Title
A STUDY OF THE ROTORFERMENTOR AND THE KENETICS OF ETHANOL FERMENTATION

Authors
Margaritis, Argyrios
Wilke, Charles R.

Publication Date
1975-07-01

LBL-3278

A STUDY OF THE ROTORFERMENTOR AND THE KINETICS OF ETHANOL FERMENTATION

Argyrios Margaritis* and Charles R. Wilke

July 1975

Prepared for the U. S. Energy Research and Development Administration under Contract W-7405-ENG-48

*Filed as a Ph. D. thesis

LBL-3278

DISCLAIMER

A STUDY OF THE ROTORFERMENTOR AND THE KINETICS OF ETHANOL FERMENTATION

Abstract

Argyrios Margaritis

A bench scale pilot plant was designed and built to test the feasibility of the Rotorfermentor as a device for potential use in the fermentation industry. The Rotorfermentor is a fermentation device designed to achieve high cell concentrations. This is achieved by filtration through a rotating microporous membrane enclosed inside the fermentor. The cell-free filtrate along with other metabolic products go through the membrane while the growing cells are left inside the fermentor. The simultaneous cell growth and cell concentration is the essential characteristic of the Rotorfermentor which in principle may replace the functions of an ordinary continuous stirred tank fermentor plus cell centrifuge. Depending on particular process conditions the application of the Rotorfermentor may result in lower capital investment costs.

The operational feasibility of the Rotorfermentor has been demonstrated by carrying out transient growth ethanol fermentation experiments. Both the cell

concentration and ethanol productivity per unit fermentor volume were found to be much higher than those for an ordinary C.S.T. fermentor.

Basic ethanol fermentation kinetic studies on Saccharomyces cerevisiae ATCC #4126 were carried out in an ordinary C.S.T. fermentor. It was found that both oxygen and glucose concentration affect the production of cell mass and ethanol as well as endogenous metabolism. At high glucose concentrations increases in oxygen concentration produced very small effects while at low glucose concentrations the oxygen effect was maximal.

A STUDY OF THE ROTORFERMENTOR AND THE KINETICS OF ETHANOL FERMENTATION

ACKNOWLEDGEMENTS

The authors wish to thank Professor Robert L. Pigford, Department of Chemical Engineering, and Professor James A. Bassham, Associate Director of the Chemical Biodynamics Laboratory, Lawrence Berkeley Laboratory for reviewing this dissertation. The expert advice and help of Mr. Gene Miner, Mechanical Department, Lawrence Berkeley Laboratory is acknowledged. Many thanks for valuable discussions and help go to Dr. Campbell W. Robinson, Mr. Lynn A. Williams, Mr. Gerald Cysewski and Mr. Paul Carroad. Special thanks are due to Mrs. Frances Wilcox for her expert typing.

This work was performed under the auspices of the United States Atomic Energy Commission through the financial support of the Lawrence Berkeley Laboratory.

CHAPTER I

INTRODUCTION

Bacterial concentrations in liquid cultures reach a certain maximum level which is characteristic of the strain and culture conditions. This maximum concentration of microorganisms, grown in ordinary batch or continuous culture conditions, is usually in the order of a few grams of dry weight of cell mass per liter of broth.

A review of the literature (Dagley et al., 1953; Finn, 1966; Hinshelwood, 1946; Monod, 1949; Sinclair and Stokes, 1962) reveals that one or a combination of the following three main factors limit maximum cell concentration: exhaustion of a limiting substrate, accumulation of toxic metabolic end product(s), and lack of available oxygen in the case of aerobic systems. In order to overcome these limiting factors, it is necessary to devise special fermentor systems. These systems should provide for continuous feeding of fresh medium, removal of toxic end products from the broth, and adequate oxygen supply.

In addition, it is possible to develop fermentation systems where high cell concentrations could be maintained. Since the rate of bacterial growth is

proportional to cell concentration, high cell productivities per unit fermentor volume may be obtained. In cases where a metabolic product is growth-associated, i.e., its production rate is proportional to cell production rate, then high cell productivities means high metabolic product productivities as well. This is the case in ethanol fermentation where the rate of ethanol production is proportional to the rate of yeast cell production.

The Rotorfermentor is a device designed to achieve high cell concentrations in batch and continuous cultures. The cells can be retained in the fermentor by filtration through a rotating microporous membrane while the metabolic products in the broth are continuously removed through the membrane. This dual function of cell growth and concentration with the simultaneous removal of any metabolic products are the essential characteristics of the Rotorfermentor. This makes the Rotorfermentor useful as a potential device that may be used to replace both an ordinary C.S.T. fermentor and a cell separator. The increase in productivity per unit fermentor volume over that of an ordinary C.S.T. fermentor may result in lower capital investment costs in a conventional microbial process where cell growth and cell separation are involved. Sortland and Wilke (8) applied the method to obtain Streptococcus faecalis cultures of up to 40% packed cell volume.

In this dissertation the theoretical basis of design and operation of the Rotorfermentor are reviewed along

with experimental results. Chapters V and III deal with the hydrodynamic characteristics of the Rotorfermentor covering the filtration characteristics of the rotating microporous membrane and power requirements, respectively. Chapter IV describes experiments designed to assess the mass transfer capacity of the Rotorfermentor. This is important in the case of aerobic microbial systems which require oxygen. Mass transfer coefficient values ($K_L a$) for oxygen are reported at different rotational speeds of the rotating membrane.

Chapter VI deals with basic studies of ethanol fermentation using Saccharomyces cerevisiae ATCC #4126. Both batch and continuous fermentation experiments are reported by employing an ordinary C.S.T. fermentor. The object of these experiments is to optimize ethanol production by finding the effects of glucose concentration and oxygen concentration.

Chapter VII covers the theory on the kinetics of dense cell culture along with some batch and transient fermentation experiments using the Rotorfermentor. Ethanol and cell productivities results obtained from an ordinary C.S.T. fermentor are also compared with those obtained from the Rotorfermentor. Some attempt is being made to assess the economic feasibility of the Rotorfermentor as a device for potential use in the fermentation industry.

This ethanol fermentation experimental study is part of an overall research program (Wilke and Rosenbluth, 1970; Wilke and Mitra, 1974) devoted to the conversion of waste cellulosic materials to glucose by enzymatic hydrolysis and subsequent conversion of glucose to alcohol via fermentation.

References Cited in Chapter I

1. Dagley, S., A. Dawes, and S. M. Foster, J. Gen. Microbiol., 8:314-322 (1953).

2. Finn, R. K., J. Ferment. Technol., 44:305-310 (1966).

3. Hinshelwood, C. N., The Chemical Kinetics of the Bacterial Cell, The Clarendon Press, Oxford, England, 1946.

4. Monod, J., Annu. Rev. Microbiol., 3:371-394 (1949)

5. Sinclair, N. A., and J. L. Stokes, J. Bacteriol., 83:1147-1154 (1962).

6. Rosenbluth, R. F., and C. R. Wilke, SERL Report No. 70-9. College of Engineering and School of Public Health, U.C., Berkeley (1970).

7. Mitra, G., and C. R. Wilke, Enzymatic Utilization of Wastes Cellulosic, LBL Report 2334 (1974).

8. Sortland, L. D., and Wilke, C. R. Kinetics of a Dense Culture Fermentation, L.R.L. Report, UCRL-18340 (1968).

CHAPTER II

EXPERIMENTAL APPARATUS

2.1 Overall Flow Diagram.

Figure 2.1.1 is an overall schematic flow diagram of the experimental apparatus used. The apparatus is composed of five main parts, the Rotorfermentor unit, the medium supply system, the recycle system, and the steam sterilization system.

Saturated steam at 121°C is introduced to the liquid medium supply tank, the gas-liquid separator, and the R-f chamber. In this way the whole apparatus is sterilized with steam before any fermentation run is begun. Live steam goes through a steam trap and then through a pressure regulator, which controls the pressure of the saturated steam from 0 to 25 p.s.i.g. before it is introduced to the fermentation apparatus.

Liquid nutrient medium is sterilized separately in 20 liter carbuoy bottles and then transferred aseptically to the supply tank.

The medium supply tank is made of stainless steel and it has a 20-inch diameter and 24-inch height, giving a storage capacity of about 100 liters. The tank is baffled and provided with a 4-inch impeller, which keeps the medium well-mixed. A glass level gauge connected to

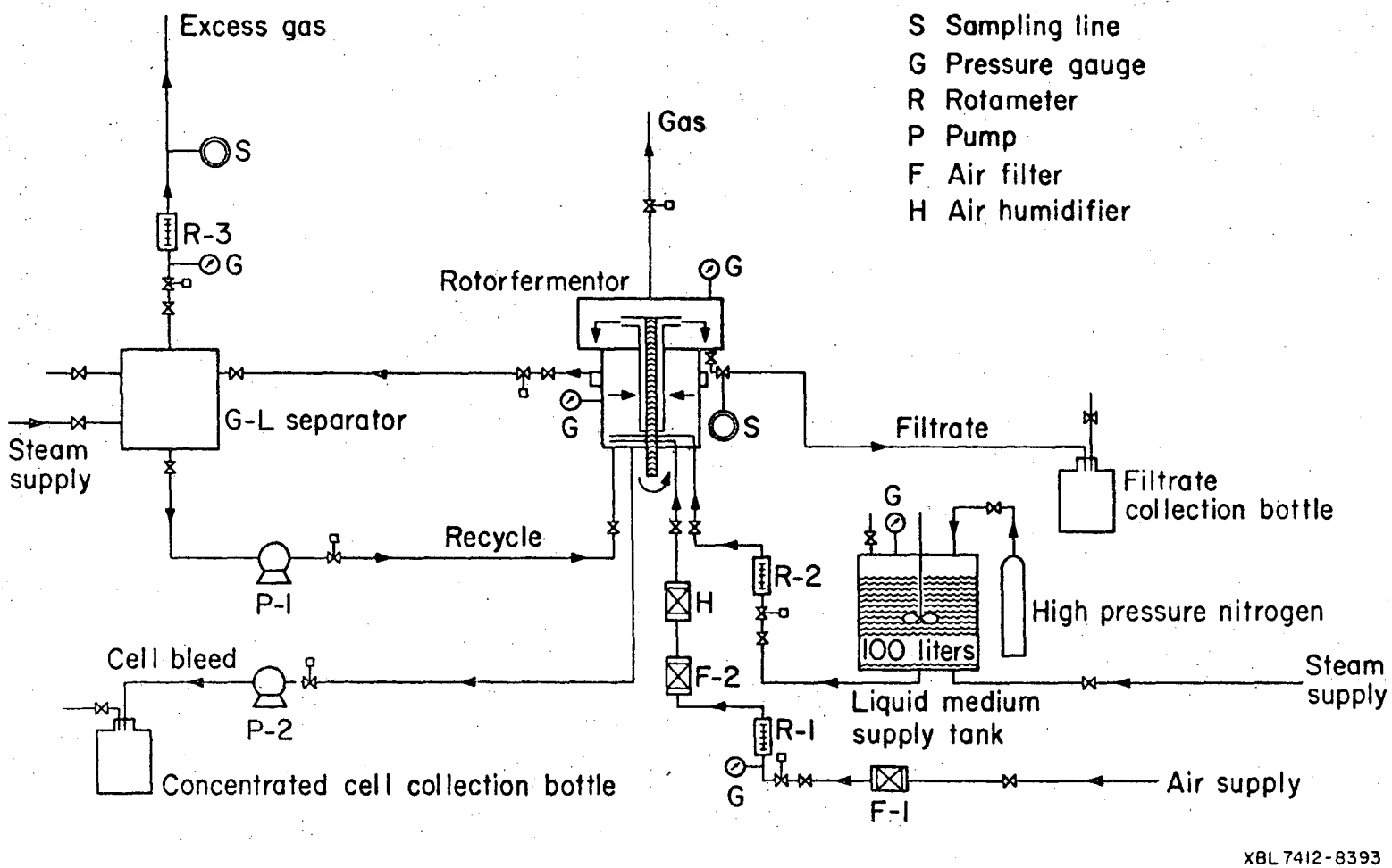

Fig. 2.1.1. Flow diagram of the Rotorfermentor apparatus.

the side of the tank indicates the level inside. A pressure gauge attached to the top indicates the pressure inside the tank. The supply tank is designed to take up to 100 p.s.i.g. pressure. High purity dry nitrogen is used to pressurize the medium inside the supply tank. The nitrogen cylinder is equipped with a pressure regulator that maintains a constant pressure from 0 to 60 p.s.i.g. This pressure is used as the driving force for cell filtration through the rotating membrane which is enclosed inside the Rotorfermentor. The sterile liquid medium that comes out of the supply tank goes through a pressure controller and metered with rotameter R-2. This rotameter is steam sterilizable and made of noncorrosive materials. The line that connects rotameter R-2 and the Rotorfermentor chamber has a one-way check valve which prevents possible back flow. This also prevents possible passage of growing cells from the Rotorfermentor to the sterilized nutrient medium in the supply tank.

The recycle system which includes the recycle pump P-1 and the gas-liquid separator is to be used in the case of aerobic systems where the excess air coming out of the Rotorfermentor must be separated from the liquid phase. Recycle pump P-1 is a positive displacement helical type Moyno pump, which has a stainless steel helical rotor and viton seals, and is steam sterilizable. This pump is especially suited for dense viscuous

slurries. The gas-liquid separator is a cylindrical chamber made of transparent pyrex glass. All piping and valves are made of stainless steel which minimizes problems of corrosion.

The Rotorfermentor assembly includes the rotating membrane which is enclosed in the fermentation chamber and the filtrate chamber on top which is separated from the fermentation chamber. A more detailed description of the Rotorfermentor assembly and the rotating membrane is given in Sections 2.2 and 2.3.

In this apparatus provision is also made for aerobic systems where aeration of the growing culture inside the Rotorfermentor is necessary. The air must be free of microorganisms before it is introduced and this is done by passing the air through specially designed air filters. These filters are packed columns made of 16 micron diameter glass-wool fibers. House supply air goes through the first filter F-1 which has 2-inch diameter and about 9-inch length. This is used as a preliminary filter where possible impurities such as dust or small oil drops are collected. Then the air goes through a controller and pressure regulator and metered with rotameter R-1. This rotameter can withstand relatively high pressures. Before the air enters the Rotorfermentor it is filtered again through filter F-2. It is made of glass-wool fibers 16 micron in diameter and the packed column has a diameter of

3 inches and 24 inches length. This sterile air is then passed through humidifier H which is a packed column filled with stainless steel wire mesh and sterile water. In this way the air entering the Rotor-fermentor is sterile and saturated with water.

In a typical run the whole apparatus is first thoroughly cleaned and washed and then sterilized for approximately 1 hour with saturated steam at 121°C. Then sterilized medium is introduced aseptically into the supply tank and pressurized to the desired pressure ranging from 2 to about 12 p.s.i.g. depending on the flow rate desired and pressure drop across the rotating membrane. The medium then flows through rotameter R-2 into the fermentation chamber. An impeller attached to the bottom of the rotating membrane provides vigorous agitation and keeps the culture well-mixed. The nutrients in the liquid medium are utilized by the growing microorganisms inside the chamber. The metabolic products, such as ethanol in the case of ethanol fermentation, are filtered through the rotating membrane while the cells are left inside the fermentation chamber. The filtrate flows through the membrane into the filtrate chamber and then collected in a bottle. The dense cell culture is maintained by continuously supplying liquid medium until a desired cell concentration is achieved. If a steady-state is desired then a cell bleed is taken through pump P-2 at a specified flow

rate. Pump P-2 is a positive displacement helical type Moyno pump. Both positive displacement pumps P-1 and P-2 are connected to two-speed controllers which control the r.p.m. of the pumps and therefore the flow rates.

Temperature inside the Rotorfermentor is controlled by means of a temperature recorder-controller. When the temperature rises above the set point temperature then a Solenoid valve opens allowing cooling water to flow through a cooling coil which is installed inside the Rotorfermentor chamber.

The pressure inside the Rotorfermentor chamber is recorded by means of a membrane type pressure gauge. This gauge is connected with a diaphragm membrane transducer with a line pneumatically filled with oil. This diaphragm transducer is used to separate the pressure gauge from the bacterial culture and thus eliminating contamination problems.

2.2 Rotorfermentor Unit.

Figure 2.2.1 is a full-scale assembly drawing of the Rotorfermentor unit. It consists of three main parts: the fermentation chamber, the rotating microporous membrane, and the filtrate chamber. All parts are made of 316 stainless steel. The heavy arrows through the rotating membrane show the direction of filtrate flow into the filtrate chamber. Liquid nutrients are evenly distributed by means of a liquid medium sparger. A cooling coil of 1/4-inch diameter inside the fermentation chamber is used to maintain constant temperature. Figure 2.2.2 shows the Rotorfermentor assembly unit without the filtration membrane. The vertical measuring ruler is divided in cm. units.

Figure 2.2.3 shows the fermentation chamber resting on its base support and the filtrate chamber. The fermentation chamber has 10-inch O.D. with 1/8-inch wall thickness and 13-inch height. There are four viewing windows two on each side and a mounting flange on which the temperature probe and pressure diaphragm are mounted. The windows are equipped with glasses 5 inches in diameter and 1/2-inch thickness. They are made of pyrex glass and can withstand pressures up to 50 p.s.i.g. and high temperatures. Viton O-rings are used to seal the windows and all other parts of the unit.

The filtrate chamber has 12.5-inch diameter and 8-inch height. The two viewing windows, 5 inches in

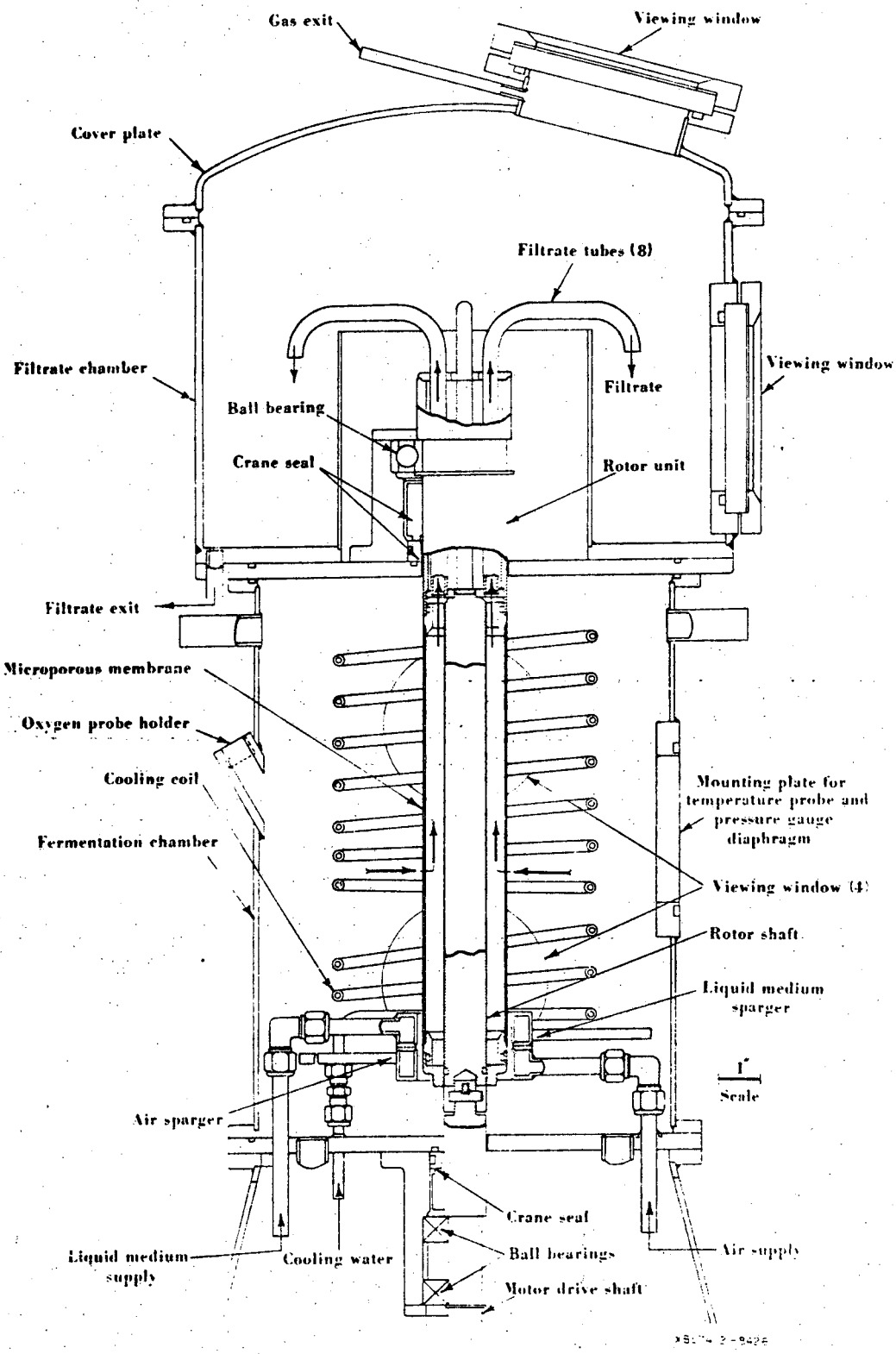

Fig. 2.2.1. Assembly drawing of the Rotorfermentor unit.

diameter, are attached on the side and on the top cover plate of the filtrate chamber. A side flange is also used to which a pressure gauge is attached. Any trapped gas or air that comes along with the liquid filtrate separates out in the filtrate chamber and comes out through an exit tube at the top of the cover plate.

Figure 2.2.4 shows the top view of the filtrate chamber. Also visible are the ball bearings and housing. The filtrate tubes (8) are attached to the rotor and filtrate is discharged through them as they rotate. Not shown in Fig. 2.2.4 is a 1/4-inch cooling coil which is placed around the ball bearing housing in order to remove the heat generated by the crane seal and ball bearings during rotation.

Figure 2.2.5 shows both the air and liquid spargers. Each sparger is made of a distribution ring and eight tubes which are evenly distributed on a radial direction. In the case of air sparger each tube has six holes of 0.0135-inch diameter, giving a total of 48 evenly spaced holes. Likewise the liquid sparger has six holes of 0.020-inch diameter per tube giving a total of 48 holes. The air and liquid spargers are assembled together as shown in Fig. 2.2.6. The air sparger is at the bottom and liquid sparger at the top. This arrangement insures adequate and uniform mixing of both nutrient medium and air inside the fermentation chamber, resulting in better oxygen mass transfer rates.

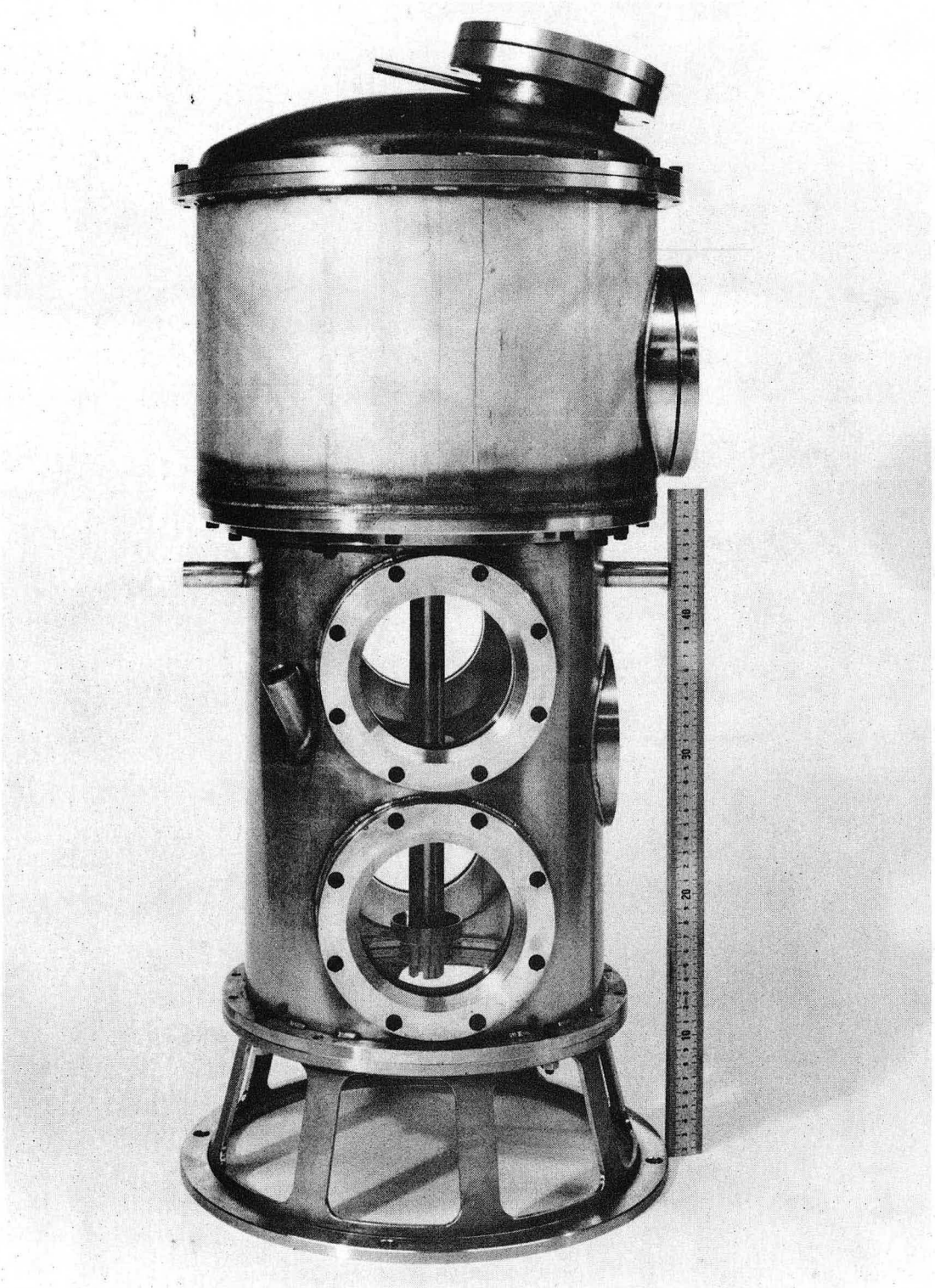

XBB 718-3815

Fig. 2.2.2. Rotorfermentor unit without the membrane.

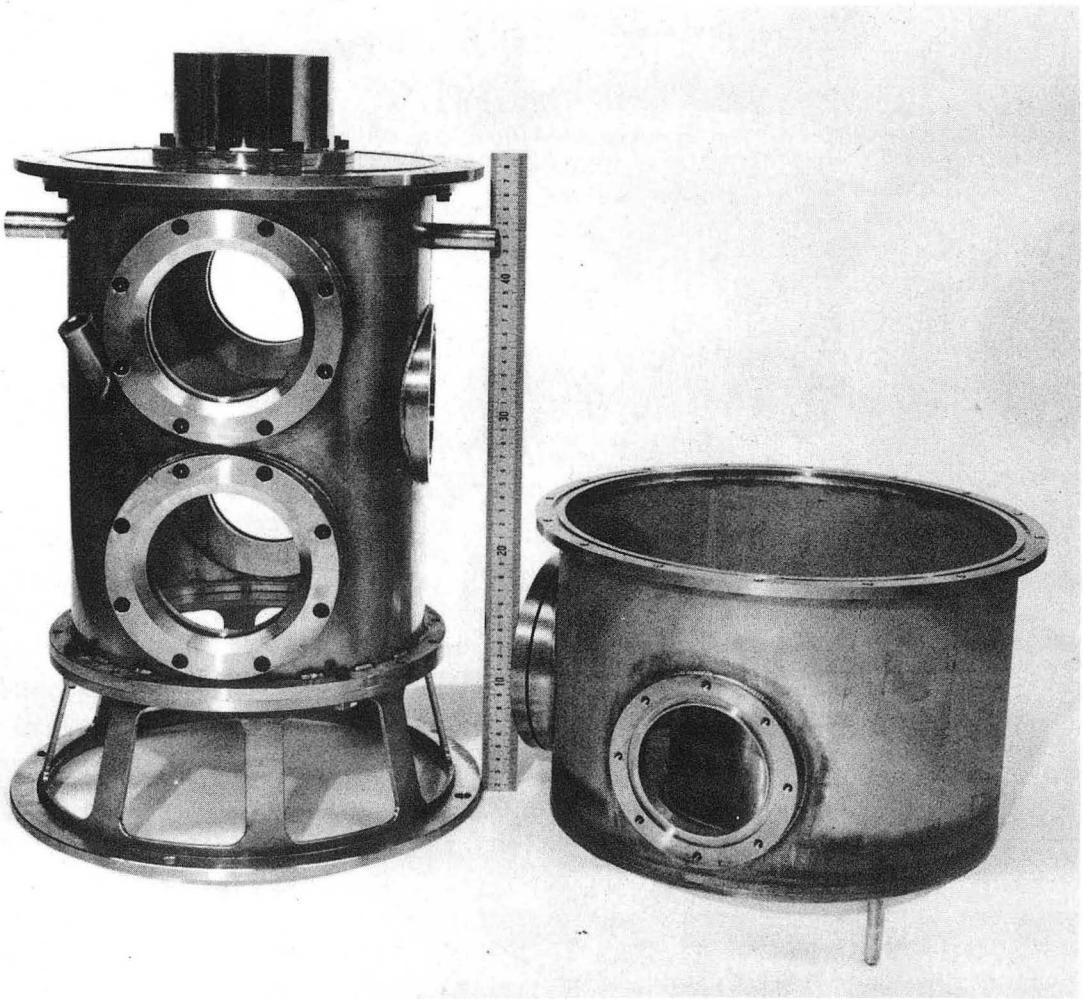

XBB 718-3814

Fig. 2.2.3. The Fermentation chamber (left) and the filtrate chamber (right).

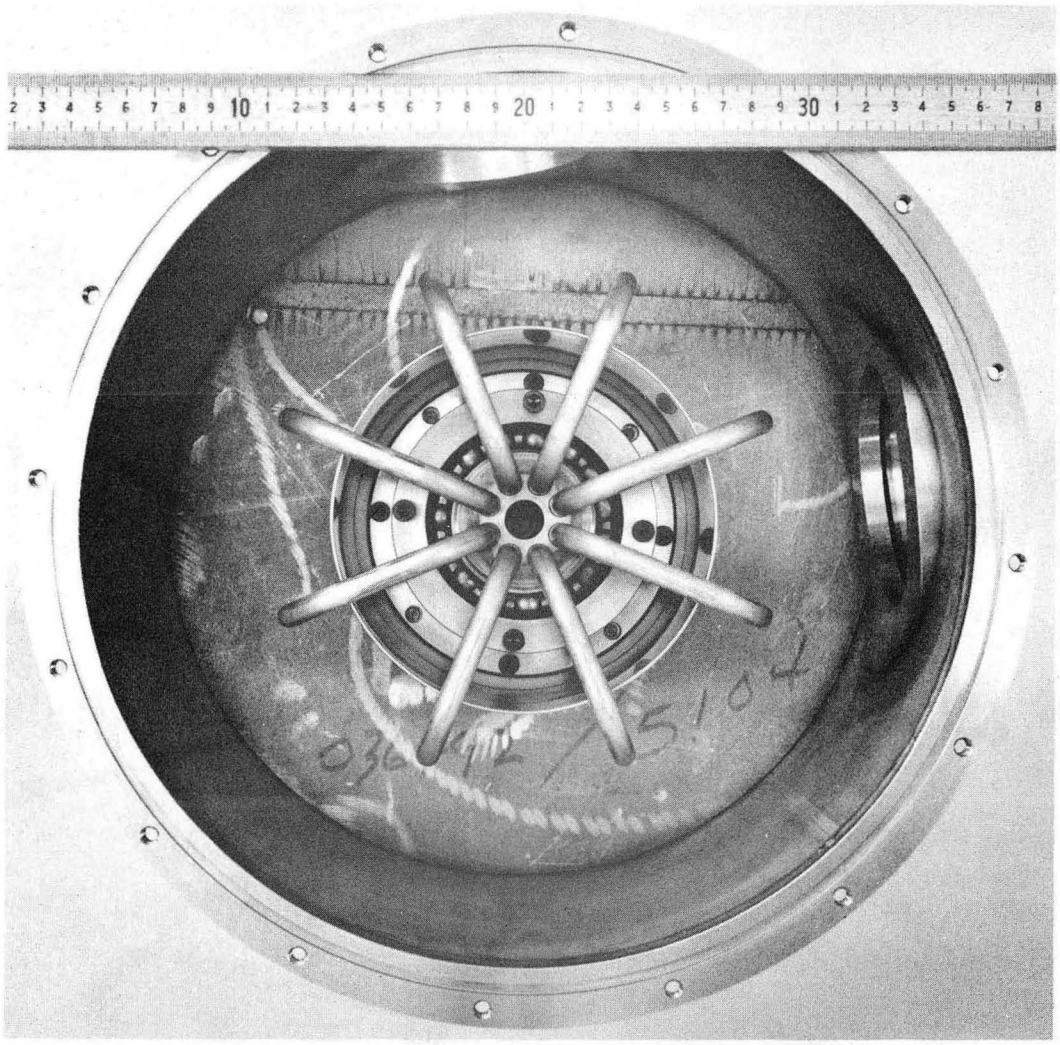

XBB 718-3809

Fig. 2.2.4. Top view of the filtrate chamber.

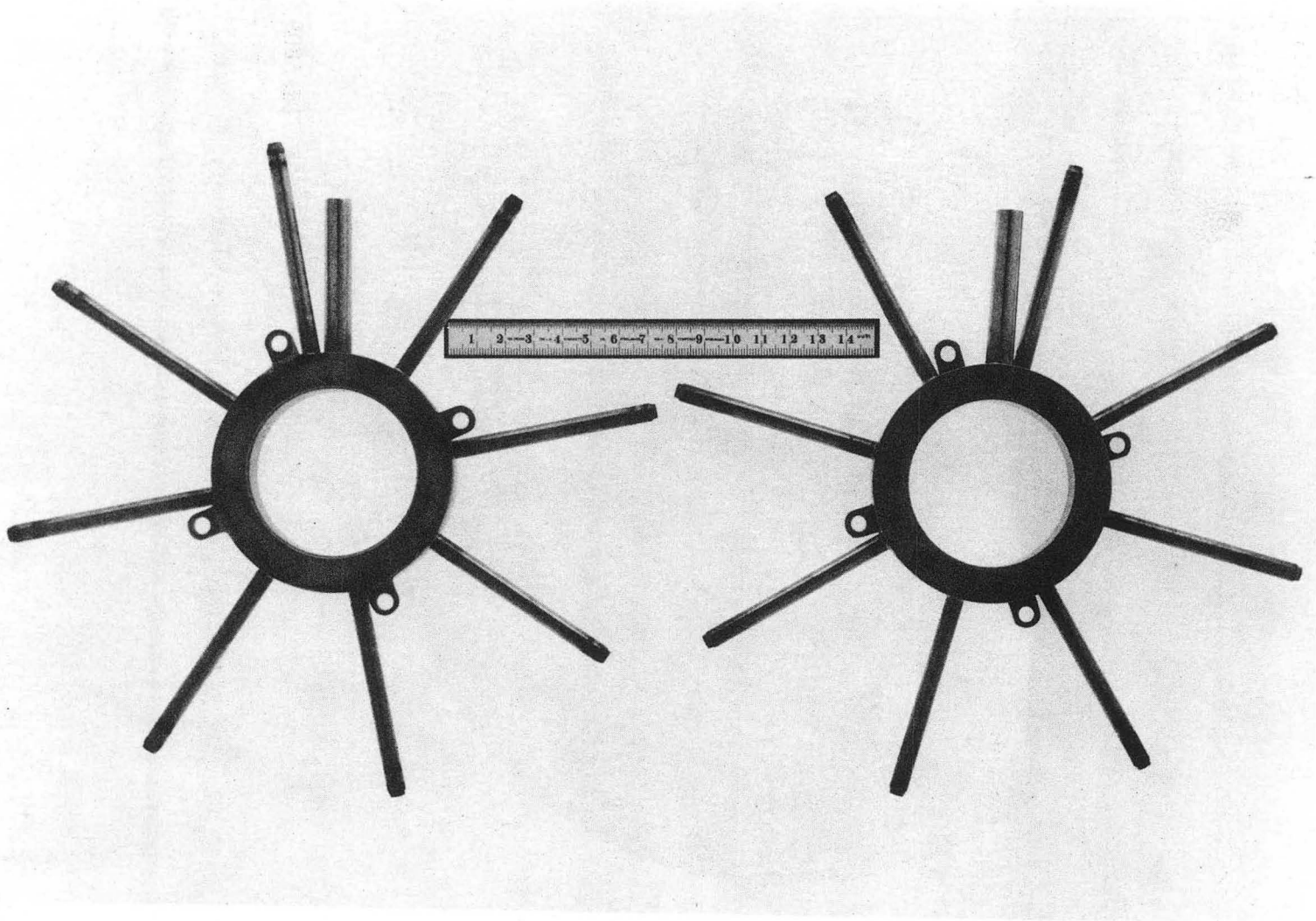

XBB 718-3811

Fig. 2.2.5 Air sparger(left) and liquid sparger(right).

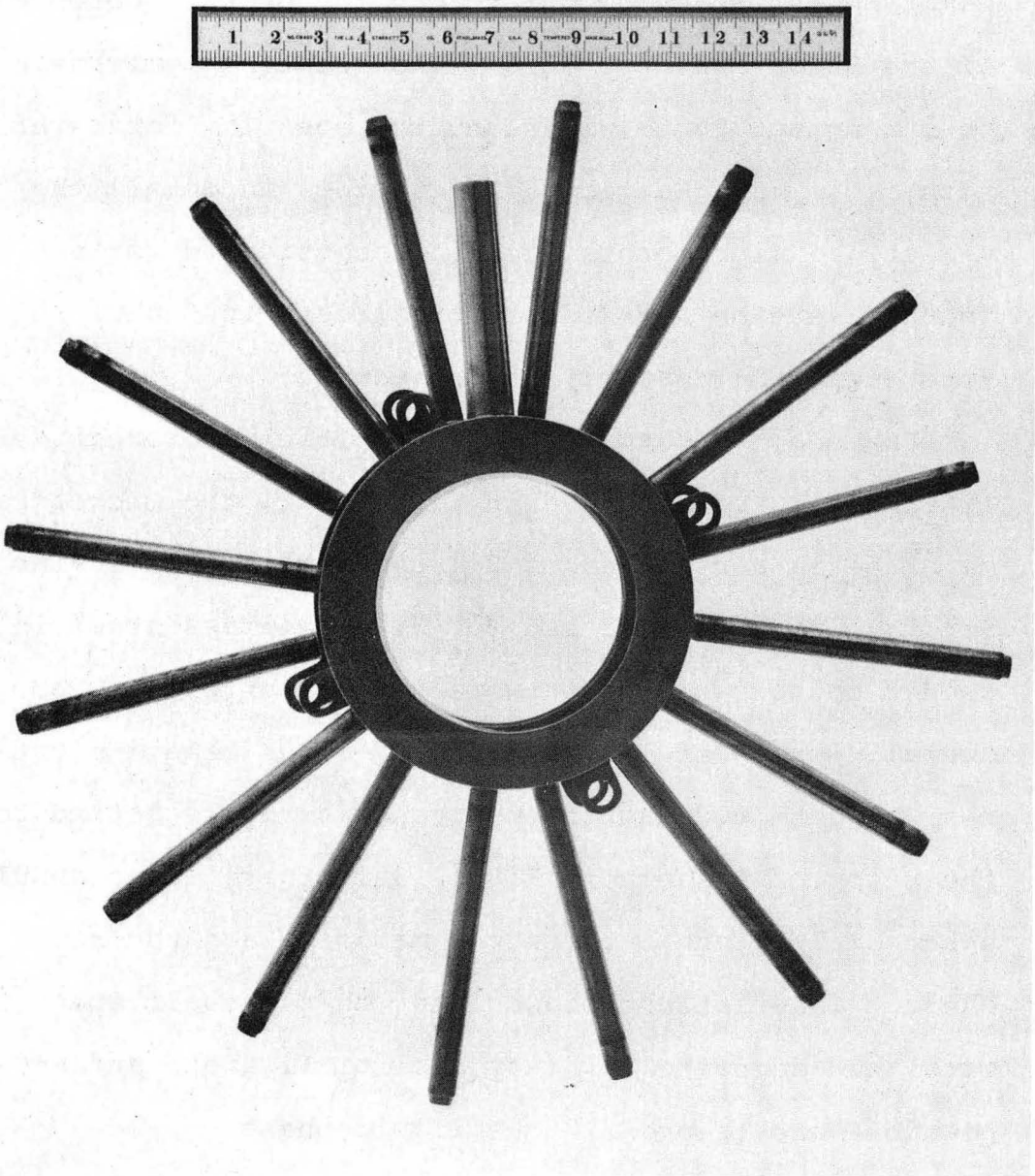

XBB 718-3819

Fig. 2.2.6. Air and liquid sparger assembly.

2.3 Membrane-Rotor Assembly

The design and efficient operation of the rotating membrane is of key importance in the overall performance of the Rotorfermentor unit. The rotating membrane must be strong enough to withstand the shearing forces at high r.p.m.'s. Section 5.2 describes in detail the variety of microporous membranes considered for use. In this section a brief pictorial description of the rotor-membrane assembly is presented.

For exact dimensions regarding the rotor unit refer to Fig. 2.2.1. As shown in Fig. 2.3.1, the microporous membrane is a cylinder of 2-inch diameter and 10-inch length. The membrane made of 316 stainless steel is welded on both sides to two end fittings giving an overall length of 11 inches. "O" rings make a tight seal at both ends as the membrane is snugly fitted to the rotor. As shown in Fig. 2.3.1, there is an annular space of 1/2 inch between the membrane and the rotor shaft. Calculations showed that this annualr space is more than adequate for easy flow of filtrate and any possible gas trapped in the liquid phase.

Figure 2.3.2 shows the rotor unit without the membrane. The rotor shaft has 1 inch diameter and the upper part has 2 inch diameter over which a ball bearing fits and supports the rotor. Eight tubes of 3/8-inch O.D. are symmetrically distributed at the top of the rotor, giving adequate cross sectional area for the

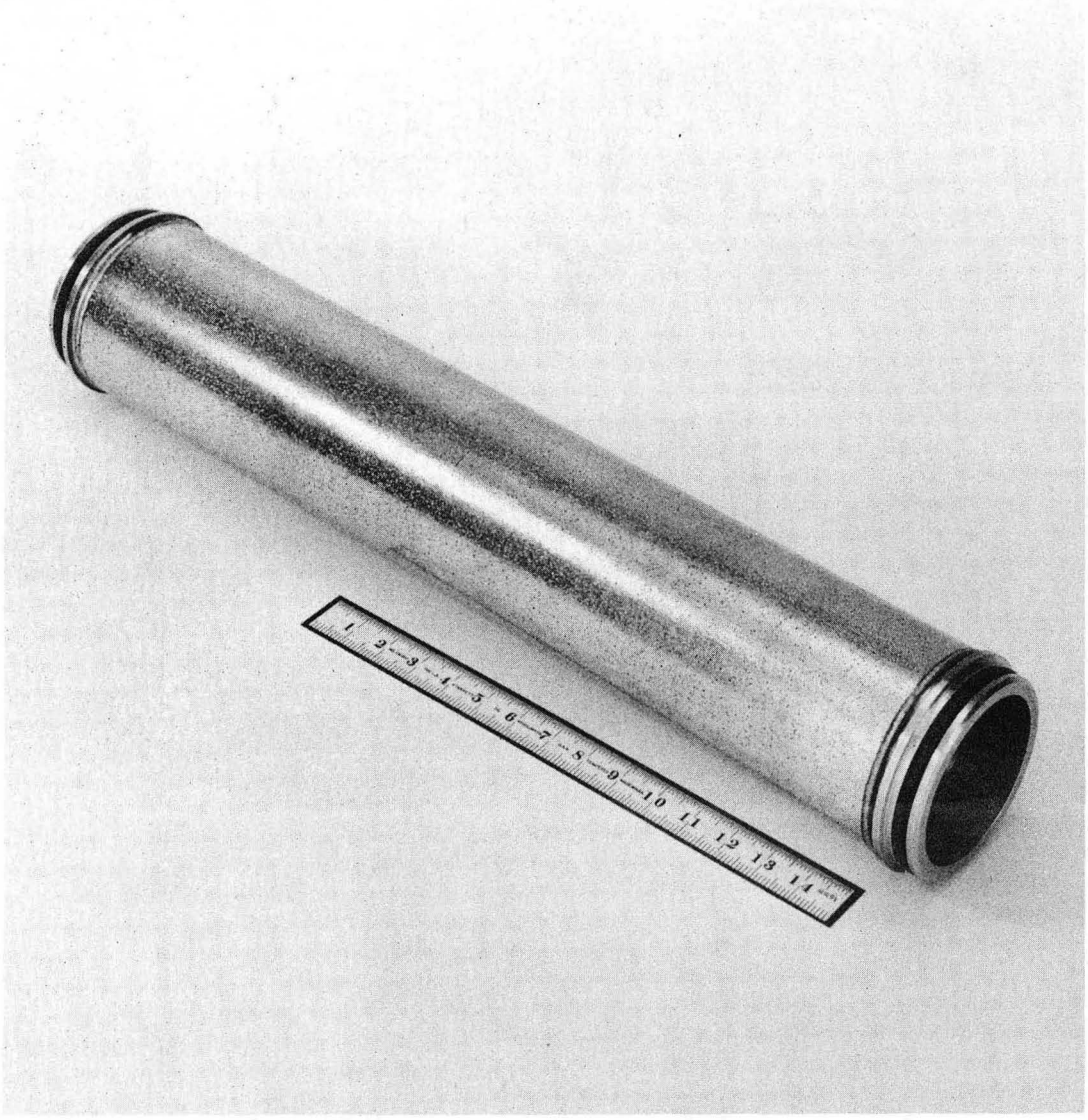

XBB 718-3817

Fig. 2.3.1. Metallic Microporous membrane.

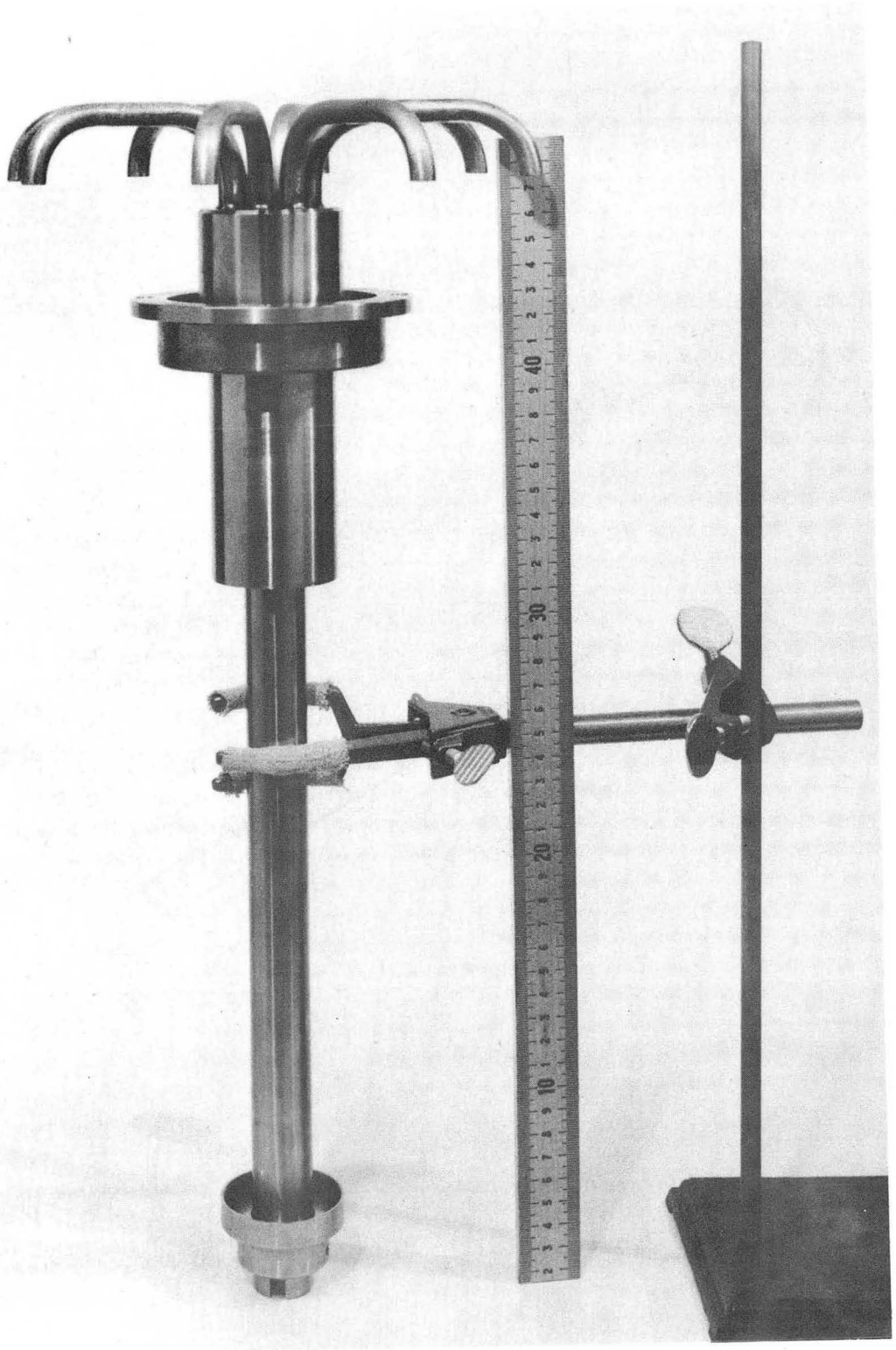

XBB 718-3813

Fig. 2.3.2. Rotor shaft.

filtrate flow. The rotor unit has a total length of 19 inches. The vertical ruler shown in Fig. 2.3.2 is divided in cm units.

Not shown in Fig. 2.3.2 is a Crane seal which fits under the ball bearing and forms a tight seal between the fermentation chamber and filtrate chamber. This is a type 9 seal manufactured by John Crane Company and is made of two parts. The upper part is fastened to the rotor and rotates along with it and a Teflon spring loaded wedge prevents any leakage. This Teflon material is impervious to acids, other corrosives, and solvents and can withstand temperatures up to 500°F. The spring is made of 316 stainless steel. The rotating upper part of the Crane seal comes in contact with a stationary ring which is fastened on the plate that separates the filtrate chamber from the fermentation chamber. All the friction occurs between the surface of the upper rotating ring which is made of graphite and the lower stationary ring made of a Tungsten-carbide alloy. These materials can withstand temperatures from -350°F to 750°F and are impervious to practically all known acids, solvents, and corrosives. This type 9 Crane seal is recommended for pressures up to 200 p.s.i. A similar Crane seal is used at the bottom end of the Rotor unit.

Figure 2.3.3 shows the deassembled rotor unit. The membrane that has two Viton "O" rings on both sides is first fit against the upper part of the rotor and then

the lower end fitting is pressed and fitted against the lower end of the membrane. Six set screws are used to fasten the lower end fitting to the rotor shaft. The result is shown in Fig. 2.3.4 which shows the final complete assembled rotor-membrane unit. The filtrate is driven through the pores of the membrane and comes out at the top eight tubes and discharged into the filtrate chamber shown earlier.

Figure 2.3.5 shows the bottom driving shaft (left) and the shaft fits to the bottom part of the rotor unit shown in Fig. 2.3.4. Two ball bearings are used to insure a rigid drive unit and eliminate possible waggling. The other item in Fig. 2.3.5 (right) is a six-blade impeller of 4-inch diameter. This impeller is to be used when the fermentor unit is used without the rotor i.e. as an ordinary C.S.T.R. fermentor.

The bottom part of the drive shaft shown in Fig. 2.3.5 (left) is connected through a torque meter to a variable speed motor unit. This is a three-phase Reeves motor of 1.5 h.p. The speed can be easily changed from 320 r.p.m. to 4,200 r.p.m. by turning a wheel that changes the gear ratio and stays constant. A Weston tachometer measures the r.p.m. The torque meter is attached between the motor shaft and the bottom shaft of the rotor. This is a Bex-Ometer torque meter, 5/8-inch collet, Model 63, and can measure from 0 to 25 pound-inch torque.

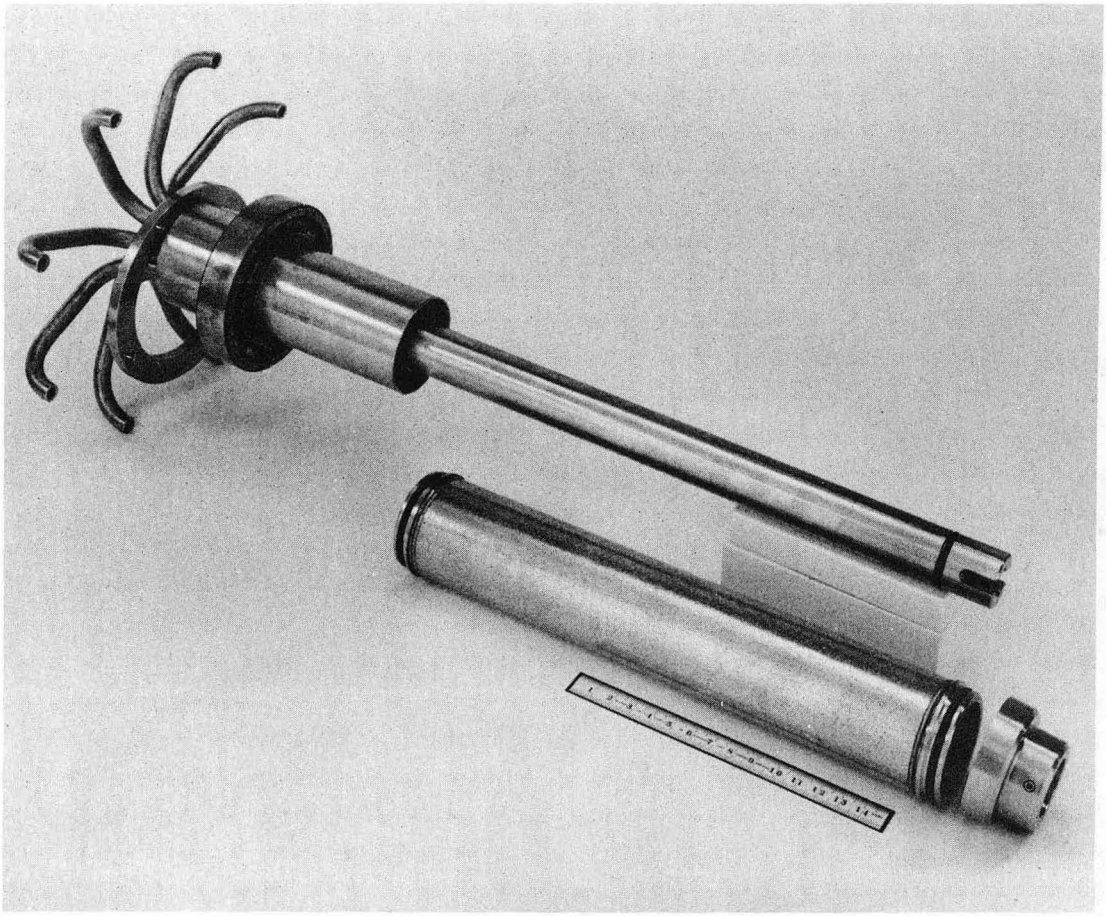

XBB 718-3818

Fig. 2.3.3. Rotor shaft and membrane

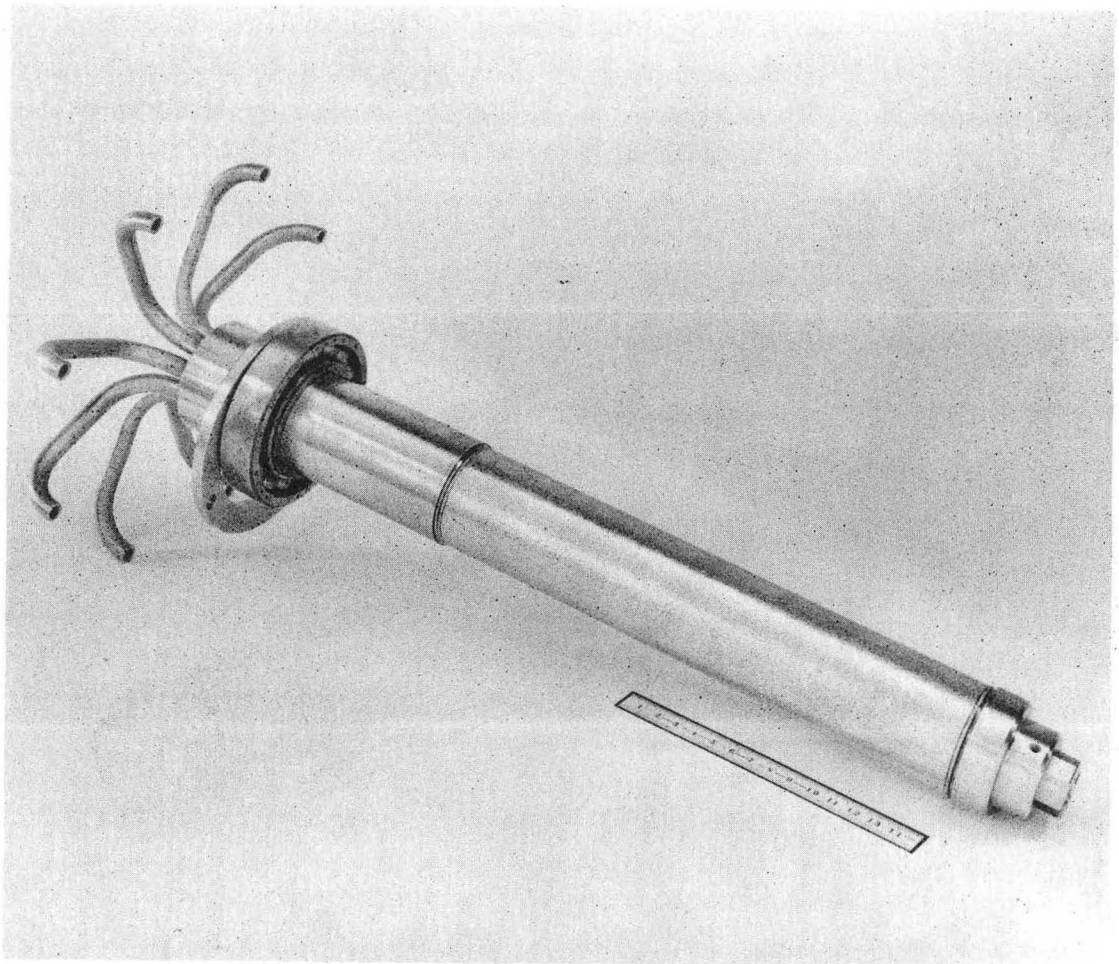

XBB 718-3816

Fig. 2.3.4. Assembled rotor unit

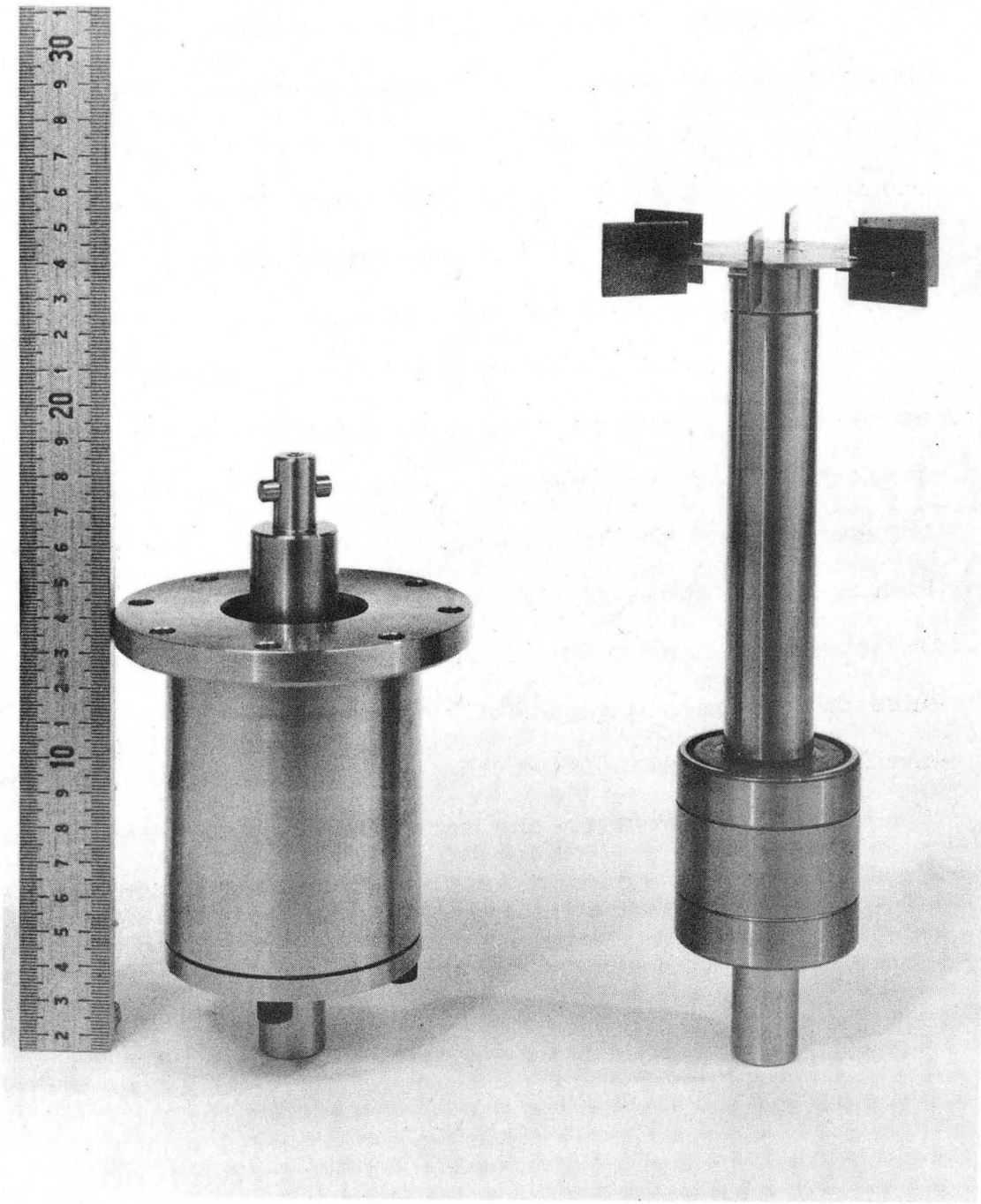

XBB 718-3812

Fig. 2.3.5. Drive shaft (left) and six blade impeller (right)

In order to measure the power consumed by the rotor both the torque and r.p.m. are needed. A stroboscope is used by means of which the r.p.m. is measured and the torque is read on the torque meter scale. The results of power consumption at various r.p.m. are presented in Section 3.1.

Figure 2.3.6 shows part of the experimental apparatus. Beginning from left to right is the Rotor-fermentor unit followed by the gas-liquid separator in the center and the medium supply tank on the right. Figure 2.3.7 shows the assembled Rotorfermentor unit. On the right hand side of the Rotorfermentor the pressure diaphragm along with the temperature probe are easily distinguished. At the bottom of the Rotorfermentor the driving shaft with the torque meter are shown along with part of the motor driving unit. Part of the instrumentation panel is shown on the left.

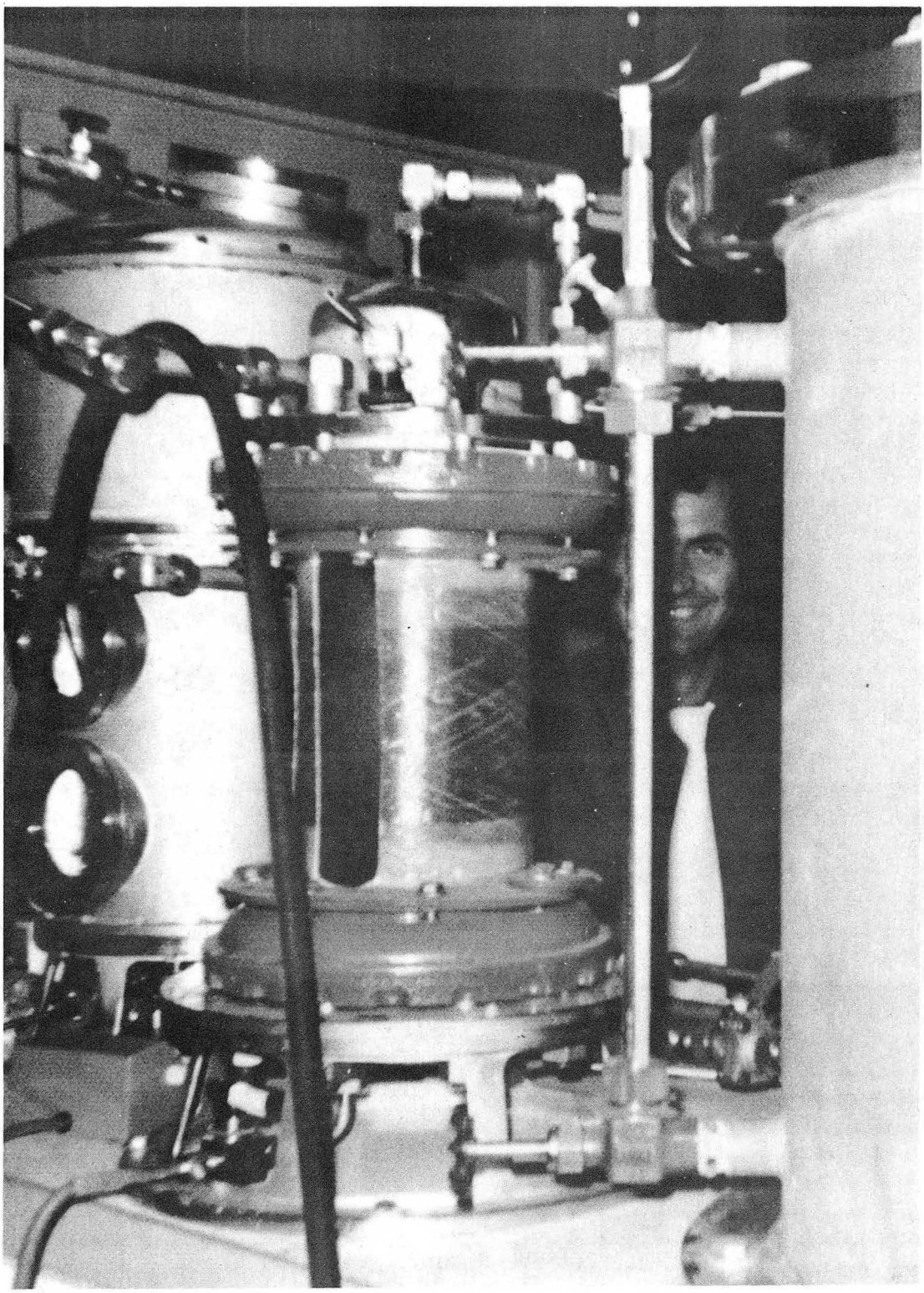

CBB 752-1317

Fig. 2.3.6. The Rotorfermentor unit (left), the gas-liquid separator (center), and the medium supply tank (right).

CBB 752-1315

Fig. 2.3.7. The Rotorfermentor unit.

CHAPTER III

HYDRODYNAMIC CHARACTERISTICS OF THE ROTORFERMENTOR

The hydrodynamic characteristics of the rotating membrane inside the Rotorfermentor chamber are of key importance in the overall performance of the unit. The hydrodynamics of the rotating membrane will affect not only mixing of the liquid but also power consumption and the filtration performance of the membrane. In this section some basic theoretical principles are reviewed and experimental results are also presented for the 2-inch diameter metallic microporous membrane.

3.1. Theoretical Considerations.

When the cylindrical membrane rotates, the fluid elements adjacent to the membrane surface are also subjected to rotational motion. At low rotor speeds, laminar flow conditions exist in the annulus between the rotor surface and the wall of the fermentation chamber. This case is adequately described by Schlicting (1). However, as the rotor speed is increased, a critical value is reached beyond which fully turbulent flow conditions are developed in the annulus. Turbulence in the vicinity of the rotor is characterized by the dimensionless Taylor Number T_a defined by Equation 3.1.1

$$T_a = \frac{4}{9} D^4 \left(\frac{\omega}{\nu}\right)^2 \qquad 3.1.1$$

where

D = rotor diameter, cm

$\omega = 2\pi N$ = angular velocity of rotor, radians/sec

N = revolution per sec, sec^{-1}

$\nu = \mu'/\rho$ = kinematic viscosity, cm^2/sec

μ' = viscosity of fluid, g/cm sec

ρ = density of fluid, g/cm^3

According to Chandrasekhar (2), the critical Taylor Number, T_c, beyond which turbulence occurs is equal to 3.1×10^4, although the critical Taylor Number is also a function of the annulus width. At rotor speeds well beyond the critical value, Donnely and Simon (3) obtained an empirical relationship between the angular velocity, ω, annulus width, d, and the torque transmitted by the rotor to the fluid. Batchelor (4) provides a theoretical analysis of the experimental results, postulating a steady flow pattern in the axial plane passing through the annulus, as shown in Fig. 3.1.1.

The peripheral velocity of the fluid elements adjacent to the membrane varies with distance. At very small distances away from the membrane surface, i.e., about 50 μ or less, the fluid elements do not "see" the membrane curvature. Therefore, in order to simplify the

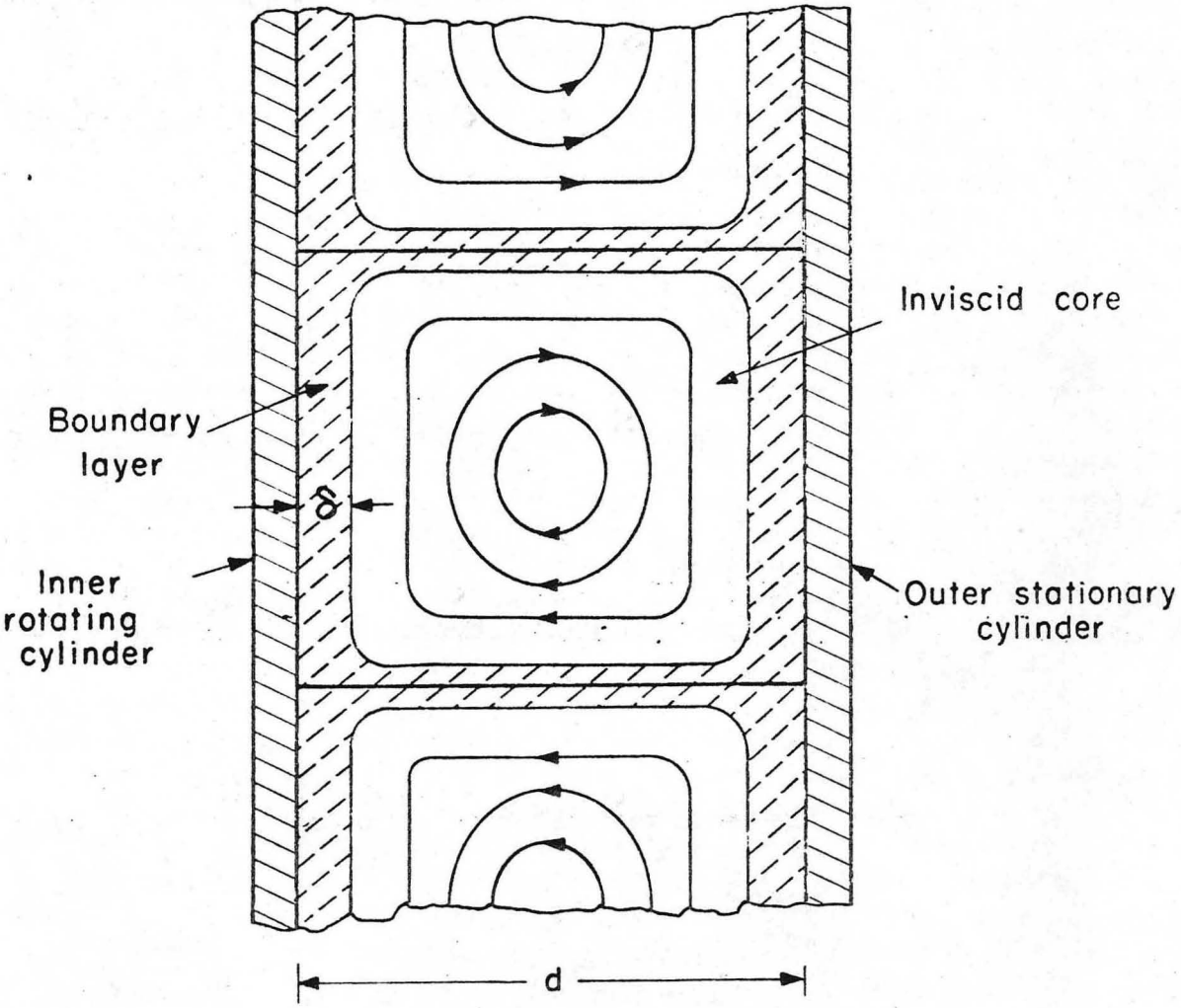

Fig. 3.1.1. Flow patterns in the axial plane. After Batchelor (4).

analysis, a good approximation can be made by neglecting the membrane curvature and assuming flow past a flat plate. For turbulent flow conditions past a flat plate, the velocity profile in the boundary layer is given by Von Karman's (5) universal velocity profile in the form:

$$v = v_o (1 - ax) \qquad 3.1.2$$

where

v = peripheral (tangential) velocity of liquid element at distance x from the membrane surface, cm/sec

v_o = peripheral velocity of membrane, cm/sec = πDN

$a = \frac{\tau_w g_c}{\mu v_o}$, cm^{-1}

τ_w = shear stress at the membrane surface, g/cm^2

$g/cm^2 = \frac{f}{2} \frac{\rho v_o^2}{g_c}$

f = friction factor, a function of Reynold's Number

g_c = gravitational constant = 980 cm/sec^2

In the derivation of Equation 3.1.2, it is assumed that there is no appreciable effect of the fluid radial flow on the peripheral velocity profile.

Figure 3.1.2 is a plot of the Von Karman velocity profile for two different viscosities at various speeds of the 2-inch diameter rotor.

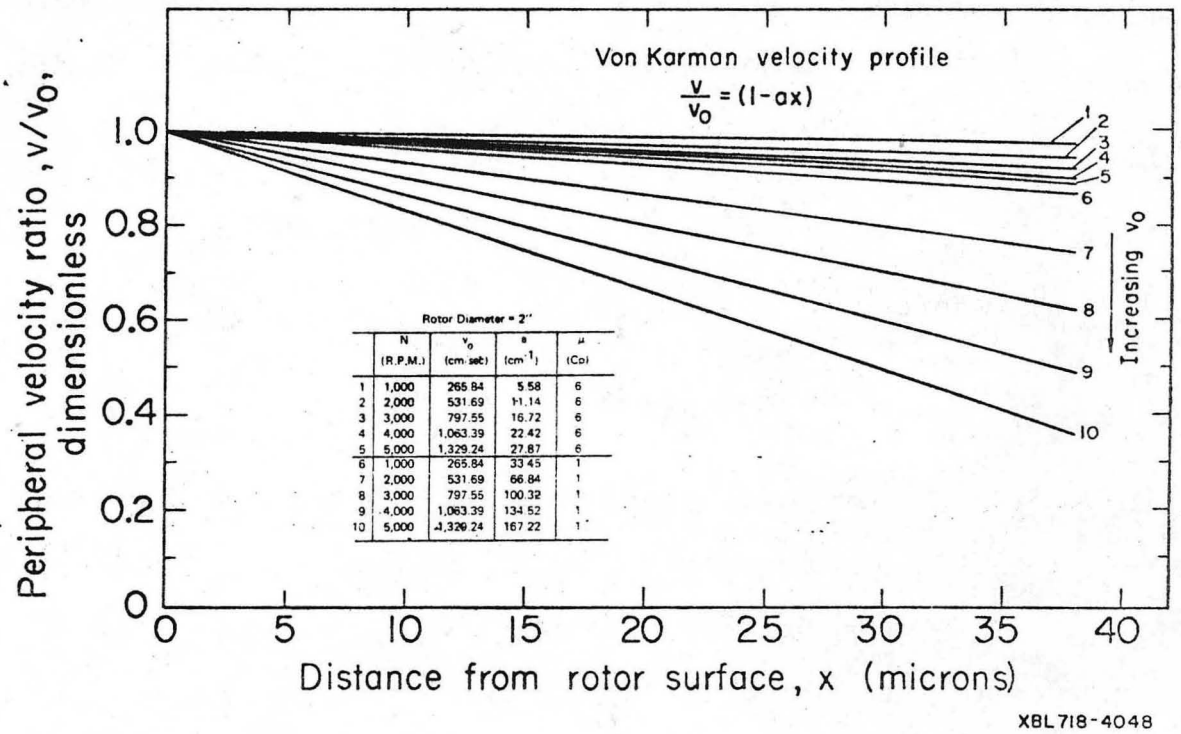

	N (R.P.M.)	v_0 (cm. sec)	a (cm^{-1})	μ (Co)
1	1,000	265.84	5.58	6
2	2,000	531.69	11.14	6
3	3,000	797.55	16.72	6
4	4,000	1,063.39	22.42	6
5	5,000	1,329.24	27.87	6
6	1,000	265.84	33.45	1
7	2,000	531.69	66.84	1
8	3,000	797.55	100.32	1
9	4,000	1,063.39	134.52	1
10	5,000	1,329.24	167.22	1

Fig. 3.1.2. The Von Karman velocity profile.

Another important variable is the power consumed by the rotor which is transmitted to the fluid in the annulus. The power consumption is a function of the rotor geometry and speed plus the physical properties of the fluid. Equation 3.1.3 shows the power consumption for a cylinder rotating in a Newtonian fluid, under fully turbulent flow conditions.

$$P = (1.272 \times 10^{-8}) (f\rho LD^4N^3) \qquad 3.1.3$$

where

$$\frac{\pi^4}{2\ g_c \times 33{,}000} = 1.272 \times 10^{-8}$$

P = power consumption, hp

ρ = density of fluid, lb./ft^3

f = friction factor

L = length of cylinder, ft.

D = diameter of cylinder, ft.

N = rotational speed of cylinder, rpm

Figure 3.1.3 is a plot of rotor speed against power consumed for various rotor diameters from 1 to 8 inches calculated for a system of 6 centipose viscosity. This corresponds in properties to the cell suspension of Streptococcus faecalis obtained by Sortland and Wilke (6,7). Values of the friction factor at different Reynold's Numbers were obtained from Theodorsen and Regier (8).

The membrane used to measure power consumption and

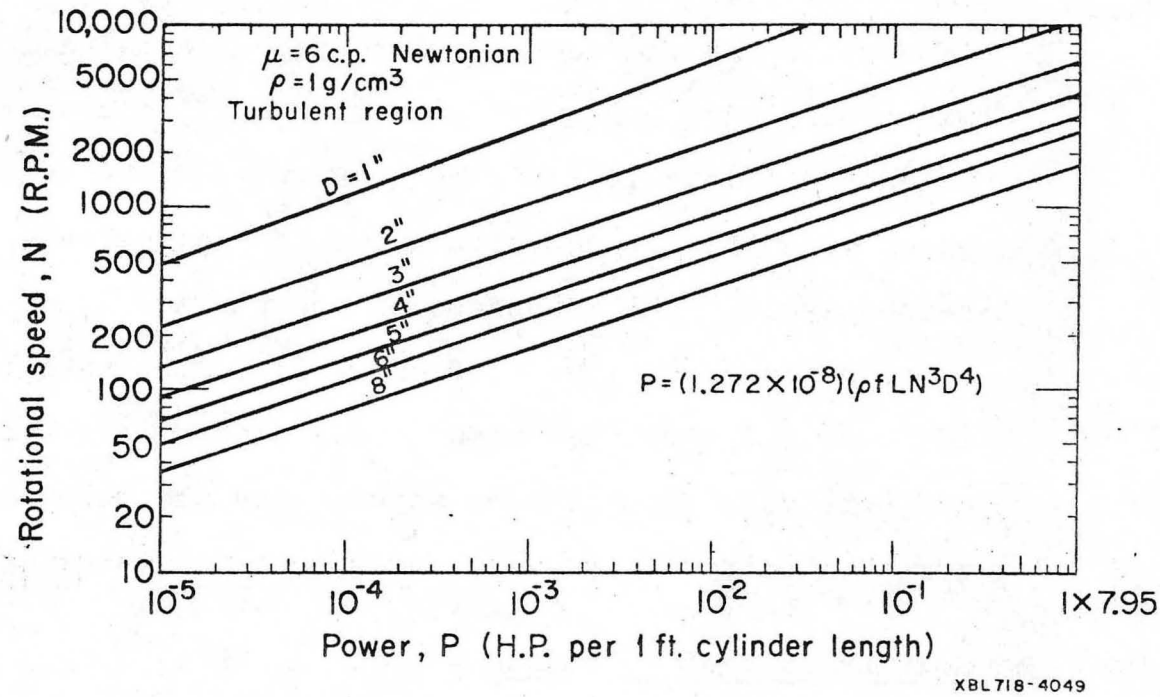

Fig. 3.1.3. Power requirements of rotating cylinders (turbulent region).

rates of yeast filtration (Section 5) is made of 316 porous sintered stainless steel. This is a Grade H membrane of 1/16" thickness made by Pall Trinity Micro Corporation and has a nominal pore size of 5 microns. However, Scanning Electron micrographs revealed a much wider pore size distribution than the "5" micron size cited for. This is revealed in Figures 3.1.4 and 3.1.5 which show the top and side views of the membrane respectively. The roughness of the surface is notable at both magnifications X100 and X500. Also both the top view and side view show no difference in structure and pore size distribution which means the membrane has a rather uniform structure throughout its thickness.

3.2 Experimental Results

The power consumption by the 2-inch diameter grade H sintered steel membrane was measured in both aerated and nonaerated pure water. Then from those experimental data friction factor f was calculated and plotted against the Reynold's Number.

The torque experienced by the membrane surface is measured by means of a torque meter. A stroboscope is used to measure the R.P.M. of the rotating rotor and also read the torque on the torque meter scale by means of the flashing light of the stroboscope. The torque meter scale is calibrated in lb-inch units. Then for a given rotor speed N r.p.m. and torque T lb-inch the

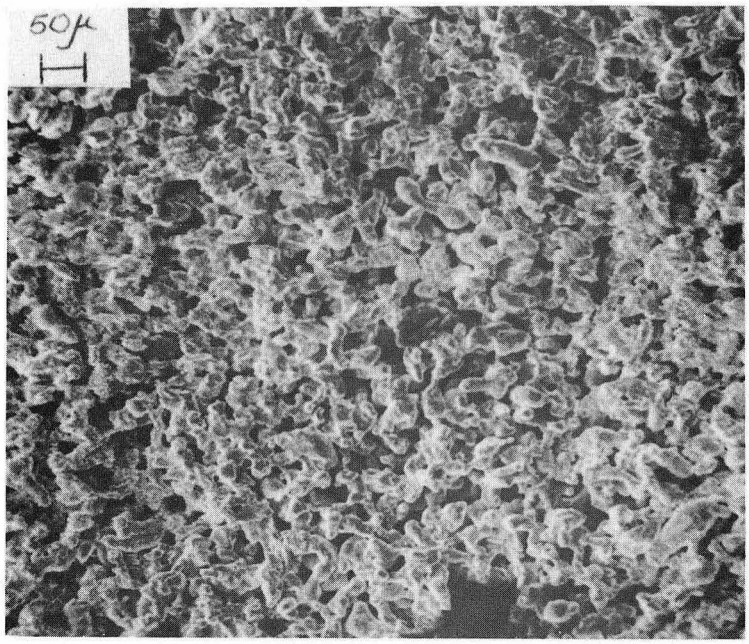

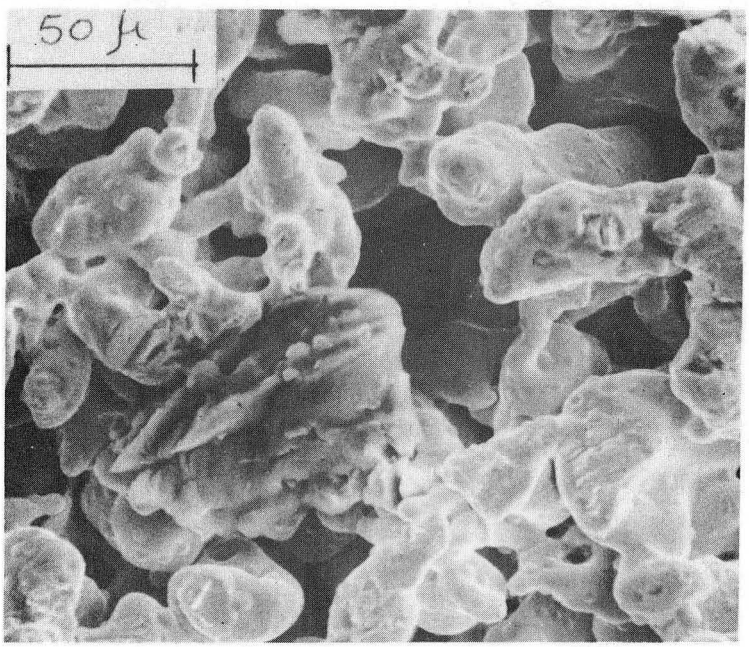

XBB 754-3045

Fig. 3.1.4. Scanning electron micrograph of sintered stainless steel membrane. Top view.

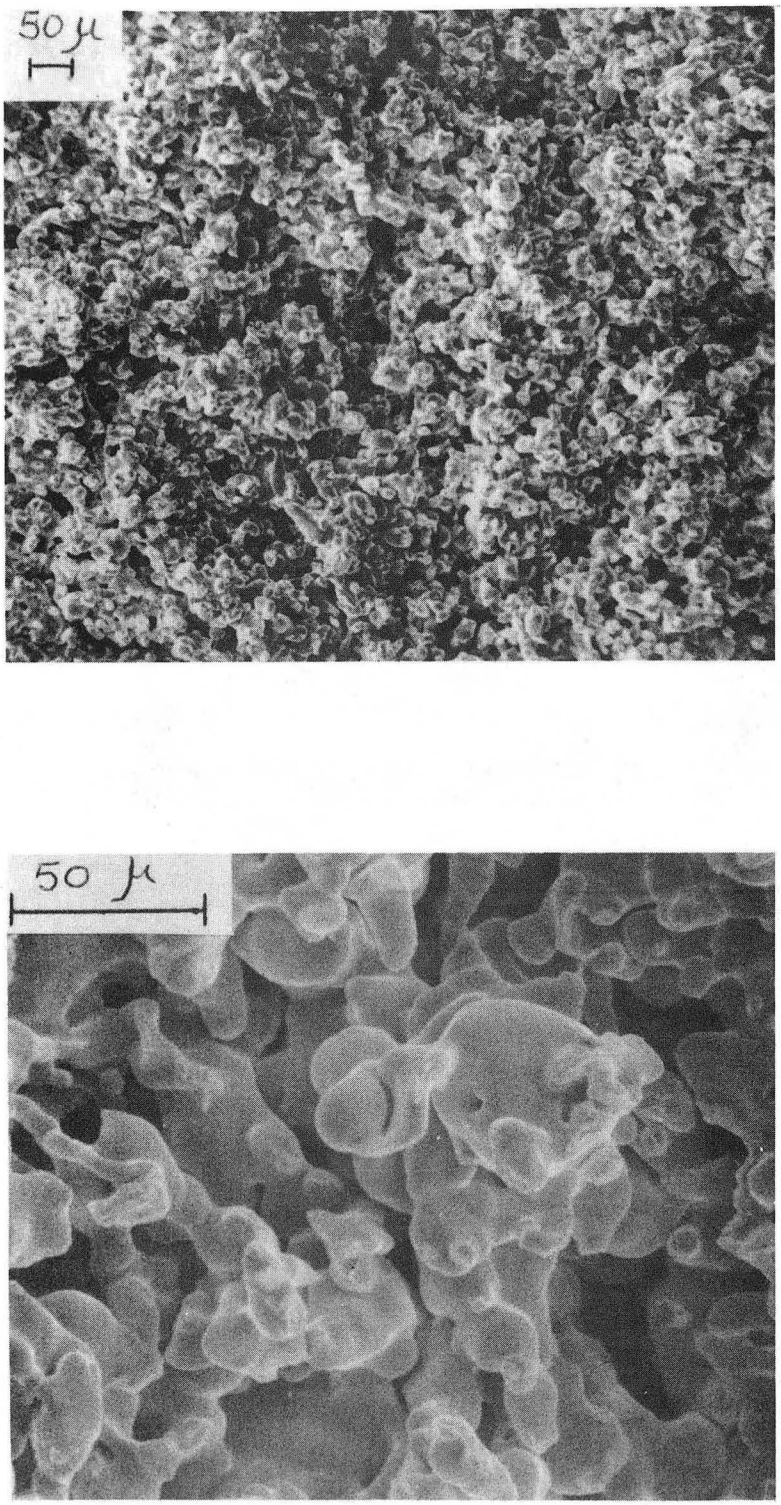

XBB 754-3044

Fig. 3.1.5. Scanning electron micrograph of sintered stainless steel membrane. Side view.

corresponding power P is given by Equation 3.2.1.

$$P = N \times T \qquad 3.2.1$$

where

P = power, lb-inch/min.

N = rotational speed, min^{-1}

T = torque, lb-inch

Prior to each run the rotor is operated at various r.p.m. in the pressure of air only. This "dry" run is used to measure the torque due to resistance that comes from the two Crane Seals and ball bearings at both ends of the rotor. The "dry" torque is then subtracted from the total torque in order to find the net torque due to the resistance of the water only.

Table 3.2.1 summarizes experimental results obtained for pure water at 25°C. From these data values of friction factor f were calculated using Equation 3.1.3 and the density and viscosity of water at 25°C. Two dimensionless groups are used to correlate data. The Reynold's Number, N_{R_e}, defined by Equation 3.2.2 and the Power number, N_p, defined by Equation 3.2.3.

$$N_{R_e} = \frac{N D_i^2 \rho}{\mu} \qquad 3.2.2$$

where

N_{R_e} = Reynold's Number, dimensionless

N = rotational speed of rotor, min^{-1}

D_i = rotor diameter, ft.

ρ = fluid density, lb./ft^3

μ = fluid viscosity, lb./ft-min

$$N_P = \frac{P\ g_c}{N^3 D_i^5\ \rho} \qquad 3.2.3$$

where

N_P = Power number, dimensionless

P = ungassed power input to the fluid, ft-lb/min

g_c = 32.2 ft/min^2

The calculated results at various R.P.M. are shown in Table 3.2.2.

Figure 3.2.1 is a plot of power input to pure water against the rotational speed of the rotor. This log-log plot gives a slope of 2.95 which is pretty close to the theoretical value of 3, the exponent of rotational speed N as given in Equation 3.1.3.

Figure 3.2.2 shows the calculated values of friction factor f at different Reynolds numbers. The solid and dotted lines show experimental results of Theodorsen and Regier (8) for solid rotating cylinders which have different degrees of surface roughness. This roughness is expressed as grains of 40-mesh sand per square inch of surface area. Our data lie closer to 310 grains/in^2 line. As revealed from Scanning Electron microscope photographs (Fig. 3.1.4) the membrane surface is composed of stainless steel grains of approximately

50 microns. This is pretty close to the 40-mesh size sand grains used by Theodorsen and Regier(8). Although the size of grains in Grade H membrane is pretty close to the cylinder used by Theodorsen and Regier (8), we do not know if the number of grains per square inch is the same in both cases. Nevertheless, the closeness of our data to that of Theodorsen and Regier (8) may suggest that the degree and size of surface roughness may be approximately the same in both cases.

Figure 3.2.3 is a plot of Power number against Reynold's Number. For comparative purposes the results of two different impellers (9) are also shown.

Table 3.2.3 shows experimental results for aerated pure water at 25°C. As shown in Figure 3.2.4, the log-log plot of power against rotational speed gives a slope of 1.60, which is less than the slope of 2.95 obtained for pure water in Figure 3.2.1.

TABLE 3.2.1

Power Consumption in Pure Water

Rotor Speed N (R.P.M.)	Torque, lb-inch)			Power, $P=N\ T_\eta$	
	Total, T	"Dry", T_d	Net, T_η	(lb-inch/min)	(ft-lb/min)
368	20.7	20.1	0.6	203.5	16.96
530	19.5	18.5	1.0	547.2	45.6
740	19.8	18.0	1.8	1,322.4	110.2
950	22.8	19.3	3.5	3,333.6	277.8
1170	21.7	17.5	4.2	4,896.0	408.0
1370	23.0	16.5	6.5	8,904.0	742.0
1560	23.7	15.8	7.9	12,396.0	1,033.0
1870	26.1	12.5	13.6	25,380.0	2,115.0
2,080	26.9	11.0	15.9	33,048.0	2,754.0

Rotor diameter = 2 inch. Rotor length = 10 inches

Membrane = Grade H. Temperature = 25°C

TABLE 3.2.2

Friction Factor in Pure Water

Rotor Speed N (R.P.M.)	Reynold's No. N_{Re}	Friction Factor f	Power No. N_P
368	1.78×10^4	0.020	4.86
530	2.56×10^4	0.018	4.37
740	3.57×10^4	0.016	3.89
950	4.58×10^4	0.019	4.63
1170	5.65×10^4	0.015	3.65
1370	6.61×10^4	0.017	4.07
1560	7.53×10^4	0.016	3.89
1870	9.03×10^4	0.019	4.62
2,080	10.03×10^4	0.018	4.37

TABLE 3.2.3

Power Consumption in Aerated Water

Rotor Speed N (R.P.M.)	Torque, lb-inch			Power, $P=N\ T_\eta$	
	Total, T	"Dry," T_d	Net, T_η	(lb-inch/min)	(ft-lb/min)
393	16.5	15.2	1.3	512	42.7
507	16.2	14.8	1.4	706	58.8
730	16.8	14.7	2.1	1,509	125.8
930	16.3	14.1	2.2	2,030	169.2
1140	16.0	13.7	2.3	2,604	217.0
1375	16.9	14.3	2.6	3,515	292.9
2,100	20.5	18.1	2.4	4,908	409.0

Rotor diameter = 2 inch. Rotor length = 10 inch

Air flow rate = 13.2 Std. lit/hr. Temp. = 25°C

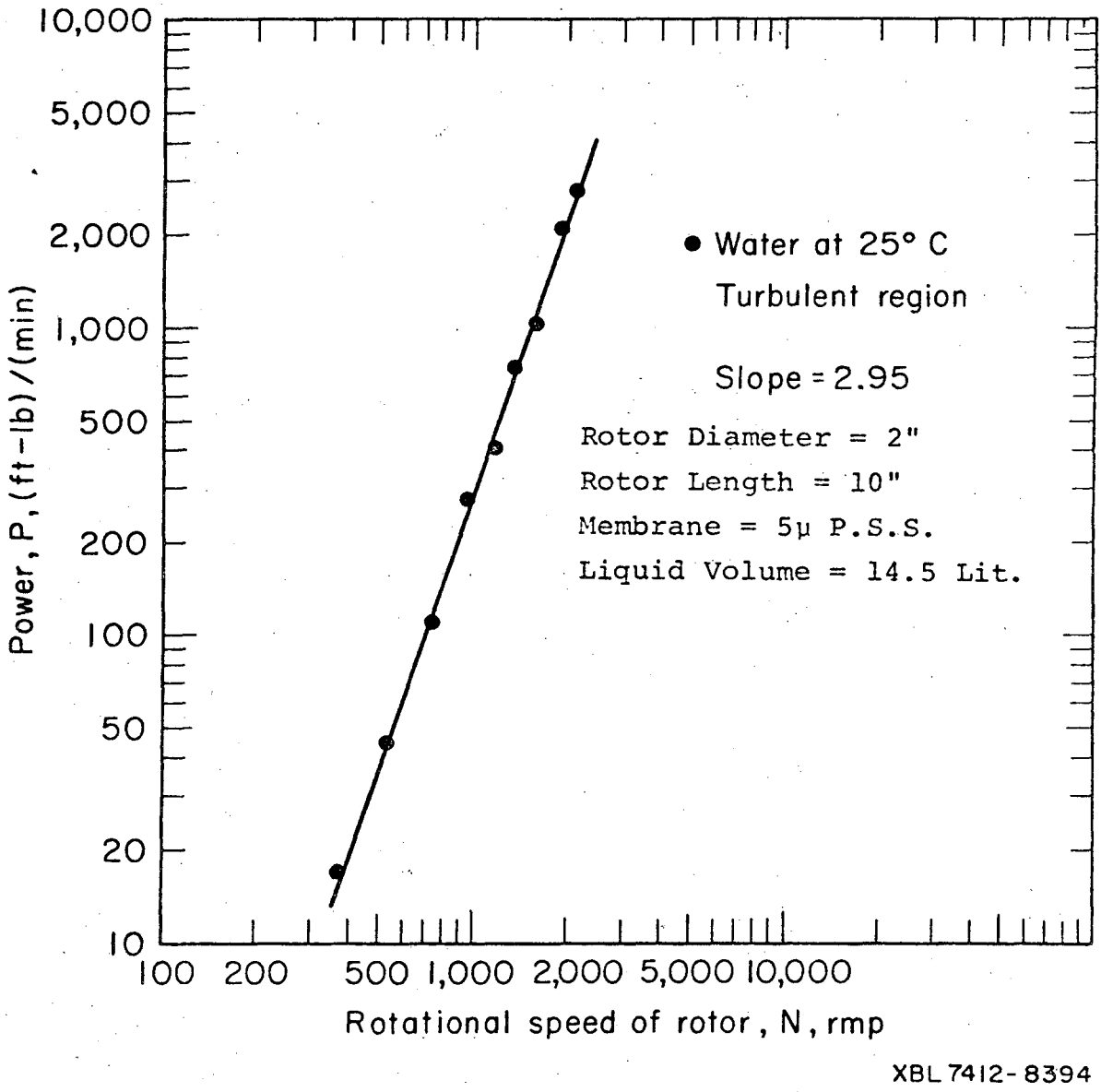

Fig. 3.2.1. Power consumption in pure water by the 2-inch diameter stainless steel membrane, Grade H.

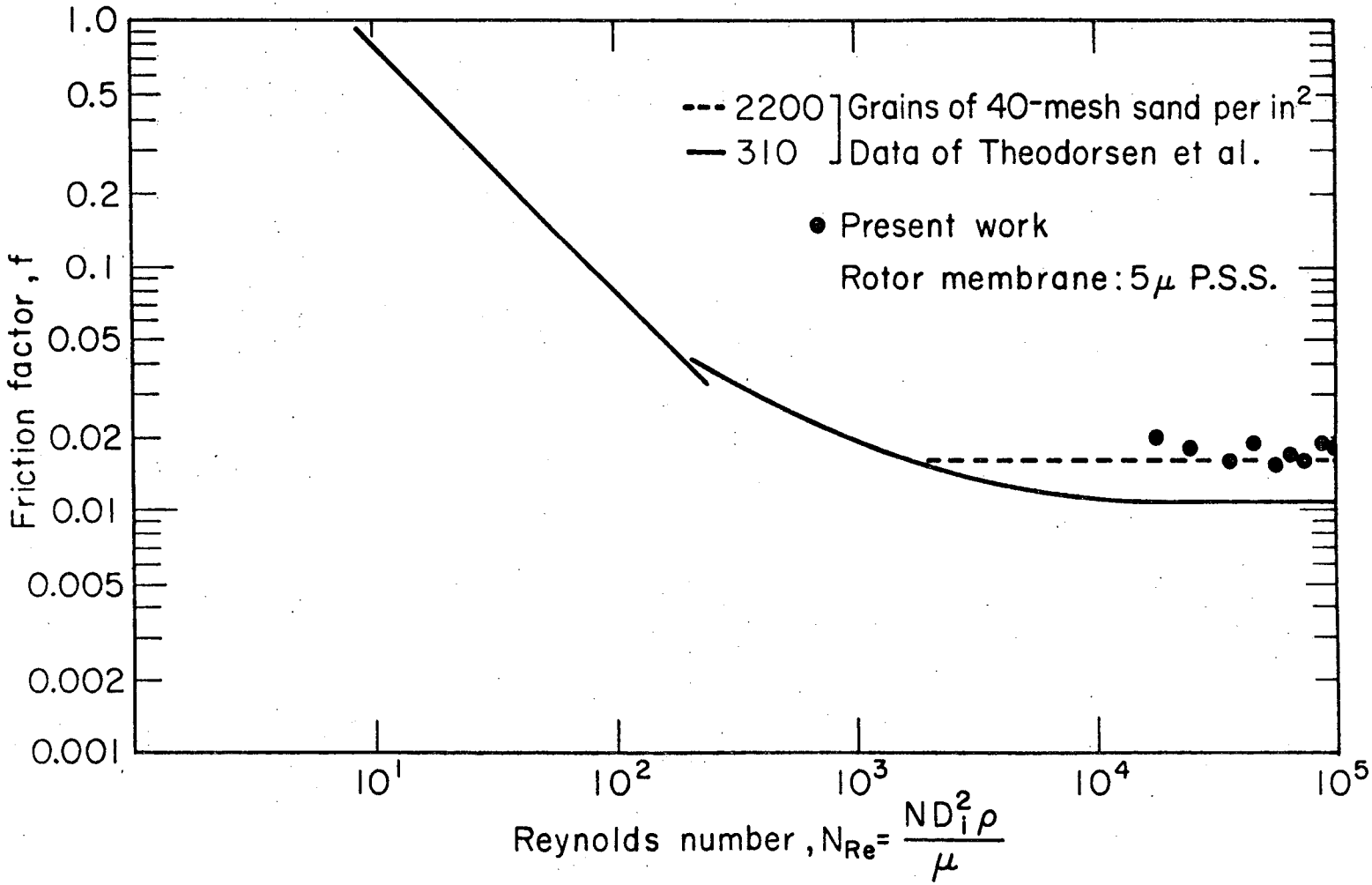

Fig. 3.2.2. Friction factor of rotating Grade H membrane. XBL 7412-8402

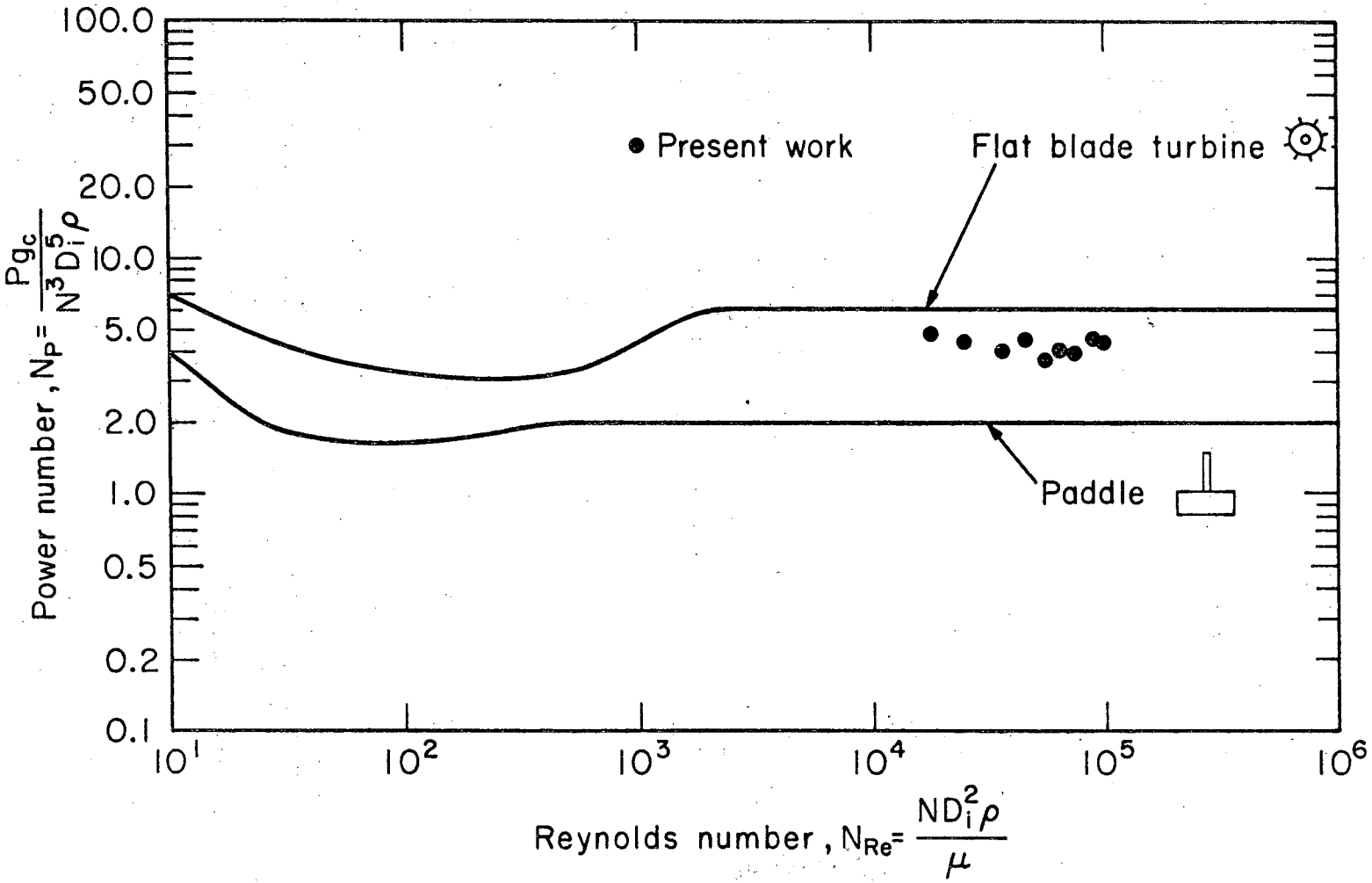

Fig. 3.2.3. Power number against Reynold's number. XBL 7412-8403

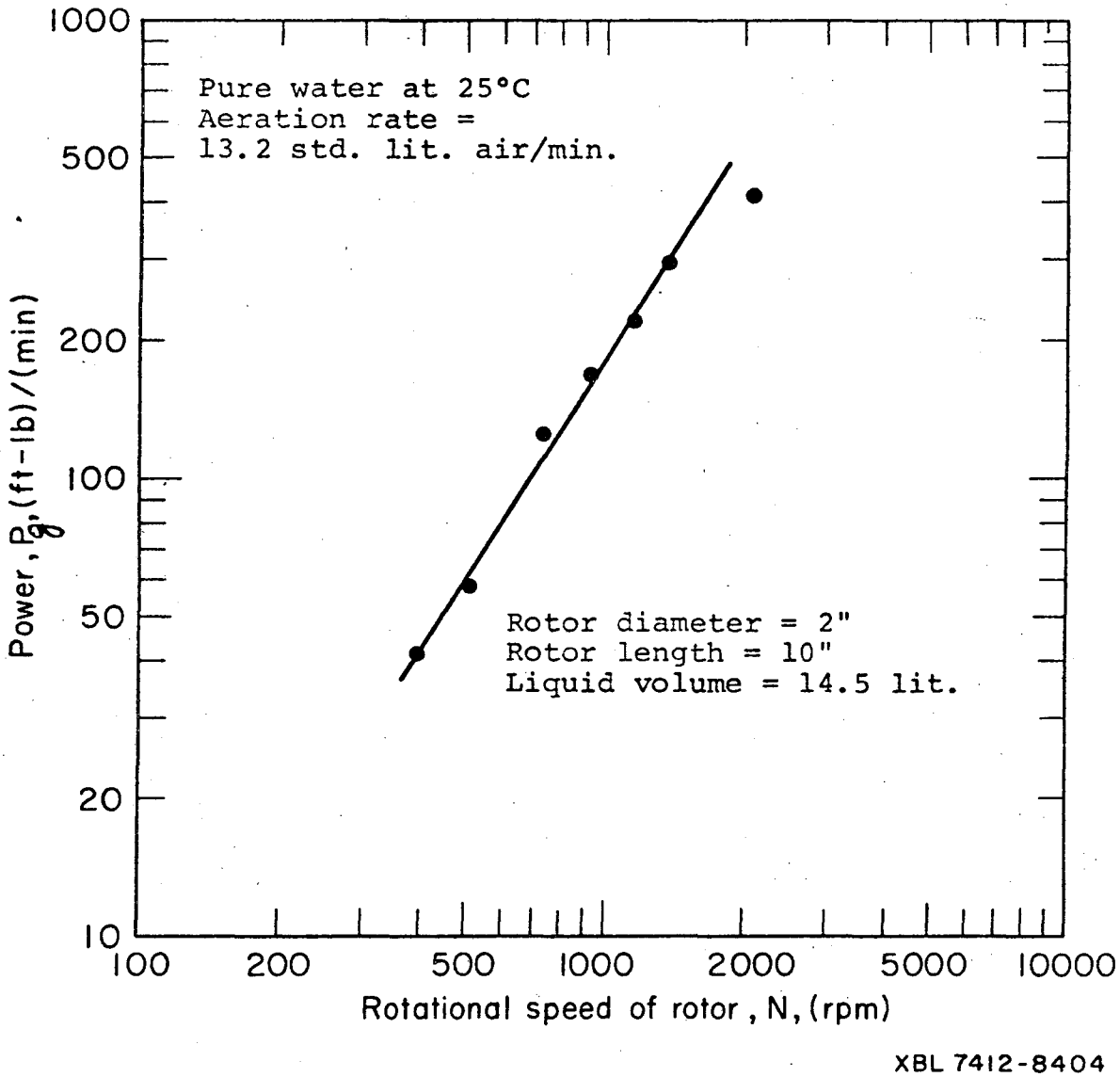

Fig. 3.2.4. Power consumption in aerated water.

References Cited in Chapter III

1. Schlicting, H., Boundary Layer Theory, McGraw-Hill Book Co., Inc., New York, 1960.

2. Chandrasekhar, S., The Stability of Viscous Flow Between Rotating Cylinders, Proc. Royal Soc., (London), A246, 301-311 (1958).

3. Donnely, R. J., and N. J. Simon, An Empirical Torque Relation for Supercritical Flow Between Rotating Cylinders, J. Fluid Mechanics, 7, 401-416 (1960).

4. Batchelor, G. K., A Theoretical Model of the Flow at Speeds Far Above the Critical, J. Fluid Mechanics, 7, 416-418 (1960).

5. Von Karman, T., Trans. Amer. Soc. Mech. Eng., 61, 705 (1939).

6. Sortland, L. D., and C. R. Wilke, Kinetics of a Dense Culture Fermentation, Lawrence Radiation Lab. Report, UCRL-18340 (1968).

7. Sortland, L. C., and C. R. Wilke, Growth of Streptococcus faecalis in Dense Culture, Biotech., Bioeng., 11, 805-841 (1969).

8. Theodorsen, T., and A. Regier, Experiments on Drag of Revolving Discs, Cylinders and Streamline Rod at High Speeds, NACA Report No. 793, pp. 367-384 (1945).

9. Aiba, S., Humphrey, A. E., Millis, N. F., Biochemical Engineering, Academic Press, Inc., New York, 1973, Second Edition.

CHAPTER IV

MASS TRANSFER CHARACTERISTICS OF THE ROTORFERMENTOR

In many microbial processes where aerobic microorganisms are employed the rate of oxygen supply may be the limiting step determining both the rate of cell mass production and metabolic product yield. When we talk about oxygen limitation we assume that other components in the liquid medium such as carbon or nitrogen source, minerals, vitamins, and other nutrients are not limiting the growth of microorganisms. It is especially important in the case of facultative aerobic microorganisms, which can grow both in the absence or presence of oxygen. In this case, the oxygen level in the liquid phase will affect the type of metabolic pathway and thus the nature and rate of production of metabolic products. Such an example is the production of ethanol by Saccharomyces cerevisiae. Experimental results presented in Section 6.5.3 of this dissertation show that the oxygen concentration in the liquid phase has an appreciable effect on the rate of both cell mass production and ethanol production.

Strohm et al. (1) found that frequently the cell yield of microorganisms having high oxygen demand is limited by the rate of oxygen supply provided other

nutrients are not limiting.

The principle of achieving high cell densities by filtration through a rotating microporous membrane has been used by Sortland (2) in the anaerobic fermentation of glucose to lactic acid by Streptococcus faecalis. In that case, there were no oxygen limitation problems and therefore no aeration was needed.

An attempt is being made in the present study to extend the use of the dense cell culture filtration technique to aerobic systems. As mentioned earlier, some aeration is needed during yeast growth and ethanol production. Because of aeration requirements, it is necessary to characterize the oxygen mass transfer capability of the Rotorfermentor unit. This section describes the method used and experimental results obtained.

4.1 The Volumetric Mass Transfer Coefficient $K_L a$.

During the aeration of a liquid medium in which microorganisms are growing, the oxygen must travel from the air bubbles through the liquid phase and to the microorganism. This overall transfer process consists of a number of steps in series. Each step has a particular resistance to oxygen transfer depending on the system being considered. The first step is the transfer of oxygen from the bulk of dispersed gas phase to the gas-liquid interface. Secondly, a physical equilibrium is established at the gas-liquid interface and transfer of oxygen across any interfacial resistance. The third step in the transfer of oxygen from the gas-liquid interface to the bulk of the liquid phase. The fourth step is the transfer from the bulk of the liquid to the liquid-microorganism interface followed by the fifth step, which is the oxygen transfer through the cell wall and membrane. Once inside the microorganism the oxygen is consumed by a variety of biochemical reactions in the presence of oxidation-reduction enzymes. As in the case of other processes in series, the slowest one is the rate limiting step. Extensive theoretical and experimental investigation has shown that in many cases the transfer of oxygen from the gas-liquid interface to the bulk of the liquid phase (third step) is the overall rate-controlling step.

The overall volumetric mass transfer coefficient for the third step is $K_L a$. This coefficient is used to characterize the mass transfer capability of stirred tank fermentors. Likewise, in our case the mass transfer coefficient $K_L a$ is used to characterize the Rotorfermentor.

A variety of investigators, who studied the absorption of oxygen or other sparingly-soluble gases in stirred tanks, have found that

$$K_L a \propto (P_G/V_L)^n (v_s)^m \qquad 4.1.1$$

where:

$K_L a$ = overall volumetric mass transfer coefficient, $sec.^{-1}$

K_L = overall mass transfer coefficient based on liquid phase concentration difference, cm/sec.

a = interfacial gas-liquid area per unit liquid volume, cm^2/cm^3.

P_G = agitation power input to gassed liquid, $ft\text{-}lb_f/min$.

V_L = volume of gas-free liquid phase, $ft.^3$

v_s = superficial gas velocity based on the cross-sectional area of the tank, cm/sec.

m,n = empirical dimensionless constants.

In addition to power input per unit liquid volume and superficial velocity, some investigators (3,4) found

that $K_L a$ is also affected by the liquid phase viscosity, density, interfacial tension and diffusion coefficient. Recently Robinson and Wilke (5,6) found that the ionic strength of the liquid solution is an important variable which affects $K_L a$.

There are basically two methods of measuring $K_L a$. The first method involves the measurement of dissolved oxygen tension in the aqueous phase in situ, using a probe of the galvanometric type. The theory of the oxygen probe's behavior and its applicability to both steady-state and transient experimental conditions is adequately described by Robinson and Wilke (5) and others (19,20). In this study, the sulphite oxidation method is used. The rate of oxidation of sulphite ion to sulphate with cupric ion as a catalyst is used to determine $K_L a$ (7,8,9,10,13,14,15). Although the physical or chemical properties of sulphite solution do not exactly correspond to those of actual fermentation media these systems have been used to design or scale-up aerobic fermentation processes. Having this in mind the $K_L a$ results presented here should be used as a useful guide that gives a good estimate of the $K_L a$ values one might expect when the actual fermentation medium is used.

The importance of maintaining adequate values of $K_L a$ in a aerobic system is shown in Eq. 4.1.2. For a given microorganism at steady-state conditions, the rate

of supply of oxygen from the gaseous phase to the liquid phase, $K_L a(C_{equ}-C_L)$, is equal to the rate of oxygen consumption by the microorganisms, $Q_{O_2} X$.

$$Q_{O_2} X = K_L a(C_{equ} - C_L) \qquad 4.1.2$$

where:

Q_{O_2} = respiration rate coefficient of microorganism, m moles O_2/hr. gm. cell

X = cell concentration, gm. cell/lit

$K_L a$ = volumetric mass transfer coefficient, $hr.^{-1}$

C_{equ} = equilibrium oxygen concentration at gas-liquid interface, m moles O_2/lit

C_L = oxygen concentration in the bulk of liquid phase, m moles O_2/lit

As shown in Eq. 4.1.2 for a given microorganism that has a respiration rate coefficient Q_{O_2}, the maximum value of $K_L a$ that can be attained will also dictate the maximum value of cell concentration that may be obtained, provided oxygen is the limiting substrate.

4.2. The Sulphite Oxidation Method.

The oxidation of sulphite ion to sulphate is given by Eq. 4.2.1

$$Na_2SO_3 + \frac{1}{2} O_2 \xrightarrow{Cu^{++}} Na_2SO_4 \qquad 4.2.1$$

Srivastava, McMillan and Harris (17) found the sulphite oxidation reaction to be first order with respect to oxygen but zero order with respect to sulphite concentration in the range 0.08 to 0.16 M. Also Fuller and Crist (18) and Cooper et al. (7) found that the rate of oxygen absorption was independent of the concentration of sulphite ion above a minimum value of 0.08 M to 0.17 M. In the present study the concentration of sulphite ion used at the start of reaction is 0.5 M. In this case oxygen absorption from the gaseous phase to liquid phase is followed by chemical reaction with $SO_3^{=}$ according to Eq. 4.2.1. Depending upon the relative magnitude of the chemical reaction rate and the physical mass transfer rate, the presence of a chemical reaction may affect the overall absorption rate capability of the system in different ways. Those systems have been classified to different reaction regimes as for example has been done by Astarita (11) and Danckwerts and Sharma (12). Astarita distinguishes four such regimes as the chemical reaction rate increases, i.e. the kinetic, diffusional, fast reaction, and instantaneous reaction regimes. The rate of absorption with chemical

reaction in the sulphite oxidation system has been found to occur in the near-fast reaction regime (7,13, 14). Cooper et al. (7) who first used the sulphite oxidation method and Phillips and Johnson (14) found that the rate of oxygen absorption with reaction was proportional to the oxygen partial pressure in the gas phase. Because oxygen is a sparingly soluble gas and the chemical reaction rate is fast, the concentration of oxygen in the bulk of liquid phase C_L is essentially zero. Furthermore, we assume that the fermentor is well-mixed so that the equilibrium oxygen concentration at the gas-liquid interface C_{equ} is in equilibrium with the air stream leaving the fermentor. Under those assumptions we set up an oxygen mass balance at steady-state conditions. The rate of oxygen transfer from the gas-liquid interface to the bulk of the liquid is given by Eq. 4.2.2

$$Q = K_L a (C_{equ} - C_L) \qquad 4.2.2$$

where:

Q = rate of oxygen absorption, $\frac{\text{moles } O_2 \text{ absorbed}}{\text{lit. hr.}}$

$K_L a$ = volumetric mass transfer coefficient, hr.^{-1}

C_{equ} = equilibrium oxygen concentration at the gas-liquid interface, moles/lit.

C_L = oxygen concentration in the bulk of liquid phase, moles O_2/lit.

At steady-state the rate of oxygen transfer Q is equal to the rate of oxygen disappearance according to reaction 4.2.1, as measured by the rate of disappearance of sulphite ion $SO_3^{=}$. Therefore, since $C_L \simeq 0$, we have

$$-\frac{1}{2}\frac{\Delta[SO_3^{=}]}{\Delta t} = (K_L a)\ (C_{equ}) \qquad 4.2.3$$

where:

$[SO_3^{=}]$ = concentration of sulphite ion, moles/lit.

t = time, hr.

The equilibrium concentration is given by Henry's Law

$$C_{equ} = \frac{\bar{P}_{out}}{H} \qquad 4.2.4$$

where:

$\bar{P}_{out}$ = partial oxygen pressure in the air stream coming out of the fermentor, atm.

H = Henry's constant, atm. lit/mole O_2.

The value of Henry's constant H must be corrected for ionic strength of solution as described by Danckwerts (16).

The partial pressure of oxygen in the outlet air stream may be obtained from an oxygen mass balance and is given by Eq. 4.2.5

$$P_{out} = 0.209 - \frac{QV_L RT}{F_G} \qquad 4.2.5$$

where:

P_{out} = outlet oxygen partial pressure, atm. O_2

0.209 = partial oxygen pressure of inlet air stream, atm. O_2

Q = rate of oxygen absorption, $\frac{\text{moles } O_2}{\text{lit. hr.}}$, defined in Eq. 4.2.2

V_L = volume of liquid solution, lit.

R = 0.0821 lit-atm/mole °K

T = temperature, °K

F_G = volumetric flow rate of air coming in, lit/hr.

Substituting Eqs. 4,2.5 and 4.2.4 into Eq. 4.2.3 and rearranging we have:

$$K_L a = \frac{QH}{[0.209 - \frac{QV_L RT}{F_G}]} \qquad 4.2.6$$

As mentioned earlier the value of Q is determined from the slope of the $[SO_3^{=}]$ versus time t line. The rate of $[SO_3^{=}]$ disappearance with time is measured by the iodometric technique, i.e.

$$Q = \frac{1}{2} \frac{\Delta[SO_3^{=}]}{\Delta t} \qquad 4.2.7$$

Iodometric Technique

The fermentor chamber was filled with 0.5 M Na_2SO_3 solution to which cuprous sulphate was added to give a catalyst concentration of 10^{-3}M $CuSO_4$. Then aeration begins and samples are taken at various time intervals and analyzed for $SO_3^=$ concentration using an iodometric titration.

The iodometric titration consists of the following reaction steps. First 2 ml. of sample are taken from the fermentor and reacted with 40 ml. of 0.1N iodine solution so that all $SO_3^=$ is converted to $SO_4^=$ according to Eq. 4.2.8.

$$Na_2SO_3 + I_2 + H_2O \longrightarrow Na_2SO_4 + 2HI \qquad 4.2.8$$

The excess amount of I_2 left over from reaction 4.2.8 is determined by back titration with sodium thiosulfate according to Eq. 4.2.9.

$$I_2 + 2\ Na_2S_2O_3 \longrightarrow Na_2S_4O_6 + 2\ Na\ I \qquad 4.2.9$$

A starch indicator is used to determine end point of titration. One can relate the amount of tiosulfate titrant used to the concentration of $SO_3^=$ ion in the original sample:

$$[SO_3^=] = 20Y - \frac{Zv}{4} \qquad 4.2.10$$

where:

$[SO_3^{=}]$ = concentration of $SO_3^{=}$ in the sample, moles $SO_3^{=}$/lit.

Y = molarity of I_2 solution, moles I_2/lit. = 0.05M = 0.1N

Z = molarity of thiosulfate solution, moles $S_2O_3^{=}$/lit. = 0.1M

v = volume of thiosulfate titrant used, ml.

Differentiate Eq. 4.2.10 w.r.t. time to get the slope of the line $SO_3^{=}$ versus time.

$$\frac{\Delta[SO_3^{=}]}{\Delta t} = 0 - (0.025)\ \frac{\Delta v}{\Delta t} \qquad 4.2.11$$

One can plot titration data directly, i.e. ml. of thiosulfate used, v, against time, t, and obtain the slope required. Therefore, the rate of absorption, Q, is given by:

$$Q = (0.0125)\ \frac{\Delta v}{\Delta t} \qquad 4.2.12$$

4.3 Experimental Results

There are three sets of experimental runs which correspond to three different modes of operation of the Rotorfermentor. In the first set which includes runs S_2, S_3, S_5 and S_6 the K_La is evaluated for pure bubble aeration. The only mixing is that due to air bubbles coming out of the ring sparger at different air flow rates. The geometry and dimensions of the air sparger have been described in Section 2.2.

The second set includes runs S_7, S_8, S_9 and S_{11} in which we have bubble aeration plus the effect of recycling through the gas-liquid separator, the recycle pump, and back into the Rotorfermentor chamber. In this set of runs we want to assess the contribution of additional mixing through the recycle line to K_La values. These runs act as a guide as to what increases in K_La are expected due to recycling.

The third set includes runs S_{12}, S_{13}, S_{14}, and S_{15}. In this set of experiments we have bubble aeration plus agitation due to the rotation of the 2-inch diameter metallic membrane. Standard size baffles inside the Rotorfermentor chamber prevents vortex formation. In these runs there is no recycling.

The titration results for runs S_2, S_3, S_5 and S_6 are shown in Figure 4.3.1 where the volume of thiosulfate used in titration is plotted against time. The numerical results are shown in Tables A-1, A-2, A-3 and

A-4 Appendix A. From the slope of the straight line and using Equation 4.2.12 we first find the rate of oxygen absorption Q. Then the value of the volumetric mass transfer coefficient $K_L a$ is calculated by using Equation 4.2.6. Values of $K_L a$ along with other pertinent experimental data for bubble aeration are shown in Table 4.3.1.

Figure 4.3.2 is a plot of $K_L a$ against air superficial velocity V_s for bubble aeration.

Figure 4.3.3 shows the titration results for recycle runs S_7, S_8, S_9 and S_{11} and a comparison is made with run S_5 for bubble aeration. All recycle runs were performed at the same aeration rate of 32.4 S.C.F.H. but at different recycle rates. Those recycle rates were controlled by changing the speed of the recycle pump. Run S_{11} was conducted at the same recycle rate as run S_7 but in addition the 2-inch diameter stainless steel membrane was rotated at 1,040 R.P.M. This test run S_{11} would represent the case where we have recycle through the gas-liquid deparator and filtration through the rotating membrane in the Rotorfermentor chamber.

The titration results for runs S_7, S_8, S_9 and S_{11} are shown in Tables A-5 through A-8 in Appendix A.

Table 4.3.2 summarizes the results obtained for recycle runs.

As seen from the results in Table 4.3.2 we have a significant contribution to $K_L a$ values due to additional mixing during recycling.

In the third set of experiments values of $K_L a$ are determined in the Rotorfermentor chamber. Air is introduced through the ring sparger and mixing comes from the 2-inch diameter metallic membrane which is rotated at different speeds. The power input to the gassed liquid comes from the rotating membrane, and there is no recycle. Figure 4.3.4 shows titration results of runs S_{12}, S_{13}, S_{14} and S_{15}. The numerical data for runs S_{12} through S_{15} are shown in Tables A-9 to A-12 in Appendix A. Table 4.3.3 shows summarized results for Rotorfermentor runs at different rotational speeds corresponding to different power inputs.

Figure 4.3.5 is a plot of $K_L a$ against power per unit liquid volume for the Rotorfermentor runs. The linearity of those results in a log-log plot is in agreement with equation 4.1.1.

Table 4.3.1 Bubble Aeration Results

Run No.	Air Flow Rate F_g, (S.C.F.H.)	Superficial Air Velocity, V_s, (cm/sec)	Volumetric Mass Transfer Coeff., K_La, ($hr.^{-1}$)
S_2	23.6	0.368	85.5
S_3	6.3	0.0984	75.5
S_4	32.4	0.507	89.0
S_5	34.0	0.53	89.0

Table 4.3.2 Recycle Runs.

Run No.	Aeration F_g (S.C.F.H.)	Rotor Speed, (R.P.M.)	Recycle Rate, (Lit/Min)	K_La ($hr.^{-1}$)
S_7	32.4	0	9.2	285
S_{11}	32.4	1,040	9.2	348
S_8	32.4	0	2.54	108
S_9	32.4	0	6.57	190
S_5	32.4	0	0	89.0

Table 4.3.3 Rotorfermentor Results

V_L = 13 lit.		V_s = 0.507 cm/sec		Temp. = 25°C
Run No.	Rotor Speed (R.P.M.)	Power per unit volume, P_g/V_L		K_La ($hr.^{-1}$)
		($ft.\text{-}lb./min/ft^3$)	(H.P./1,000 gal)	
S_{12}	500	130.05	0.527	72.5
S_{14}	800	278.1	1.125	95.3
S_{13}	1,000	391.0	1.582	99.8
S_{15}	1,500	707.0	2.863	109.0

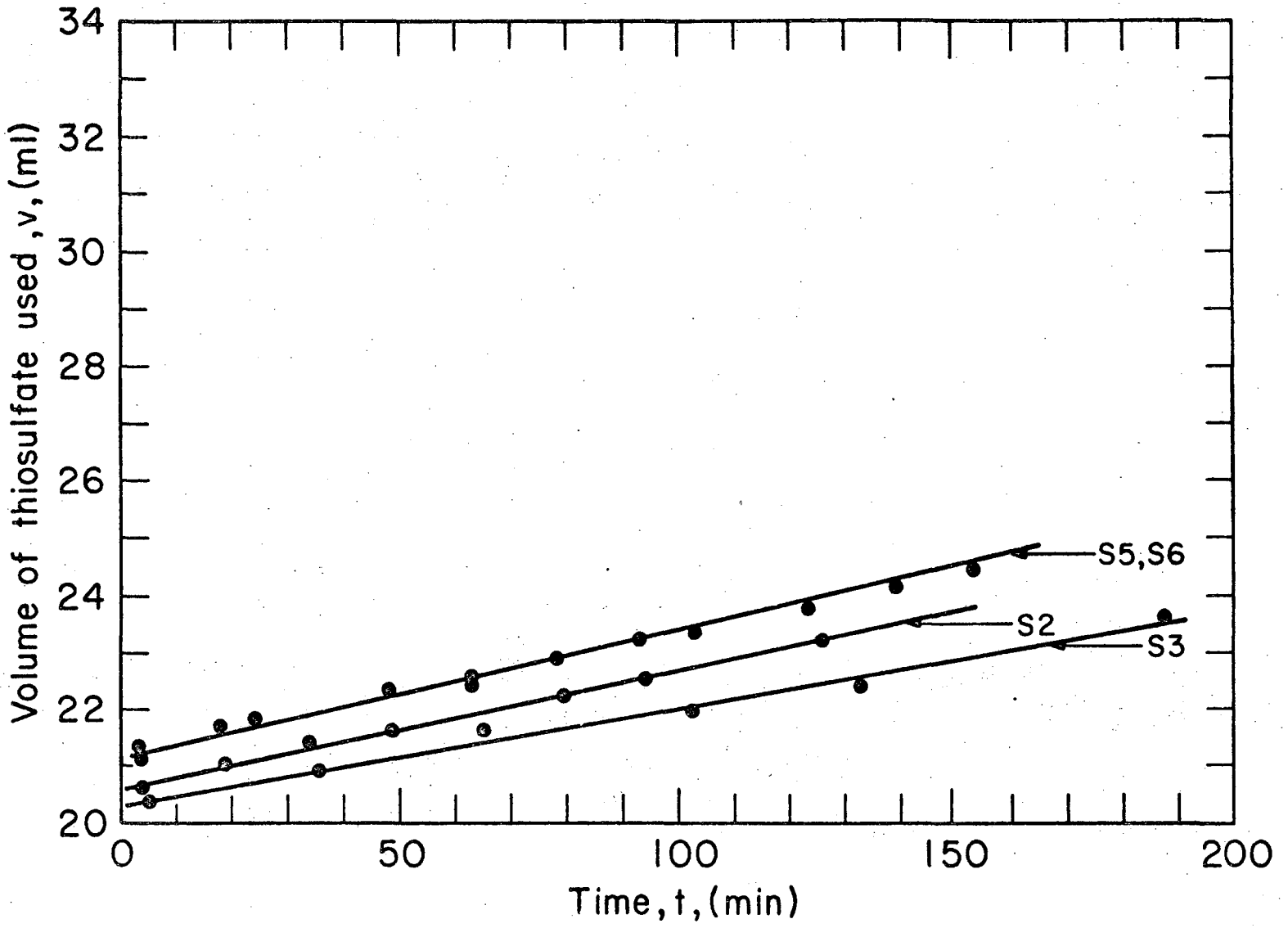

Fig. 4.3.1. Titration results for bubble aeration. Sulphite oxidation method. XBL 7412-8405

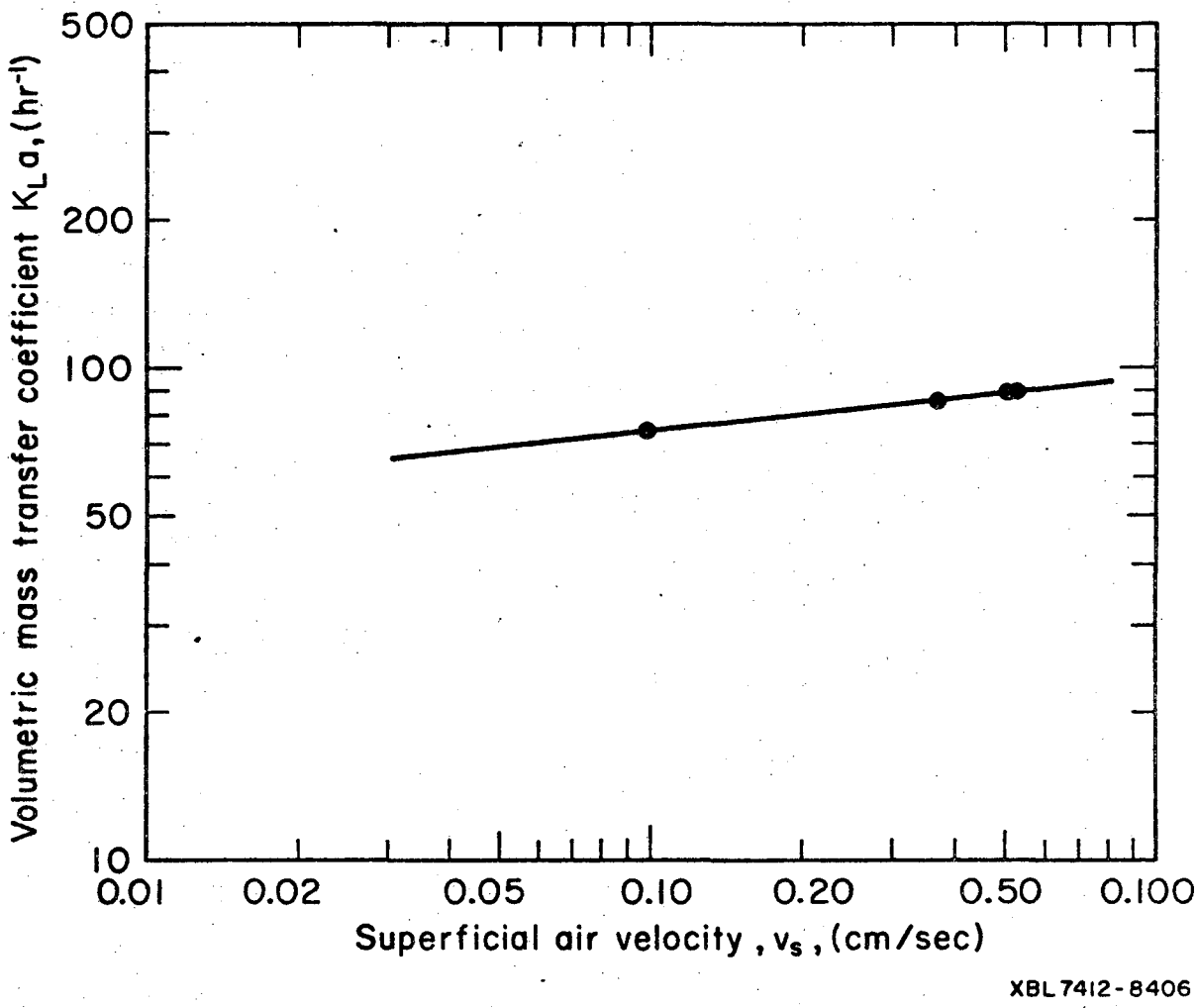

Fig. 4.3.2. Bubble aeration in the Rotorfermentor.

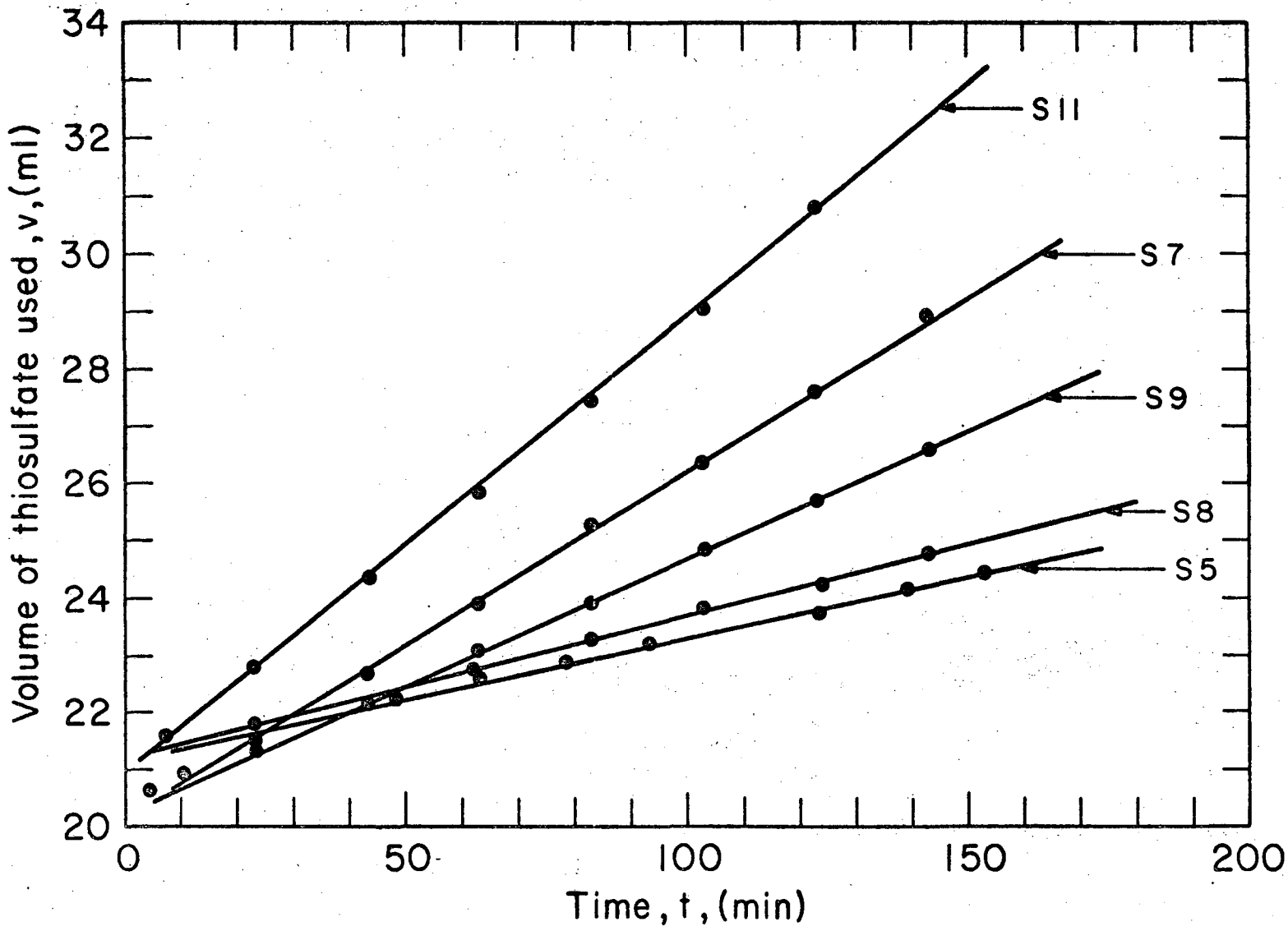

XBL7412-8407

Fig. 4.3.3. Titration results for recycle runs.

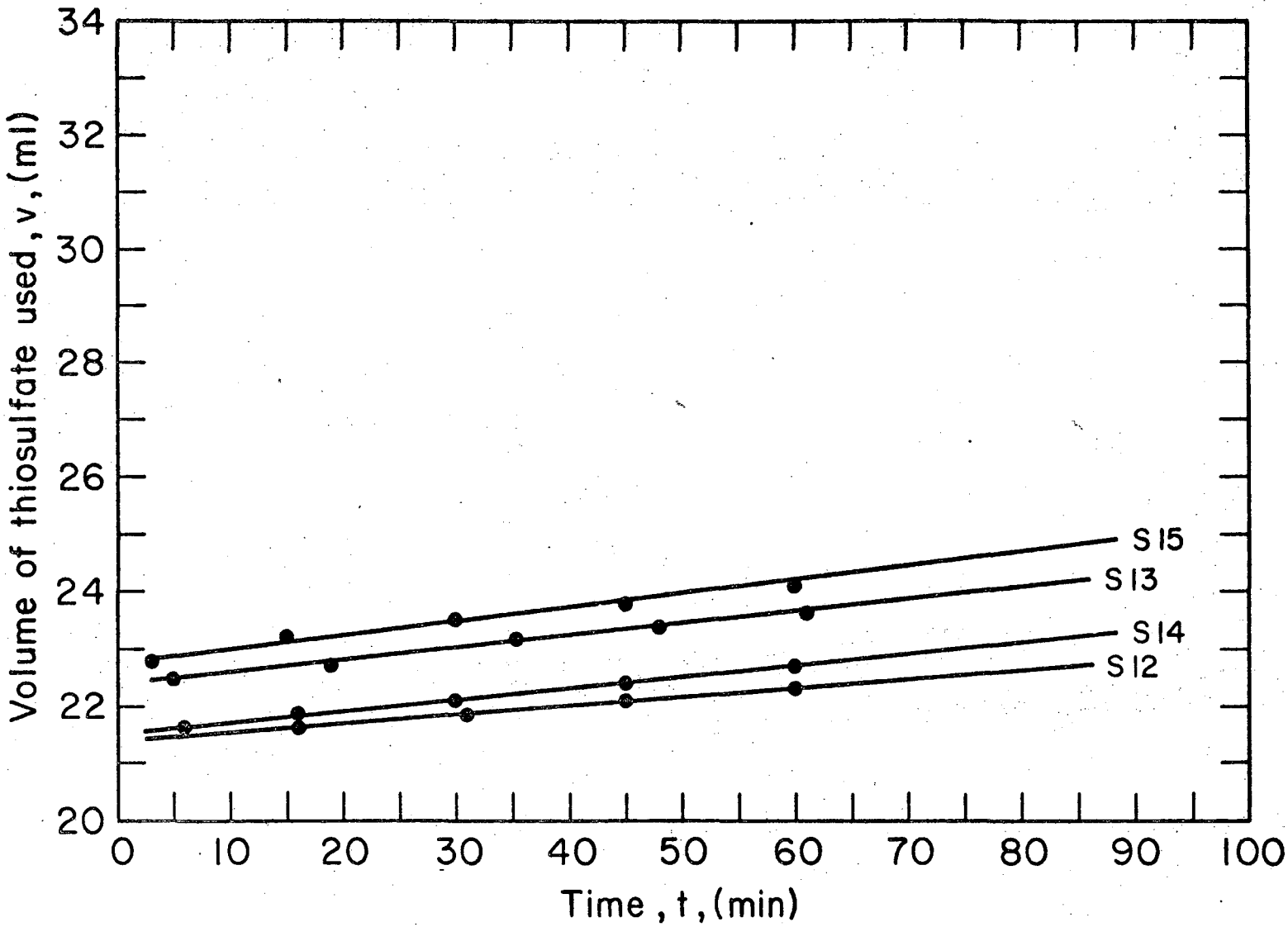

XBL 7412-8408

Fig. 4.3.4. Titration results for Rotorfermentor runs.

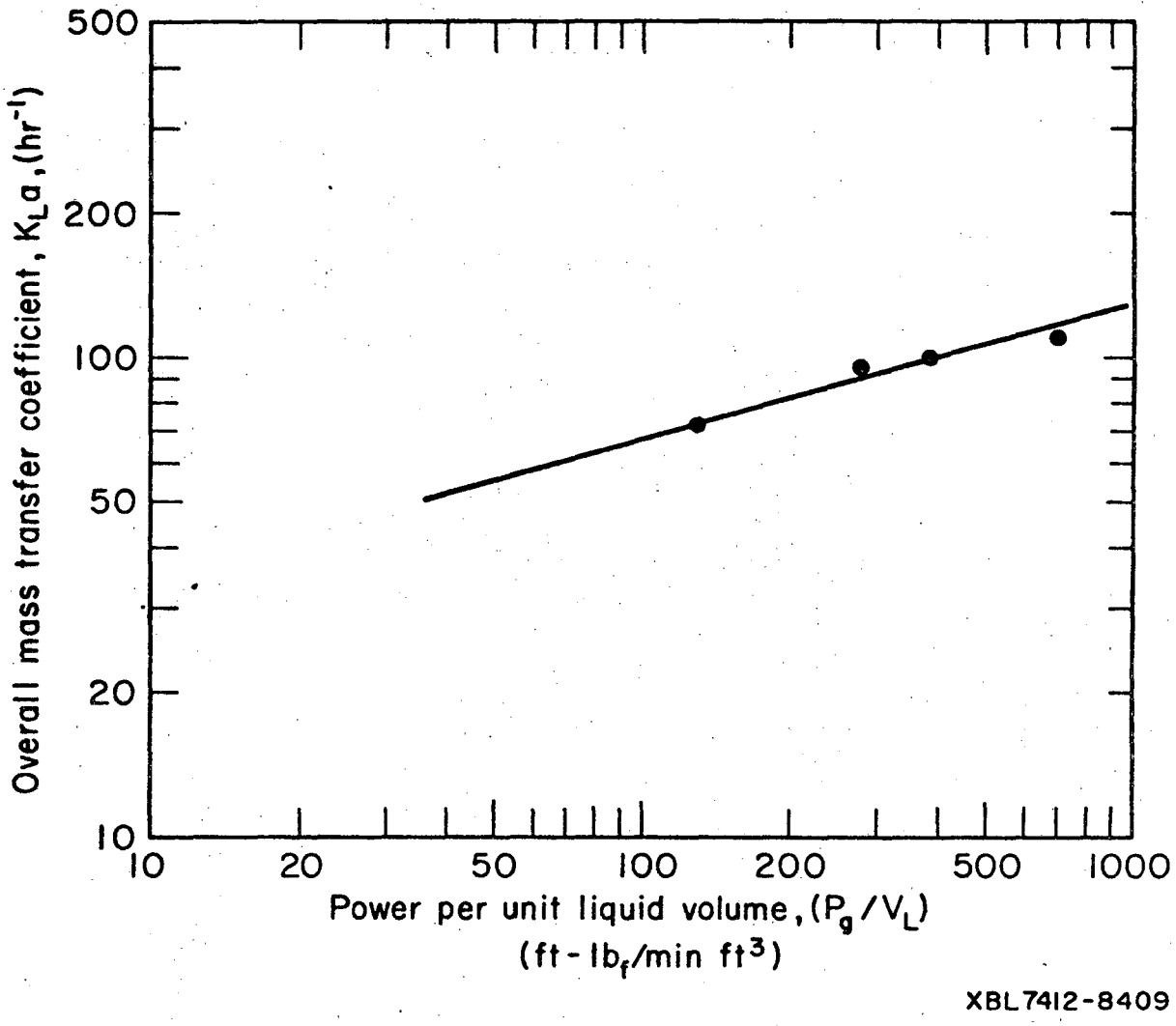

Fig. 4.3.5. Overall oxygen mass transfer coefficient in the Rotorfermentor. V_s = 0.507 cm/sec.

A P P E N D I X- A

Table A-1. Titration Results of Run S_2

V_L = 4.96 lit F_g = 23.6 S.C.F.H. Air. Temp=22° C.

Time	PH	Volume Thiosulfate Used, (ml)
3.2	9.2	20.65
18.4	9.3	21.05
33.4	9.4	21.35
48.4	9.5	21.60
65.1	9.6	21.67
79.3	9.7	22.25
93.5	9.8	22.50
126.2	9.8	23.20

Table A-2 Titration Results of Run S-3

V_L = 5.0 lit F_g = 6.3 S.C.F.H. Temp =22.5° C.

Time (Min)	PH	Volume Thiosulfate Used, (ml.)
5.2	9.0	20.40
35.2	9.1	20.95
65.3	9.2	21.80
102.0	9.2	22.00
132.3	9.4	22.33
187.2	9.5	23.60

Table A-3 Titration Results of Run S-5

V_L = 5.0 lit F_g = 32.4 S.C.F.H. Temp = 22.5° C.

Time	PH	Volume Thiosulfate Used (ml)
3.3	9.0	21.55
23.3	9.1	21.95
63.2	9.4	22.55
83.2	9.6	23.15
103.1	9.7	23.25

Table A-4. Titration Results of Run S-6

V_L = 5.0 lit F_g = 34.0 S.C.F.H. Temp. =22° C.

Time	PH	Volume Thiosulfate Used (ml)
3.3	9.0	21.35
18.1	9.1	2170
48.1	9.3	22.30
63.1	9.4	22.55
78.2	9.5	22.85
93.1	9.6	23.15
123.0	9.7	23.80
139.0	9.7	24.10
153.0	9.7	24.35

Table A-5 Titration Results of Run S-7

V_L=16.0 lit. F_g=32.4 S.C.F.H. Recycle = 3.2 lit/min

Temp.=2.5° C

Time (min)	PH	Volume Thiosulfate Used. (ml)
3.75	8.9	20.8
23.1	9.2	21.55
43.2	9.6	22.65
63.0	9.7	23.90
83.0	9.7	25.20
103.0	9.7	26.30
123.0	9.7	27.60
143.0	9.7	28.90

Table A-6 Titration Results of Run S-8

V_L=16.0 Lit. F_g = 32.4 S.C.F.H. Recycle =2.54 lit/min

Temp = 25.1° C

Time (min)	PH	Volume Thiosulfate Used, (ml)
7.0	9.0	21.60
23.1	9.1	21.80
43.0	9.3	22.25
62.2	9.6	22.75
83.1	9.7	23.25
103.0	9.8	23.88
124.0	9.8	24.20
143.0	9.8	24.80

Table A-7 Titration Results of Run S-9

V_L =16.0 lit. F_g=32.4 S.C.F.H. Recycle =6.57 lit/min
Temp.=25°C.

Time (min)	PH	Volume Thiosulfate Used, (ml.)
10.2	9.3	21.25
23.1	9.6	21.55
43.0	9.8	22.20
63.0	9.8	23.05
83.1	9.8	23.90
103.1	9.8	24.85
122.4	9.8	25.70
143.0	9.8	26.60

Table A-8 Titration Results of Run S-11

V_L=16 lit. F_g=32.4 S.C.F.H. Recycle =9.2 lit/min
Rotor speed =1,040 R.P.M. Temp = 25° C.

Time (min)	PH	Volume Thiosulfate Used, (ml.)
8.0	9.7	21.90
23.1	9.8	22.80
43.1	9.8	24.40
63.1	9.8	25.80
83.1	9.7	27.50
103.0	9.7	29.10
123.0	9.6	30.80

Table A-9 Titration Results of Run S-12

V_L=13 lit. V_s=.507 cm/sec Rotor Speed =500r.p.m.

Temp.=25° C.

Time (min)	PH	Volume Thiosulfate Used (ml.)
16.1	9.2	21.60
31.2	9.4	21.85
45.0	9.5	22.15
60.1	9.7	22.30

Table A-10. Titration Results of Run S-13

V_L=13 lit. V_s=.507 cm/sec. Rotor Speed = 1,000 r.p.m.

Temp.= 25° C.

Time (min)	PH	Volume Thiosulfate Used (ml)
5,0	9.7	22.50
19.1	9.7	22.75
35.3	9.6	23.20
48.1	9.7	23.40
6o.2	9.8	23.65

Table A-11 Titration Results of Run S-14

V_L=13 lit. V_s=0.507 cm/sec. Rotor Speed =800 r.p.m.

Temp.=25° C.

Time (Min)	PH	Volume Thiosulfate Used (ml)
6.30	9.2	21.60
16.0	9.4	21.90
30.0	9.5	22.10
45.1	9.7	22.43
60.1	9.8	22.70

Table A-12 Titration Results of Run S-15

V_L =13 lit. V_s= 0.507 cm/sec. Rotor Speed=1,500 r.p.m.

Temp.=25° C.

Time (min)	PH	Volume Thiosulfate Used (ml)
3.0	9.8	22.80
15.1	9.8	23.20
30.0	9.7	23.50
45.1	9.8	23.80
60.0	9.8	24.10

CHAPTER V

FILTRATION CHARACTERISTICS OF THE ROTATING MEMBRANE

Filtration through the rotating membrane is of extreme importance to the overall performance of the Rotorfermentor since low filtration rates may become the limiting factor in achieving high cell densities. This section covers the theoretical background on filtration. Two modes of filtration are covered, the "centrifugal" filtration where no cake is present due to high centrifugal forces and "cake" filtration where a cake of particles is present on the rotating membrane surface.

Experimental results are presented on yeast filtration using the 2-inch diameter Grade H sintered steel membrane. Also some filtration results are presented on polystyrene particles using a 10% open area Mallory metallic membrane.

5.1 Theory of Filtration.

5.1.1 "Centrifugal" Filtration.

Consider any particle in the boundary layer near the membrane surface moving with a peripheral velocity v at a distance r from the rotor axis. The particle is subjected to a centrifugal force, F_c given by Eq. 5.1.

$$F_c = (m_{eff})\left(\frac{v^2}{r\, g_c}\right) \tag{5.1}$$

where

m_{eff} = effective particle mass, $= \frac{\pi}{6} D_p^{\,3} (\rho_p - \rho)$, for spheres

F_c = centrifugal force, g_f

D_p = particle diameter, cm

ρ_p = particle density, g/cm^3

ρ = density of the fluid, g/cm^3

Substituting for v from Eq. 3.1.2 and rearranging, we get

$$F_c = \left(\frac{\pi}{6} D_p^3 \Delta\rho\right)\left(\frac{v_o^2}{r\, g_c}\right)(1 - ax)^2 \qquad (5.2)$$

where

$\Delta\rho = \rho_p - \rho$

The centrifugal force tends to throw the particle away from the membrane surface. If at the same time there is a filtrate flow radially into the membrane, the particle experiences a drag force, F_D, which tends to carry the particle towards the membrane. The drag force acting on the particle is given by Eq. 5.3.

$$F_D = \left(\frac{C_D}{2g_c}\right)(A_p \rho\, u^2) \qquad (5.3)$$

where

C_D = drag coefficient, a function of the particle Reynold's No. Re_p, and $Re_p = \frac{D_p u}{\nu}$

A_p = projected area of particle in the direction of motion, cm^2 $A_p = \frac{\pi D_p^2}{4}$ for spherical particles

u = radial liquid velocity, cm/sec; also $u = cm^3/sec\ cm^2$, i.e. filtrate flux through the membrane.

For small relatively light particles, as in the case of bacteria, the gravity and buoyancy forces acting are negligible compared with the two dominant forces F_c and F_D. Furthermore, for small values of u, so that $Re_p < 0.03$, we assume viscous flow and Stoke's

Law is applicable.

$$C_D = \frac{24}{Re_p} = \frac{24\mu}{\rho D_p u} \tag{5.4}$$

Substituting Equation 5.4 into Equation 5.3 gives

$$F_D = \left(\frac{3\pi}{g_c}\right)(\mu D_p u) \tag{5.5}$$

From Equations 5.2 and 5.5 we see that for a given set of filtration conditions, the particle size D_p is important since F_c is proportional to D_p^3, while F_D is proportional D_p. For a given particle size and density, F_c can be changed by varying the rotor speed, N., while F_D can be controlled independently through u by changing the pressure inside the fermentation vessel.

Dividing Equation 5.1 by Equation 5.5 and noting that $r = R_o + x \simeq R_o$, since the rotor radius $R_o >> x$, we get Equation 5.6,

$$\frac{F_c}{F_D} = \left(\frac{\Delta\rho}{18\mu u R_o}\right)\left(D_p^2\ v^2\right). \tag{5.6}$$

Figure 5.1.1 shows the interplay between the two forces F_c and F_D as the particle rotates with a linear peripheral velocity v and simultaneously exposed to drag force F_D due to filtrate flux u.

If $F_c > F_D$ at the membrane surface, i.e. $x = 0$, particles in the liquid will not reach the surface, but rather will reach an equilibrium position at a distance $x = x_{equ}$, where $F_c = F_D$. It is assumed that the particles are carried by the fluid at the same peripheral velocity which varies with distance according to Equation 3.1.2. This mode of operation prevents the particles from touching the membrane surface and thus

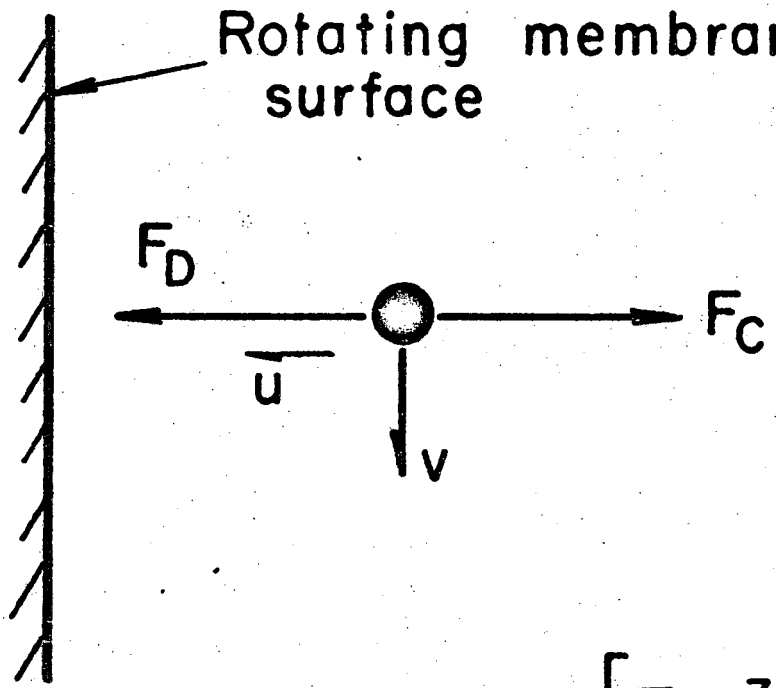

$$F_C = \left[\frac{\pi}{6} D_p^3 (\rho_p - \rho)\right] \left[\frac{v^2}{r g_c}\right]$$

$$F_D = \left(\frac{3\pi\mu}{g_c}\right) (D_p u)$$

XBL718-4139

Fig. 5.1.1. Centrifugal and drag forces on a rotating particle.

prevents cake formation or possible plugging of membrane pores. The higher the F_c/F_D ratio at $x = 0$, the greater the equilibrium distance x_{equ}, and theoretically a clear boundary layer region free of particles could exist adjacent to the membrane surface. In this case it would be possible to use membranes with large pores with corresponding large filtration rates. We shall call this mode of operation "centrifugal" filtration. Equation 5.6 does not include particle to particle interaction and is applicable only to Newtonian fluids. For a given set of values of $\Delta\rho$, μ, R_o, and equilibrium conditions such that $F_c/F_D = 1$, Equation 5.6 can be used to predict theoretical filtration rates, u, at different values of D_p and v. Such a plot of v versus u at different D_p values for the 2-inch rotor is shown in Figure 5.1.2 The theoretical results shown in Figure 5.1.2 are only those for dilute non-interacting particle suspensions. The theoretical equilibrium distance, x_{equ} away from the membrane at which $F_c = F_D$ is determined from the particle's peripheral velocity v using Equation 3.1.2 and also shown in Figure 5.1.2. Therefore, the thickness of the clear boundary layer free of particles will be given by x_{equ} minus the particle radius. Another important assumption to be remembered in interpreting the theoretical results in Figure 5.1.2 is that the particle moves in a viscous boundary layer with a peripheral velocity v which is not affected by the radial filtrate flux u. However, in real dense suspensions of particles there is a particle to particle interaction which may tend to reduce the centrifugal force effects giving lower filtration rates u at a given rotational speed of the membrane.

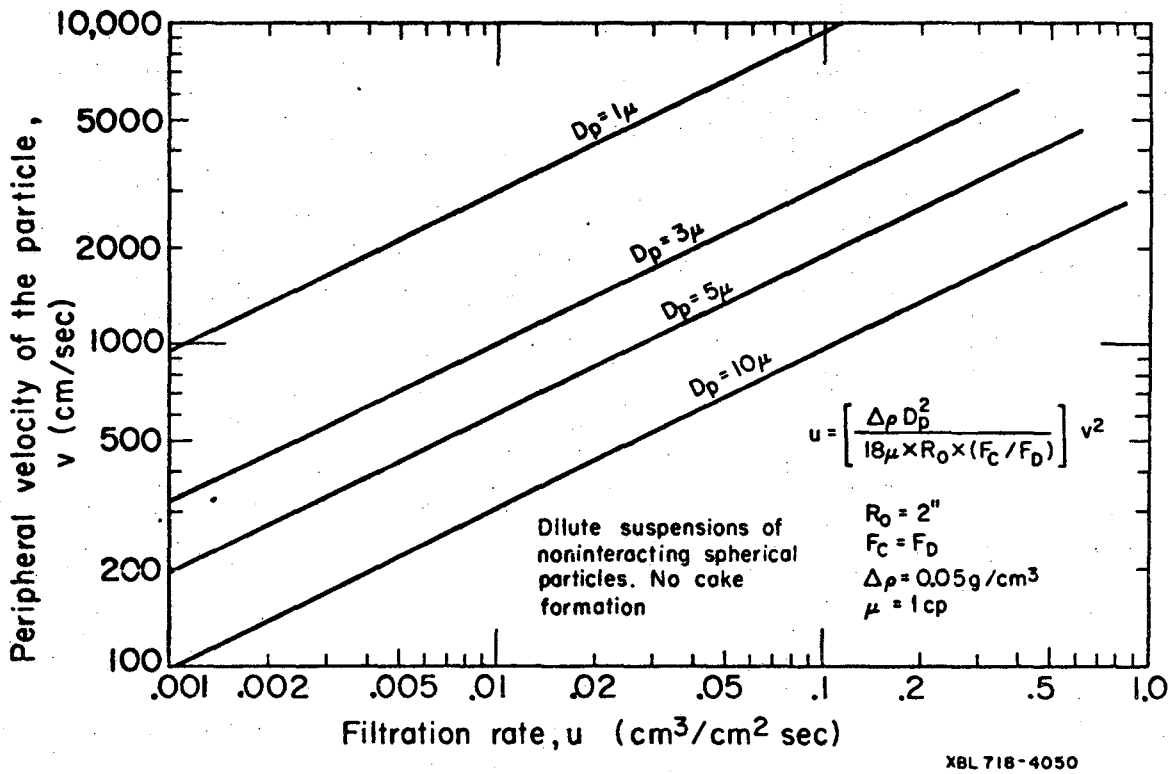

Fig. 5.1.2. Theoretical filtration rates for dilute suspensions without cake formation.

Therefore, when one tries to compare the theoretical filtration rates for "centrifugal" type filtration the idealized assumptions made must be carefully examined. Under those idealized assumptions a maximum filtrate flux u_{max} might be obtained for no cake formation provided

$$F_D \leq F_c \tag{5.7}$$

$$\text{or } \frac{3\pi}{g_c} \mu D_p u_{max} \leq \frac{\pi}{6} D_p^3 \Delta\rho \frac{v_o^2}{rg_c} (1 - ax)^2 \tag{5.8}$$

At the membrane surface $x = 0$ and rearranging Equation 5.8, we get

$$u_{max} \leq \frac{\Delta\rho}{18\mu} D_p^2 \frac{2v_o^2}{D_i} \tag{5.9}$$

Introducing the centrifugal factor Z into Equation 5.9, we get

$$u_{max} < \left[\frac{\Delta\rho\ g_c\ D_p^2}{18\mu}\right] Z \tag{5.10}$$

where

$Z = \frac{2v_o^2}{D_i\ g_c}$, dimensionless centrifugal factor

D_i = membrane diameter, cm.

v_o = peripheral velocity of membrane, cm/sec.

$= \pi D_i N$

5.1.2. "Cake" Filtration.

If $F_c < F_D$ at the membrane surface, i.e. $x = 0$, the particles will touch the surface with resultant cake formation, provided the pore size of the membrane is smaller than the particle size so that the particles do not go through. For a given r.p.m. and pressure inside the vessel at the beginning of a steady-state run, the cake thickness will start building up until a constant thickness is achieved. Correspondingly the filtration rate will be high at the beginning and then decrease slowly until it reaches a limiting constant value, u_∞. This type of filtration we shall call "cake" filtration. Bhagat and Wilke (1) developed a model which includes the effects of centrifugal and drag forces as well as the diffusion of particles away from the cake to the bulk of the fluid. This theoretical model is shown in Figure 5.1.3. The convective flux is due to bulk fluid flow through the cake and membrane, the diffusion flux includes both eddy and molecular diffusion and is due to the concentration gradient of particles, and the centrifugal flux is due to contrifugal force. Introducing the centrifugal flux term in the diffusion equation in terms of mass fluxes as proposed by Bird, Stewart, and Lightfoot (2) we have Equation 5.11

$$N_P = c(N_P + N_\ell) - \rho_s(D+\varepsilon)\frac{dc}{dx} + u_t\rho_s c \qquad (5.11)$$

where

N_P = mass flux of particles with respect to fixed coordinates, gm/cm^2 sec.

N_ℓ = mass flux of liquid with respect to fixed coordinates = filtrate mass flux through membrane, gm/cm^2 sec

c = weight fraction of particles, $\frac{\text{gm solids}}{\text{gm suspension}}$

ρ_s = density of suspension, gm/cm^3

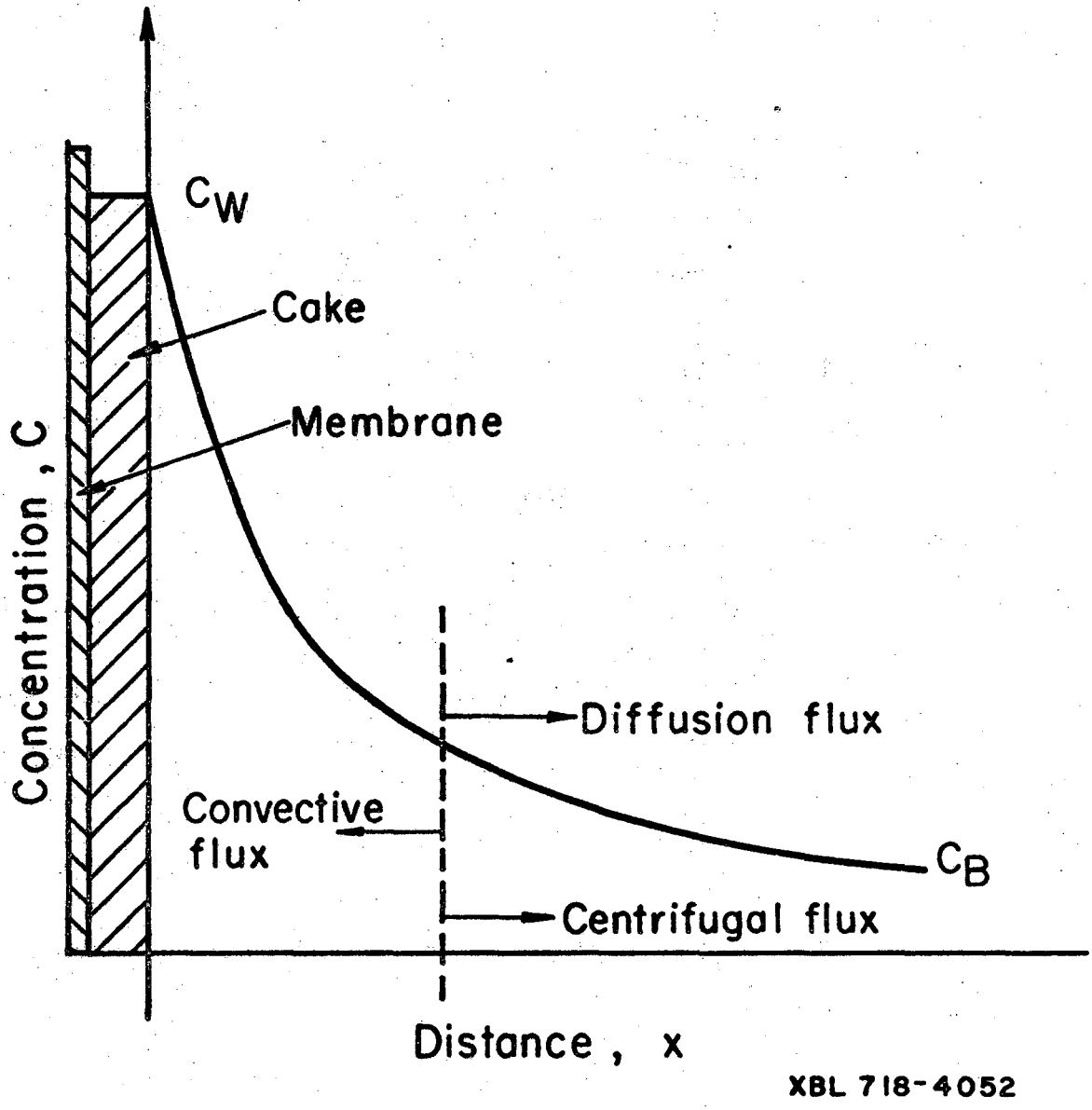

Fig. 5.1.3. Theoretical model for filtration with "cake" formation.

D = molecular diffusivity of particles, cm^2/sec

ε = eddy diffusivity, cm^2/sec

u_t = terminal velocity of particles subjected to centrifugal force, cm/sec

x = distance away from the cake surface, cm.

The first term on the right hand side of Equation 5.11, $c(N_\ell + N_P)$, is the mass flux of particles resulting from the bulk motion of the fluid while the second term is the mass flux of particles resulting from the diffusion superimposed on the bulk flow. The third term is the mass flux of particles resulting from the centrifugal pressure developed by the rotating membrane.

Equation 5.11 gives the relationship between various fluxes from the beginning of filtration up to the time when a constant cake thickness develops on the rotating membrane giving rise to a constant filtrate flux u_∞. When the limiting filtrate flux u_∞ is reached then there is no more net transport of particles towards the membrane surface and a steady-state is established. This means that there is no net flux of particles across any plane parallel to the membrane surface. Under those steady-state conditions, the net particle flux $N_P = 0$, and the convective flux due to pressure drop across the membrane must equal to diffusion flux due to concentration gradient plus the centrifugal flux due to centrifugal pressure.

$$N_\ell c = \rho_s (D+\varepsilon) \frac{dc}{dx} + u_t \rho_s c \qquad (5.12)$$

rearranging we get

$$(D+\varepsilon) \frac{dc}{dx} = c\left(u_t - \frac{N_\ell}{\rho_s}\right) \qquad (5.13)$$

The liquid flux N_ℓ is given by

$$N_\ell = \rho u \tag{5.14}$$

where

ρ = liquid density, gm/cm^3

u = liquid linear velocity, the same as volumetric filtrate flux, cm/sec or cm^3/cm^2 sec.

Substitute Equation 5.14 into Equation 5.13 and rearranging we have

$$-(D+\varepsilon)\frac{dc}{dx} = c\left(\frac{\rho}{\rho_s}u - u_t\right) \tag{5.15}$$

In order to integrate Equation 5.15 we need to express the terminal velocity u_t and eddy diffusivity, ε, as functions of distance x and can estimate the molecular diffusivity D for large spherical particles by the Stokes-Einstein equation as recommended by Wilke and Chang (3). We further assume that the volumetric filtrate flux, u, is essentially constant throughout the thickness, x, of the boundary layer next to the cake surface. This is a good assumption because the flux area through which the filtrate must flow does not change significantly within the boundary layer thickness. Furthermore we assume that the particle acquires its terminal velocity u_t at any position x instantaneously.

The terminal velocity of the particle due to centrifugal force at any distance x is given by Equation 5.16

$$u_t = \frac{\Delta\rho\, g_c\, D_P^2}{18\mu}\; Z\,(1-ax)^2 \tag{5.16}$$

Since at the cake surface x = 0 then

$$u_{t_o} = \frac{\Delta\rho\, g_c D_p^2}{18\mu}\, z \qquad (5.17)$$

and at any distance, x, we have

$$u_t = u_{t_o}\,(1-ax)^2 \qquad (5.18)$$

A large number of empirical equations have been proposed which correlate the eddy diffusivity, ε, with distance, x, in the turbulent boundary layer. However, all of those correlations deal with turbulent flow in pipes. No work has been reported on eddy diffusivity for turbulent flow in rotating cylinders. We assume that near the membrane surface the "curvature" of the membrane is negligible and can approximate flow conditions to those past a pipe wall. Wasan, Tien, and Wilke (4) developed a correlation for eddy diffusivity for mass and heat transfer in pipes. Thus correlation is given by Equation 5.19.

$$\frac{\varepsilon}{\gamma} = \frac{4.16 \times 10^{-4}\, x^{+3} - 15.15 \times 10^{-6}\, x^{+4}}{1 - 4.16 \times 10^{-4}\, x^{+3} + 15.15 \times 10^{-6}\, x^{+4}} \qquad (5.19)$$

for

$$0 \leq x^+ \leq 20$$

where

ε = eddy diffusivity, cm^2/sec

ν = kinematic viscosity, $cm^2/sec = \mu/\rho$

x^+ = dimensionless distance

$$= \left(\frac{\tau_w\, g_c}{\rho}\right)^{1/2} \left(\frac{x}{\nu}\right)$$

τ_w = shear stress at the membrane surface, gm_f/cm^2

For small values of x^+ i.e. $x^+ < 5$, Equation 5.19 can be approximated by Equation 5.20.

$$\frac{\varepsilon}{\nu} = 4.16 \times 10^{-4} x^{+3} \tag{5.20}$$

For example for $x^+ = 5$ Equation 5.20 gives a ε/ν value 14.6% less than the value obtained by Equation 5.19. This difference is much less for values $x^+ < 5$. Substituting for x^+ in Equation 5.20 we have

$$\varepsilon = \frac{4.16 \times 10^{-4}}{\nu^2} \left(\frac{\tau_w g_c}{\rho}\right)^{3/2} x^3$$

or

$$\varepsilon = \varepsilon_o x^3 \tag{5.21}$$

As mentioned earlier the molecular diffusivity, D, for large spherical particles can be estimated by using Stokes-Einstein equation in the following form

$$D = \frac{kT}{3\pi\mu D_p} \tag{5.22}$$

where

D = molecular diffusivity, $cm^2/sec.$

k = Boltzman constant = 1.37×10^{-16} engs/°K

T = absolute temperature, °K

μ = liquid viscosity, poise = gm/cm-sec.

D_p = particle diameter, cm.

Rearranging Equation 5.15 we get

$$-\frac{dc}{c} = \left(\frac{\rho u}{\rho_s}\right)\left(\frac{dx}{D + \varepsilon}\right) - \left(\frac{u_t\, dx}{D + \varepsilon}\right) \tag{5.23}$$

Integrate both sides of Equation 5.23

$$-\int\frac{dc}{c} = \left(\frac{\rho u}{\rho_s}\right)\int\frac{dx}{D + \varepsilon} - \int\frac{u_t\, dx}{D + \varepsilon} + b \tag{5.24}$$

Substitute Equation 5.18 into Equation 5.24 to get

$$-\int\frac{dc}{c} = \left(\frac{\rho u}{\rho_s}\right)\int\frac{dx}{D+\varepsilon} - u_{t_o}\int\frac{(1-\alpha x)^2}{D+\varepsilon}\,dx + b \qquad (5.25)$$

Substituting Equation 5.21 into 5.25 and expanding the second term in Equation 5.25, we get

$$-\ell n\ c = \frac{\rho u}{\rho_s\ \varepsilon_o}\int\frac{dx}{\frac{D}{\varepsilon_o}+x^3} - \frac{u_{t_o}}{\varepsilon_o}\left[\int\frac{dx}{\frac{D}{\varepsilon_o}+x^3} - 2\alpha\int\frac{x dx}{\frac{D}{\varepsilon_o}+x^3} + \alpha^2\int\frac{x^2\,dx}{\frac{D}{\varepsilon_o}+x^3}\right] + b \qquad (5.26)$$

Let

$$\frac{D}{\varepsilon_o} = B^3$$

Then substituting for the proper integrals (4) we get Equation 5.27

$$-\ell n\ C = \frac{\frac{u\rho}{\rho_s} - u_{t_o}}{\varepsilon_o}\left[\frac{1}{6B^2}\ \ell n\ \frac{(B+x)^2}{B^2 - Bx + x^2}\right.$$
$$\left. + \frac{1}{B^2\sqrt{3}}\ \tan^{-1}\ \frac{2x - B}{B\sqrt{3}}\right] + \frac{2\alpha u_{t_o}}{\varepsilon_o}\left[\frac{1}{6B}\ \ell n\ \frac{B^2 - Bx + x^2}{(B+x)^2}\right.$$
$$\left. + \frac{1}{B\sqrt{3}}\ \tan^{-1}\ \frac{2x - B}{B\sqrt{3}}\right] - \frac{u_{t_o}}{3\varepsilon_o}\ \ell n(B^3 + x^3) + b \qquad (5.27)$$

In Equation 5.27 the only variables are the concentration of solids c and distance x. In order to evaluate the integration constant b we need two boundary conditions. From Figure 5.1.3 we have

B.C. #1 at $x = 0$ $\quad c = c_w$

B.C. #2 at $x = \delta$ $\quad c = c_B$

Here δ is the boundary layer thickness for mass transfer. There is no available correlation for δ in rotating cylinders. However, an approximation can be made by assuming that $x = \delta$ at $v = \frac{v_o}{2}$. Then from Equation 3.1.2 we get

$$\delta = \frac{1}{2\alpha} \tag{5.28}$$

Applying the boundary conditions we get

$$\ell n \frac{c_w}{c_B} = \frac{\frac{\rho u}{\rho_s} - u_{t_o}}{\varepsilon_o} \left[\frac{1}{6B^2} \ell n \frac{(B+\delta)^2}{B^2 - B\delta + \delta^2} + \frac{1}{B^2\sqrt{3}} \left(\tan^{-1} \frac{2\delta - B}{B\sqrt{3}} - \tan^{-1} \left(\frac{-1}{\sqrt{3}} \right) \right) \right] + \frac{2\alpha u_{t_o}}{\varepsilon_o}$$

$$\left[\frac{1}{6B} \ell n \frac{B^2 - B\delta + \delta^2}{(B+\delta)^2} + \frac{1}{B\sqrt{3}} \left(\tan^{-1} \frac{2\delta - B}{B\sqrt{3}} - \tan^{-1} \left(\frac{-1}{\sqrt{3}} \right) \right) \right]$$

$$- \frac{u_{t_o}}{3\varepsilon_o} \ell n \left(\frac{B^3 + \delta^3}{B^3} \right) \tag{5.29}$$

We can further simplify Equation 5.29 by noting that B is very small compared with δ i.e $B \ll \delta$.

If $B \ll \delta$ then the following terms in the right hand side of Equation 5.29 are further approximated.

$$\ell n \frac{(B+\delta)^2}{B^2 - B\delta + \delta^2} \simeq \ell n \frac{\delta^2}{\delta^2} = 0$$

$$\tan^{-1} \frac{2\delta - B}{B\sqrt{3}} \simeq \tan^{-1} \infty = \frac{\pi}{2}$$

$$\tan^{-1} \left(\frac{-1}{\sqrt{3}} \right) = -\frac{\pi}{6}$$

$$\ell n \frac{B^2 - B\delta + \delta^2}{(B+\delta)^2} \qquad \ell n \frac{\delta^2}{\delta^2} = 0$$

Then Equation 5.29 reduces to Equation 5.30

$$\ell n \frac{c_w}{c_b} = \left(\frac{\frac{\rho u}{\rho_s} - u_{t_o}}{\varepsilon_o}\right)\left(\frac{1}{B^2\sqrt{3}}\right)\left(\frac{2\pi}{3}\right)$$

$$+ \left(\frac{2\alpha\, u_{t_o}}{\varepsilon_o}\right)\left(\frac{1}{B\sqrt{3}}\right)\left(\frac{2\pi}{3}\right) - \frac{u_{t_o}}{3\varepsilon_o}\,\ell n\left(\frac{B^3 + \delta^3}{B^3}\right) \qquad (5.30)$$

In cases where $\rho_s - \rho = \Delta\rho$ is small or in cases of dilute suspensions $\rho/\rho_s \simeq 1.0$. In addition, for most cases second and third terms of the right hand side of Equation 5.30 are much smaller than the first term and can be neglected. Under those conditions Equation 5.30 can be approximated with Equation 5.31.

$$\ell n \frac{c_w}{c_b} = \left(\frac{u - u_{t_o}}{\varepsilon_o}\right)\left(\frac{2\pi}{3\sqrt{3}\, B^2}\right) \qquad (5.31)$$

It must be remembered that Equation 5.31 represents steady-state filtration conditions in the presence of a constant thickness cake at the rotating membrane. The value of u is the steady-state limiting filtrate flux which we shall denote as u_∞. Solving for u in Equation 5.31 we get Equation 5.32.

$$u_\infty = u_{t_o} + \left(\frac{3\sqrt{3}\, B^2\, \varepsilon_o}{2\pi}\right)\left(\ell n \frac{c_w}{c_b}\right) \qquad (5.32)$$

or

$$u_\infty = u_{t_o} + 0.8724\, B^2\, \varepsilon_o\, \ell n \frac{c_w}{c_b}$$

or

$$u_\infty = u_{t_o} + u_D \qquad (5.33)$$

In Equation 5.33 the limiting filtrate flux, u_∞, is made up of two terms the centrifugal term, u_{t_o}, and diffusion term u_D. We can further simplify u_D by substituting for B and ε_o.

$$u_D = (0.8274)\left(\frac{D}{\varepsilon_o}\right)^{2/3} (\varepsilon_o)\ \ln \frac{c_w}{c_b} \qquad \text{or}$$

$$u_D = (0.8274)\ (D)^{2/3}\ (\varepsilon_o)^{1/3}\ \ln \frac{c_w}{c_b} \qquad (5.34)$$

In summary, then, the limiting filtrate flux at steady-state conditions, u_∞, is given by Equation 5.33 while Equations 5.17 and 5.34 give the centrifugal and diffusional filtrate flux components respectively.

5.1.3 Batch Filtration at Constant Pressure and No Membrane Rotation.

In this mode of operation the pressure drop across the cake and membrane is maintained constant at no membrane rotation. The theory and assumptions for constant pressure batch filtration are beyond the scope of this dissertation and are adequately described by McCabe and Smith (5). The purpose of the constant pressure batch runs is to determine the filtration characteristics of the yeast cake and the resistance to filtrate flow by the membrane.

For constant pressure batch filtration, the relationship between the volume of filtrate collected V and time θ is given by Equation 5.35

$$\frac{\Delta\theta}{\Delta V} = K_P V + B \qquad (5.35)$$

where

K_P = slope = $\dfrac{\alpha C \mu}{A^2(-\Delta P)g_c}$

B = intercept = $(R_m \mu)/A(-\Delta P)g_c$

V = volume of filtrate, cm^3

θ = time, sec.

C = mass of solids per unit filtrate volume, gm/cm^3

α = specific cake resistance, cm/gm

μ = viscosity of filtrate, gm/cm-sec.

A = filtration area, cm^2

ΔP = pressure drop across cake and membrane, gm_f/cm^2

R_m = filter medium resistance, cm^{-1}

According to Equation 5.35 when the reciprocal of filtrate rate is plotted against the volume of filtrate a straight line should result that has a slope K_p and intercept B. The specific cake resistance α is given by Equation 5.36

$$\alpha = (K_p A^2 \Delta P \, g_c)/C\mu \tag{5.36}$$

and the filter medium resistance is given by Equation 5.37

$$R_m = (BA\Delta P \, g_c)/\mu \tag{5.37}$$

The total pressure drop across the stationary membrane is equal to the pressure drop across the cake plus the pressure drop across the membrane itself. When the membrane rotates, however, an additional pressure must be overcome which is the centrifugal pressure acting away from the rotating membrane.

The centrifugal pressure drop for the cylindrical membrane is given by Equation 5.38

$$P_c = \frac{\rho \omega^2}{g_c} \int_{r_1}^{r_2} r dr = \frac{\rho}{2g_c} \left(r_2^2 - r_1^2 \right) \omega^2 \tag{5.38}$$

where

P_c = centrifugal pressure, p.s.i.

ω = angular rotor velocity = $2\pi N$

ρ = liquid density, lb./ft^3

r_1 = radius of rotor shaft, ft.

r_2 = radius of membrane, ft.

Note that in our case the difference $r_2 - r_1$ is the annulus width between the solid rotor shaft and the membrane surrounding it. We assume that this annulus is filled with filtrate and that all fluid elements within the annulus have the same angular velocity

ω as that of the rotor.

In our system we have $r_1 = 0.5"$, $r_2 = 1"$, $\rho = 62.3$ lb/ft^3 then substituting those values Equation 5.38 for the 2" rotor becomes

$$P_c = 0.383 \times 10^{-6} N^2 \qquad (5.39)$$

where

P_c = centrifugal pressure, p.s.i.

N = rotational speed, r.p.m.

Therefore, for filtration with membrane rotation one must overcome the centrifugal pressure P_c and the pressure drop across the cake and membrane itself.

5.2. Membrane Selection

In view of the fact that the rotating membrane is exposed to high shear it must be mechanically strong and durable. It must be sterilizable and must have the proper pore size distribution so that no microorganisms may go through and possibly plug the pores. Furthermore, the membrane must give relatively high filtration rates at moderate pressure drops, and must be non-corrosive when exposed to nutrient media. Another important criterion for selection is that the membrane must be economical and readily available.

A variety of membranes has been tested and checked for filtration capacity at various pressure drops. The results are shown in Figure 5.2.1. The filtrate volumetric flux, u, is plotted against pressure drop for pure water at 23°C. The first membrane is made by Mallory Metallurgical Company and has 10% open area made of perforations which are irregularly shaped. Microscopic examination showed that those irregularly shaped perforations have an average size of approximately 250 microns. The membrane is made of 316 stainless steel and it has a thickness of 0.010 inch. This membrane is mechanically stable and gives very high filtration rates, but obviously it cannot be used for filtration of microorganisms that range in size 1 to 5 microns. This membrane could be used in situations where the particle size is more than 250 microns.

The other two membranes, Grade F and Grade H are made by Pall Trinity Micro Corporation. Both are made of sintered porous stainless steel and have 1/16 inch thickness. As shown in Figures 3.1.4 and 3.1.5 the pores are very irregular and there is a high degree of tortuosity across the thickness of the membrane. These pores are the intersticial open space between the sintered stainless stell granules that make up the membrane. The sintering process involves the heating of stainless steel powder made of very small granules at temperatures well above 1,000°C and partial annealing before final cooling. Grade F has an average pore size of 20 microns and Grade H has 5 micron average pore size. As mentioned earlier, scanning electron microscope observation revealed a much wider pore size distribution than that cited for by the manufacturer.

The other two membranes made by Millipore Corporation are Grade WS and WH. These are Microweb filters made of standard cellulose ester Millipore filters reinforced with fine monofilament nylon cloth, which gives added strength to the membrane. They have a thickness of 150 microns. Grade WS has a mean pore size of 3.0 microns with a pore size variation ±0.9 microns. Grade WH has a pore size of 0.45 microns ±0.02 microns, and a porosity of 45%. They are not steam-sterilizable; however, they can be sterilized with

ethylene oxide of U.V. radiation, or by exposure to 75% ethanol solution.

In selecting any of the membranes discussed so far it is important that the particle size is smaller than the pore size of the membrane so that plugging of the pores is minimized.

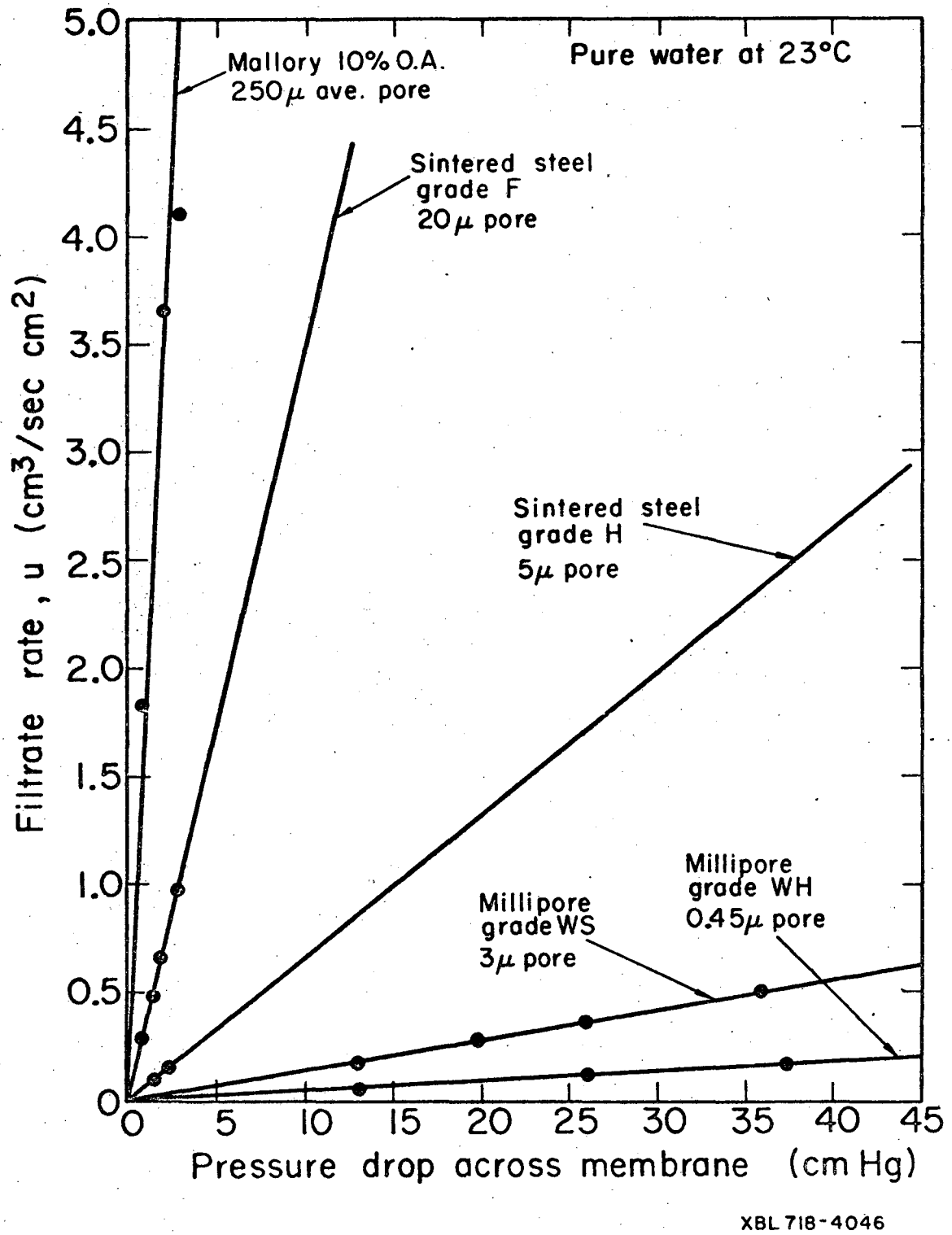

Fig. 5.2.1. Filtration rates for pure water.

5.3 Experimental Results

5.3.1 "Centrifugal" Filtration

In order to check the principle of "centrifugal" filtration as outlined in Section 5.1.1 a test run was performed using a 6-inch diameter rotor to which a Mallory metallic membrane of 10% open area was attached. This membrane is strong and has an average pore size of approximately 250 microns. These pores are fairly large when compared with the polystyrene particles used which have a size range 6 to 14 microns.

In this experiment, 80 liters of dilute suspension of 0.1% solids in water was prepared and charged into the 100 liter capacity supply tank. The solids used are made by Dow Chemical Company and they are uniform spheres of latex made from Styrene Divinyl-benzene copolymer. The 6-inch diameter metallic membrane was rotated at 2,500 r.p.m. and the pressure in the supply tank was adjusted so that a volumetric filtrate flux of 0.047 cm^3/cm^2 sec was achieved through the rotating membrane. In this experiment there was no solids bleed except the bleed of small sized particles that went through the membrane with the filtrate. As a result, there was a net accumulation of solids inside the filtration chamber. A traveling probe was used to take samples at various distances x away from the rotating membrane. The results are shown in Figure 5.3.1. Solids

concentration in the filtrate going through the membrane and inside the filtration chamber are plotted against time. As seen from Figure 5.3.1 the solids concentration in the filtrate is almost constant while that inside the chamber increases linearly with time in accordance with a mass balance equation. The data also show that there was no concentration gradient along distance x (measured in inches) which is an indication of adequate mixing conditions in the annulus between the filtration chamber and the membrane. It is obvious from the results shown in Figure 5.3.1 that since we have particles ranging from 6 to 14 microns the smaller ones are not subjected to high enough centrifugal force and are carried along with the filtrate. The larger particles are subjected to high enough centrifugal forces and therefore retained inside the chamber. Some theoretical calculations are presented in order to show the relative equilibrium position of particles that fall in the size range between 6 to 14 microns.

Figure 5.3.2 is the theoretical Von Karman velocity profile based on experimental conditions of run number 2. We assume that any particle present within the boundary layer will have the same peripheral velocity v as that predicted by the Von Karman velocity profile. We further assume that this peripheral velocity profile is not affected by the radially directed filtrate flux u.

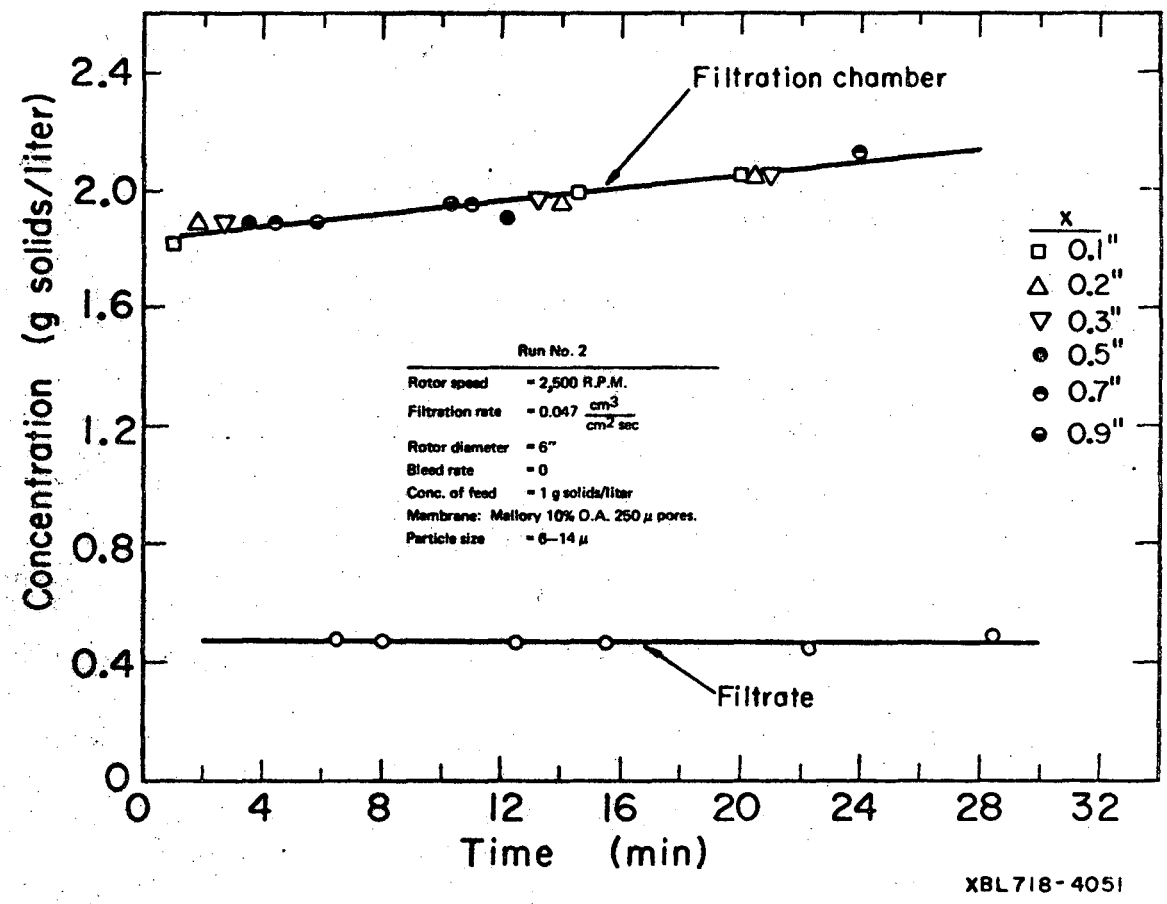

Fig. 5.3.1. Filtration results of dilute polystyrene suspension.

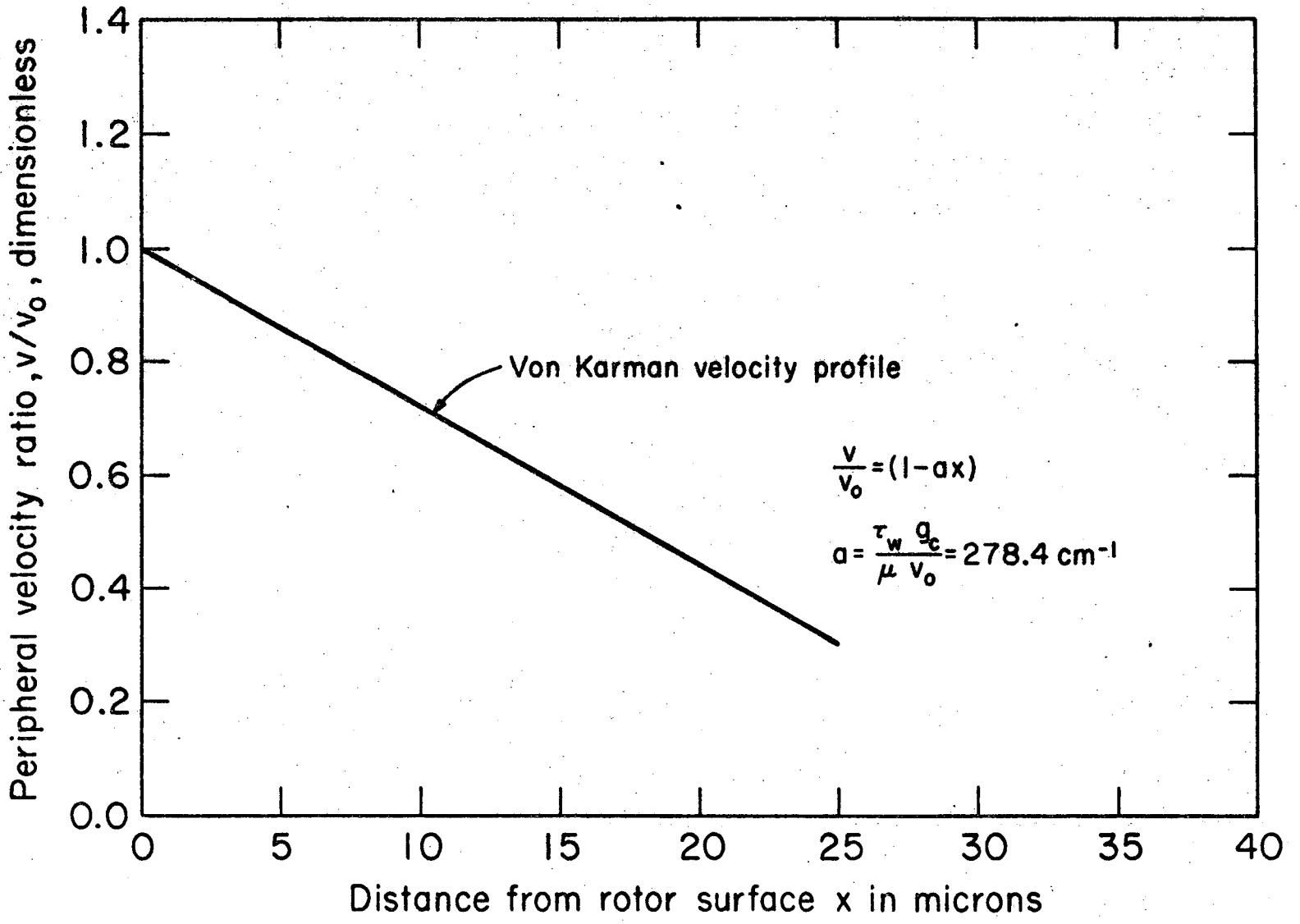

XBL7412-8401

Fig. 5.3.2. Von Karman velocity profile.

To check if turbulent conditions exist in the annulus between the rotating membrane and the filtrate chamber we calculate the Taylor number according to equation 3.1.1

$$T_a = \frac{4}{9} (15.24)^4 \left(\frac{2\pi \times 41.7}{0.9 \times 10^{-2}}\right) = 2.03 \times 10^{13}$$

which is much greater than 3.1×10^4 beyond which turbulence exists.

Then we use equation 5.6 to find the ratio of centrifugal to drag force F_C/F_D at various distances x away from the membrane.

For the experimental conditions of run number 2 we have

$Re = 1.66 \times 10^6$

$f = 0.0025$ for smooth cylinders, taken from Theodorsen and Regier.

$\nu = \mu/\rho = 0.9 \times 10^{-2}$ cm^2/sec.

$D = 15.24$ cm.

$\rho_p = 1.052$ bm/cm^3

$N = 2{,}500$ r.p.m.

$u = 0.047$ cm^3/cm^2 sec.

$\Delta\rho = 0.052$

The shear stress at the wall is given by

$$\tau_w = \left(\frac{f}{2}\right) \left(\frac{v_0^2}{g_c}\right) = \left(\frac{2.5 \times 10^{-3}}{2}\right)$$

$$\left(\frac{1 \times (3.14 \times 15.24 \times 41.7)^2}{980}\right) = 5.1 \text{ gm}_f/\text{cm}^2$$

The term a is given by

$$a = \frac{\tau_w g_c}{\mu v_0} = \frac{5.1 \times 980}{9 \times 10^{-3} \times 3.14 \times 15.24 \cdot 41.7}$$

$$= 278.4 \text{ cm}^{-1}.$$

Then the Von Karman velocity profile becomes

$$v = (1{,}995.5)\ (1 - 278.4x). \qquad 5.40$$

Figure 5.3.2 is a plot of equation 5.40.

The ratio of centrifugal to drag force is given by

$$\frac{F_C}{F_D} = \left[\frac{5.2 \times 10^{-2}}{18 \times 0.009 \times 0.047 \times 7.62}\right]\ [D_p^2 V^2] \quad \text{or}$$

$$\frac{F_C}{F_D} = (0.89817)\ (D_p^2 v^2) \qquad 5.41$$

Table 5.3.1 summarizes calculated theoretical results for F_C/F_D ratios at different distances x away from the rotating membrane and for three particle sizes 6, 10, and 14 microns. In order to find the equilibrium distance x for each particle size we read that x value at which $F_C/F_D = 1$. For each particle size as the distance x increases the F_C/F_D ratio decreases.

Figure 5.3.3 is a schematic drawing that shows the relative particle sizes and corresponding equilibrium

Table 5.3.1 "Centrifugal" Filtration

$X \times 10^4$ (cm)	V/V_0	V (cm/sec)	F_c/F_D Ratio		
			$D_P = 6\mu$	$D_P = 10\mu$	$D_P = 14\mu$
0	1.0	1,996			
2	0.94	1,876	1.14		
4.2	0.88	1,758	1.00		
6	0.83	1,656	0.88	2.46	
8	0.78	1,547	0.77	2.14	4.21
10	0.72	1,437	0.67	1.85	3.63
15	0.58	1,157	0.43	1.20	2.36
16.8	0.53	1,055	0.36	1.00	1.95
20	0.44	878	0.24	0.69	1.36
23	0.36	714	0.16	0.46	1.00
25	0.30	598	0.11	0.33	0.62

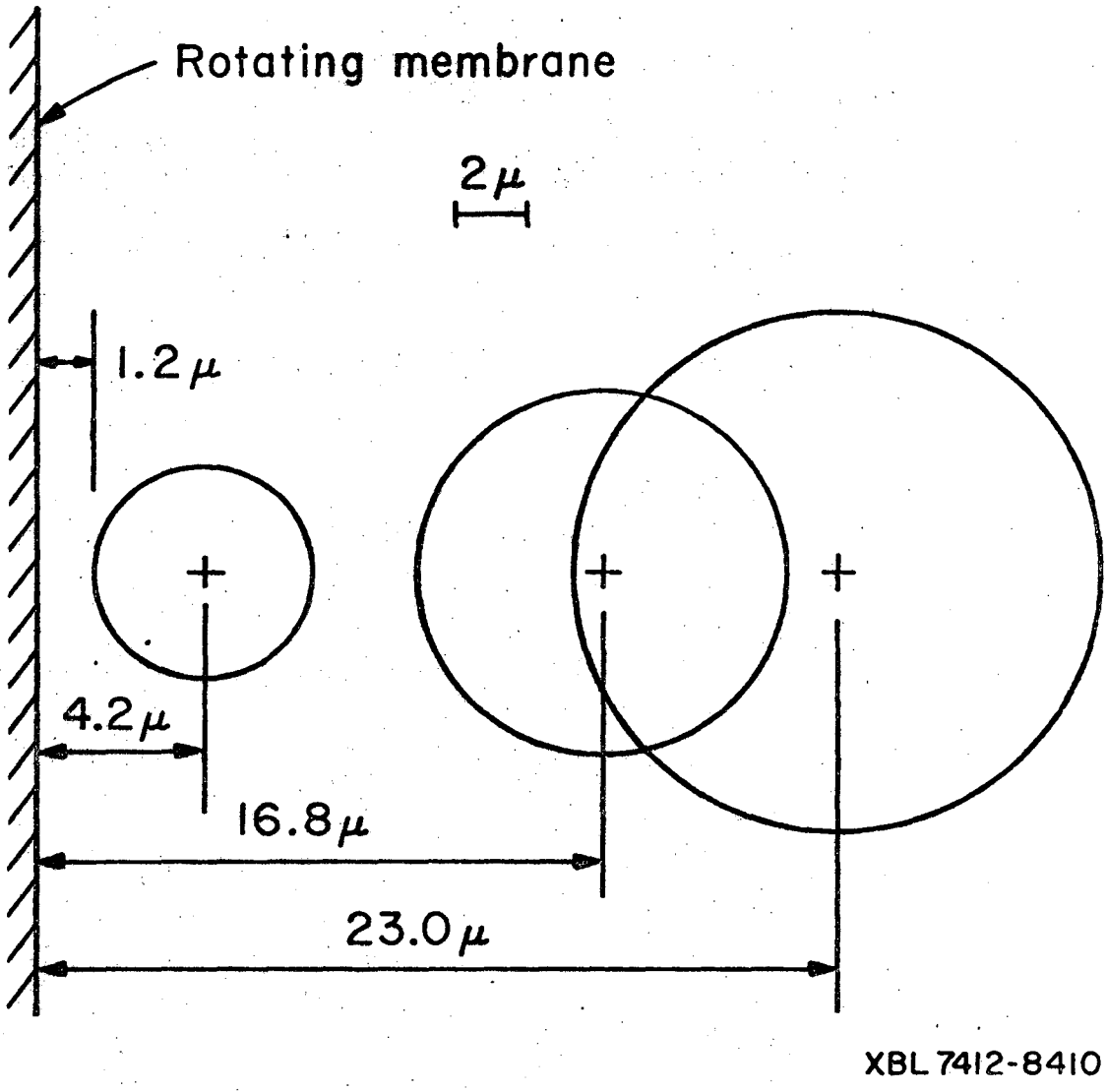

Fig. 5.3.3. Equilibrium position of polystyrene particles during "centrifugal" filtration.

distances predicted by the "centrifugal" filtration theory calculations. These calculations predict that all size particles from 6 to 14 microns should not reach the membrane surface or go through the membrane pores. However, experimental results indicate that we do have some particles going through the membrane. This may be explained by one or a combination of the following possible reasons:

1. Due to the radial filtrate flux u going toward the membrane the Von Karman velocity profile will tend to shift to the left and therefore resulting in lower peripheral particle velocities. This, of course, means lower centrifugal forces acting on the particle than predicted by the theory.
2. Since we have a range of particle sizes there is bound to be some particle to particle interaction. This interaction may result in some displacement from the mean equilibrium position. For the smaller size particles which are close to the membrane surface this displacement may be large enough to force the particles through the membrane pores.
3. For those particles which happen to be next to a membrane pore the drag force will be much larger than that experienced away from the pore. This is due to the fact that the pores

constitute only 10% of the membrane area and the filtrate velocity u will be much larger at the pores than away from the membrane surface. This, of course, will result in drag forces larger than those predicted by the theory. Reasons number 1 to number 3 alone or in combination will result in some particles of the smaller size going through the membrane pores. Therefore in "centrifugal" filtration sufficiently large centrifugal forces must operate so that a relatively large particle-free layer develops around the membrance surface.

5.3.2 "Cake" Filtration

In this set of experiments the 2-inch diameter sintered stainless steel membrane was used. This is a Grade H membrane shown in Figures 3.1.4 and 3.1.5 and discussed in Section 5.2. Baker's yeast made by Red Star Company was used at different concentrations. Microscopic observations showed that the yeast cell size varied between 3 to about 5 microns. The flow diagram of the experimental apparatus used is shown in Figure 2.1.1. The supply tank was changed with approximately 50 liter yeast suspension in tap water and pressurized with nitrogen to the desired pressure. A four-blade turbine impeller mounted on top of the supply tank was used to agitate the yeast suspension and keep it well mixed. The yeast suspension was first changed into the Rotorfermentor chamber by opening the supply tank valves. As soon as the chamber was filled up, the membrane was rotated by setting the motor at the desired speed. The filtrate at the beginning of filtration had yeast cells but as the cake started building up, the filtrate finally cleared up with no cells present. The pressure drop between the Rotorfermentor chamber and the filtrate chamber was recorded by a membrane transducer-pressure gauge system, as described in Section 2.1. The temperature was controlled by means of a cooling coil inside the chamber. During the course of filtration the filtrate was collected and weighed as

a function of time. From these data the filtrate flow rate was obtained as a function of time. For each run the pressure drop for filtration ΔP was maintained constant. This was done by pressurizing the supply tank with nitrogen at a desired pressure, which was maintained constant by means of a pressure regulator valve located between the nitrogen cylinder and the supply tank. All three filtration experiments were carried out at a constant membrane rotational speed of 640 r.p.m.

The filtration results of run FY-7 are shown in Table 5.3.1. The pressure drop was maintained at 15.5 p.s.i. and the yeast suspension was 3.16 gm. wet cell per liter of solution which is equal to 0.9 gm. dry wt./lit. The moisture content of the cells was 71.5% as received from the manufacturer in cake form. The membrane area available for filtration for the 2-inch diameter membrane was 365 cm^2. As seen from Table 5.3.1, the filtrate flux is high at the beginning of filtration and it decreases with time as the cake thickness increases. The filtrate flux reaches a constant value corresponding to a constant cake thickness.

Table 5.3.2 shows filtration results of run FY-12 for a pressure drop of 24.3 p.s.i. and yeast concentration 3.16 gm. wet cell per liter.

Table 5.3.3 shows the results of run FY-16. The pressure drop was maintained at 26.5 p.s.i. and the

yeast concentration was increased to 19.3 gm. wet cells per liter which is equal to 5.5 gm. dry weight per liter of solution.

The results of runs FY-7, FY-12 and FY-16 are plotted in Figure 5.3.4. Comparing the results of runs FY-7 and FY-12, we note that at the beginning of filtration the filtrate flow rate is proportional to pressure drop ΔP. However, as the steady-state cake thickness is reached, which is different for the two runs, the filtrate flow rate is the same, i.e., seems to be independent of pressure drop ΔP. This is in agreement with the results of Bhagat and Wilke (1) who found that at a given r.p.m. the steady-state filtrate flux is given by

$$u \propto \frac{\Delta P}{l}$$

where l is the cake thickness. At a given r.p.m. as ΔP is increased, the cake thickness l also increases so that the ratio $\Delta P/l$ remains the same, giving the same value of u. This explains why u seems to be independent of ΔP at steady-state conditions.

Bhagat and Wilke (1) studied the filtration of dilute suspensions 0.1% to 0.05% solids of 1.3 to 14 microns polystyrene particles. No attempt was made to study the possible effect of particle concentration on u at steady-state. In run FY-16 the ΔP was almost the same as for run FY-12 but the yeast concentration

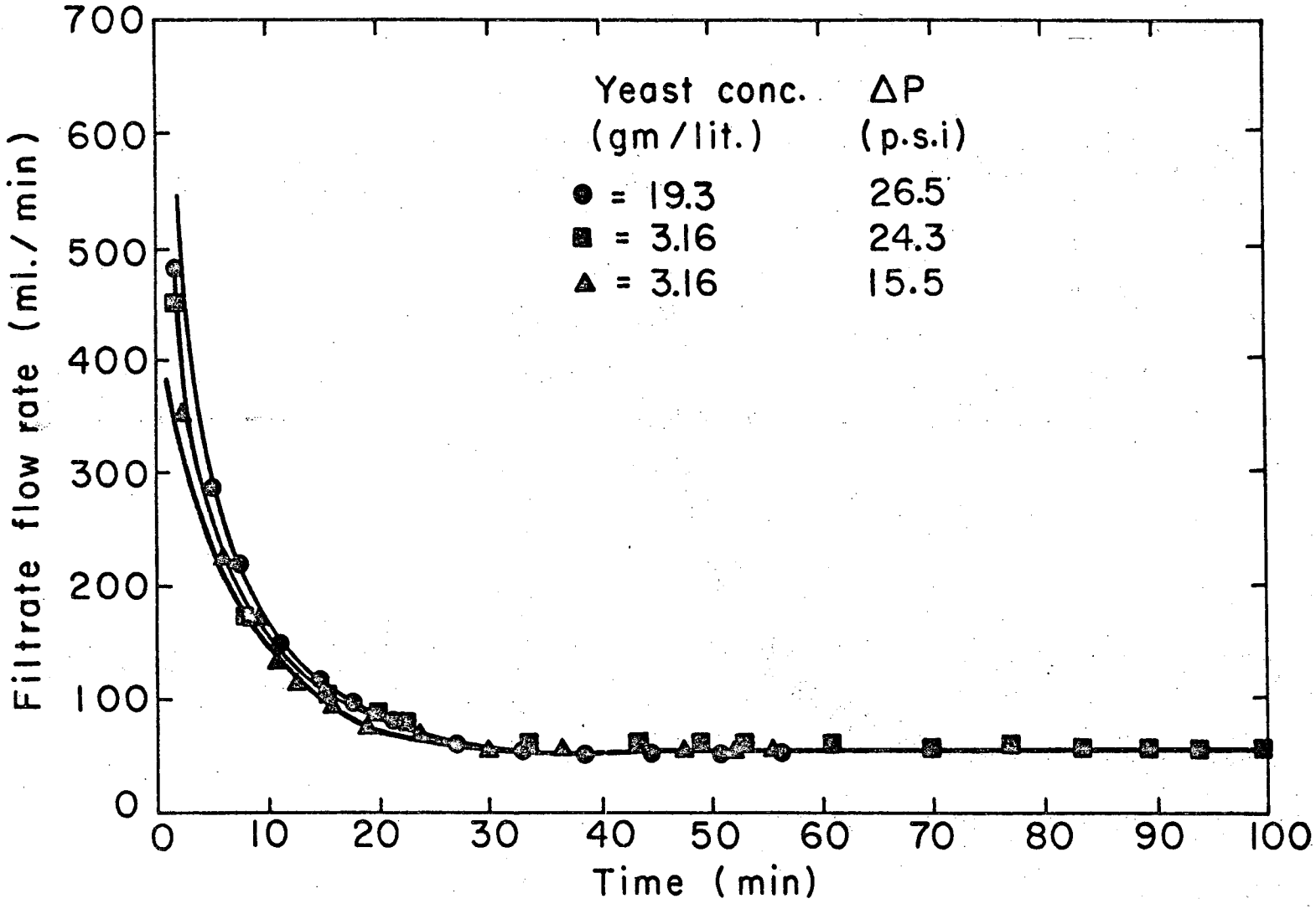

XBL756-3075

Fig. 5.3.4. Filtration at Constant Rotational Speed 640 R.P.M.

Table 5.3.1. Filtration Results of Run FY-7

ΔP = 15.5 p.s.i. N = 640 r.p.m. C = 3.16 gm/lit

Time t (min.)	Filtrate weight (lb.)	ΔV (lit.)	Δt (min.)	Filtrate Rate (lit/min)	Average time, $\bar{t}$ (min.)
0	0.000				
		1.634	4.56	0.358	2.28
4.56	3.575				
		0.673	3.00	0.226	6.06
7.56	5.057				
		0.423	2.50	0.169	8.81
10.06	5.994				
		0.171	1.30	0.132	10.71
11.36	6.369				
		0.312	2.79	0.112	12.75
14.15	7.057				
		0.353	3.71	0.095	16.00
17.86	7.837				
		0.198	2.74	0.072	19.23
20.60	8.275				
		0.411	6.25	0.066	23.72
26.85	9.183				
		0.339	6.49	0.052	30.09
33.34	9.933				
		0.354	6.47	0.055	36.57
39.81	10.716				
		0.283	5.44	0.052	42.53
45.25	11.341				
		0.226	4.34	0.052	47.42
49.59	11.841				
		0.226	4.43	0.051	51.80
54.02	12.341				
		0.155	2.93	0.053	55.49
56.95	12.684				

Table 5.3.2. Filtration Results of Run FY-12

ΔP = 24.3 p.s.i. N = 640 r.p.m. C = 3.16 gm./lit.

Time t (min.)	Filtrate weight (lb.)	ΔV (lit.)	Δt (min.)	Filtrate Rate (lit./min)	Average time, $\bar{t}$ (min.)
0	0.000				
		1.930	4.25	.453	2.15
4.25	4.250				
		1.376	8.08	.171	8.29
12.33	7.250				
		0.653	6.36	.103	15.51
18.69	8.688				
		0.255	2.82	.091	20.10
21.51	9.250				
		0.426	5.27	.081	22.14
26.78	10.188				
		0.921	13.08	.071	33.32
39.86	12.188				
		0.454	7.20	.063	43.46
47.06	13.188				
		0.242	4.06	.060	49.09
51.12	13.688				
		0.255	4.18	.061	53.21
55.30	14.250				
		0.682	11.50	.059	61.05
66.80	15.750				
		0.369	6.74	.055	70.17
73.54	16.563				
		0.409	7.16	.057	77.12
80.70	17.478				
		0.312	5.88	.053	83.64
86.58	18.125				
		0.313	5.75	.054	89.45
92.33	18.813				
		0.284	5.17	.055	94.91
97.50	19.438				
		0.312	5.47	.057	100.23
102.97	20.125				
		0.327	5.77	.057	105.85
108.74	20.813				
		0.426	7.30	.058	112.39
116.04	21.750				

Table 5.3.3. Filtration Results of Run FY-16

ΔP = 26.5 p.s.i. N = 640 r.p.m. C = 19.3 gm./lit

Time t (min.)	Filtrate weight (lb.)	ΔV (lit.)	Δt (min.)	Filtrate Rate (lit/min)	Average time, $\bar{t}$, (min.)
0	0.000				
		2.045	4.22	0.484	2.11
4.22	4.500				
		0.426	1.48	0.288	4.96
5.70	5.437				
		0.738	3.32	0.222	7.36
9.02	7.062				
		0.653	3.37	0.150	11.2
13.39	8.500				
		0.312	2.62	0.119	14.7
16.01	9.187				
		0.313	3.16	0.099	17.6
19.17	9.875				
		0.368	4.56	0.081	21.5
23.73	10.687				
		0.369	6.17	0.060	26.8
29.90	11.500				
		0.341	6.10	0.056	33.0
36.00	12.250				
		0.255	4.91	0.052	38.5
40.91	12.812				
		0.369	7.24	0.051	44.5
48.15	13.625				
		0.284	5.63	0.050	51.0
53.78	14.250				
		0.255	5.03	0.051	56.3
58.81	14.812				

was increased to 19.3 gm/lit., i.e., an almost six-fold increase over that of run FY-12. As shown in Figure 5.3.4, the steady-state filtrate flux u is the same for both runs and is not affected by the increase in yeast concentration. It is not known, however, if u will continue to be unaffected at much higher yeast concentrations.

5.3.3 Batch Filtration at No Membrane Rotation

In this set of experiments the pressure drop across the cake and membrane was maintained constant during the whole batch run. The experimental procedure used was the same as that described in Section 5.3.2, the only difference being that the 2-inch diameter Grade H membrane was not rotated. The purpose of these constant pressure batch runs was to determine the filtration characteristics of the yeast cake and the resistance to filtrate flow by the membrane. The filtrate volume V was collected as a function of time and the reciprocal of filtrate rate was correlated according to equation 5.35. From these data the specific cake resistance α and the filter medium resistance R_m were calculated.

Table 5.3.4 shows experimental results of run FY-14. The slurry concentration was 0.77 gm. dry yeast/lit. and the pressure drop was maintained constant at 7.8 p.s.i. The membrane used was the sintered steeel Grade H of 5 micron nominal pore size and had a total surface area

of 365 cm.^{2}

Table 5.3.5 shows results of run FY-3 which was carried out at 10 p.s.i. and a slurry concentration of 0.87 gm. dry yeast/lit. Table 5.3.6 shows the results of run FY-5 at 15 p.s.i. and 0.5 gm. dry yeast/lit. Table 5.3.7 shows data for run FY-10 which was carried out at a pressure of 30 p.s.i. and a slurry concentration of 0.30 gm. dry yeast/lit.

Figure 5.3.5 is a plot of $\Delta t/\Delta V$ against volume of filtrate V. As we see the experimental results correlate into a straight line relationship as predicted by equation 5.35. The slope K_p and intercept B for each run is used to calculate the specific cake resistance α and filter medium resistance R_m. The summarized results are shown in Table 5.3.8. The specific cake resistance and medium resistance R_m are plotted against pressure drop ΔP as shown in Figures 5.3.6 and 5.3.7 respectively.

The value of specific cake resistance increases with pressure drop ΔP as shown in Figure 5.3.6, indicating that the yeast cake is compressible. The filter medium resistance R_m does not seem to depend on ΔP remaining almost constant for the pressure range covered. The values of α and R_m obtained seem to be within typical ranges. Although no data exist on values of α for yeast cake a rough comparison could be made with the

batch constant pressure filtration data for water suspensions of $CaCO_3$. For example, at $\Delta P = 6.7$ p.s.i. the value of α for $CaCO_3$ suspensions was found to be 1.65×10^{11} ft/lb. or 0.11×10^{11} cm/gm as reported by McCabe and Smith (5). The value of α for yeast filtration at $\Delta P = 7.8$ p.s.i. was found to be 5.89×10^{11} cm/gm. Yeast cake seems to have much higher α values than those for $CaCO_3$ cake. This may be due to the fact that yeast cells being much more compressible than $CaCO_3$ solid grains tend to form very closely packed cake of very low permeability resulting in relatively high values of α.

The value of R_m for $CaCO_3$ filtration at $P = 6.7$ p.s.i. was reported by McCabe and Smith (5) to be 1.97×10^{10} ft. or 0.065×10^{10} cm. No mention is made of the type of filter medium used. In our case for the 5 micron sintered steel membrane used the value of R_m at $\Delta P = 10$ p.s.i was found to be 0.712×10^{10} cm.

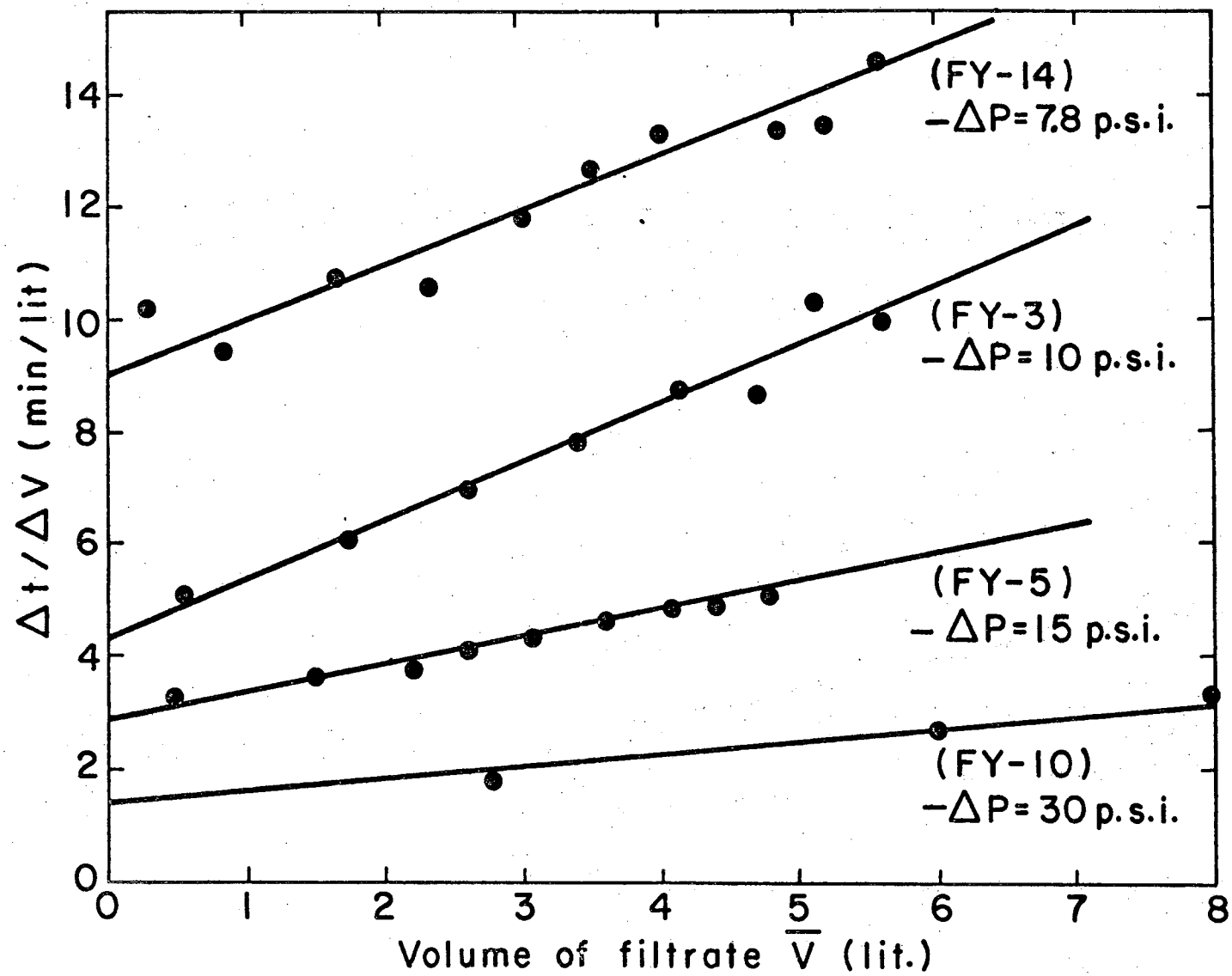

Fig. 5.3.5. Batch Filtration of Yeast Slurry
Rotor Speed = 0 R.P.M.; 5μ P.S.S. Membrane

XBL756-3081

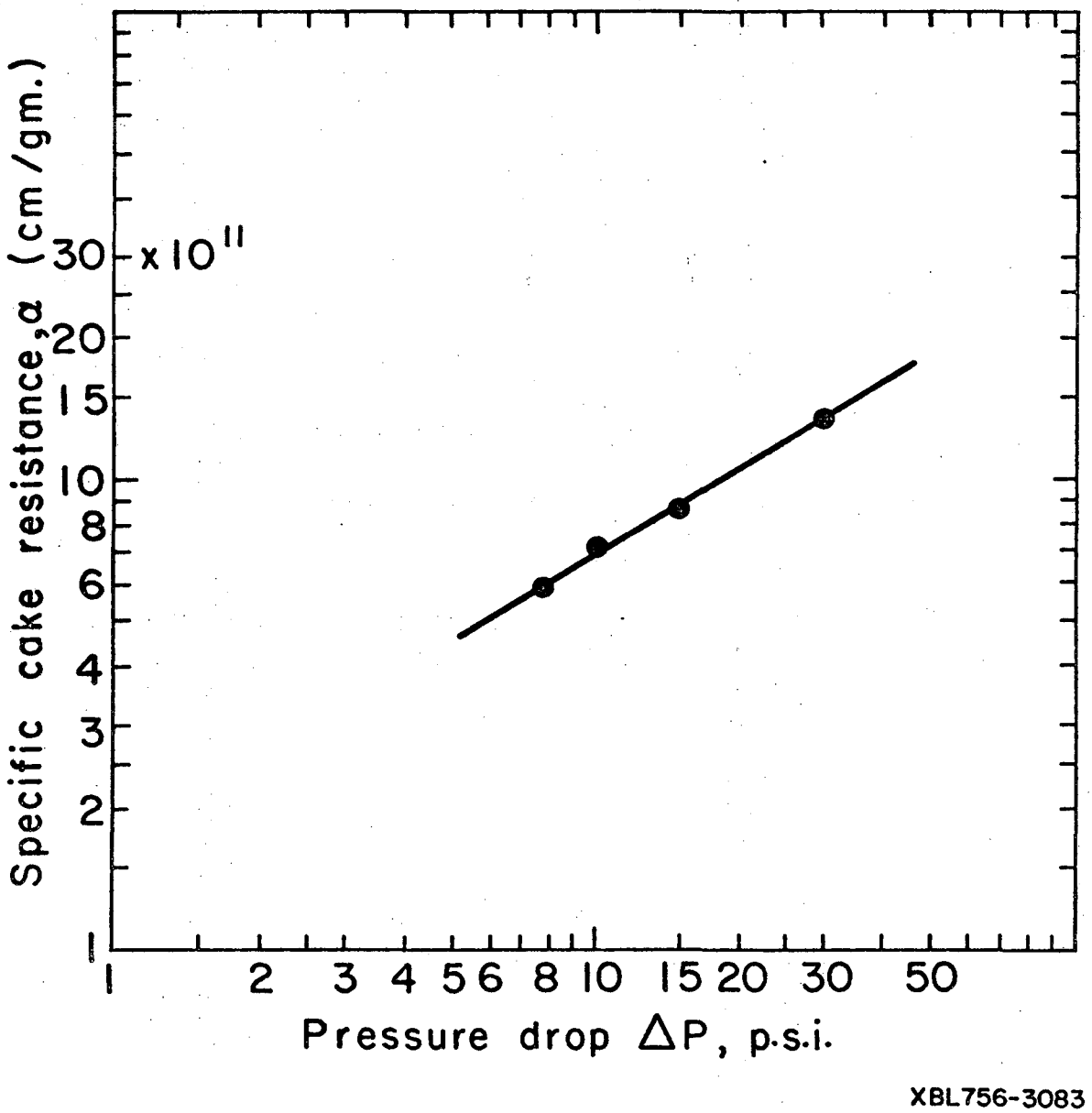

Fig. 5.3.6. Specific Cake Resistance vs. Pressure Drop for Yeast.

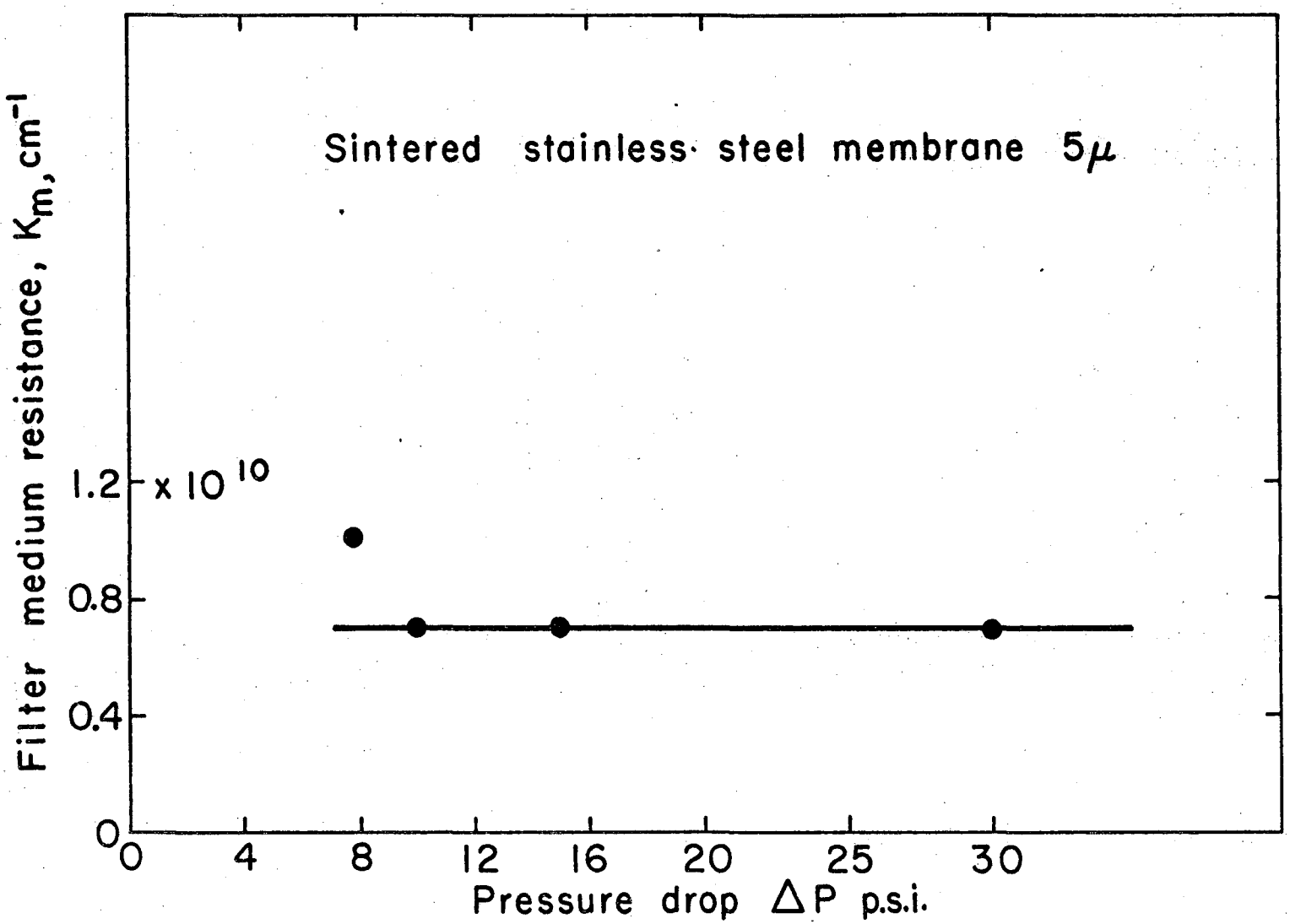

Fig. 5.3.7. Filter Medium Resistance vs. Pressure Drop. XBL756-3079

Table 5.3.4 Batch Filtration Results of Run FY-14

ΔP = 7.8 p.s.i N = 0 r.p.m. C = 0.77 gm./lit.

Time, t (min)	Filtrate Volume, V (lit)	Δt (min)	ΔV (lit)	$\Delta t / \Delta V$ (min/lit)	$\bar{V} = \frac{V_1 + V_2}{2}$ (lit)
0	0.000				
		4.70	0.454	10.35	0.227
4.70	0.454				
		7.63	0.821	9.31	0.865
12.33	1.275				
		8.54	0.795	10.74	1.672
20.87	2.070				
		5.97	0.570	10.48	2.355
26.84	2.640				
		7.47	0.630	11.85	2.955
34.31	3.270				
		6.46	0.510	12.68	3.525
40.77	3.780				
		6.45	0.480	13.44	4.02
47.22	4.260				
		5.98	0.400	14.95	4.46
53.20	4.660				
		4.80	0.360	13.33	4.84
58.00	5.020				
		5.80	0.440	13.20	5.24
63.80	5.460				
		5.77	0.400	14.40	5.66
69.57	5.860				

Table 5.3.5. Batch Filtration Results of Run FY-3

ΔP = 10 p.s.i N = 0 r.p.m. C = 0.87 gm./lit.

Time t (min)	Filtrate Volume, V (lit)	Δt (min)	ΔV (lit)	$\Delta t / \Delta V$ (min/lit)	$V = \frac{V_1 + V_2}{2}$ (lit)
0	0				
		5.70	1.105	5.16	0.552
5.70	1.105				
		7.55	1.250	6.04	1.73
13.25	2.355				
		3.15	0.455	6.87	2.582
16.38	2.810				
		8.52	1.080	7.88	3.350
24.90	3.890				
		4.44	0.510	8.72	4.145
29.34	4.400				
		4.46	0.520	8.58	4.66
33.80	4.920				
		4.00	0.380	10.53	5.11
37.80	5.300				
		5.71	0.575	9.93	5.59
43.51	5.875				

Table 5.3.6 Batch Filtration Results of Run FY-5

ΔP = 15 p.s.i. N = 0 r.p.m. C = 0.50 gm./lit

Time t (min)	Filtrate Volume, V (lit)	Δt (min)	ΔV (lit)	$\Delta t / \Delta V$ (min./lit)	$V = \frac{V_1 + V_2}{2}$ (lit)
0	0.000				
		3.03	0.908	3.34	0.454
3.03	0.908				
		4.09	1.137	3.60	1.477
7.12	2.045				
		1.22	0.338	3.61	2.214
8.34	2.383				
		1.82	0.457	3.98	2.611
10.16	2.840				
		1.90	0.450	4.22	3.065
12.06	3.290				
		2.90	0.630	4.60	3.605
14.96	3.920				
		1.34	0.280	4.78	4.060
16.30	4.200				
		1.92	0.400	4.80	4.400
18.22	4.600				
		1.39	0.281	4.94	4.74
19.61	4.881				

Table 5.3.7 Batch Filtration Results of Run FY-10

ΔP = 30 p.s.i N = 0 r.p.m. C = 0.30 gm./lit.

Time t (min)	Filtrate Volume V (lit)	Δt (min)	ΔV (lit)	$\Delta t / \Delta V$ (min/lit)	$V = \frac{V_1 + V_2}{2}$ (lit)
0	0.000				
		5.48	3.730	1.47	2.74
5.48	3.730				
		1.04	0.340	2.71	6.00
6.52	4.070				
		2.90	0.850	3.41	7.97
9.42	4.920				
		0.90	0.230	3.91	9.87
10.32	5.150				
		2.34	0.600	3.89	11.49
12.66	5.750				
		1.10	0.250	4.40	13.21
13.76	6.000				
		1.30	0.280	4.64	14.41
15.06	6.280				

Table 5.3.8

Run No.	ΔP (p.s.i.)	Slurry Conc. C (gm. dry cell/lit)	Slope K_p (min./lit)	Intercept B (min/lit)	Specific Cake Resistance α (cm/gm) X 10^{10}	Medium Resistance R_m ($cm.^{-1}$) X 10^{11}
FY-14	7.8	0.77	0.962	9	5.89	1.16
FY-3	10	0.87	1.045	4.3	7.26	0.712
FY-5	15	0.50	0.48	2.8	8.71	0.696
FY-10	30	0.30	0.221	1.4	13.36	0.696

References Cited in Chapter V

1. Bhagat, A. K., and C. R. Wilke, Filtration Studies with Ultrafine Particles, Lawrence Radiation Laboratory Report UCRL-16574 (1966).

2. Bird, R. B., Stewart, W. E., and Lightfoot, E. N., Transport Phenomena, John Wiley and Sons, Inc., New York (1960).

3. Wilke, C. R., and Chang, P., A. I. Ch. E. Journal, 1(2), 270 (1955).

4. Selby, S. M., C. R. C. Standard Mathematical Tables, Chemical Rubber Company, Ohio (1970), 18th Edition.

5. McCabe, W. L., and Smith, J. C., Unit Operations of Chemical Engineering, New York, McGraw-Hill, Inc. (1956).

CHAPTER VI

ETHANOL FERMENTATION KINETICS

In this section a series of experiments are described on the kinetics of ethanol fermentation using Saccharomyces cerevisiae ATCC #4126. Both batch and steady-state continuous experiments were carried out with emphasis on the effects of oxygen and glucose concentration on ethanol productivities. An ordinary 1 liter stirred tank fermentor was used for both batch and continuous experiments. In addition, a brief description is given on the metabolism and morphology of the yeast cell.

6.1 Yeast Morphology.

Yeast cells of the Saccharomyces genera are oblate spheroids which reproduce asexually by a process called budding. A bud appears at the end of the long axis of the cell which grows in size until it reaches almost the size of the mother cell and then separates. Depending on growth conditions such as pH temperature and nutrient composition the complete cycle from the time a bud appears to the time of separation from the mother cell takes about two to three hours. The same cell can undergo the budding process several times before it dies.

The number of buddings a cell went through can be found by noting the number of scars left on the cell surface. This can be easily seen by looking at the cell surface using an ordinary optical microscope.

Hartwell et al. (1) proposed a genetic control model to explain the cell division cycle in Saccharomyces cerevisiae. This is shown schematically in Figure 6.1. The mitotic cell division of eukaryotic yeast cells is accomplished through a sequence of events. A time interval G1 separates the previous cell division from the initiation of DNA synthesis. Chromosome replication is accomplished during the DNA synthesis period, S, which usually occupies about a third of the cell cycle. Another time interval, G2, separates the completion of DNA synthesis from prophase, which is the beginning of mitosis, M. A fast sequence of changes in chromosome structure and movement takes place during the short mitotic period which results in the precise separation of sister chromatids to daughter nuclei. Mitosis is followed by cytokinesis, the partitioning of the cytoplasm into two daughter cells with separate plasma membranes.

Microscopic observation of distillers' yeast during budding is reported by de Becze (2).

Figure 6.2 shows exponentially grown cells of Saccharomyces cerevisiae ATCC #4126. The top part shows

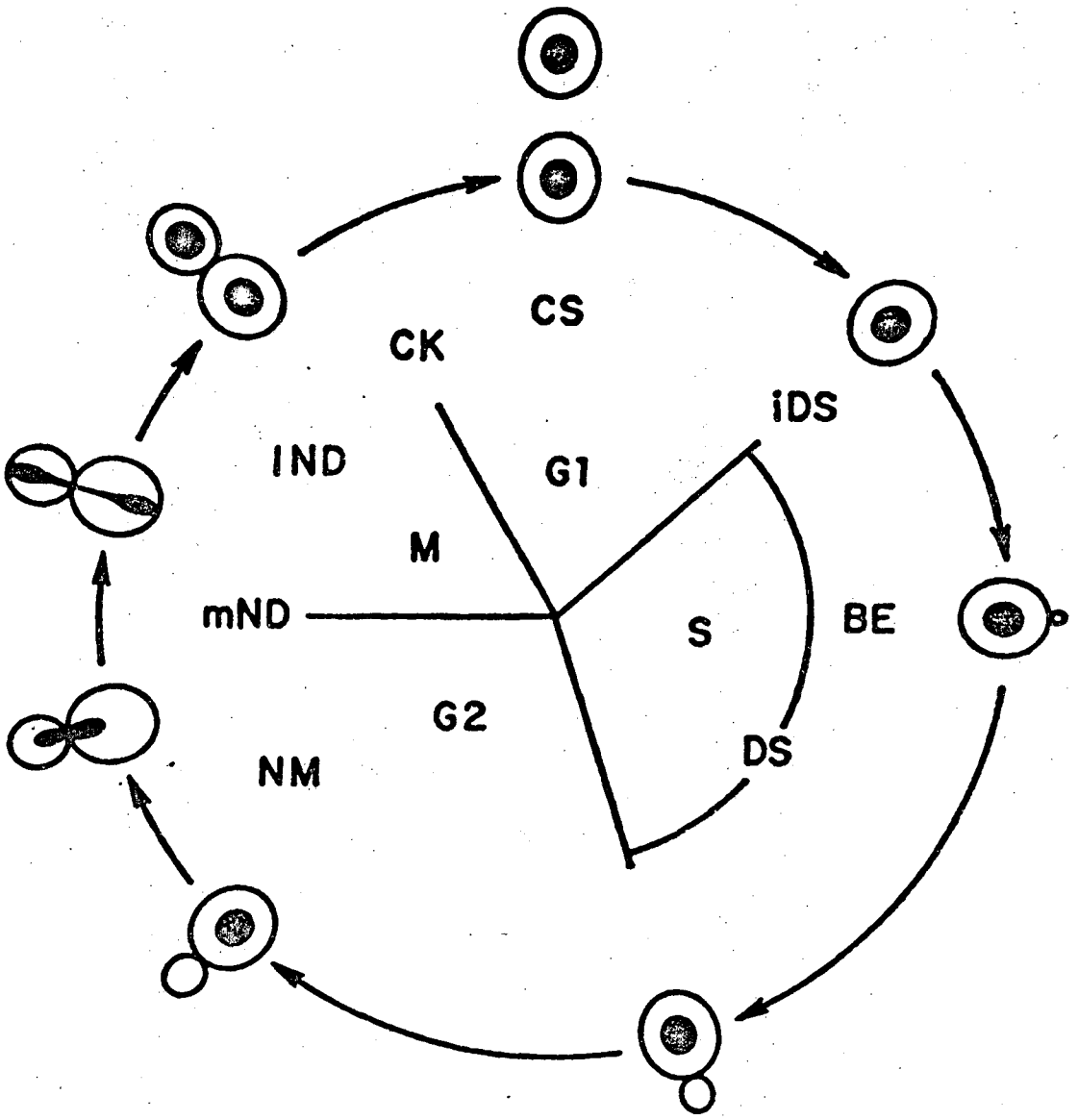

XBL 754-934

Fig. 6.1. Sequence of events in the cell division cycle of yeast. After Hartwell et al. (1).

typical stages of four different cells at four different phases of budding. Notice the progressive growth in bud size until the two cells are ready to separate. The bottom part of Figure 6.2 shows typical cells at various stages of growth. The morphology of yeast cells depends strongly on the presence or absence of essential nutrients such as oxygen and glucose. Figure 6.3a shows cells in stationary or resting phase 32 hours after inoculation when practically all glucose has been exhausted. Notice the appearance of empty-like ghost cells. In these cells most of the cytoplasm leaked out leaving only the cell wall and membrane. Figure 6.3b shows cells that were left in a fermentor for about 10 days with no mechanical agitation which resulted in the cells settling at the bottom of the fermentor. Lack of agitation prevents the distribution of nutrients and oxygen resulting in the retardation of cell growth. A brief description of the basic structural elements of yeast cell will give a better perspective in understanding metabolism and the way in which nutrients such as oxygen may affect ethanol productivities. Figure 6.4b shows a cross-section of a typical yeast cell, using an electron microscope. The basic micro-structures of a yeast cell are the following: cell wall, cytoplasmic membrane, nucleus, one or more vacuoles, mitochondria, lipid globules, volutin or polyphosphate bodies, and the cytoplasmic matrix.

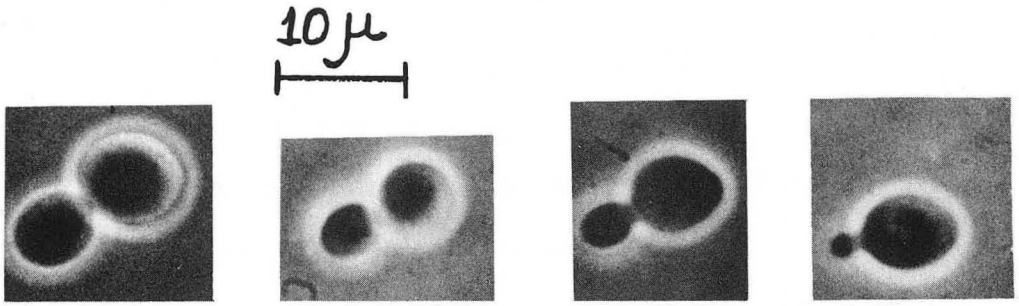

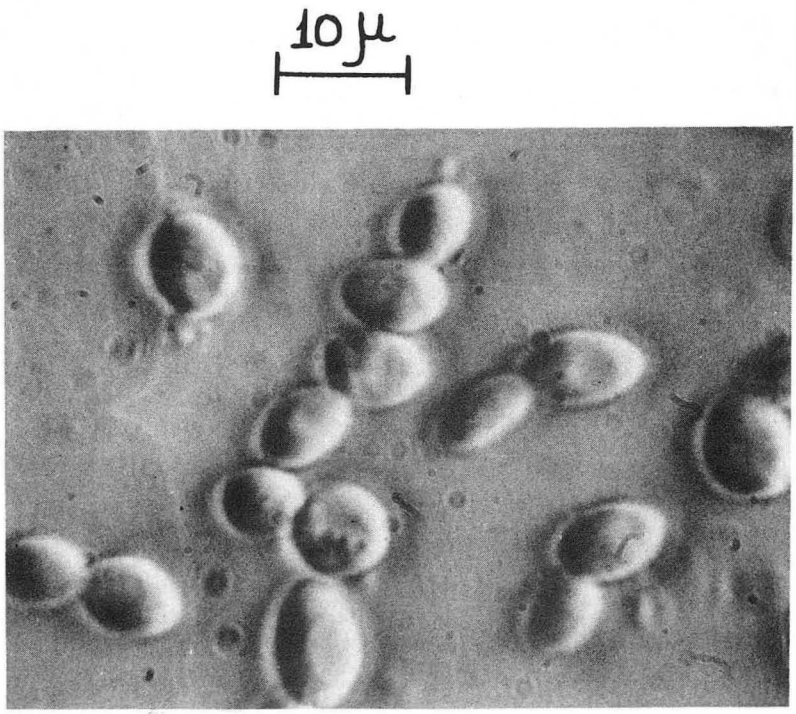

XBB 754-3047

Fig. 6.2. Division of exponentially grown cells of Saccharomyces cerevisiae ATCC 4126.

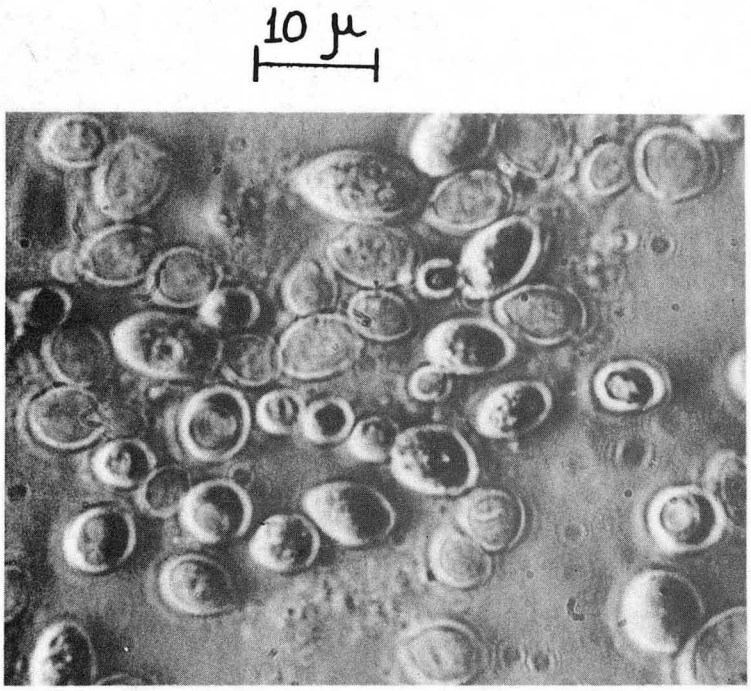

XBB 754-3046

Fig. 6.3. Morphology of yeast cells at different growth conditions

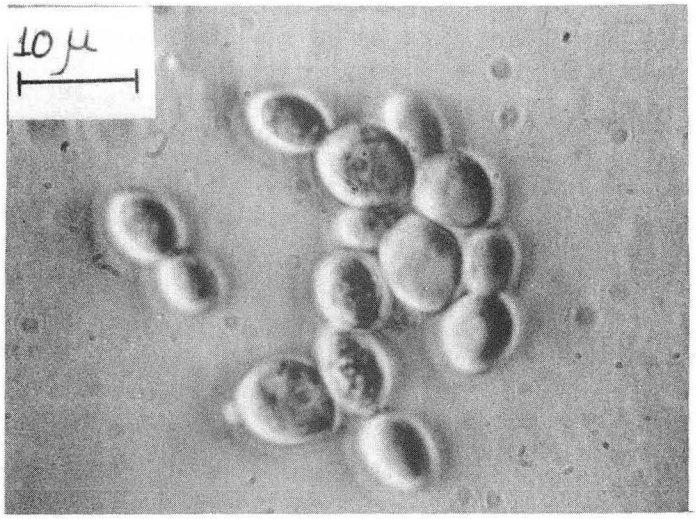

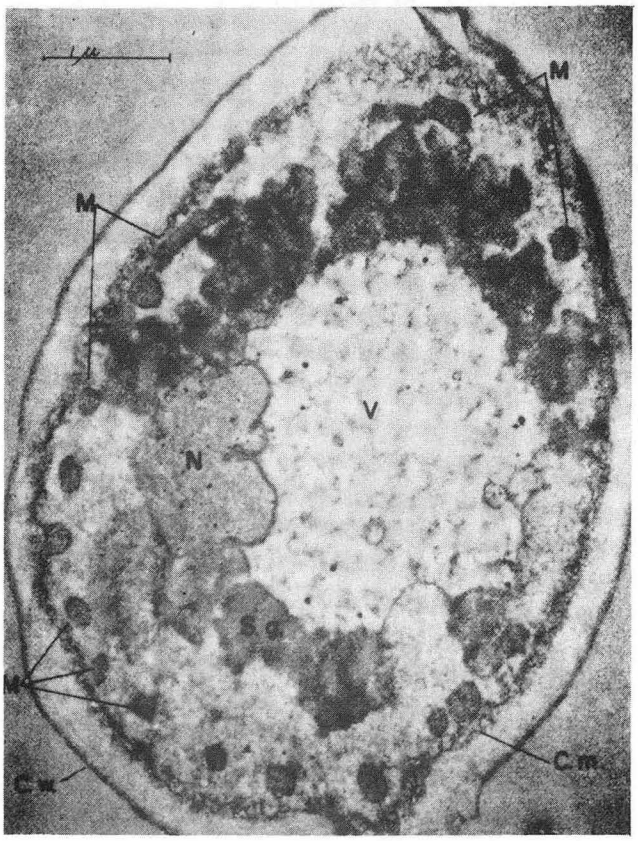

XBB 757-5655

Electron micrograph of a section of *Saccharomyces cerevisiae*. Cytoplasmic structures: cytoplasmic membrane (C.m.), cell wall (C.w.), mitochondrion (M), storage granule (S.g.) and vacuole (V) (Agar & Douglas, 1957).

Fig. 6.4 (a) Exponentially grown yeast cells.
(b) Cross-section of a yeast cell.

The cell wall. The wall can be seen with the ordinary light microscope as a distinct outline of the cell and although it is somewhat elastic, its rigidity is responsible for the particular shape which a yeast cell assumes.

Our present understanding of the chemical composition of the cell wall of yeast is based largely on the combined evidence of chemical analysis and enzymatic degradation of the walls.

The principle fraction, now known as yeast glucan, and in the early literature as "yeast cellulose," constitutes the component responsible for the shape and rigidity of the yeast cell. This highly insoluble polysaccharide had been shown to contain a preponderance of β-1,3 linkages between the glucose units which compose this polymer.

The glucan, which represents about 30-35% of the dried cell walls of Saccharomyces cerevisiae, is accompanied by a second major component, a mannan, consisting of a water-soluble polysaccharide of the sugar D-mannose. This polymer is also present in a concentration of approximately 30%.

Another component is chitin, a linear polymer of N-acetylglucosamine, in which the constituent monomeric units are linked by β-1,4 bonds. Chitin concentrations of 1-2% are found in walls of Saccharomyces cerevisiae and related species.

Wall material of baker's yeast has been reported by some to contain from 8.5-13.5% lipid material, although lower figures have been published by others.

Finally, cell-wall material is known to contain from one to several percent of inorganic materials, especially phosphate.

The cytoplasmic membrane. This structure is located directly beneath the cell wall and plays an important role in the selective permeability of the cell and in the transport of nutrients. The cytoplasmic membrane is not a smooth layer, but short invaginations into the cytoplasm are apparent when ultrathin sections of Saccharomyces cerevisiae are photographed with the electron microscope. The membrane is very thin, about 75 to 80 Å, and appears as a double layer in electron micrographs. It is composed of protein, ribonucleic acid, and lipids.

The nucleus. Although in the past many controversies raged about the location and the nature of the yeast nucleus, it is now well established, as a result of studying ultrathin sections, that yeast has a well-defined nucleus, surrounded by a double nuclear membrane. This membrane contains a number of nuclear pores, presumably for the purpose of exchanging cytoplasmic materials with nuclear components. All of the earlier work was based on staining the nucleus with specific dyes, but in most cases the details of nuclear

division could not be clearly observed. The demonstration of individual chromosomes was even more difficult, although some workers demonstrated by use of nuclear stains individual bodies which resembled chromosomes.

Vacuoles. Usually one or more vacuoles of variable size can be readily observed in yeast cells under the light microscope (Fig. 6a). Vacuoles are probably sacs of fluid of greater transparency and lower viscosity than the surrounding cytoplasm.

Other workers have found that if yeasts are grown in the presence of L-menthionine, the vacuole accumulates large amounts of S-adenosylmethionine.

Occasionally the vacuoles contain very striking bodies which consist of highly refractile polymetaphosphate or volutin.

Vacuoles are less electron-dense than the cytoplasm, so that they can be easily differentiated in electron micrographs. They are surrounded by single membranes, which appear to have diverticula, or finger-like structures, that extend deep into the cytoplasm.

Mitochondria. Yeast cells have been shown by ultrathin sectioning to contain mitochondria (varying in number from about 4 to 20), which, in Saccharomyces cerevisiae, are located fairly close to the periphery of the yeast cell. These bodies, also found in cells higher plants and animals, measure approximately 0.4-0.6

micron in lengths and 0.2-0.3 micron in diameter, and are important in the respiratory activity of yeast. Yeast mitochondria have a double-layered outer wall and contain internal membranes, or cristae, in various configurations. These cristae, which are characteristic components of mitochondria, appear to be formed by infolding of the inner layer of the membrane. For many years electron microscopic examination of ultrathin sections of yeast supported the view that there are many individual mitochondria particles per yeast cell. However, recent research by Hoffmann and Avers (3) showed that there is only one giant branched mitochondrion per cell. Three-dimensional models constructed from 80 to 150 consecutive serial sections of entire yeast cells showed that all the separate mitochondrial profiles were cross-sections through a single, branching, tubular structure about 50 to 60 microns in length and 200 to 600 Å in diameter.

Lipid globules. Most yeast cells contain small amounts of lipid in the form of globules which are stainable with fat stains such as Sudan Black or Sudan Red. These dyes penetrate the cell and accumulate in the lipid globules, staining them bluish black or red. In electron micrographs of thin sections, the lipid globules show up as the most electron-transparent bodies of the cell.

Cytoplasm. Cytoplasm is a limpid fluid encompassing finely granular material which contains the reserve polysaccharide yeast glycogen, and is rich in ribonucleic acid and protein. The last two are found primarily in small RNA-containing granules, called ribosomes, which are involved in protein synthesis.

The first step in glucose metabolism is the physical transport from the liquid medium surrounding the cell and then transport across the cell membrane. The research findings of many workers (4,5,13) has shown that the transport of glucose across the cell membrane is not an ordinary free diffusion process, but rather a catalyzed transport porcess. Once the glucose enters the cell it undergoes phosphorilation and other reactions of the glycolytic pathway. A few enzymes are located near the cell membrane such as acid phosphatase while most of the enzymes are located inside the cell. The mitochondria contain most of the respiratory enzymes, the enzymes of the tricarboxylic acid cycle and other enzymes.

6.2 Yeast Metabolism

Saccharomyces cerevisiae ATCC #4126 is a facultative anaerobe which means that it is able to grow both in the presence or absence of oxygen. Yeast cells can get all their energy requirements and synthesize all their cell components from glucose in a medium which also contains ammonium salts, other inorganic salts, vitamins, and other trace minerals. Glucose enters the cell and, depending on the level of oxygen concentration, it is catabolized into CO_2, ethanol, and water, while part of the glucose is anabolized resulting in the formation of new cell material and cell growth.

The catabolic breakdown of glucose in yeast involves the operation of three series of biochemical reactions inside the cell; the glycolytic pathway, the tricarboxylic acid cycle (TCA) and the electron transport pathway. Later on we shall examine how these pathways are connected with each other in determining the amount of ethanol produced in each cell.

The glycolytic pathway. Under strictly anaerobic conditions (i.e., complete absence of oxygen) the cell catabolizes glucose through the glycolytic pathway shown in Figure 6.5a. Each reaction step is catalyzed by a specific enzyme. Not shown in Figure 6.5a is the last two reactions in alcoholic fermentation, i.e., the conversion of pyrurate to acetaldehyde plus CO_2 and

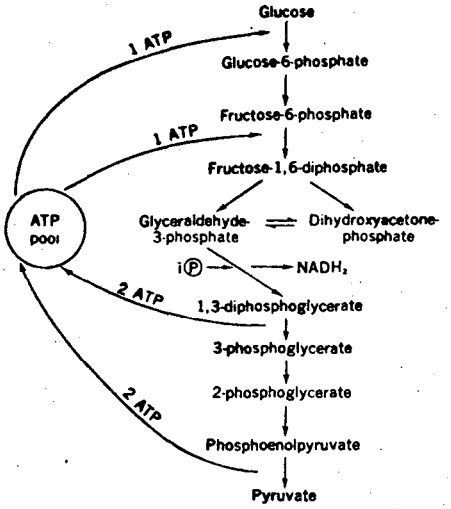

(a)

Summary: Glucose+2 ATP+2NAD⁺ ⟶ 2 Pyruvate+4 ATP+2 NADH₂

The glycolytic pathway.
iⓅ = H_3PO_4; ATP = adenosine triphosphate; NAD = nicotinamide adenine dinucleotide.

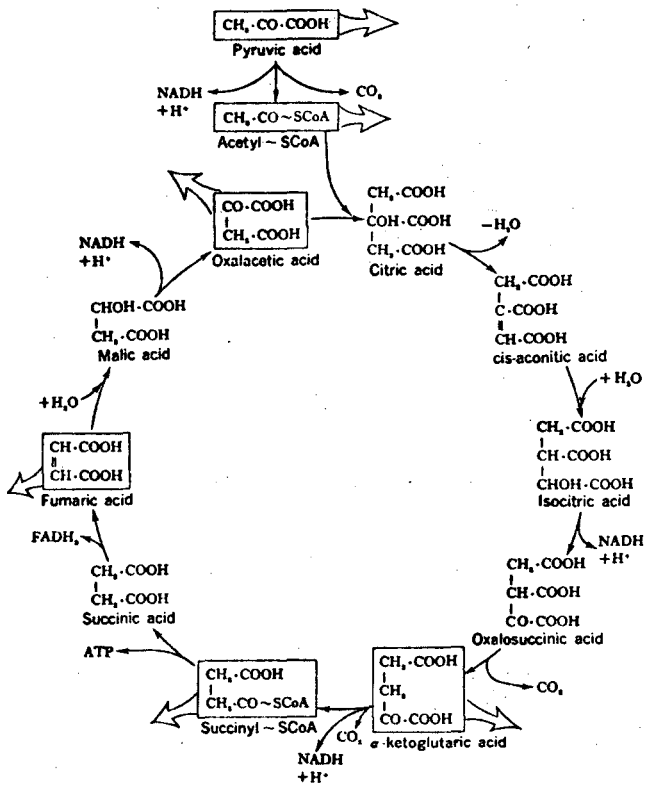

(b)

Summary: $CH_3{\cdot}CO{\cdot}COOH + 4NAD^+ + FAD \rightleftharpoons 3CO_2 + 4NADH + 4H^+ + FADH_2$

Tricarboxylic acid cycle. The compounds put inside squares are the starting compounds for synthetic reactions; α-ketoglutaric, fumaric, oxalacetic, and pyruvic acids are all concerned in amino acid formation, succinyl~SCoA is used for porphyrin synthesis, and acetyl~SCoA is needed for acetylation reactions.

XBL 752-265

Fig. 6.5. The glycolytic pathway (a), and the TCA cycle (b).

acetaldehyde to ethanol. Alcohol dehydrogenase is the enzyme that catalyzes the reaction acetaldehyde to ethanol.

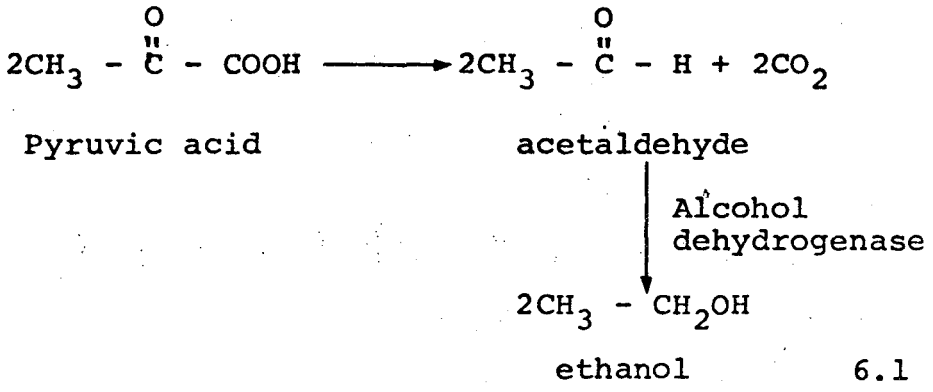

6.1

The overall reaction is that for every mole of glucose metabolized two moles of ATP are produced plus two moles of CO_2 and two moles of ethanol.

$$C_6H_{12}O_6 \longrightarrow 2C_2H_5OH + 2CO_2 + 2ATP \qquad 6.2$$

According to equation 6.2 the maximum theoretical ethanol yield is 0.511 gms. of ethanol formed per gm. of glucose metabolized. In reality though, the ethanol yield is less than the theoretical value due to the fact that some glucose is assimilated into cell mass and part of the glucose is converted into products other than ethanol such as higher alcohols, fatty acids, esters, carbonyl compounds and fusel oil.

The Tricarboxylic Acid Cycle (TCA)

When the yeast cell is exposed to aerobic conditions by supplying oxygen in the liquid phase the respiratory enzymes and the enzymes of the TCA cycle are developed (6,7,8,9,10). Under those conditions the glucose is still catabolized by passing through the glycolytic pathway until it reaches the pyruvate step. At this point some of the pyruvate goes to acetaldehyde and then ethanol plus CO_2 and some of the pyruvate enters the TCA cycle, and through the electron transport pathway is oxidized to CO_2 and H_2O. Therefore, depending on the level of oxygen concentration, part of the original glucose that enters the cell is fermented to ethanol plus CO_2 and part of it is oxidized through the TCA cycle to CO_2 and H_2O.

Figure 6.5b shows the TCA cycle reactions, where each reaction is catalyzed by a specific enzyme. Common to both glycolytic pathway and TCA cycle is the production of adenosine triphosphate (ATP). ATP is one of the most important high energy compounds in cellular metabolism, and shown in Figure 6.6a. ATP participates in many biochemical reactions inside the cell providing the necessary energy. For example, when the two terminal phosphate groups of ATP are hydrolyzed 12,000 cal. are released per phosphate. Table 6.1 shows in detail the amount of ATP produced by the glycolytic and by the TCA cycle. Under fully anaerobic condition only two ATP

Table 6.1. Amount of energy derived by microorganisms during the oxidation of glucose via glycolysis and the Tricarboxylic acid cycle.

Pathway	No. of moles of ATP formed. Algae, Yeast and Fungi	
<u>Glycolysis</u>		
Glucose → 2 Pyruvate		2
Oxidation of:		
$2NADH + 2H^+$	2 x 3 =	6
<u>TCA Cycle</u>		
Pyruvate → $3\ CO_2 + 3H_2O$		
Oxidation of:		
$4NADH + 4H^+$	4 x 3 = 12	
$1FADH_2$	1 x 2 = 2	
Succinyl~SCoA → 1ATP	$\frac{1}{15}$	
2 Pyruvate → $6CO_2 + 6H_2O$	2 x 15 =	<u>30</u>
<u>Overall</u>:		
Glucose + 30_2 → $6CO_2 + 6H_2O$	Total =	38

moles are produced, while under aerobic conditions a total of 38 moles ATP are produced per mole of glucose catabolized. This certainly shows that from the ATP production point of view the aerobic pathway is far more efficient than the strictly anaerobic glycolytic pathway.

The TCA cycle serves another important role. Many products of the TCA cycle are used as starting materials in biosynthesis reactions, such as the production of amino acids, fatty acids and other compounds. This explains the importance of some oxgygen in stimulating the cell function and growth. This is also in accordance with Pasteur's observations on anaerobiosis who found that anaerobically grown yeast degenerates in structure if periods of aerobiosis are not interspersed.

Electron transport pathway.

Many oxidation reactions in the cell are catalyzed by enzymes which have a cofactor or prosthetic group that accepts protons and electrons from the substrate and passes these via a series of electron accepting compounds, each of higher oxidation/reduction potential E_o' than the donor compound, to oxygen or other acceptor. The most important carriers of this electron transport pathway are:

1. Nicotinamide adenine dinucleotide (NAD). The nicotinamide portion of this nucleotide accepts hydrogen from a reduced substrate as shown in Figure 6.6b.
2. Flavin adenine monoculeotide (FMN) and flavin adenine dinucleotide (FAD). Riboflavin is the portion of these two nucleotides that accepts hydrogen from HADH or directly from the substrate. This is shown in Figure 6.6c.
3. Cytochromes b,c,a,a_3. All of these cytochromes have different E'_o values, but all of them have haem as the prosthetic group. The iron present in the haem group accepts electrons from the flavin carriers of lower E'_o and passes them to oxygen which combines with hydrogen ions to form water, the final product of oxidation. Figure 6.6d shows the reactions for the oxidation of a substrate via the electron transport pathway.

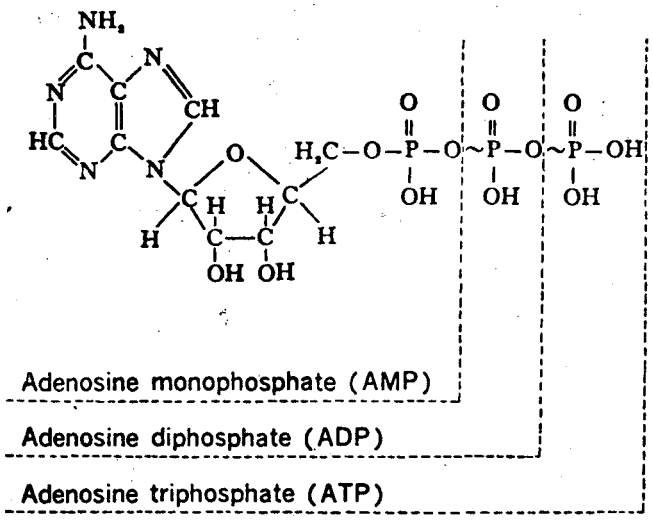

(a)

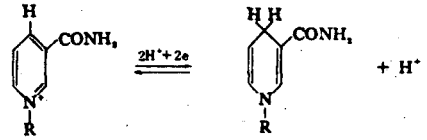

(b)

When R = ribose-phosphate-phosphate-ribose-adenine, the prosthetic group is nicotinamide adenine dinucleotide (NAD)
When R = ribose-phosphate-phosphate-ribose, 2-phosphate-adenine, the prosthetic group is nicotinamide adenine dinucleotide phosphate (NADP)

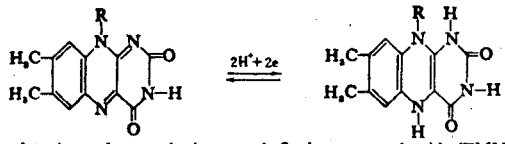

(c)

When R = ribose-phosphate, the prosthetic group is flavin mononucleotide (FMN)
When R = ribose-phosphate-phosphate-adenine, the prosthetic group is flavin adenine dinucleotide (FAD)

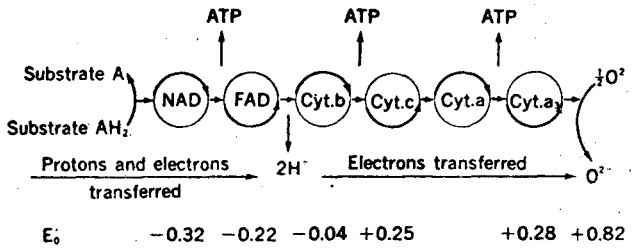

(d)

Electron transport pathway showing the oxidation/reduction potential (E_0') of the reactants; protons and electrons pass via a dehydrogenase, a flavoprotein, and cytochromes b, c, a, and a_3 to oxygen as the final electron acceptor. The sites of ATP formation are also indicated.

XBL 754-935A

Fig. 6.6. ATP (a), NADP (b), FMN (c), and electron transport pathway (d).

6.3 Regulation of glucose metabolism in yeast.

Pasteur first observed that the anaerobic fermentation of glucose to ethanol is inhibited in the presence of oxygen with a simultaneous increase in respiration. At the same time there is a decrease in glucose consumption under aerobic conditions. This is known as the "Pasteur effect." A wide variety of theories (11, 12) have been proposed in the past to explain this reversible relationship between respiration and fermentation in yeast metabolism. Most of those theories give only a partial explanation of the "Pasteur effect" phenomenon.

The most recent theory which seems to explain the "Pasteur effect" adequately is that proposed by Sols (4). This theory is based on a series of inhibition and activation feedbacks of the various key enzymes involved in the glycolytic and TCA pathway. Figure 6.7 is a schematic diagram of cellular metabolism in yeast showing the glycolytic pathway and its connection with the TCA cycle. As shown in Figure 6.7 glucose enters the cell then becomes phosphorylated to glucose-6-P then (not shown) is fructose-6-P. Fructose-6-P is again phosphorylated to fructose-1, 6-diP in the presence of the enzyme phosphofructokinase. The rest of the glycolytic pathway is abbreviated (not shown) until pyruvate, at which point pyruvate is converted to acetaldehyde (not shown) plus CO_2 and then acetaldehyde to

ethanol. Both CO_2 and ethanol are excreted out of the cell while molecular oxygen O_2 diffuses inside the cell reaching the respiratory enzymes. Then pyruvate enters the TCA cycle and, also shown schematically, are the products used in the cellular biosynthesis of fats, proteins, and nucleic acids. The two feedback mechanisms are inhibition depicted with dotted line and - sign, while activation is shown with solid line and + sign.

The enzyme phosphofructokinase that catalyzes the reaction fructose-6-P to fructose-1, 6-diP can be inhibited by ATP and citrate produced in the TCA cycle. While ammonium ion NH_4^+ and adenosine monophosphate (AMP) tend to activate phosphofructokinase. As mentioned earlier 38 ATP are produced per mole of glucose metabolized under aerobic conditions as opposed to 2ATP in the absence of oxygen. This pool of ATP produced under aerobic conditions inhibits phospho-fructokinase resulting in the accumulation of glucose-6-P which in turn inhibits the enzyme responsible for the active transport of glucose through the cell membrane. This explains why under aerobic conditions the cell needs less glucose to produce the necessary ATP than under anaerobic conditions. Also shown in Figure 6.7 is the activation by AMP on the enzyme isocitrate dehydrogenase which catalyzes the reaction

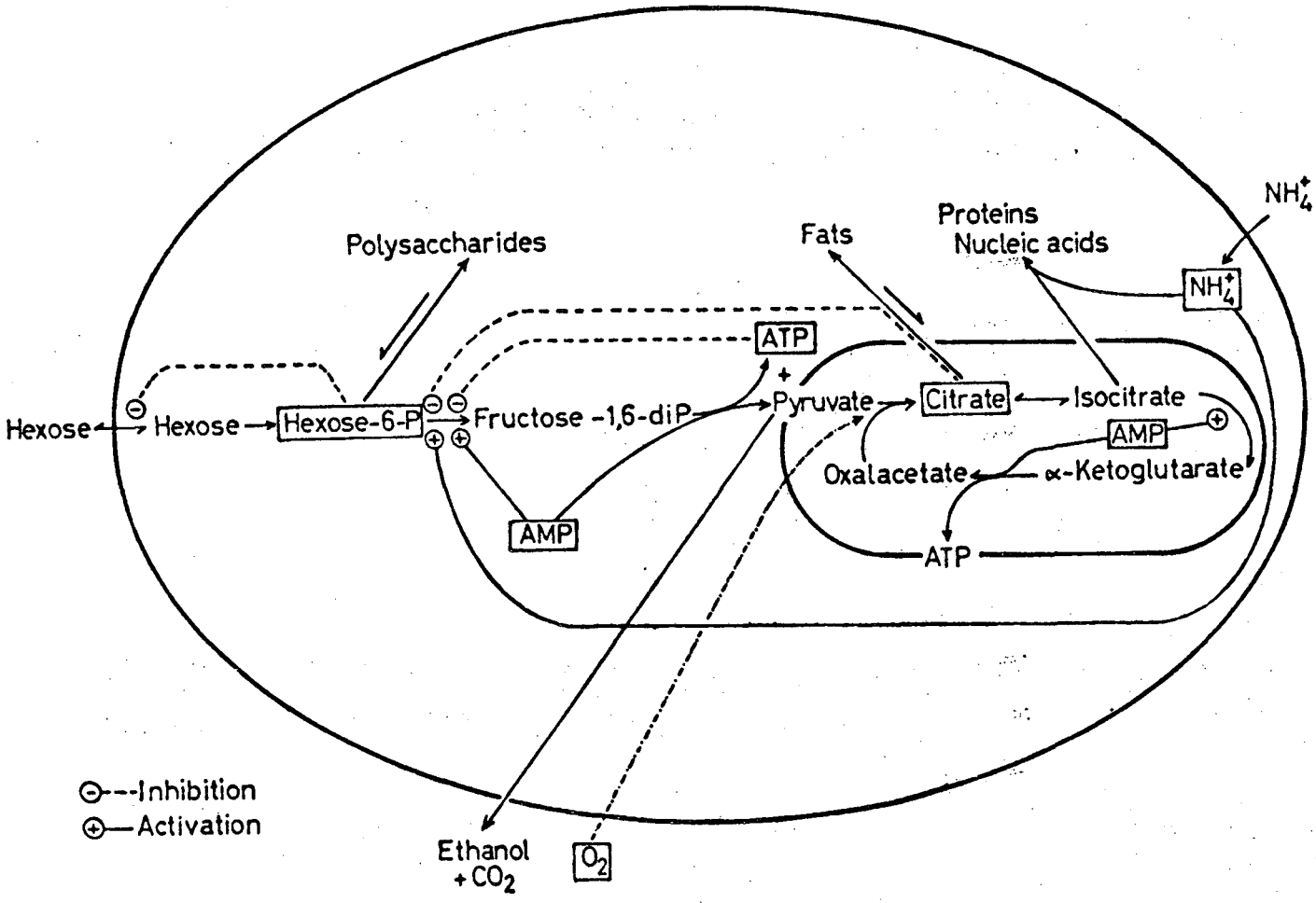

Schematic diagram of cellular metabolism.

XBL 752-266

Fig. 6.7. Proposed inhibition-activation model in yeast metabolism. After Sols (4).

isocitric acid to oxalosuccinic acid (not shown) in the TCA cycle. This sequential feedback inhibition along the main series of pathways of glucose degradation affords a fine and fast adjustment to the metabolic requirements for both energy and biosynthetic precursors. As mentioned earlier, ammonium ions NH_4^+ can counteract the inhibition of ATP on the enzyme phosphofructokinase. This is a competitive effect. Sols and Salas (14) found that inhibition by physiological concentrations of ATP can be reversed by NH_4^+ ions in the 5 to 50 mM range. Also, Holzer and Witt (15) have shown that the addition of an ammonium salt to glucose fermenting yeast causes a rapid increase of aerobic fermentation. This observation can be explained by the NH_4^+ ion activation of phosphofructokinase.

The Effect of Glucose

According to Holzer (12) a number of enzymes in yeast are repressed at high concentrations of glucose. On many occasions this enzymic repression by glucose serves a useful purpose. This is the case, for example, in the enzyme lactase (β-galactosidase) which cleaves lactose into glucose and galactose. Lactase is repressed when glucose is already present in the medium. At high glucose concentrations certain enzymes of the TCA cycle and respiration enzymes are repressed. Table 6.2 is a list of enzymes repressed by glucose given by Holzer

(12). Also high concentrations of glucose repress these enzymes to such an extent that the activation of these enzymes by oxygen is minimized. On the other hand the activation of enzymes by oxygen is maximized when the repression is minimized at low glucose concentrations. This antagonistic effect between glucose and oxygen concentration should be taken into consideration when explaining yeast fermentation results.

Table 6.2. Yeast enzymes repressed by glucose.

Invertase
Lactase
Isocitrate lyase
Malate synthase
β-glucosidase
Isocitrate dehydrogenase
Succinate dehydrogenase
Cytochrom c-oxidase
DPNH-cytochrome c-oxidoreductase
DPNH-oxidase
Alcohol dehydrogenase
Malate dehydrogenase

Among the enzymes inhibited by high glucose concentrations is alcohol dehydrogenase. As mentioned earlier

this enzyme is responsible for the conversion of acetaldehyde to ethanol. Therefore, one might anticipate a decrease in the rate of ethanol production per cell as glucose concentration reaches high levels.

Moss et al. (16) studied the antagonistic effect of glucose and oxygen in the growth of Saccharomyces carlsbergensis, a yeast used in brewing. They used a 5 liter fermentor at steady-state operating conditions, pH = 5 and conducted two sets of experiments at high and low glucose concentrations while varying oxygen concentration. When high glucose feed concentrations of 100 and 136 gm. glu/lit were used, corresponding to 27 and 37.5 gm. glu/lit inside the fermentor, then metabolism was predominantly by ethanolic fermentation and increasing oxygen concentration had no effect even when oxygen was at its saturation concentration. On the other hand, at low glucose feed concentrations of 20.2 and 24.1 gm. glu/lit, corresponding to 0.023 and 1.49 gm. glu/lit inside the fermentor, oxygen played an important role in the relative distribution of glucose between ethanolic and aerobic fermentation. Under low glucose concentration conditions they found that when oxygen concentration was 0.01 saturation then 0.8 of intake glucose metabolism was by ethanolic fermentation while at oxygen concentration near saturation glucose metabolism was 0.98 aerobic. In addition, the effect

of high glucose concentration and oxygen on cytochromes of Saccaromyces carlsbergensis was studied. It was found that cyt aa_3 varied directly with increasing oxygen concentration at low glucose concentration. However, at high glucose concentrations cyt aa_3 concentration was reduced and increasing oxygen concentration had no effect. Similarly the b type and c type cytochromes were depressed by high glucose concentrations and increasing oxygen did not have any any effect.

In view of the fact that at low glucose concentrations oxygen plays a vital role in the production of ethanol and in activating many enzymes in the yeast cell, Aiba et al. (17) used a respiration deficient yeast strain to study ethanol inhibition kinetics. This allows the study of ethanol inhibition on the yeast enzymes without the activating effect of oxygen.

6.4 A Brief Summary of Fermentation Kinetics.

The growth of microorganisms is autocatalytic in nature so that the growth rate is proportional to the number present at any time t. The constant of proportionality is called the specific growth rate and designated by μ.

$$\frac{dx}{dt} = \mu x \qquad 6.4.1$$

where:

x = concentration of microorganisms, gm/lit.

t = time, hr.

μ = specific growth rate, hr^{-1}.

Monod (30) proposed an empirical model which relates the specific growth rate μ with the concentration of growth limiting substrate.

$$\mu = \frac{\mu_{max} S}{K_s + S} \qquad 6.4.2$$

where:

μ_{max} = maximum specific growth rate, hr^{-1}

K_s = saturation constant, gm/lit.

S = concentration of growth-limiting substrate, gm/lit.

This model is analogous to the Michaelis and Menten (31) theoretical model developed for enzyme kinetics.

In batch growth μ is a function of time except for the so-called exponential growth period when $\mu = \mu_{max}$,

the growth of microorganism is not limited by any of the nutrients present. The specific growth rate μ is related to the mass-doubling time t_d which is the time required to double the cell mass of a growing microorganism.

$$t_d = \frac{\ln 2}{\mu} = 0.693/\mu \qquad 6.4.3$$

The following yields are often used in batch and continuous fermentation to characterize the efficiency of conversion of a substrate to cell mass or other products.

$$Y_{X/S} \equiv \frac{\Delta X}{-\Delta S} \qquad 6.4.4$$

where:

$Y_{X/S}$ = overall cell mass to substrate yield factor, dimensionless.

ΔX = cell mass produced, gm/lit.

ΔS = substrate consumed, gm/lit.

$$Y_{P/S} \equiv \frac{\Delta P}{\Delta S} \qquad 6.4.5$$

where

$Y_{P/S}$ = overall product to substrate yield factor, dimensionless

ΔP = product formed, gm/lit

$-\Delta S$ = substrate consumed, gm/lit.

$$Y_{P/X} \equiv \frac{\Delta P}{\Delta X} \qquad 6.4.6$$

where:

$Y_{P/X}$ = overall product to cell mass yield factor, dimensionless.

Certain substrates, especially those utilized for energy, are also involved in cell maintenance. For example, a cell can use glucose for endogenous respiration without cell growth. Therefore, especially at low glucose concentrations the yield expression must also include a factor to account for utilization of the substrate for cell maintenance. Under those conditions the total substrate utilized is equal to the substrate utilization for cell growth and that used for cell maintenance.

$$\Delta S_T = \Delta S_G + \Delta S_M \qquad 6.4.7$$

where

ΔS_T = total substrate used, gm/lit

ΔS_G = substrate used for cell growth, gm/lit

ΔS_M = substrate used for cell maintenance, gm/lit.

If $(\Delta S)_M = 0$ then $Y_{X/S}$ is constant and independent of specific growth rate μ. However, if $(\Delta S)_M > 0$ then $Y_{X/S}$ is not constant but a function of μ.

We define Y_G as the yield factor for cell growth and is given by equation 6.4.8.

$$Y_G = - \frac{(\frac{dx}{dt})_G}{(\frac{ds}{dt})_G} = - \frac{(\mu X)}{(\frac{ds}{dt})_G} \qquad 6.4.8$$

where G stands for cell growth.

Also the overall cell yield factor $Y_{X/S}$ is based on the total amount of substrate utilized and is given by equation 6.4.9.

$$Y_{X/S} = - \frac{(\frac{dx}{dt})_G}{(\frac{ds}{dt})_T} = - \frac{(\mu X)}{(\frac{ds}{dt})_T} \qquad 6.4.9$$

where $(\frac{ds}{dt})_T$ is the rate of utilization of total substrate. Furthermore, we assume that the rate of substrate utilization for maintenance is proportional to cell concentration,

$$(\frac{ds}{dt})_M = - mX \qquad 6.4.10$$

where m = specific rate constant of substrate uptake for cellular maintenance, hr^{-1}.

Differentiate equation 6.4.7 with respect to time t.

$$(\frac{ds}{dt})_T = (\frac{ds}{dt})_G + (\frac{ds}{dt})_M \qquad 6.4.11$$

Substitute equations 6.4.8, 6.4.9 and 6.4.10 into 6.4.11.

$$- \frac{1}{Y_{X/S}} \mu X = - \frac{1}{Y_G} \mu X - mX \qquad 6.4.12.$$

or rearranging

$$\frac{1}{Y_{X/S}} = \frac{m}{\mu} + \frac{1}{Y_G} \qquad 6.4.13$$

According to equation 6.4.13 if $\frac{1}{Y_{X/S}}$ is plotted against $\frac{1}{\mu}$ one should obtain a straight line with slope m and intercept $\frac{1}{Y_G}$. This linear plot is used as a test to check for the presence of endogenous metabolism in a growing cell culture.

Formation of Product

A wide variety of models have been proposed for the production of metabolic products. Three of these models have found wide use in expressing the behavior of simple fermentation systems.

1. Growth-associated model.
2. Nongrowth associated model.
3. Combined model.

In the first case the rate of product formation is related to the rate of cell growth according to equation 6.4.14.

$$\frac{dP}{dt} = \alpha \frac{dX}{dt} \qquad 6.4.14$$

where α = stoichiometric constant for the stoichiometric conversion of substrate to a single product P.

When the rate of product formation depends only on the

cell concentration then the nongrowth associated model is given by equation 6.4.15

$$\frac{dP}{dt} = \beta X \qquad 6.4.15$$

where

β = proportionality constant, hr^{-1}.

The constant β is similar to enzyme activity and can be thought of as representing so many units of product-forming activity per mass of cells.

The combined model incorporates both equations 6.4.14 and 6.4.15

$$\frac{dP}{dt} = \alpha \frac{dX}{dt} + \beta X \qquad \text{or}$$

$$\nu \equiv \frac{1}{X} \frac{dP}{dt} = \alpha\mu + \beta \qquad 6.4.16$$

where

ν = specific rate of product formation gm. product/ gm cell hour.

According to equation 6.4.16, if ν is plotted against μ one should get a straight line with slope α and intercept β.

Luedeking and Piret (32) first used the combined model to express the productivity of lactic acid fermentations. Later Aiyar and Luedeking (27) used the same model to correlate batch anaerobic data of alcohol fermentation.

Continuous Fermentation

Consider a single well mixed fermentation vessel at steady-state. Fresh medium enters the fermentor at a volumetric flow rate of F lit/hr and substrate concentration S_0 gm/lit. The fermentor has a volume V_L and the substrate cell and product concentrations inside the fermentor are S, X, and P respectively. The effluent stream has the same flow rate F lit/hr. We define dilution rate $D = F/V_L$ which is the reciprocal of residence time.

At steady-state we have the following cell mass balance.

Rate in - Rate out + Rate of generation = 0

$$0 - FX + \mu X V_L = 0 \qquad 6.4.17$$

diving by V_L and noting that $F/V_L = D$ we have

$$-D + \mu = 0 \qquad \text{or}$$

$$\mu = D \qquad 6.4.18$$

Therefore, at steady-state the dilution rate D is equal to the specific growth rate μ. However, when $D \geq \mu_{max}$ then washout will occur because the rate of removal of cell from the fermentor will be greater than the maximum possible rate of cell generation within the fermentor.

A product mass balance yields

$$0 - FP + \nu X V_L = 0 \qquad 6.4.19$$

divide by V_L and solve for ν

$$\nu = \frac{DP}{X} \qquad 6.4.20$$

Equation 6.4.20 gives ν at steady-state conditions. Similarly, the cell and product yield factors $Y_{X/S}$ and $Y_{P/S}$ are given by equations 6.4.21 and 6.4.22.

$$Y_{X/S} = \frac{\Delta X}{S_0 - S} \qquad 6.4.21$$

$$Y_{P/S} = \frac{\Delta P}{S_0 - S} \qquad 6.4.22$$

6.5 Experimental Methods.

During the course of yeast growth experiments the following variables were measured:

Glucose concentration, ethanol concentration, cell mass concentration, oxygen concentration, pH and temperature.

6.5.1 Experimental apparatus.

A 1-liter capacity Fermentation Design, Inc. fermentor was used for both batch and continuous experiments. Temperature was controlled by means of a stainless stell coil inside the fermentor and connected to a constant temperature water bath. A speed controlled magnetic stirrer bar at the bottom of the fermentor jar provided the necessary mixing needed during fermentation. Figure 6.8 is a schematic flow diagram of the fermentor system used in continuous growth experiments.

A 20-liter bottle was used for the preparation of the medium and then sterilized in an autoclave for one hour at 121°C. Pure sterile medium was fed to the top of the fermentor at a constant rate by means of a Sigmamotor peristaltic pump.

Air supply was controlled by means of a needle valve, and a rotameter with a pressure gauge were used to measure flow rates. After the rotameter the air was sterilized by passing through a glass wool fiber filter

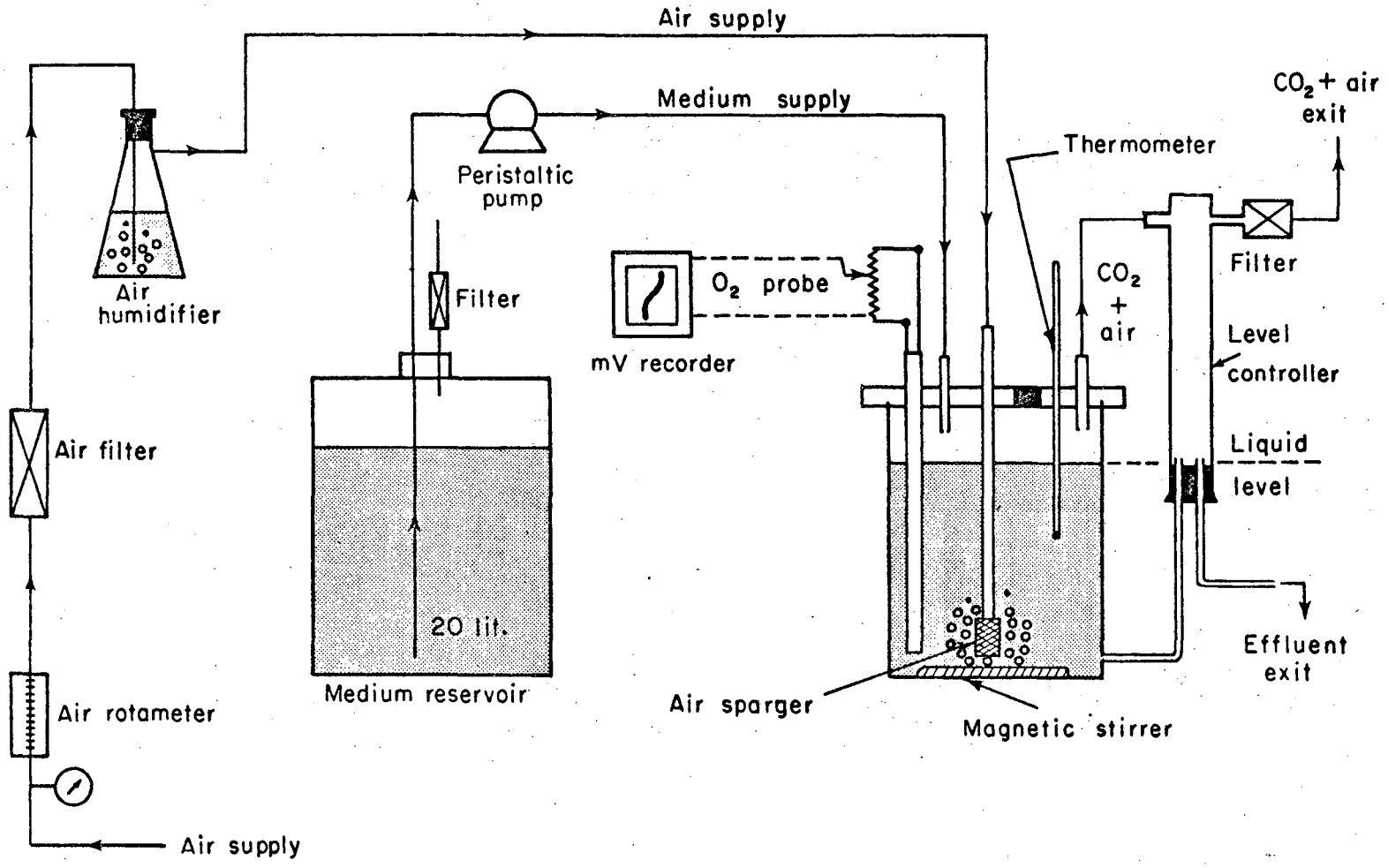

XBL754-2819

Fig. 6.8. Schematic flow diagram of the C.S.T. fermentor experimental apparatus.

pad then humidified in a bottle filled with sterile distilled water. Sterile and humidified air was then introduced in the fermentor through a fine glass sparger located near the bottom of the fermentor. The magnetic stirrer was used to break up the air bubbles and provide uniform aeration inside the fermentor. Oxygen mass transfer from the air bubbles to the liquid phase was controlled by changing the speed of the magnetic stirrer and/or the air flow rate. The liquid volume inside the fermentor was controlled by adjusting the height of a level controller which is a small tube connected to the fermentor through a flexible rubber tube. To insure an efficient level control the pressure at the top of the fermentor, due to CO_2 and air, was the same as that inside the level controller. This was done by means of a rubber tube connection between the top of the fermentor and the level controller. The CO_2 formed and air came out at the top of the fermentor, then through the top of the level controller and out into atmosphere through a glass fiber sterilizer pad. At steady-state conditions the rate of liquid inflow at the top of the fermentor equals the rate of outflow at the bottom of the level controller as shown in Figure 6.8. The liquid volume inside the fermentor was different for different experiments varying between 680 to 820 ml. Provision was made for an oxygen probe which was connected to a voltage recorder, and a thermometer.

In a typical experiment the whole apparatus was sterilized in an autoclave at 121°C for 30 minutes. The fermentor was then filled with fresh sterile medium and inoculated with 40 ml. of dilute cell suspension made by dissolving in sterile water about two loops of yeast taken from a slant. A sterilized syringe was used to inoculate the fermentor and also to withdraw samples during fermentation. At steady-state conditions for a given dilution rate a 10-ml. sample was withdrawn from the fermentor aseptically then centifuged and the supernatant was used for glucose and ethanol analysis. Samples were examined under a light microscope at x1250 to check for the presence of possible contaminating microorganisms.

6.5.2 Cell concentration.

To determine the cell concentration the optical density (absorbance) of a sample was measured in a Fischer Electrophotometer at a wavelength of 650 mμ. This optical density was converted to cell concentration by using a calibration chart as shown in Figure 6.9. This chart shows the linear relationship between dry cell mass concentration and optical density. At cell concentrations higher than about 0.45 gm. dry wt./lit there is no linearity and the samples must be properly diluted before measurement.

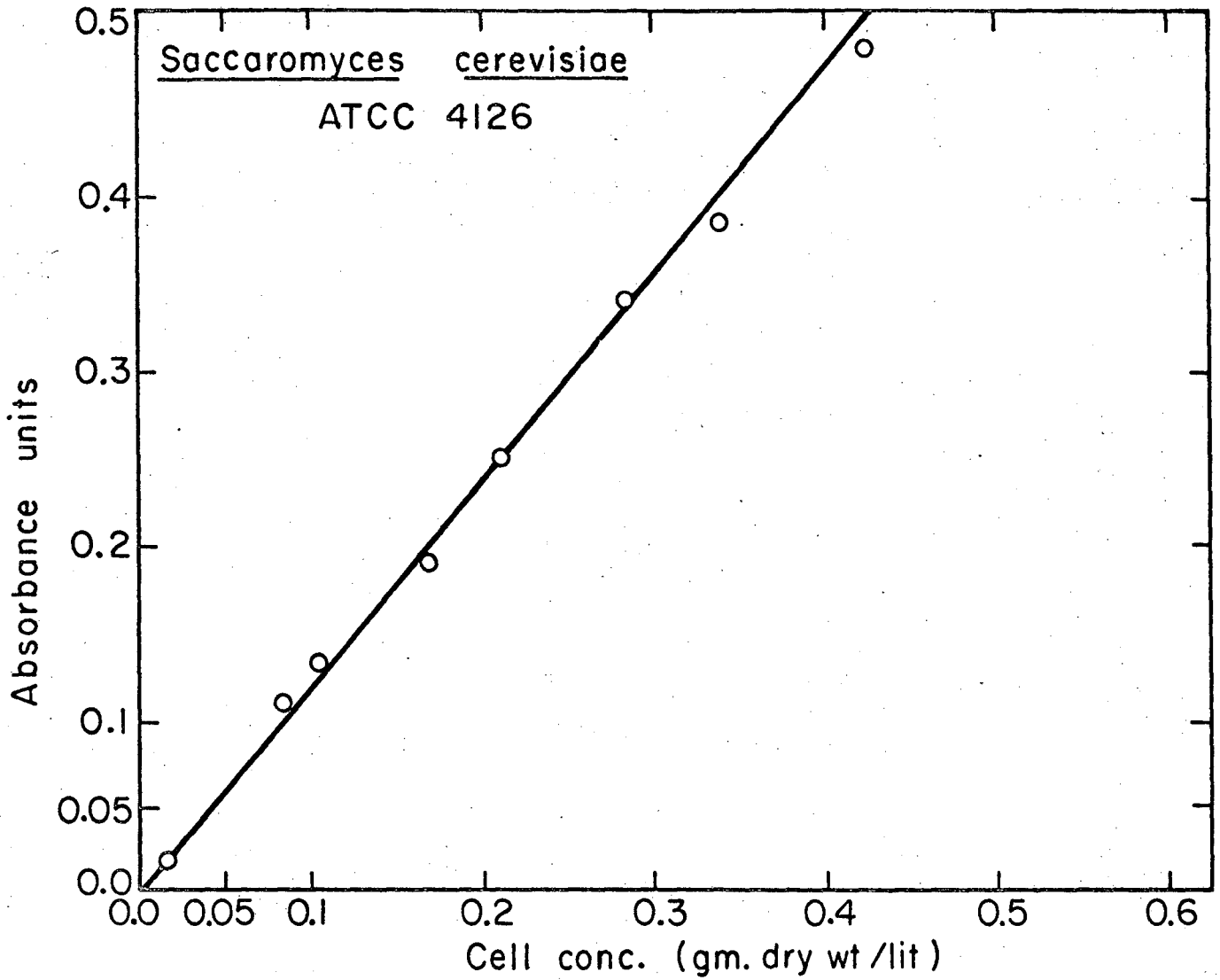

Fig. 6.9. Calibration curve for cell concentration of Saccharomyces cerevisiae ATCC 4126. XBL754-2844

6.5.3 Glucose concentration.

Glucose was determined by the dinitrosalicylic acid (DNS) method (18). One ml. of sample was added to 3 ml. of DNS reagent in a test tube mixed and placed in a boiling water bath for five minutes. Then the tube was removed from the bath and cooled to room temperature and diluted with distilled water to a final volume of 24 ml. The diluted sample was well mixed and the absorbance was measured with a Beckman DU-2 spectrophotometer at 600 mμ against an appropriate DNS reagent and water blank. The absorbance reading was converted to glucose concentration by means of a standard calibration curve prepared with known concentrations of anhydrous dextrose (Mallinckraft chemicals). The standard curve is shown in Figure 6.10.

6.5.4 Ethanol concentration.

Ethanol was measured by gas chromatography. Standard solutions of varying ethanol concentrations were first run through the chromatograph in order to obtain a standard calibration curve which correlated ethanol concentrations against areas. Then the unknown samples were run and ethanol concentrations found from chromatogram areas. Figure 6.11 shows a typical standard calibration curve. An Aerograph 1520 G-L Chromatograph was used with a 6-foot long 1/4-inch column packed with chromosorb W-acid wash type 60-80 mesh.

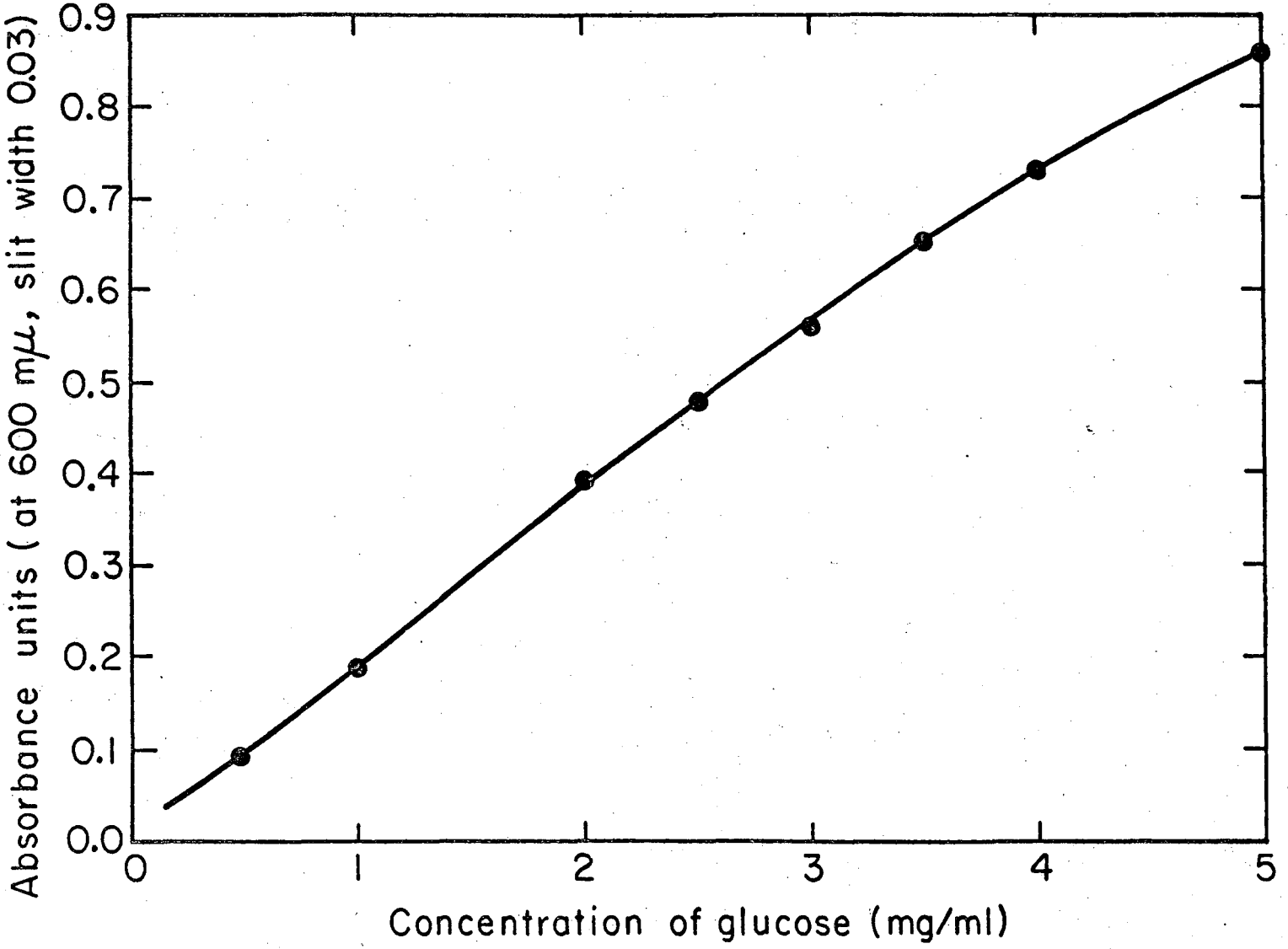

Fig. 6.10. Calibration curve for concentration of glucose by DNS method.

XBL754-2834

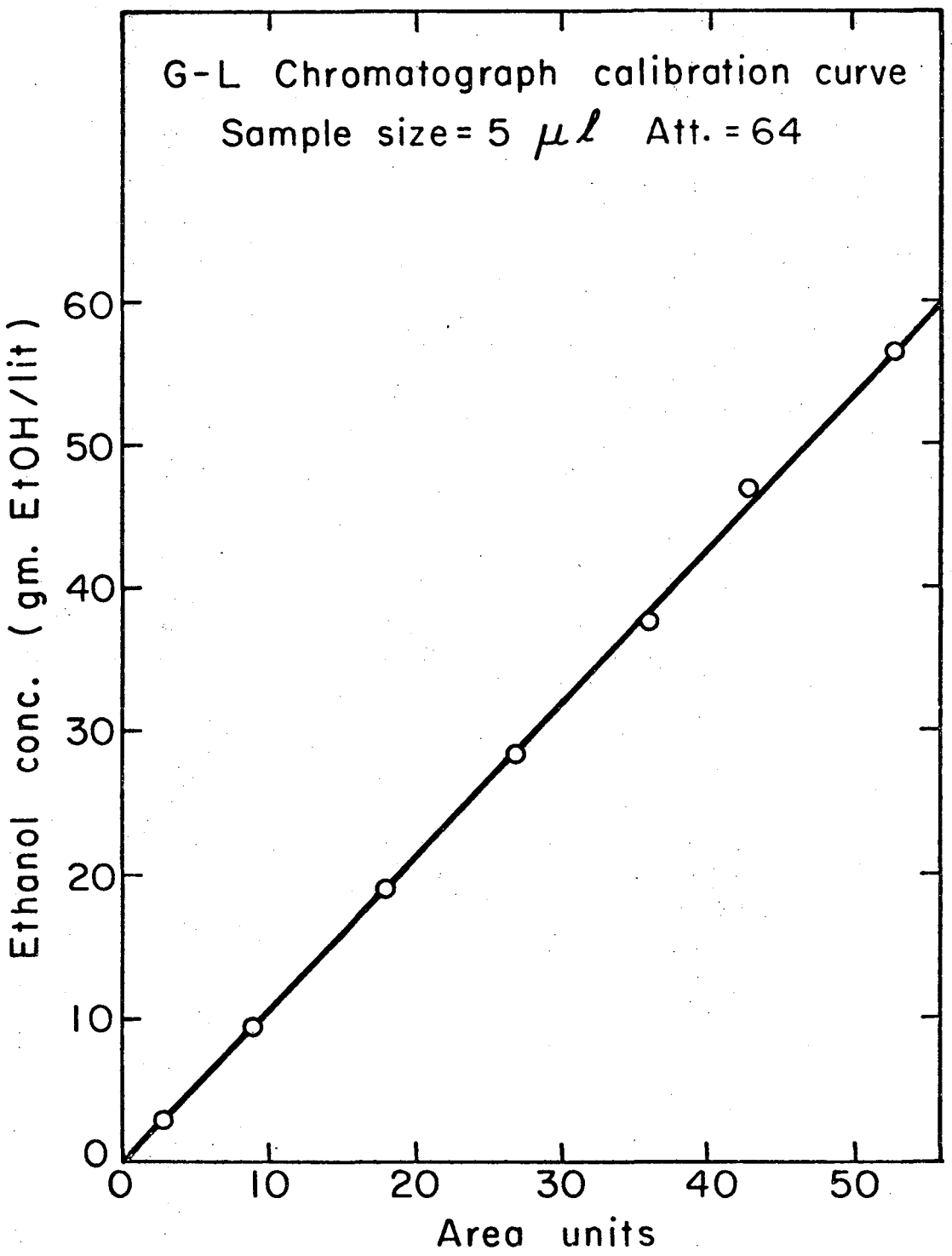

Fig. 6.11. Calibration curve for G-L chromatographic determination of ethanol concentration.

6.5.5 Oxygen concentration.

A galvanic type of electrode was used to measure the partial pressure of oxygen in the liquid phase. This probe is of the same type as that employed by Johnson et al (20) and Mancy et al (19). In this probe the silver anode and lead cathode are placed together with the supporting acetate electrolyte inside a semi-permeable protective Teflon membrane. Molecular oxygen diffuses through the membrane and is spontaneously reduced at the silver cathode and the current generated gives rise to a potential drop across a variable resistance placed outside the probe. The rate of electric current produced by the probe is proportional to the rate of oxygen diffusion through the Teflon membrane. In the presence of an acetate electrolyte the following half reactions occur in the probe:

At the silver cathode

$$O_2 + 2H_2O + 4e^- \longrightarrow 4OH^- \xrightarrow[4H^+]{} 2H_2O$$

At the lead anode

$$4Pb + 4Ac^- \longrightarrow 4PbAc + 4e^-$$

the overall reaction is:

$$O_2 + 2H_2O + 4Ac^- + 4Pb \longrightarrow 4OH^- + 4PbAc$$

At steady-state $I \propto \bar{P}_{O_2} \propto HC_L$

where:

I = current output

$\bar{P}_{O_2}$ = partial pressure of O_2 in liquid phase

H = Henry's constant

C_L = oxygen concentration in liquid phase

Robinson and Wilke (21) give a detailed analysis of the theory and operation of the oxygen probe.

Before the oxygen probe was used it was calibrated by placing it in a sulphite solution of zero oxygen concentration and pure water that was well mixed and sparged with air to insure saturation conditions at a given temperature. A 0.5M Na_2SO_3 solution containing 0.004M $CuSO_4$ was used after the solution was left for a long time to insure that all molecular oxygen in water reacts with $SO_3^{=}$. This "zero oxygen" reference solution was used at four different temperatures and the "zero" current output by the probe was measured. The results are shown in Table B.1, Appendix B. For comparative purposes the results for saturated pure water and nonaerated pure medium are also shown. Figure 6.12 shows the results for "zero" current output, Io, at different temperatures. Increase in Io with temperature is also reported by Vincent (22). The value of C_L = 57.9 μM oxygen for pure medium is in the same range

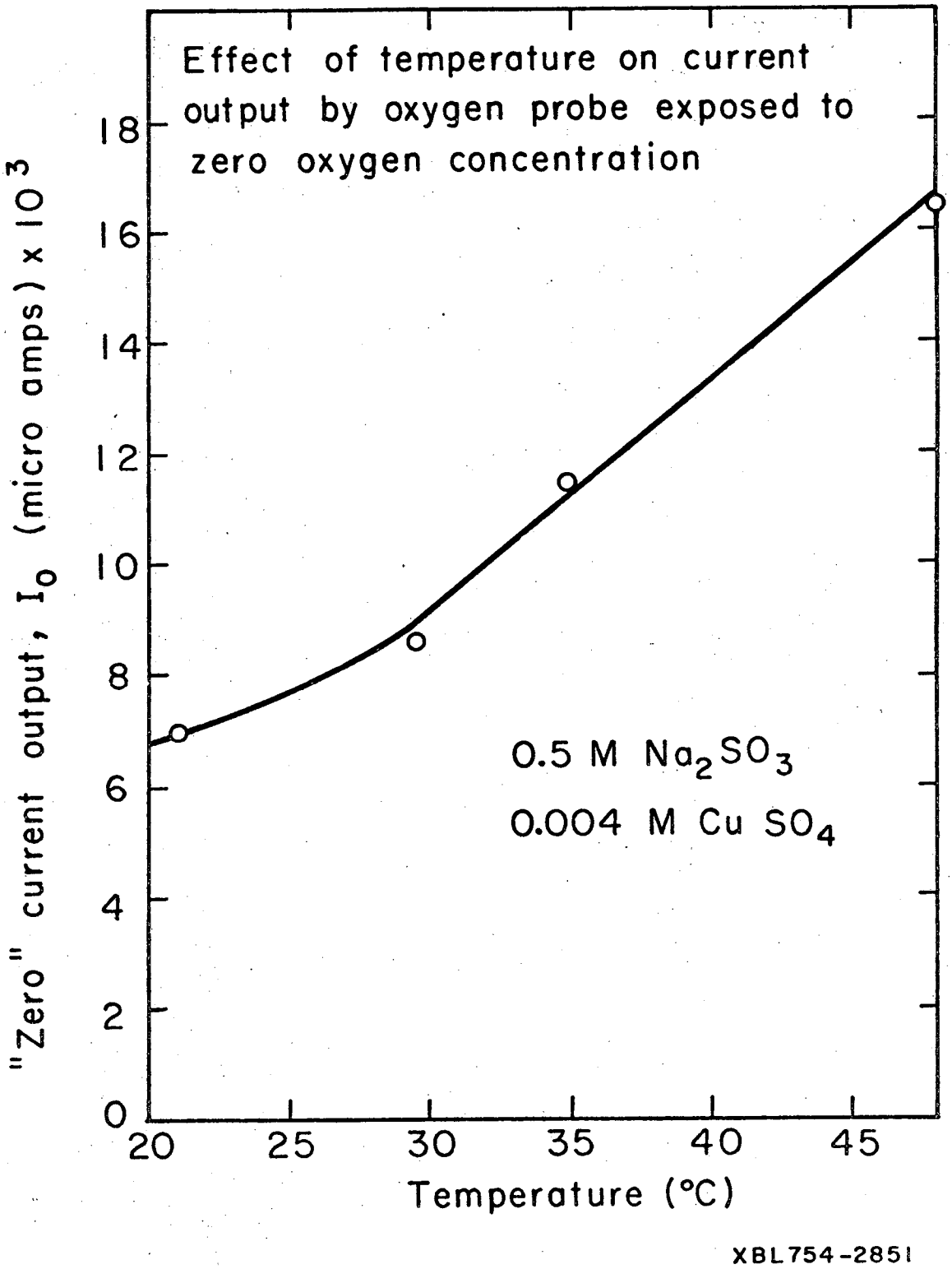

XBL754-2851

Fig. 6.12. Current output by oxygen probe exposed to zero oxygen concentration.

of oxygen concentration for pure medium of the same glucose content found by Solomons (23).

The pH of the culture was measured by a Beckman pH meter.

6.5.6 Medium composition.

The formulation of the medium used in growth experiments was based on the chemical composition of a typical yeast cell (24, 25, 26). Glucose is the energy and carbon source for yeast growth while NH_4Cl serves as nitrogen source and yeast extract is a good source of amino acids and other vitamins while the other chemicals shown in Table 6.3 are sources of minerals and salts. It was found that tap water was an adequate source of trace elements, and the formulation of a special trace elements solution was not required.

Table 6.3. Medium Composition for Saccharomyces cerevisiae ATCC #4126.

Amounts are given per liter of tap water	
Compound	Amount in gms.
Glucose*	100
Yeast extract	8
NH_4Cl	8
$Na_2HPO_4.7H_2O$	3.9
KH_2PO_4	0.5
$MgSO_4$	0.5
$CaCl_2$	0.28
Citric Acid**	4.3
Sodium Citrate**	1.25
Antifoam***	200 p.p.m.

*Glucose concentration was varied
** Citric/Citrate buffer to give pH = 4.0
*** General Electric silicone emulsion 60.

6.6 Experimental Results and Discussion.

In this section a series of continuous growth experiments is presented. Runs A, C, E and G were designed to assess the importance of glucose concentration on ethanol productivities while runs OY, OX, and Y were designed to find the effect of oxygen concentration on ethanol productivities. All experiments were conducted at 28°C and pH = 4.0±0.1. A batch run was conducted first until a certain cell density was reached. Then the continuous operation was started by continuously supplying fresh medium at a given constant flow rate. The fermentor volume was held constant while the volumetric feed rate of fresh medium was varied to accommodate different dilution rates. Steady-state was checked by sample analysis and it was found that steady-state was essentially reached after a minimum of three fermentor volume turnovers. After steady-state was reached at given dilution rate then a sample was taken from the fermentor for analyses.

6.6.1 Run A.

Approximately 20 liters of medium were prepared and autoclaved at 121°C for 45 minutes. The glucose concentration was 126.5 gm/lit and the rest of medium composition is given in Table 6.3. The medium was left to cool overnight and then it was sparged with sterile nitrogen for 14 hours to strip out most of the oxygen

present in the medium. The oxygen probe was used to measure the oxygen concentration after nitrogen sparging and was found to be 0.93 p.p.m. or 29.06 μM.

The minifermentor was first sterilized, then flushed with nitrogen and then 800 ml. of fresh sterile medium was introduced into the fermentor and inoculated. To prevent oxygen coming into the fermentor from outside nitrogen at a small flow rate was introduced, filling the empty space of approximately 200 ml. at the top of the fermentor. Therefore, the only source of oxygen was that coming from the fresh feed.

Figure 6.13 shows batch growth data where ln X is plotted against time t. The arrow indicates the point at which the constant flow of fresh medium began for the continuous operation. Figure 6.14 shows steady-state results where the cell mass, ethanol, and glucose concentrations are plotted against dilution rate D. Figure 6.15 is a plot of the overall fermentor productivity for both cell mass and ethanol against dilution rate D. Figure 6.16 is a plot of specific ethanol productivity ν against D, while Figure 6.17 shows the change in both $Y_{X/S}$ and Y_M as a function of D. Figure 6.18 is a typical plot of $1/Y_{X/S}$ against 1/D to check the presence of endogenous metabolism in yeast according to equation 6.4.13. Table 6.4 is a summary of experimental data for Run A.

Table 6.4. Summary of Data for Run A

S_0 = 126.5 gm. glucose/lit. C_{L0} = 0.93 p.p.m. pH = 4.1 T = 28°C

Dilution Rate D (hr^{-1})	Cell Mass X (gm/lit)	Glucose S (gm/lit)	Ethanol P (gm/lit)	$Y_{X/S}$	$Y_{P/S}$	Specific Ethanol Prod. ν^* (hr^{-1})	Cell Prod. DX	EtOH Prod. DP	1/D (hr)	$1/Y_{X/S}$	Rate of Glucose Uptake Rg** (hr^{-1})
0.0282	1.29	40.8	25.6	0.0151	0.30	0.558	0.0364	0.72	35.5	66.2	1.87
0.0477	1.50	56.2	20.4	0.0213	0.29	0.650	0.0716	0.972	21.0	47.0	2.24
0.09	1.28	81.6	12.0	0.0285	0.27	0.845	0.115	1.08	11.1	35.1	3.16
0.130	0.92	101.0	7.0	0.036	0.275	0.99	0.12	0.91	7.7	27.8	3.60
μ_{max} = 0.154	0	126.5	0	-	-	-	0	0	-	-	-

*ν ≡ gm. EtOH/hr. gm. cell.

**Rg ≡ gm. glucose consumed/ hr. gm. cell.

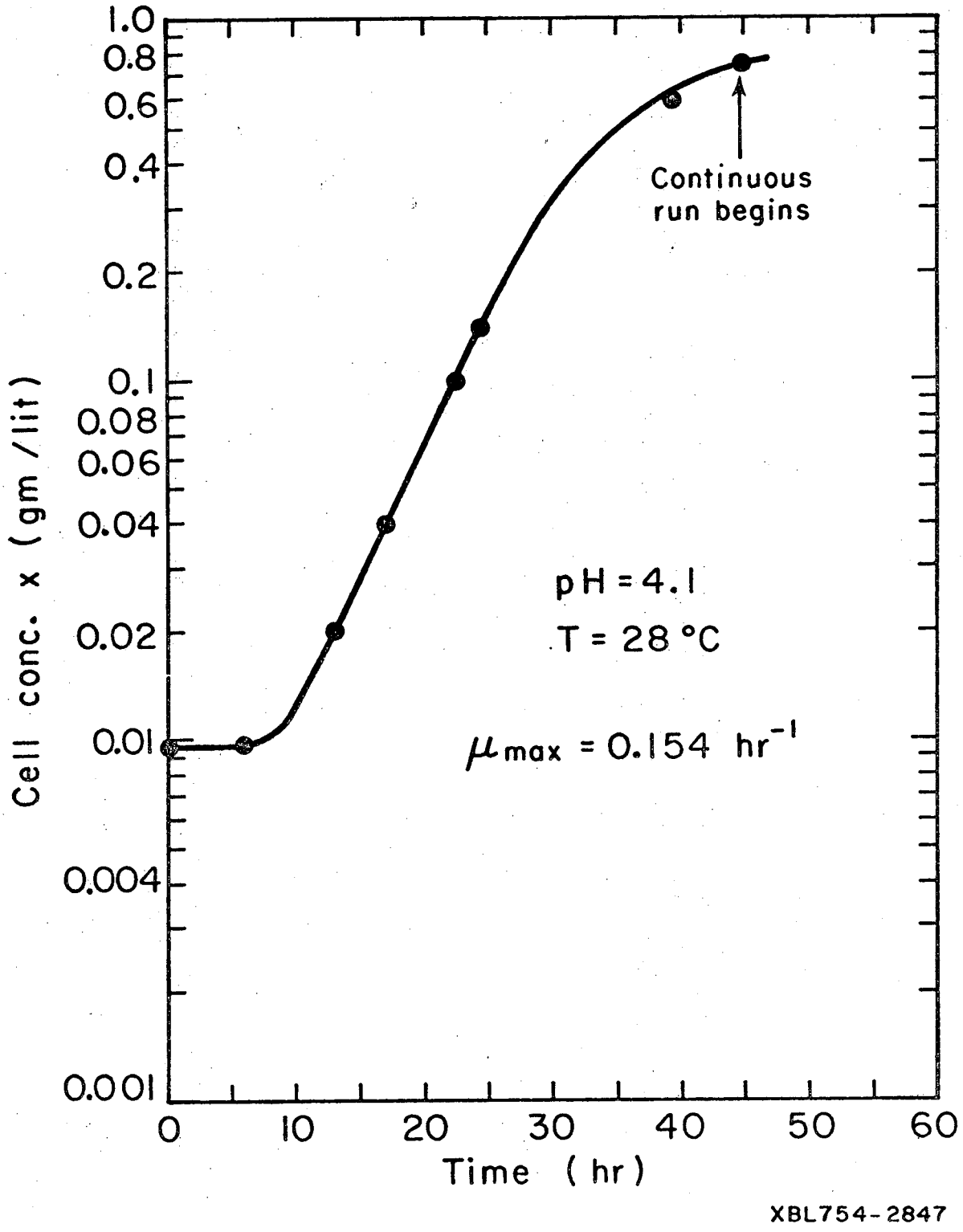

Fig. 6.13. Batch growth results for Run A.

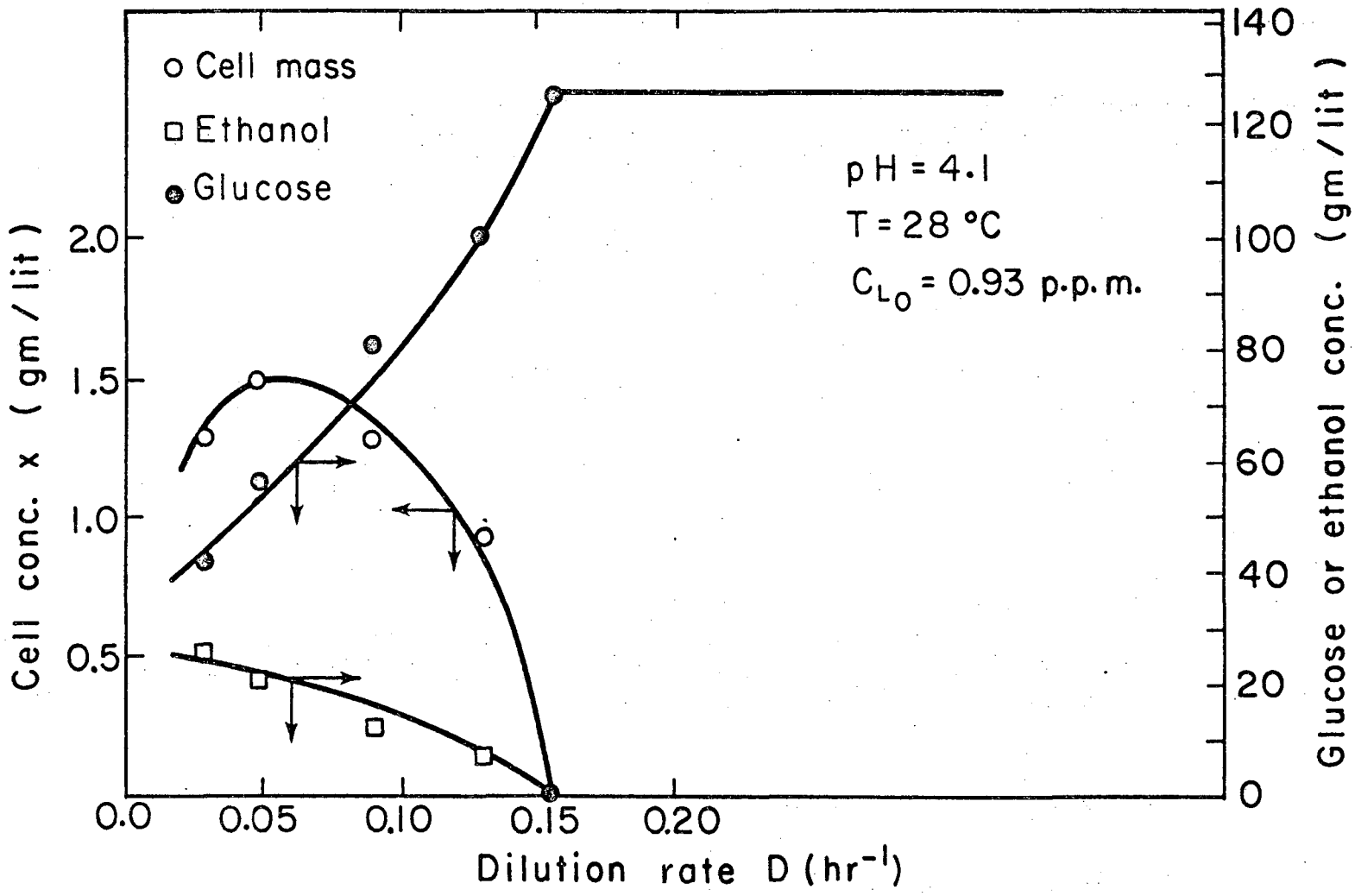

XBL754-2821

Fig. 6.14. Steady-state growth results for Run A.

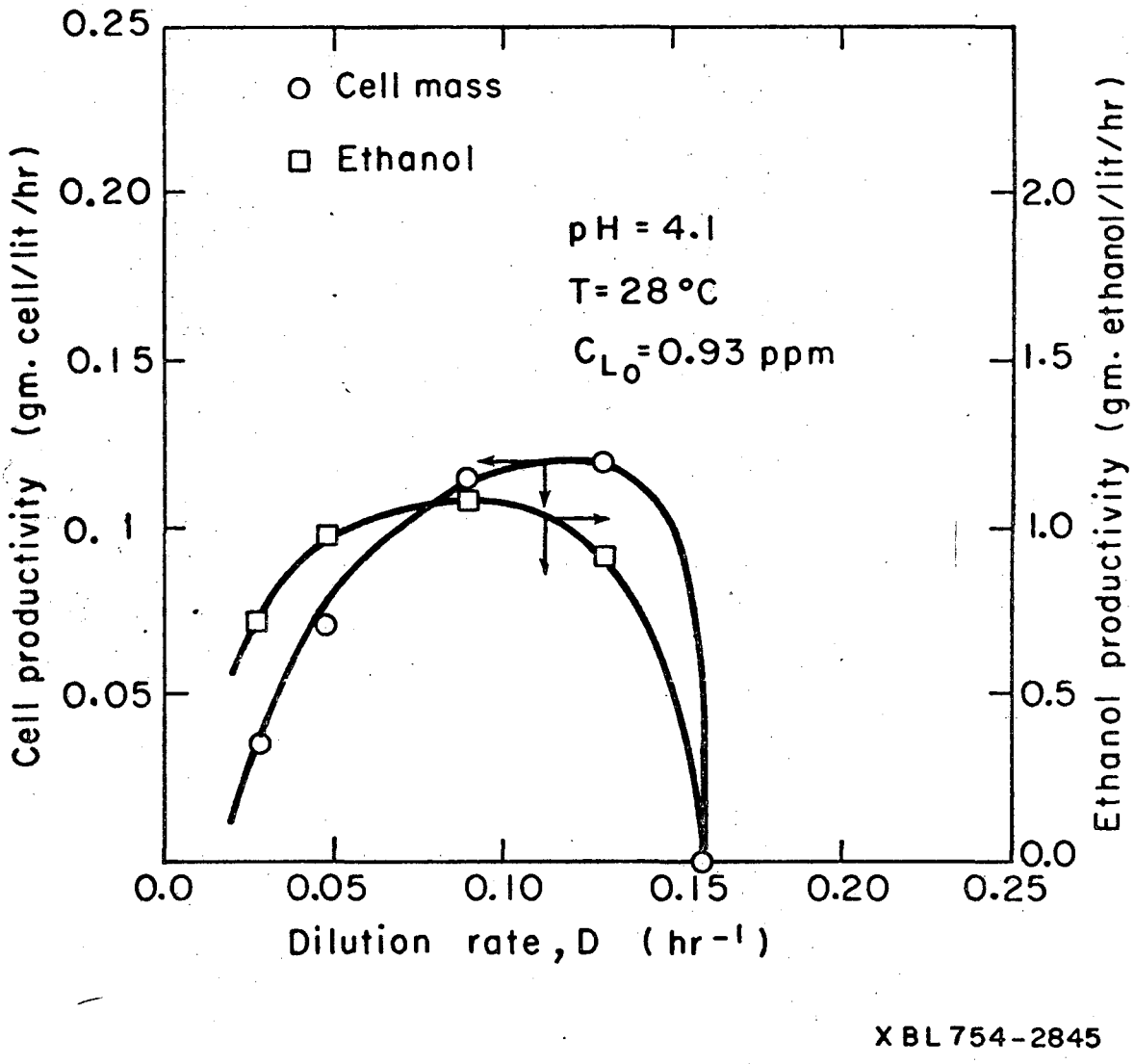

Fig. 6.15. Cell and ethanol productivity results for Run A.

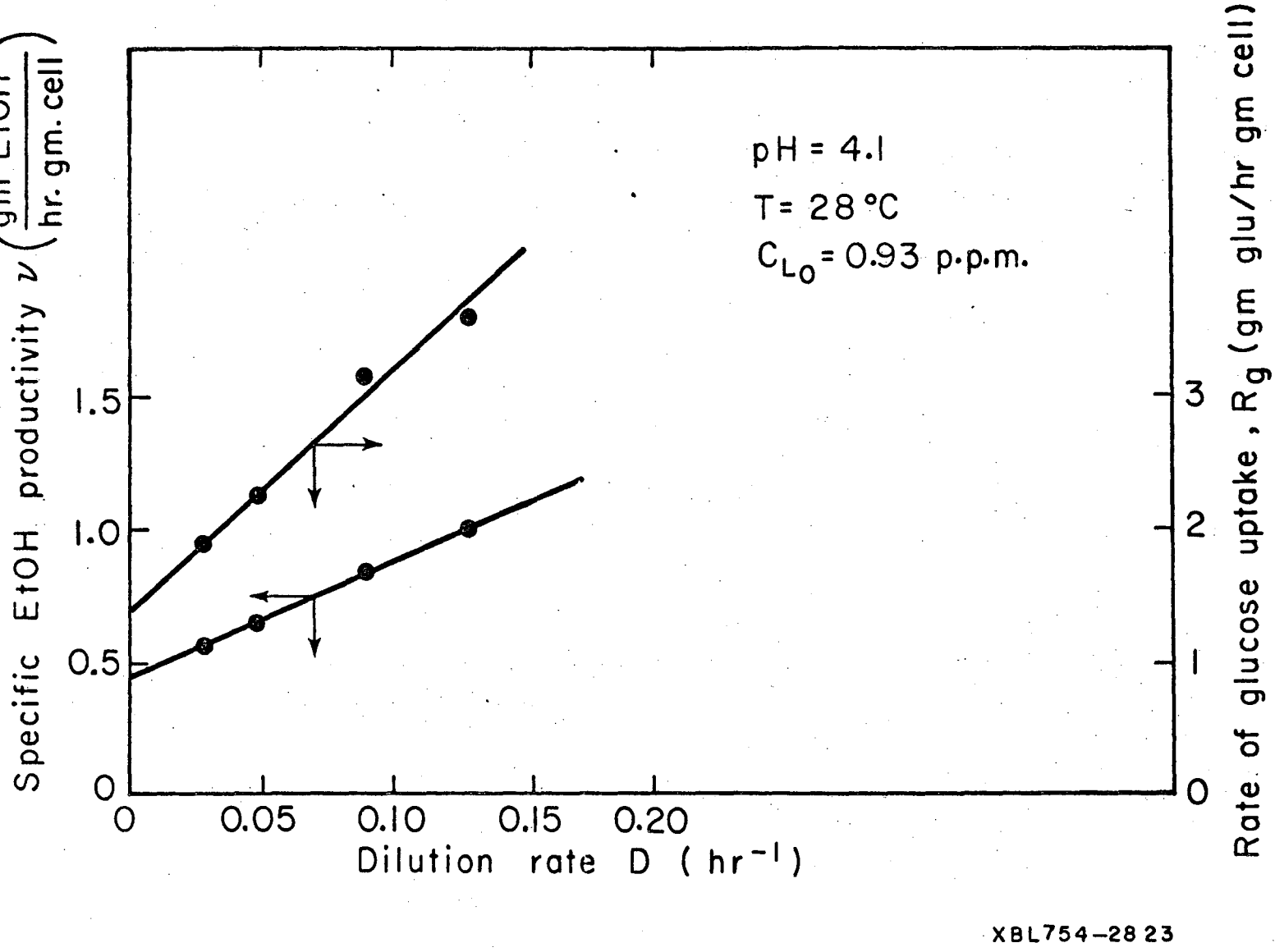

Fig. 6.16. Specific ethanol productivity and glucose uptake results for Run A.

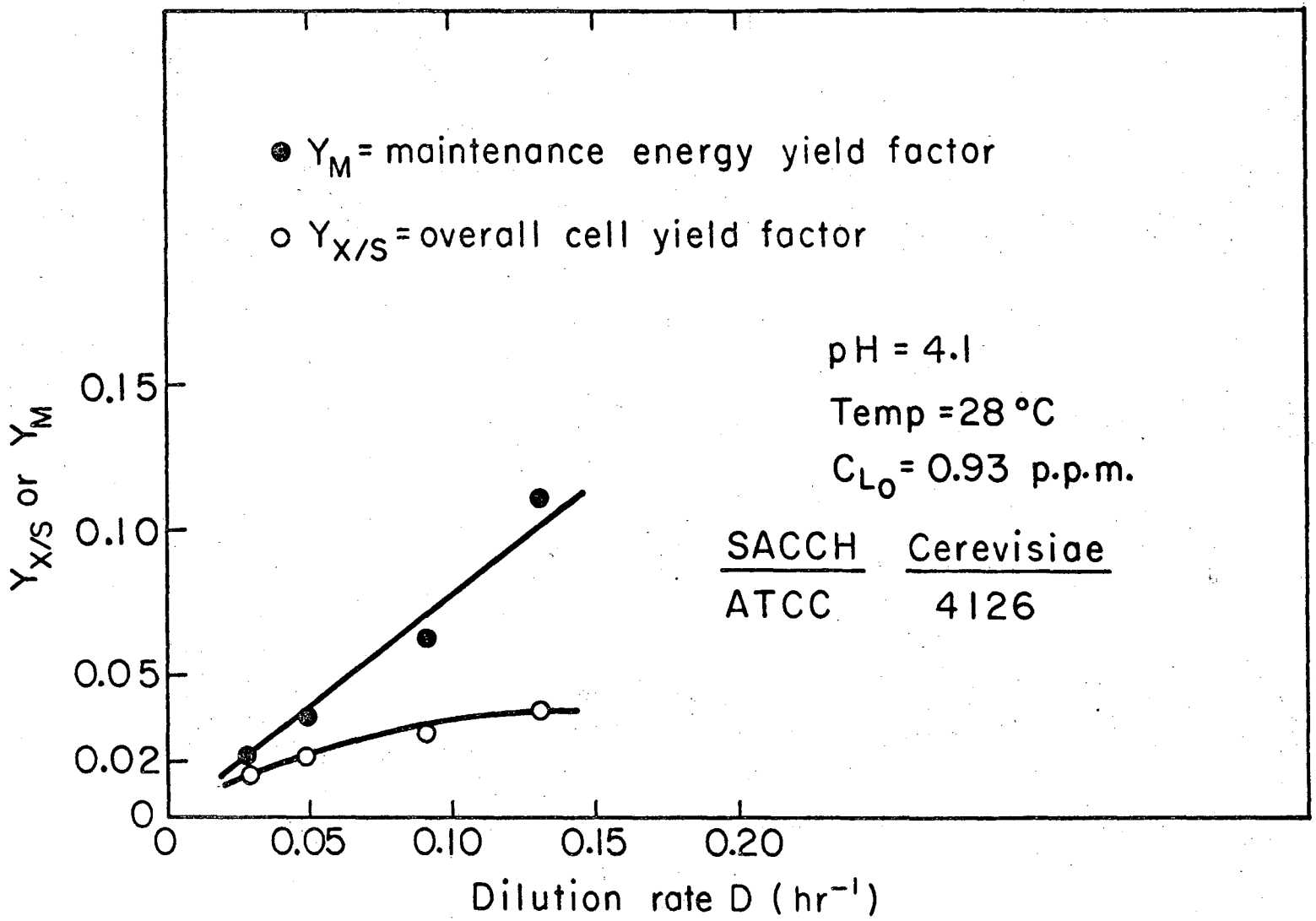

XBL754-2838

Fig. 6.17. Maintenance energy and overall cell yield factor for Run A.

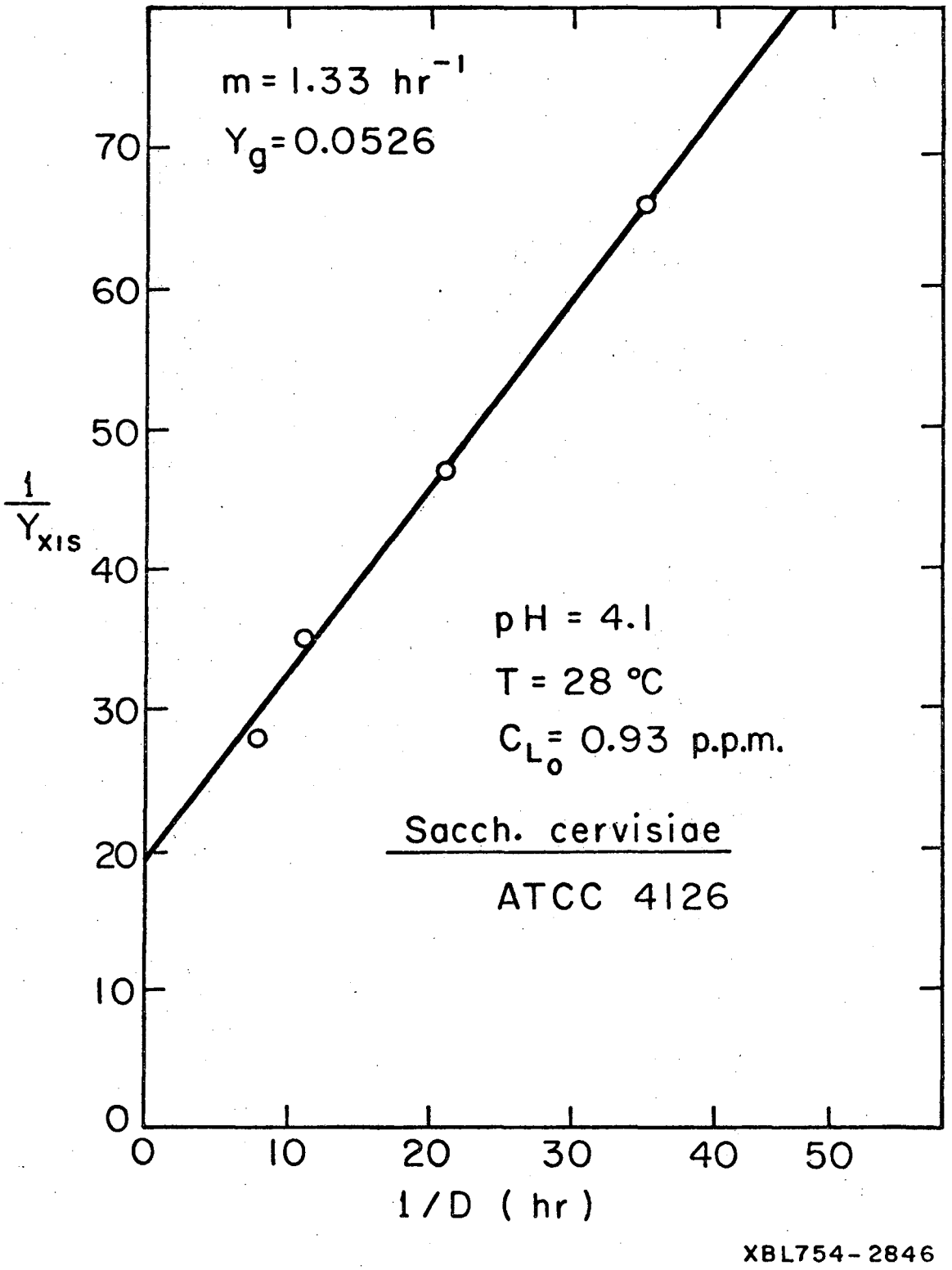

Fig. 6.18. Endogenous metabolism plot for Run A.

6.6.2 Run C.

In this run the glucose concentration was 108 gm/lit and the medium composition and sterilization conditions were the same as in run A. In order to assess the importance of oxygen in the feed as a limiting substrate the medium in this run was not flushed with nitrogen. The oxygen concentration in the sterilized medium was found to be 2.95 p.p.m. or 92.18 μM which is approximately three times greater than that in run A.

Figure 6.19 shows batch growth data. Both μ_{max} and level of cell concentration are higher than those for run A shown in Figure 6.13.

Figure 6.20 shows transient results due to a step change in dilution rate from 0.203 hr^{-1} to 0.152 hr^{-1}. As we see essentially steady-state is reached after about three fermentor volume turnovers. Figure 6.21 shows steady-state results for run C and for comparative purposes the results of run A are also included. This graph shows the effect of oxygen concentration in the feed as a limiting substrate. Both cell and ethanol concentrations are higher at the higher oxygen concentration. Figure 6.22 is a plot of cell and ethanol productivities against dilution rate. We observe that by increasing the feed concentration of oxygen by almost threefold we have approximately a threefold increase in maximum cell productivity and almost 2.5 times increase

in maximum ethanol productivity. Figure 6.23 is a plot of cell and ethanol yield constants against D. Both $Y_{X/S}$ and $Y_{P/S}$ are higher at 2.95 p.p.m. oxygen than those at 0.93 p.p.m. Figure 6.24 shows the specific ethanol productivity ν as a function of dilution rate D. The value of ν at 2.95 p.p.m. oxygen is systematically lower than that at 0.93 p.p.m. This is in agreement with the Pasteur effect as explained by Sols (4) and covered in Section 6.3. The data in Figure 6.24 correlated according to equation 6.4.16 covered in Section 6.4. At steady-state conditions $\mu = D$. The values of α and β for steady-state conditions and at different feed oxygen concentrations are given in Table 6.5. Comparison is made with the anaerobic batch data of Aiyar and Luedeking (27) at the same pH and 30°C temperature and a different Saccharomyces cerevisiae strain.

Figure 6.25 is a plot of $1/Y_{X/S}$ against 1/D for both runs A and C. This linear correlation is in accordance with equation 6.4.13, Section 6.4 and shows the effect of oxygen on endogenous metabolism. For the feed oxygen concentrations studied here the value of slope m is practically the same, i.e., 1.33 $hr.^{-1}$ while the yield constant for growth Y_g is 0.20 at 2.95 p.p.m. and 0.053 at 0.93 p.p.m. The increase in Y_g with oxygen concentration reflects similar increases in $Y_{X/S}$ with oxygen as shown in Figure 6.23. Figure 6.26 shows the

maintenance energy yield factor Y_M as a function of dilution rate D. Figure 6.26 shows that there is a linear relationship between Y_M and D and there is no appreciable difference in Y_M due to difference in feed oxygen concentration range covered here. Figure 6.27 is a comparison between $Y_{X/S}$ and Y_M at different dilution rates for run C. Table 6.6 is a summary of data for run C.

Table 6.5 Proportionality Constants for Alcoholic Fermentation

Investigator and Growth Conditions	pH	Temperature (°C)	Oxygen Concentration C_L (p.p.m.)	Slope α	Intercept β (hr^{-1})
Present work; steady-state growth	4.1	28	0.93	4.0	0.46
	4.1	28	2.95	3.33	0.45
Aiyar, Luedeking; batch anaerobic growth	4.0	30	-	0.83	0.72

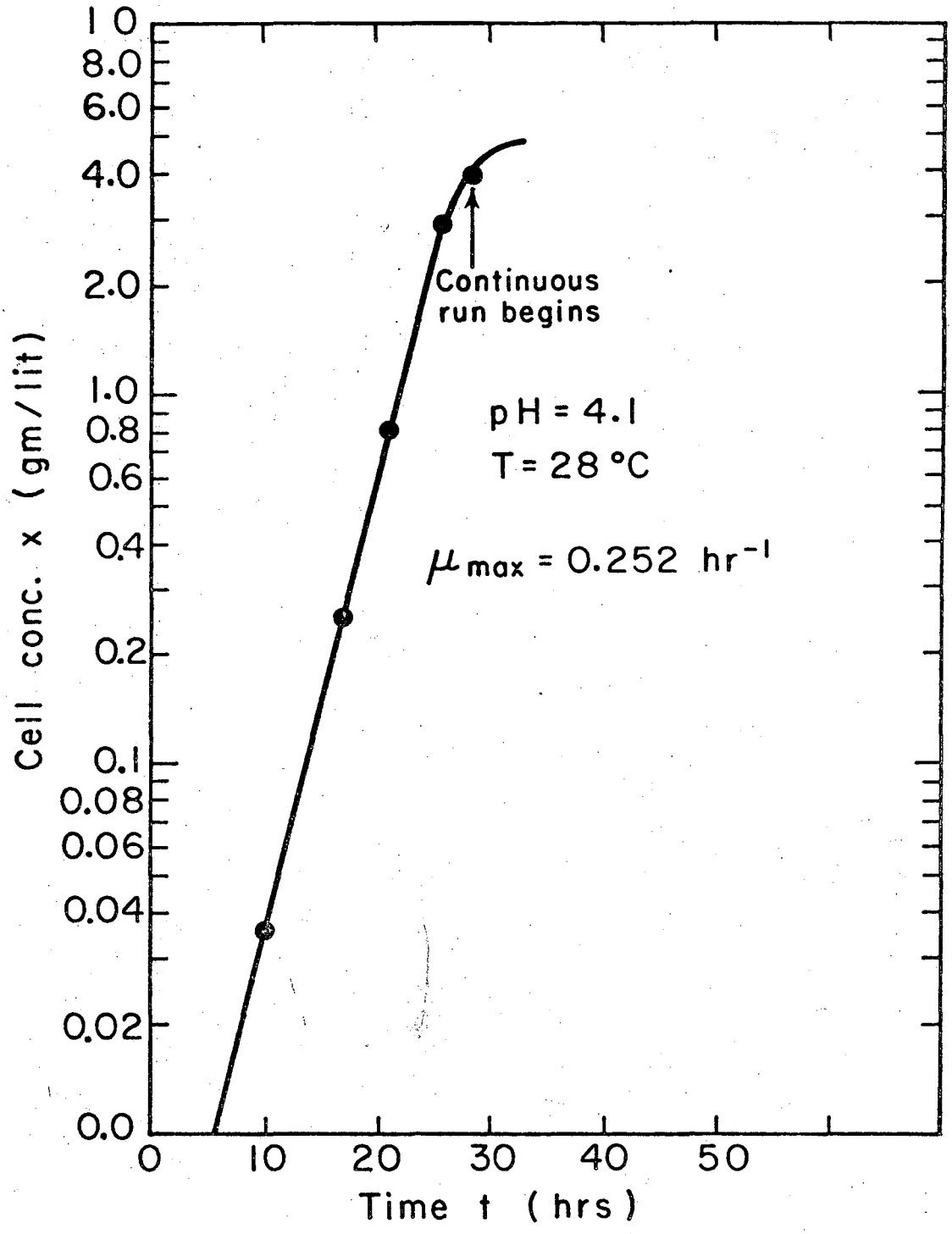

XBL754-2849

Fig. 6.19. Batch growth results for Run C.

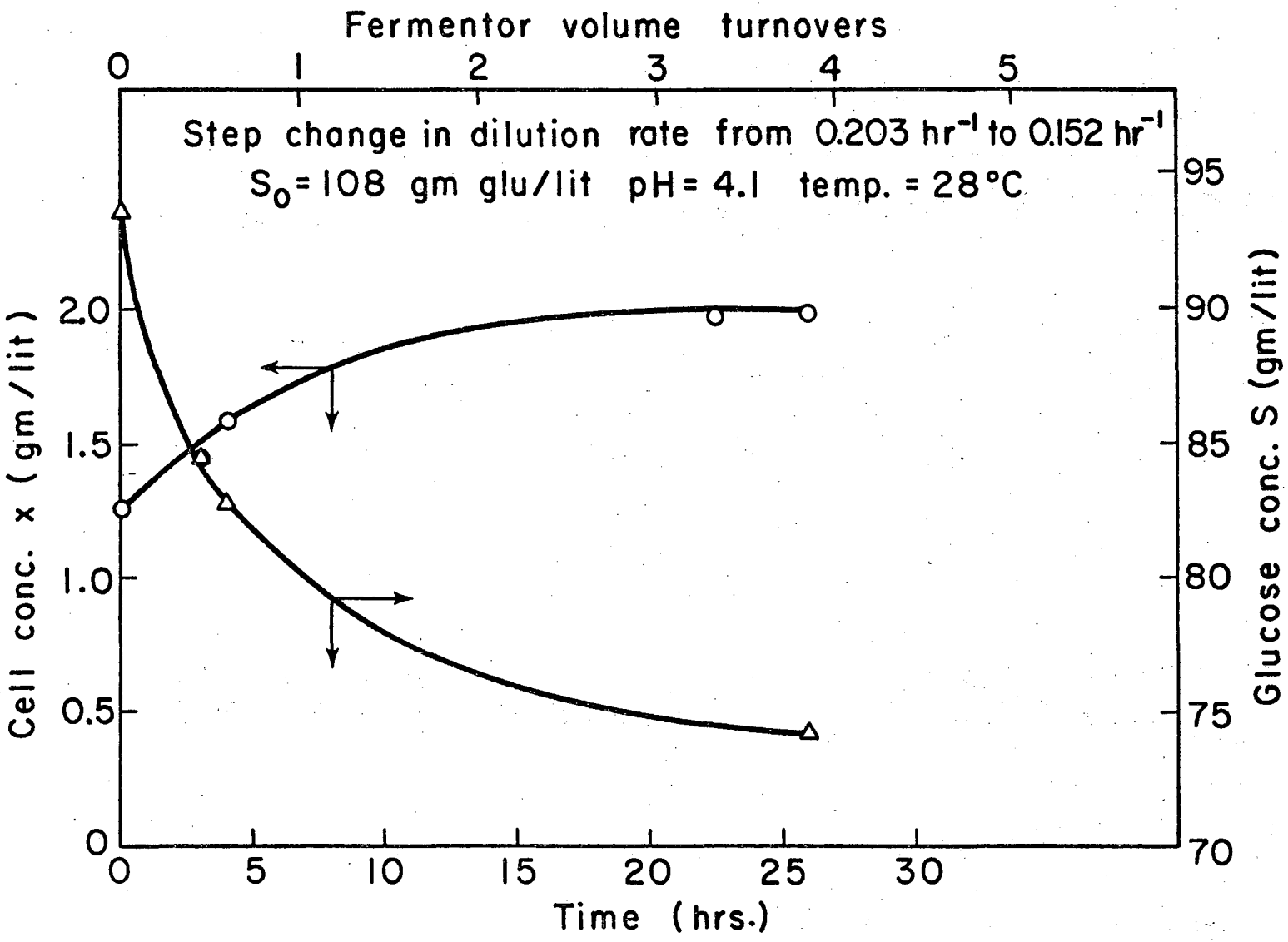

Fig. 6.20. Transient growth results due to step change in dilution rate. Run C.

XBL754-2822

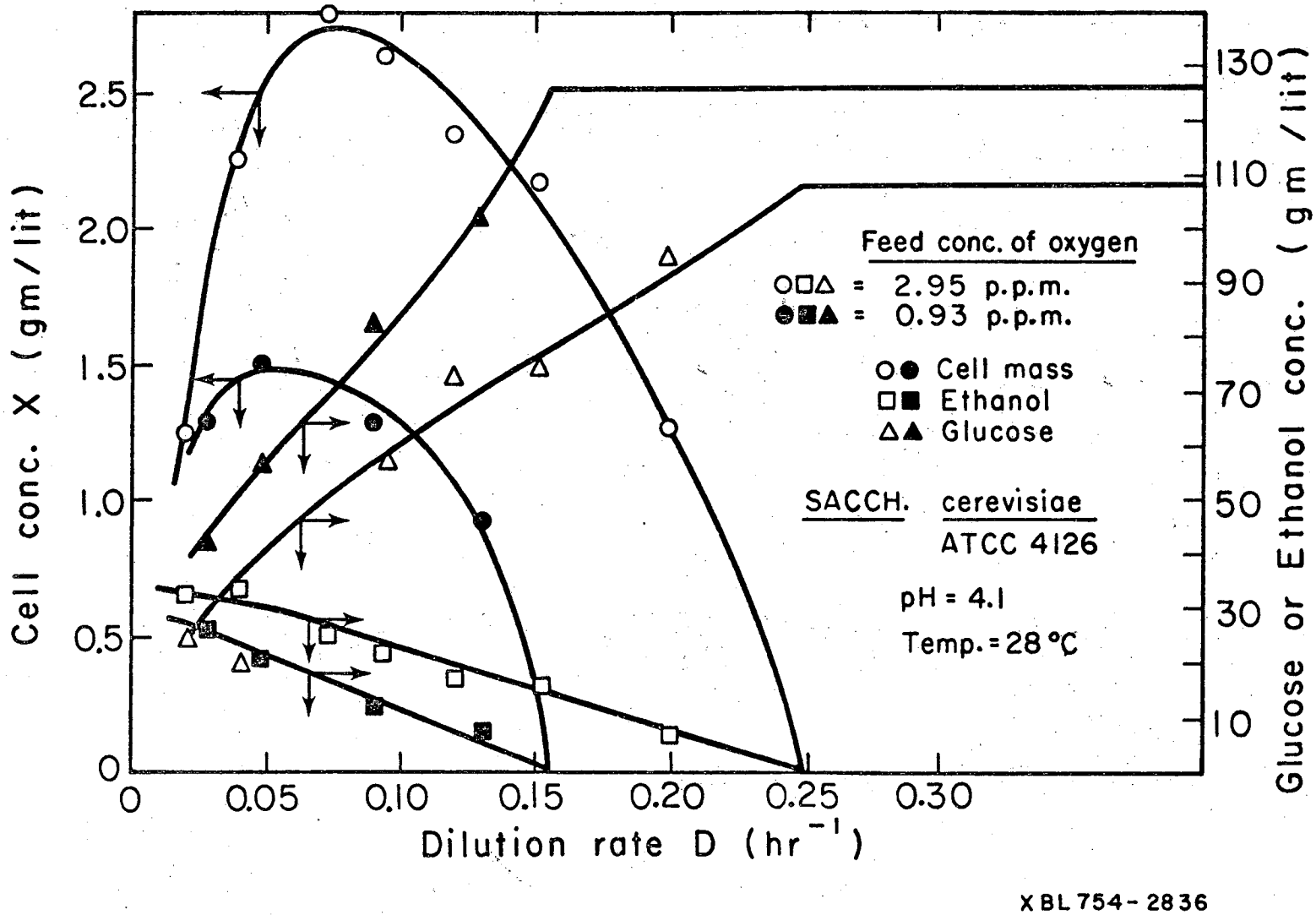

Fig. 6.21. Steady-state growth results for Runs C and A.

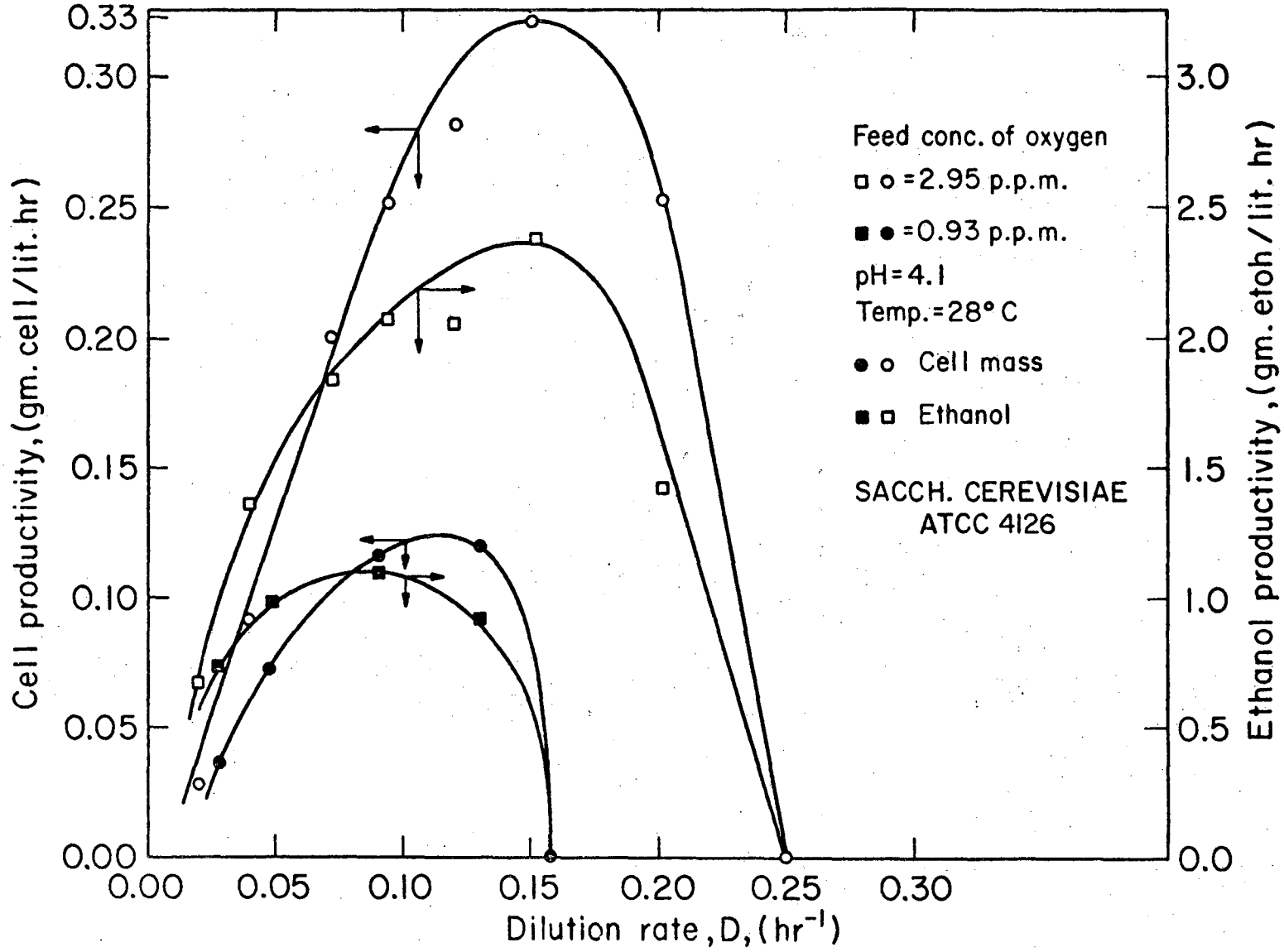

Fig. 6.22. Cell and ethanol productivity for Runs C and A.

XBL752-2236

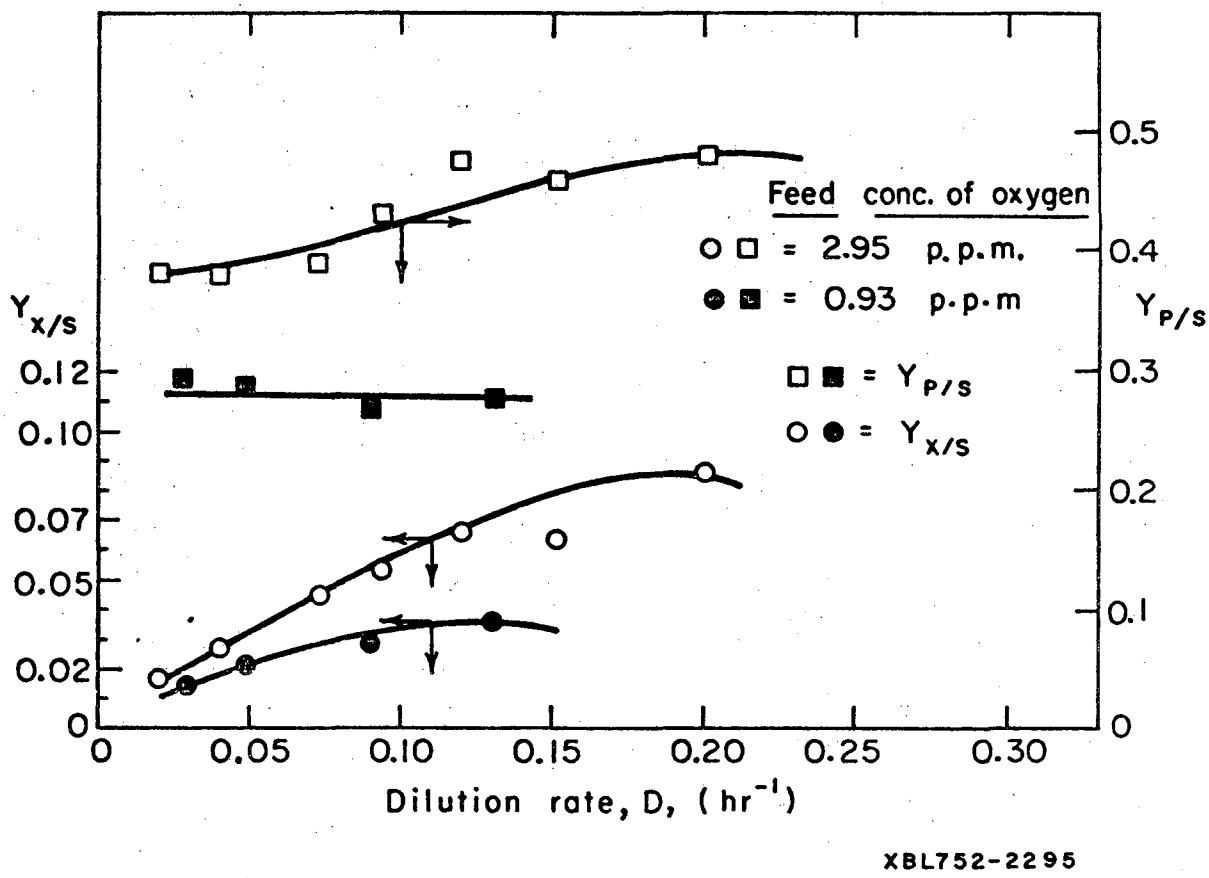

Fig. 6.23. Cell and ethanol overall yield factors for Runs C and A.

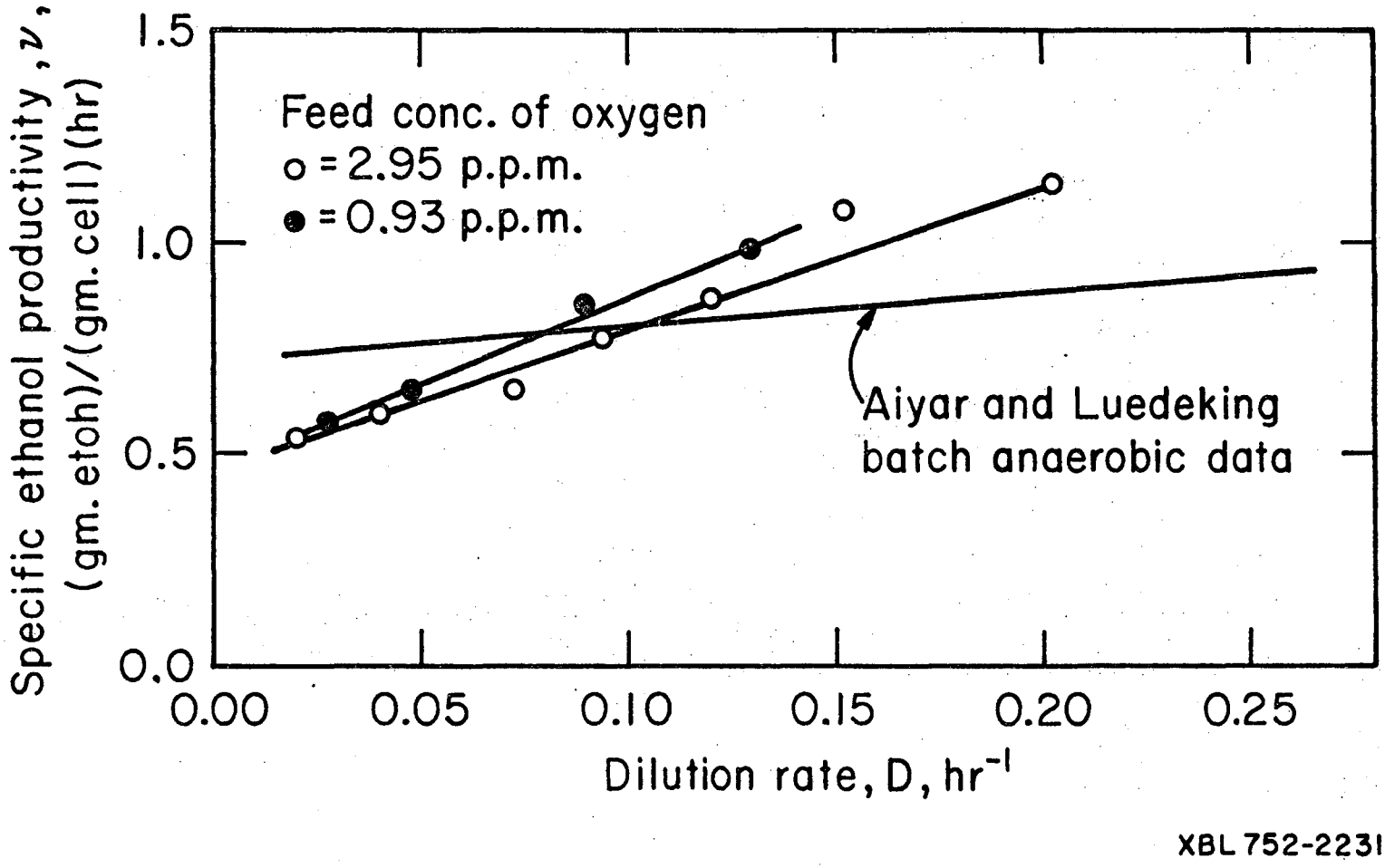

Fig. 6.24. Specific ethanol productivity for Runs C and A.

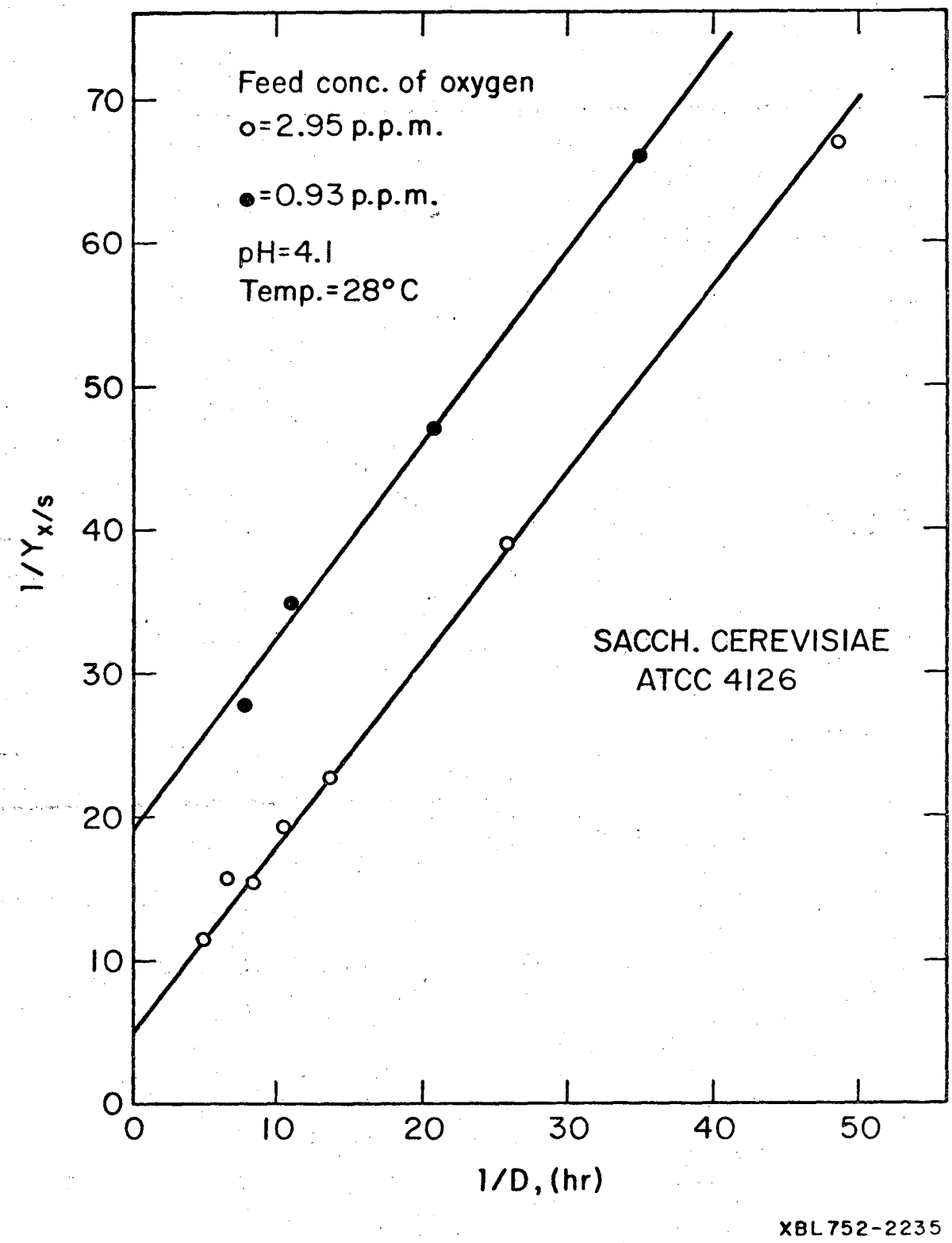

Fig. 6.25. Endogenous metabolism plot for Runs C and A.

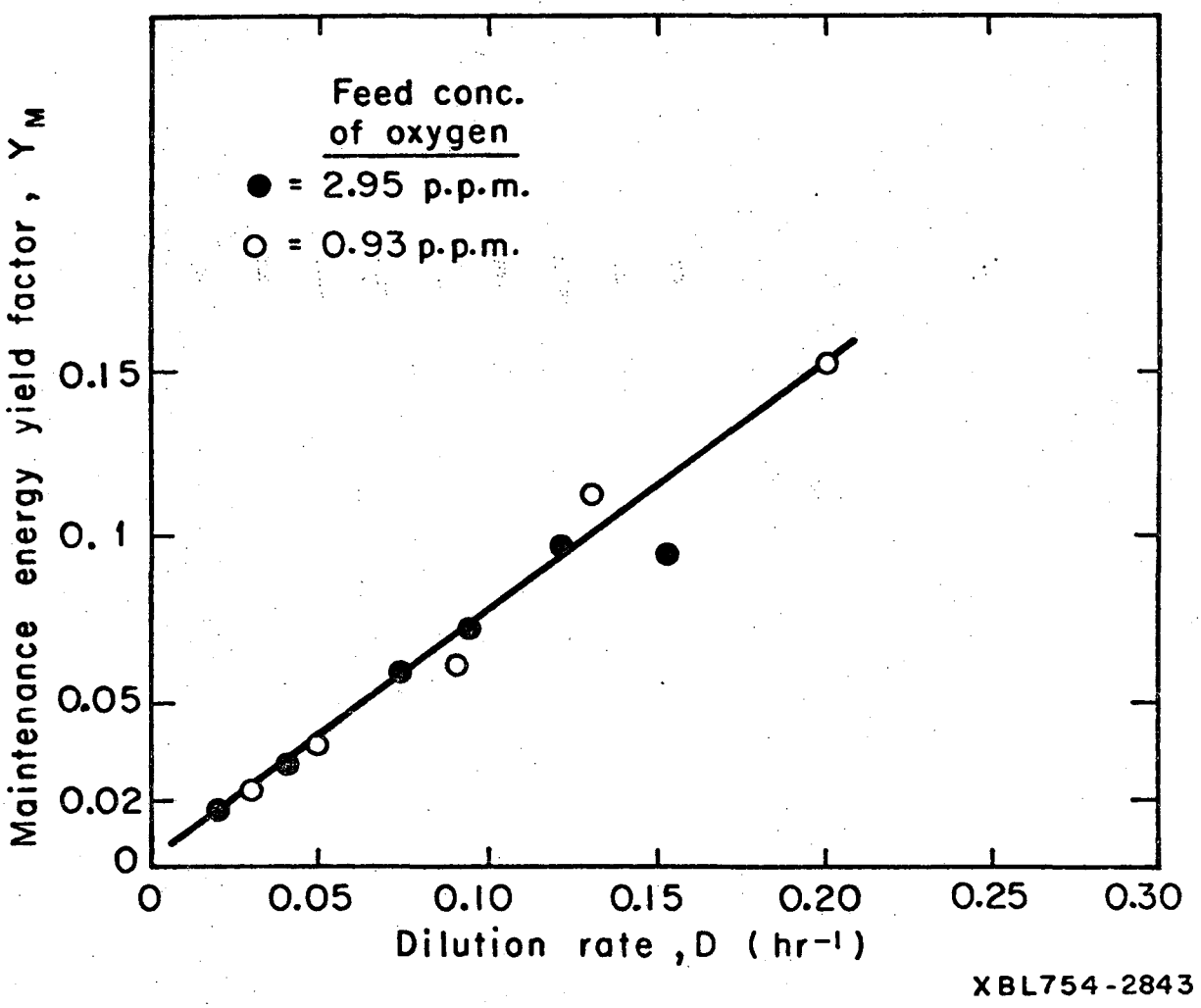

Fig. 6.26. Effect of oxygen concentration on maintenance yield factor.

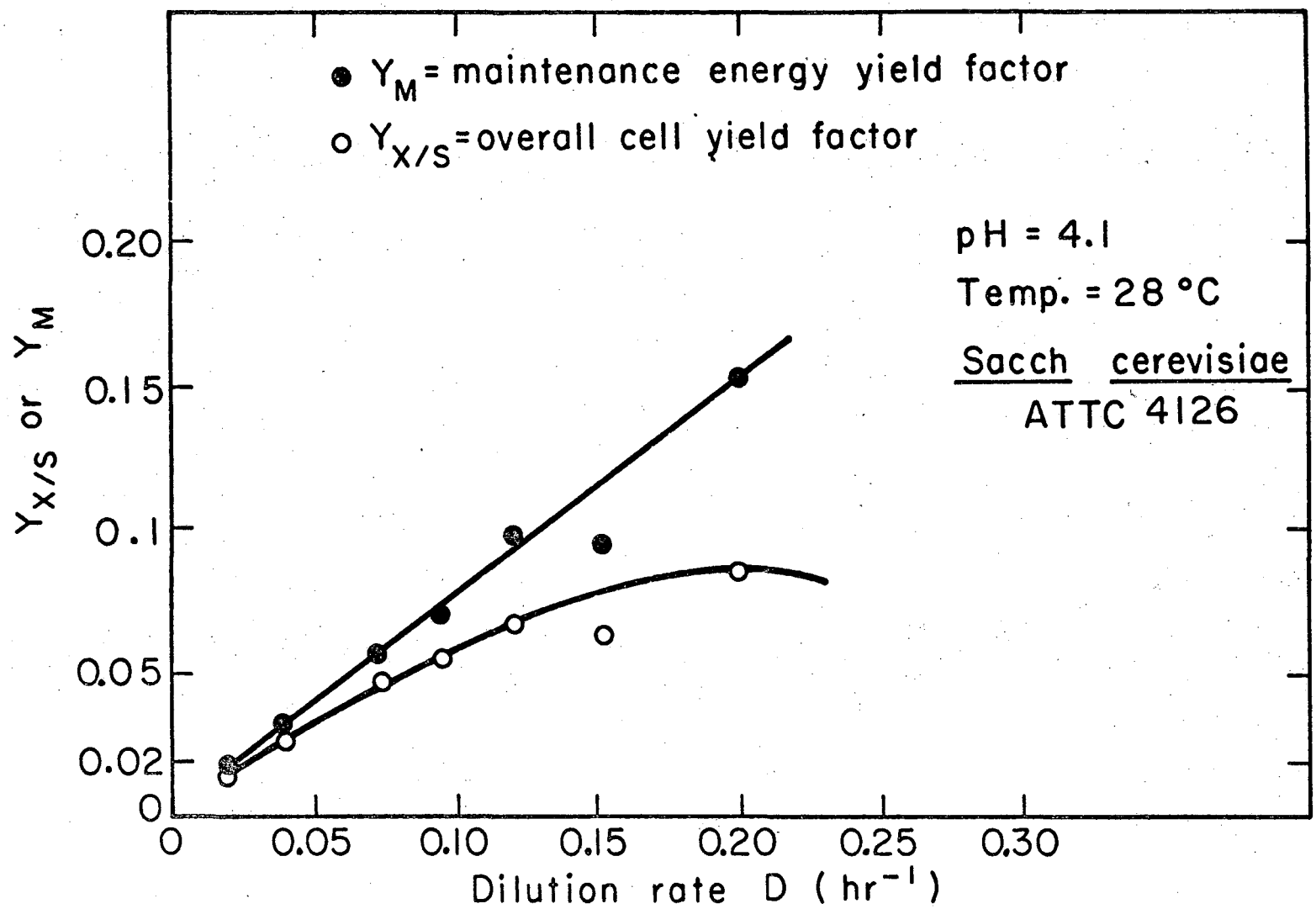

Fig. 6.27. Overall cell yield factor and maintenance yield factor for Run C.

XBL754-2840

Table 6.6 Summary of Data for Run C

S_0 = 108 gm. glu/lit C_{L0} = 2.95 p.p.m. pH = 4.1 T = 28°C

Dilution Rate D (hr^{-1})	Cell Mass X (gm/lit)	Glucose S (gm/lit)	Ethanol P (gm/lit)	$Y_{X/S}$	$Y_{P/S}$	Specific Ethanol Productivity ν^* (hr^{-1})	Cell Productivity DX	Ethanol Productivity DP	1/D (hr)	$1/Y_{X/S}$	Rate of Glucose Uptake Rg** (hr^{-1})
0.0206	1.25	24.2	32.0	0.015	0.382	0.526	0.026	0.658	48.5	67.0	1.38
0.0403	2.25	19.7	33.6	0.0255	0.380	0.600	0.091	1.35	24.8	39.2	1.58
0.0732	2.8	44.3	25.0	0.044	0.393	0.653	0.205	1.83	13.7	22.7	1.67
0.0944	2.65	56.6	22.0	0.0516	0.428	0.782	0.250	2.07	10.6	19.4	1.83
0.12	2.35	72.2	17.0	0.0656	0.475	0.868	0.282	2.04	8.33	15.3	1.83
0.152	2.17	73.8	15.7	0.0634	0.460	1.10	0.33	2.39	6.57	15.7	2.39
0.203	1.25	93.5	7.0	0.0862	0.483	1.14	0.254	1.42	4.92	11.6	2.35
0.252	0	108.0	0	-	-	-	0	0	-	-	-

*ν = gm. EtOH/hr. gm. cell.

**Rg = gm glucose consumed/hr.gm.cell.

6.6.3 Run E

The glucose concentration was 21.8 gm/lit. The oxygen concentration in the sterilized medium was 4.99 p.p.m. which is higher than that for run C. This increase in oxygen concentration (solubility) with decreasing glucose concentration is similar to the results obtained by Solomons (23).

Figure 6.28 shows steady-state results for cell mass, ethanol, and glucose concentration. The very low glucose concentrations especially at low values of D is characteristic of a typical run where glucose is the limiting substrate. This is in contrast to the relatively high glucose concentrations at low dilution rates observed in runs A and C where the feed glucose concentrations were approximately 6 and 5 times greater than that in run E. Figure 6.29 shows ethanol and cell productivity results. Figure 6.30 is a plot of ethanol and cell yield factors against dilution rate. Figure 6.31 shows the linear relationship of both specific ethanol productivity and rate of glucose uptake with the dilution rate. For the specific ethanol productivity the values of slope α and intercept β are 4.76 and 0.08 $hr.^{-1}$ respectively. The value of intercept β = 0.08 $hr.^{-1}$ is much lower than the values reported in Table 6.5. This might suggest a possible effect of glucose concentration on β.

Figure 6.32 is a plot to check endogenous metabolism at low glucose concentrations. The value of slope was found to be 0.17 $hr.^{-1}$ which is lower than the value of 1.33 $hr.^{-1}$ found for runs A and C. Again, this might suggest a possible effect of glucose concentration on m. The growth yield factor Y_g was found to be 0.11 which is approximately in the same range of Y_g values found for runs A and C. Table 6.7 is a summary of results for run E.

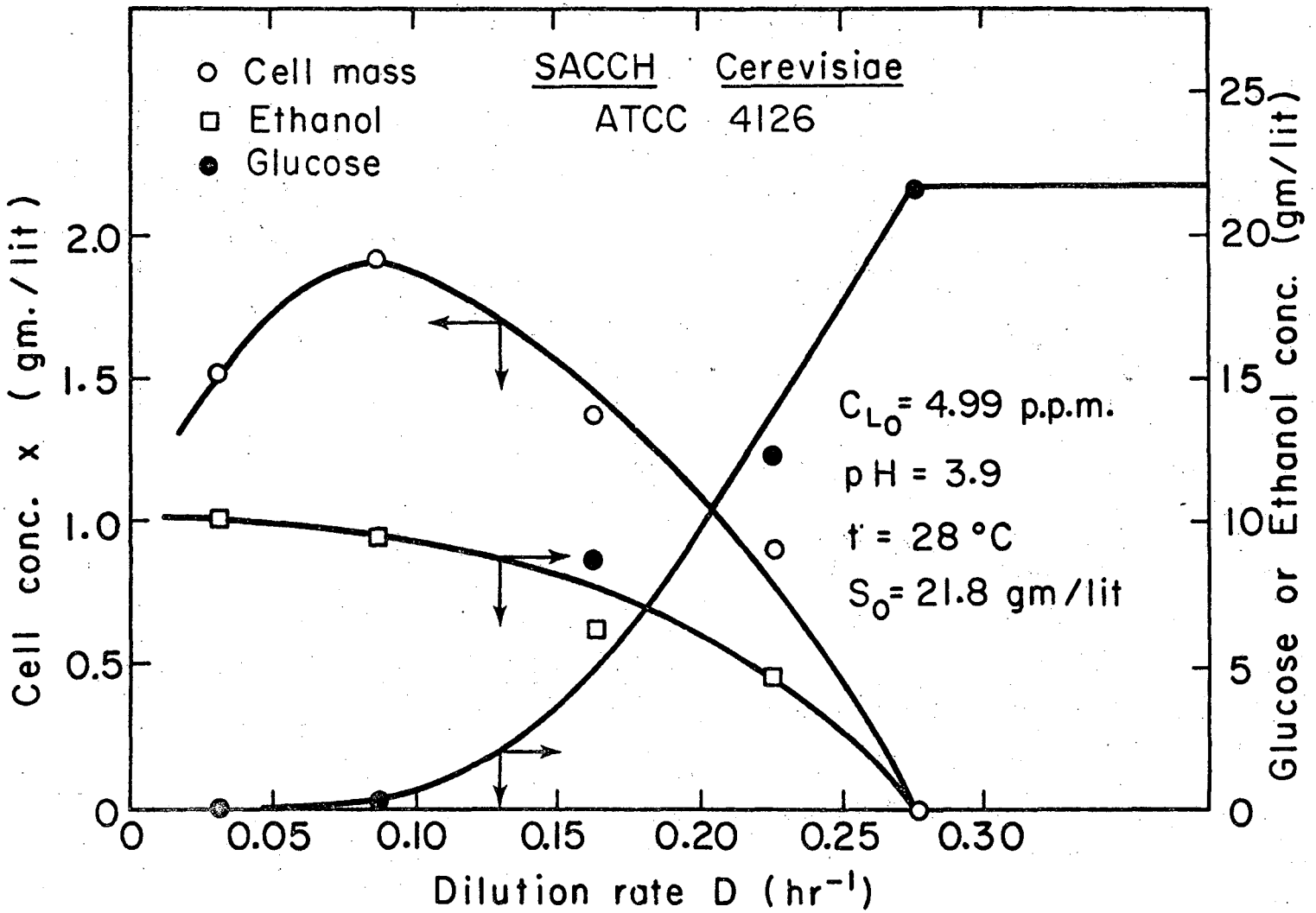

Fig. 6.28. Steady-state growth results for Run E. XBL754-2820

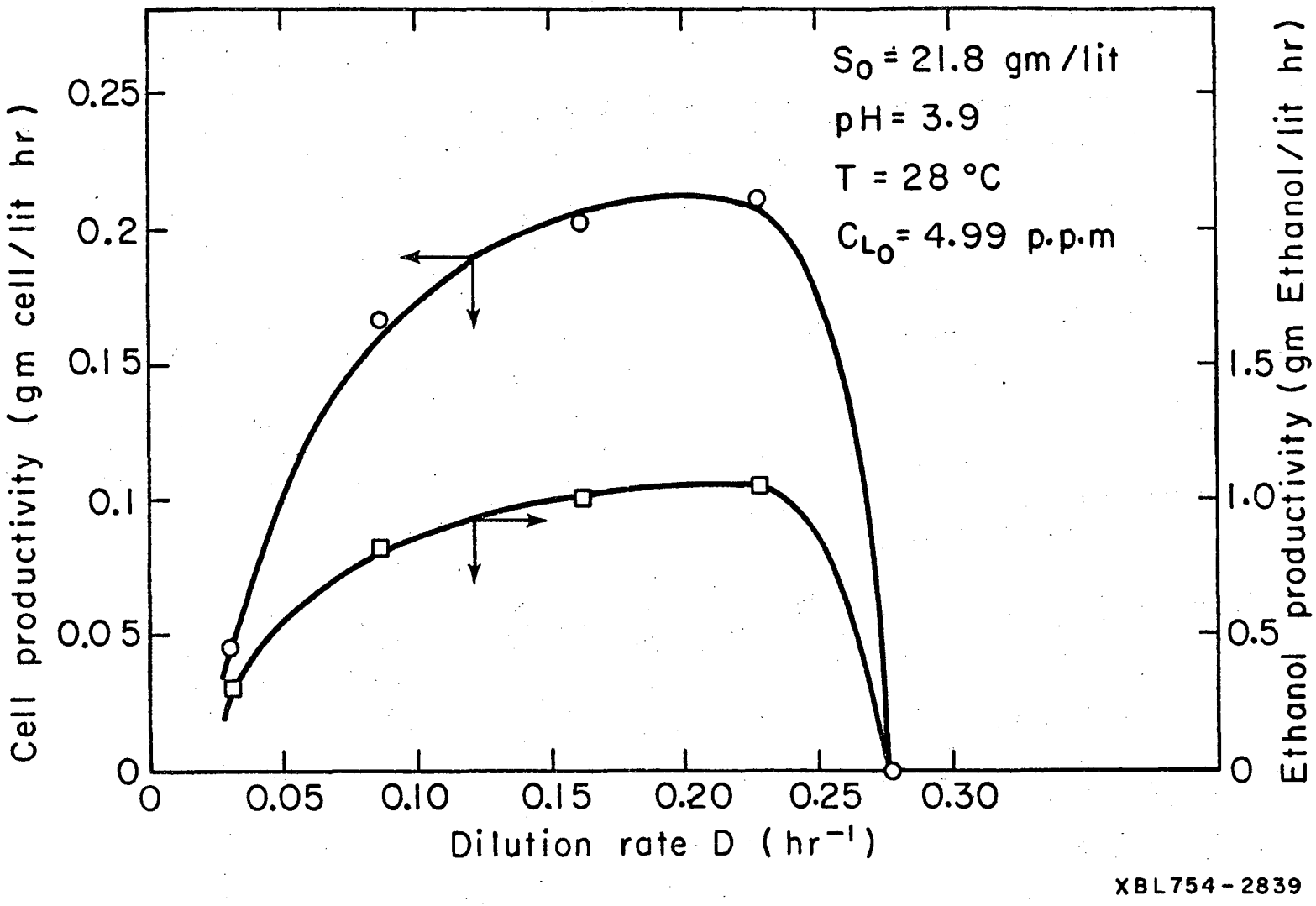

Fig. 6.29. Cell and ethanol productivity for Run E.

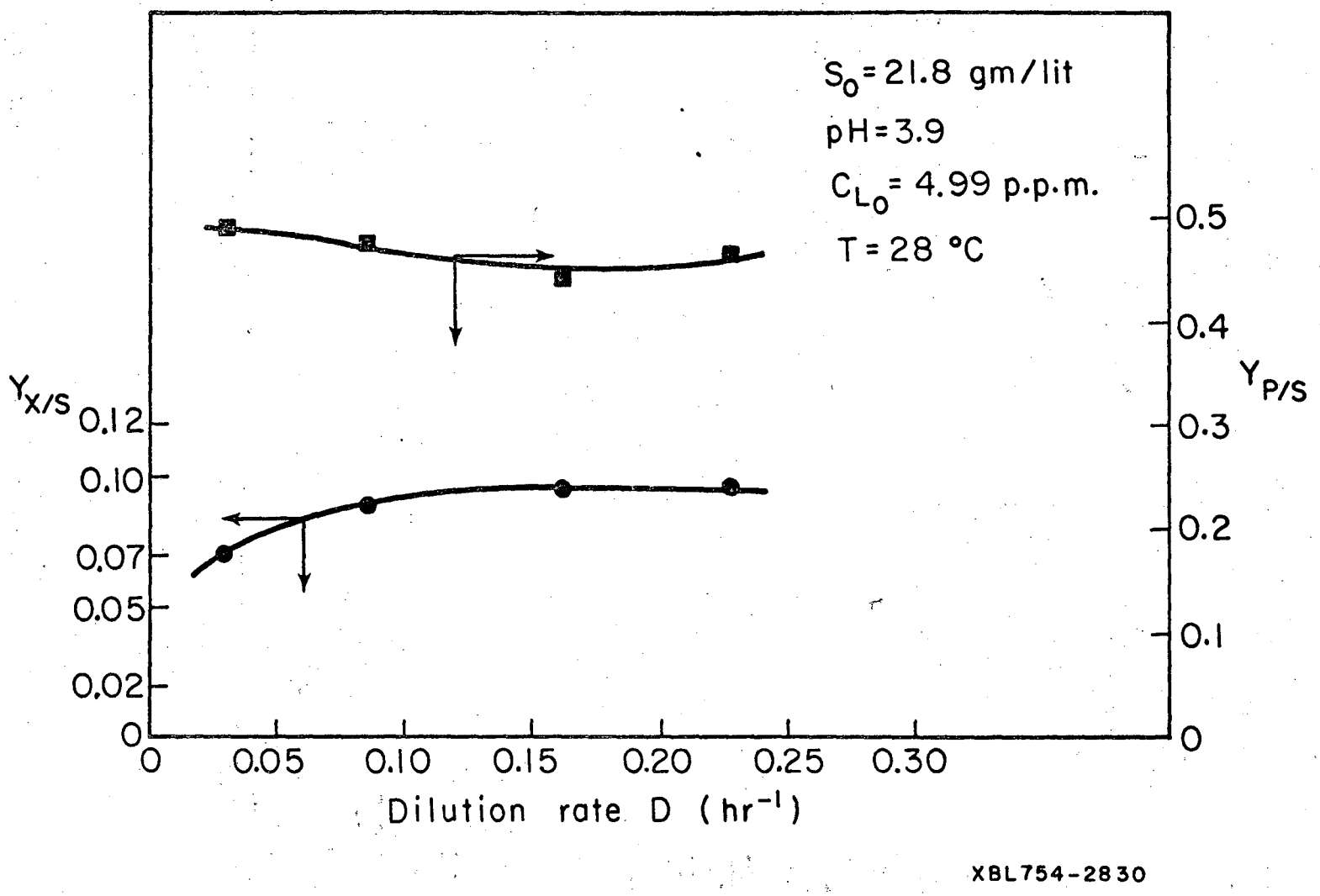

Fig. 6.30. Overall cell and ethanol yield factors for Run E.

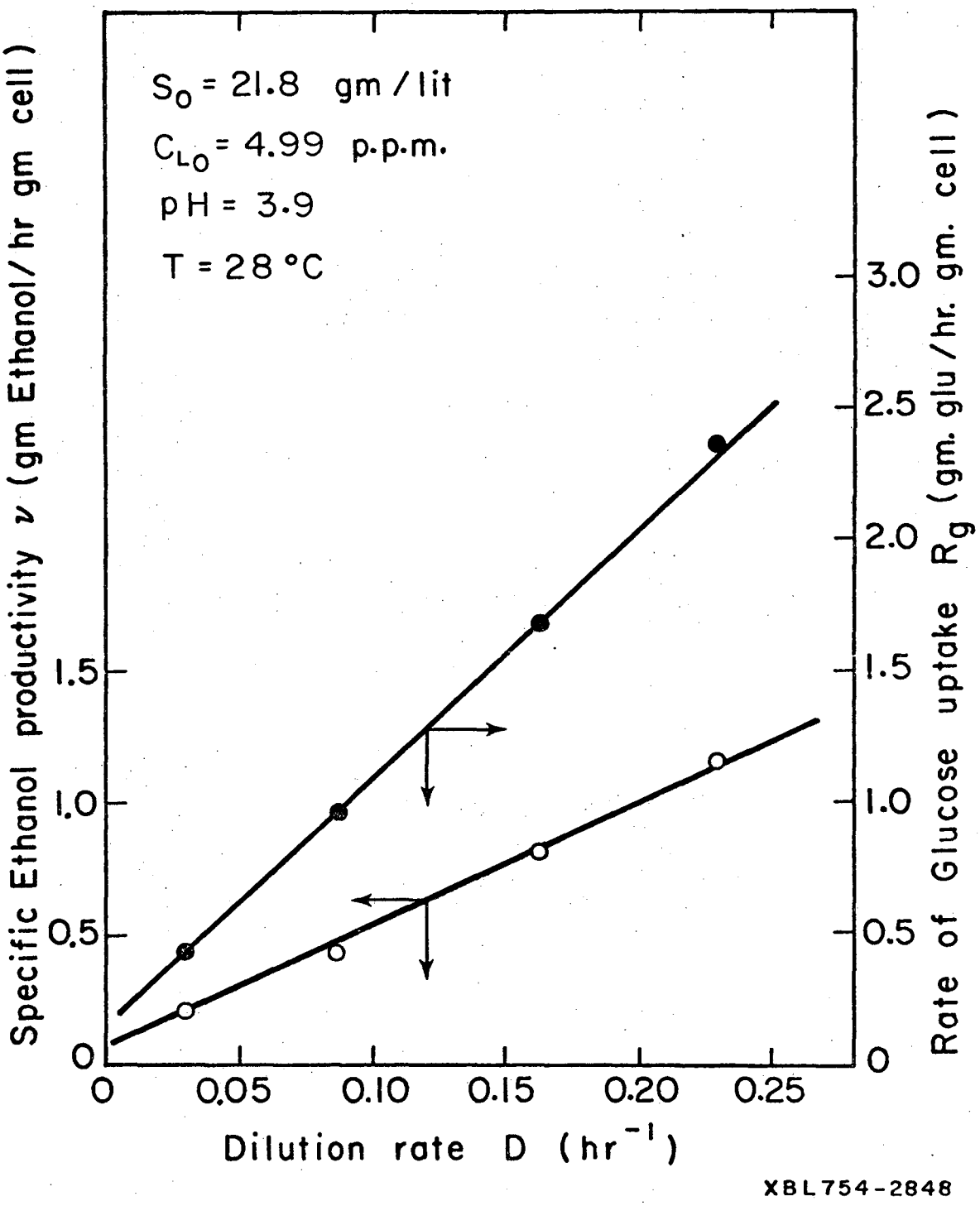

Fig. 6.31. Specific ethanol productivity and rate of glucose uptake for Run E.

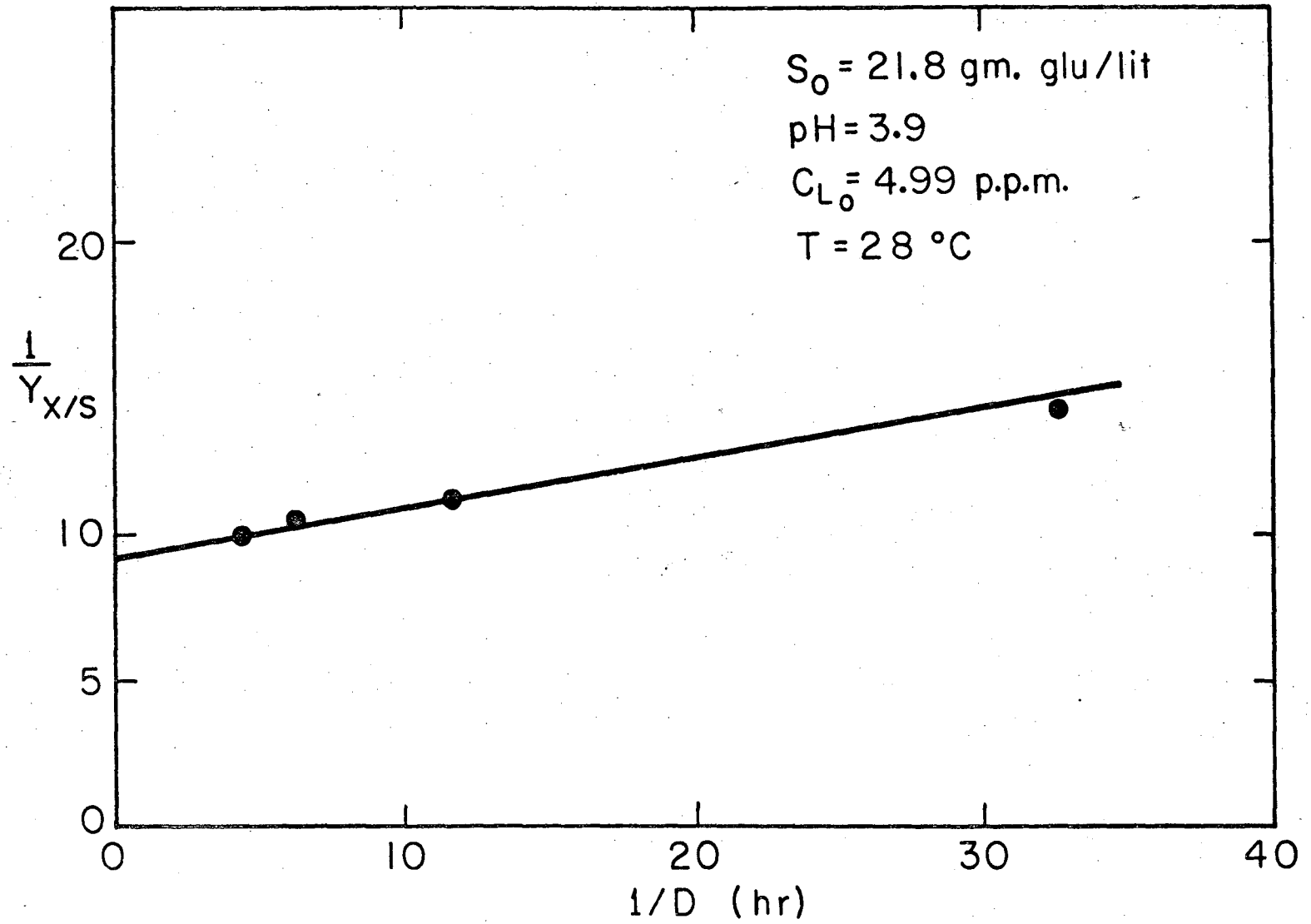

XBL754-2841

Fig. 6.32. Endogenous metabolism plot for Run E.

Table 6.7 Summary of Data for Run E

S_0 = 21.8 gm. glu/lit C_{L0} = 4.99 p.p.m. pH = 3.9 T = 28°C

Dilution Rate D (hr^{-1})	Cell Mass X (gm/lit)	Glucose S (gm/lit)	Ethanol P (gm/lit	$Y_{X/S}$	$Y_{P/S}$	Specific Ethanol Productivity ν^* (hr^{-1})	Cell Productivity DX	Ethanol Productivity DP	1/D (hr)	$1/Y_{X/S}$	Rate of Glucose Uptake Rg** (hr^{-1})
0.0304	1.53	0.03	10.2	0.0703	0.49	0.203	0.047	0.31	32.6	14.2	0.433
0.086	1.92	0.24	9.5	0.089	0.48	0.427	0.166	0.82	11.6	11.2	0.965
0.162	1.25	8.8	6.3	0.096	0.440	0.81	0.203	1.01	6.17	10.4	1.68
0.228	0.918	12.3	4.6	0.097	0.468	1.15	0.21	1.05	4.38	10.1	2.36
0.277	0	21.8	0	-	-	-	0	0	-	-	-

*ν = gm. EtOH/hr. gm. cell.

**Rg = gm. glucose consumed/hr. gm. cell.

6.6.4 Run G.

In this run the feed glucose concentration was 210 gm/lit and the oxygen concentration 4.51 p.p.m. Figure 6.33 shows batch growth data. Figure 6.34 is a plot of glucose, cell mass and ethanol concentration inside the fermentor at different dilution rates. Relatively large amounts of glucose are left over unfermentable inside the fermentor when compared with all previous runs. These steady-state data are especially important in trying to assess the effects of high glucose concentrations on specific ethanol productivity. Figure 6.35 is a plot of specific ethanol productivity ν against D with slope $\alpha = 4.0$ and intercept $\beta = 0.12\ hr^{-1}$. The results of run G are given in Table 6.8.

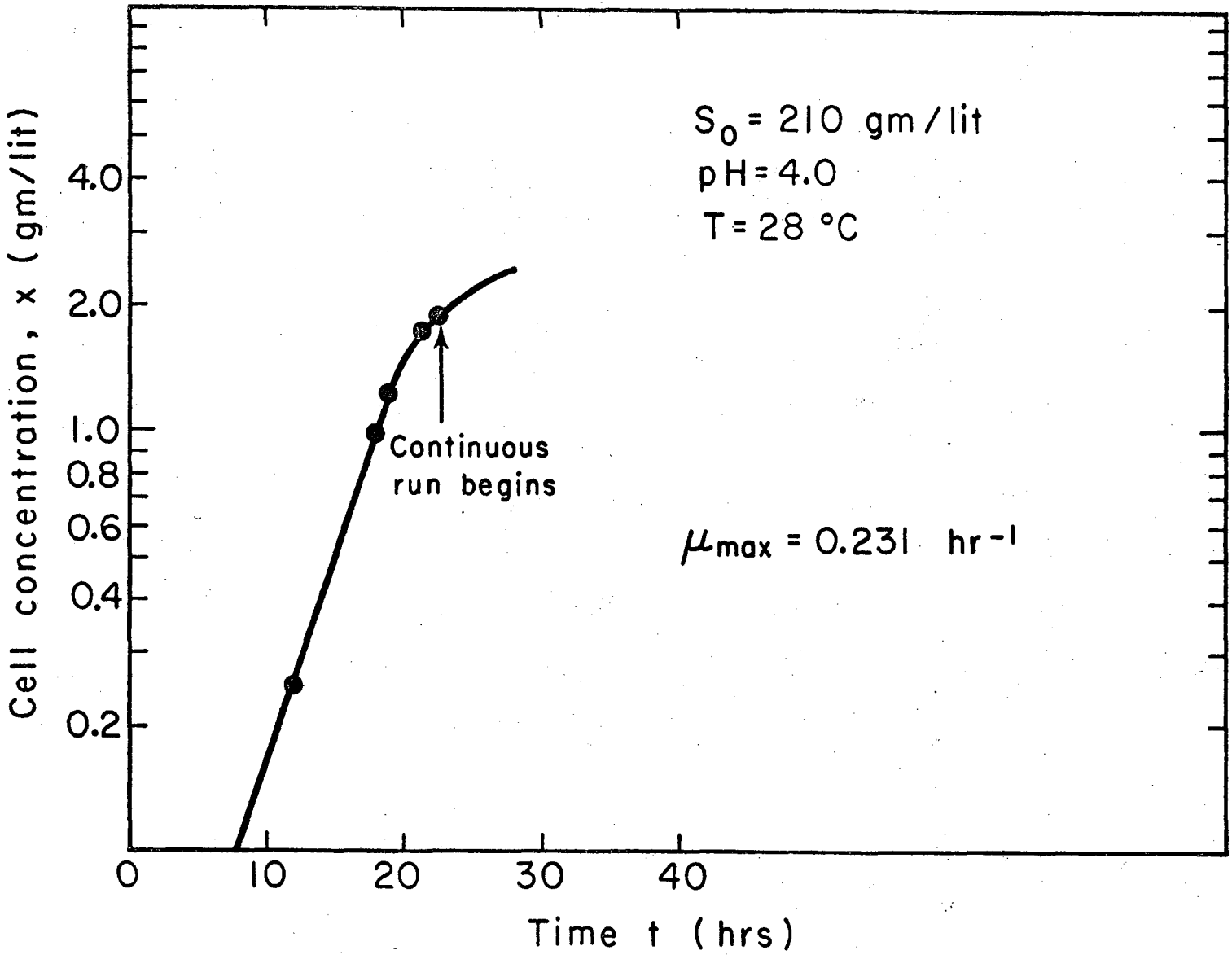

Fig. 6.33. Batch growth results for Run G.

XBL754-2824

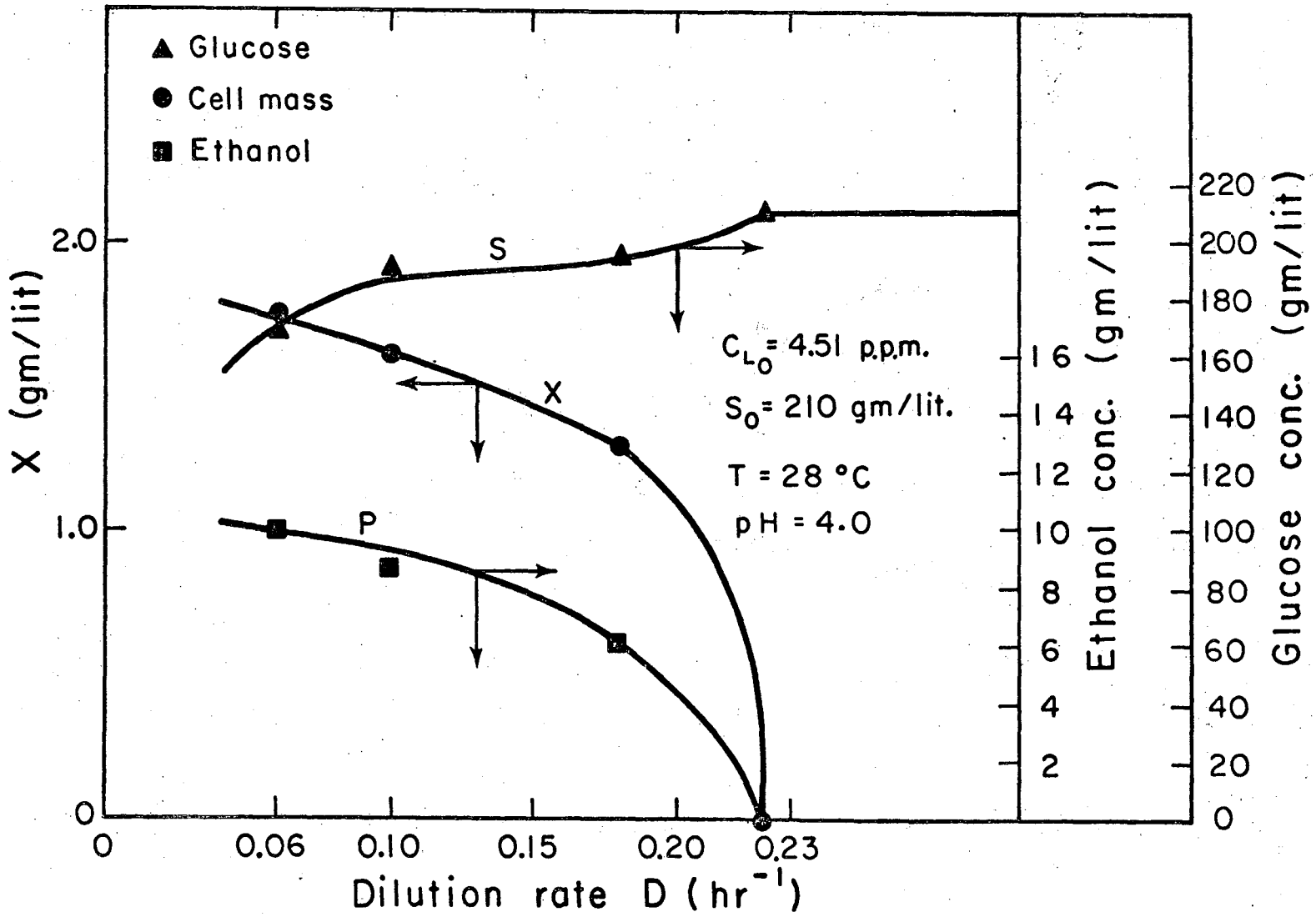

XBL754-2825

Fig. 6.34. Steady-state growth results for Run G.

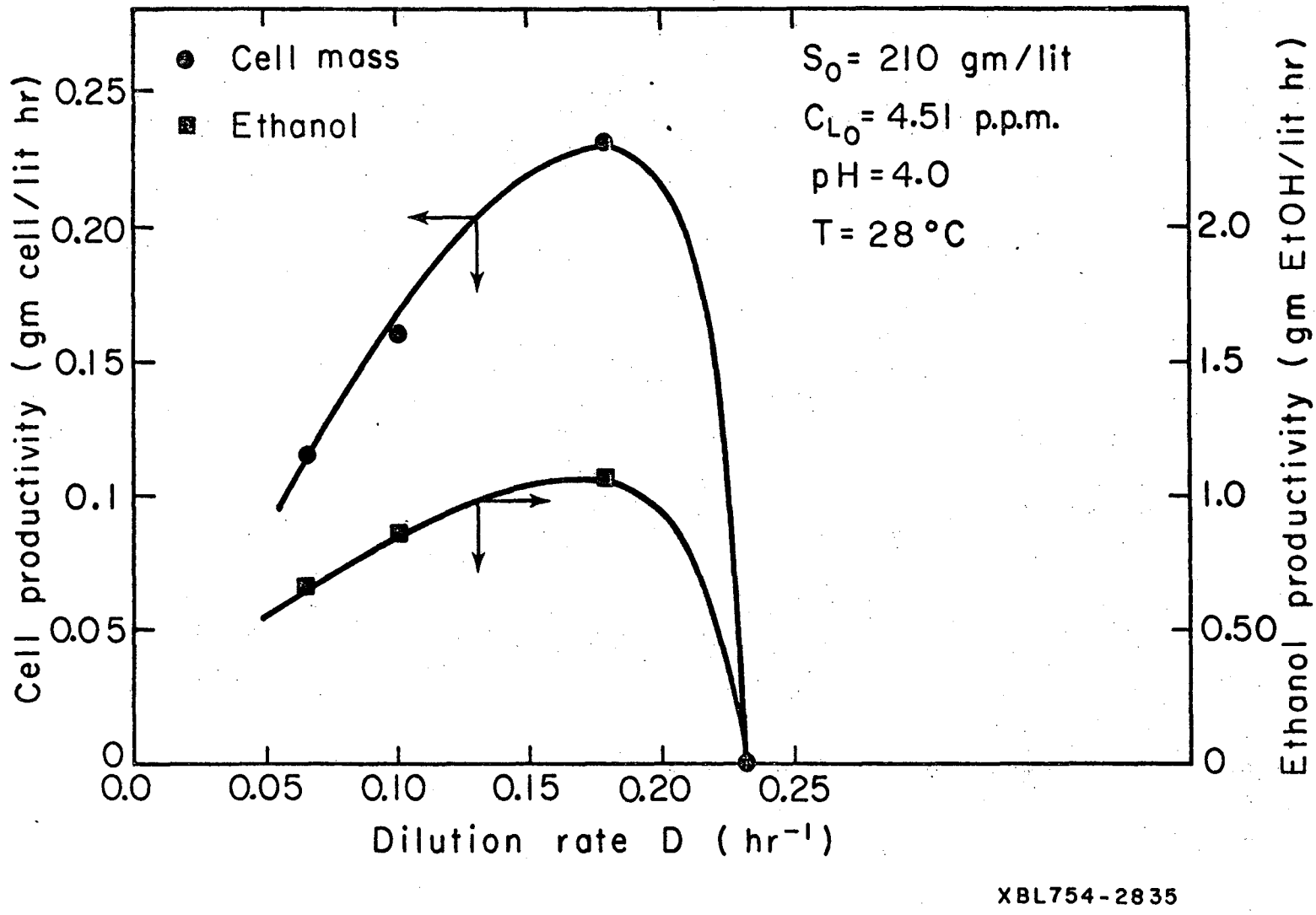

Fig. 6.35. Cell and ethanol productivity for Run G.

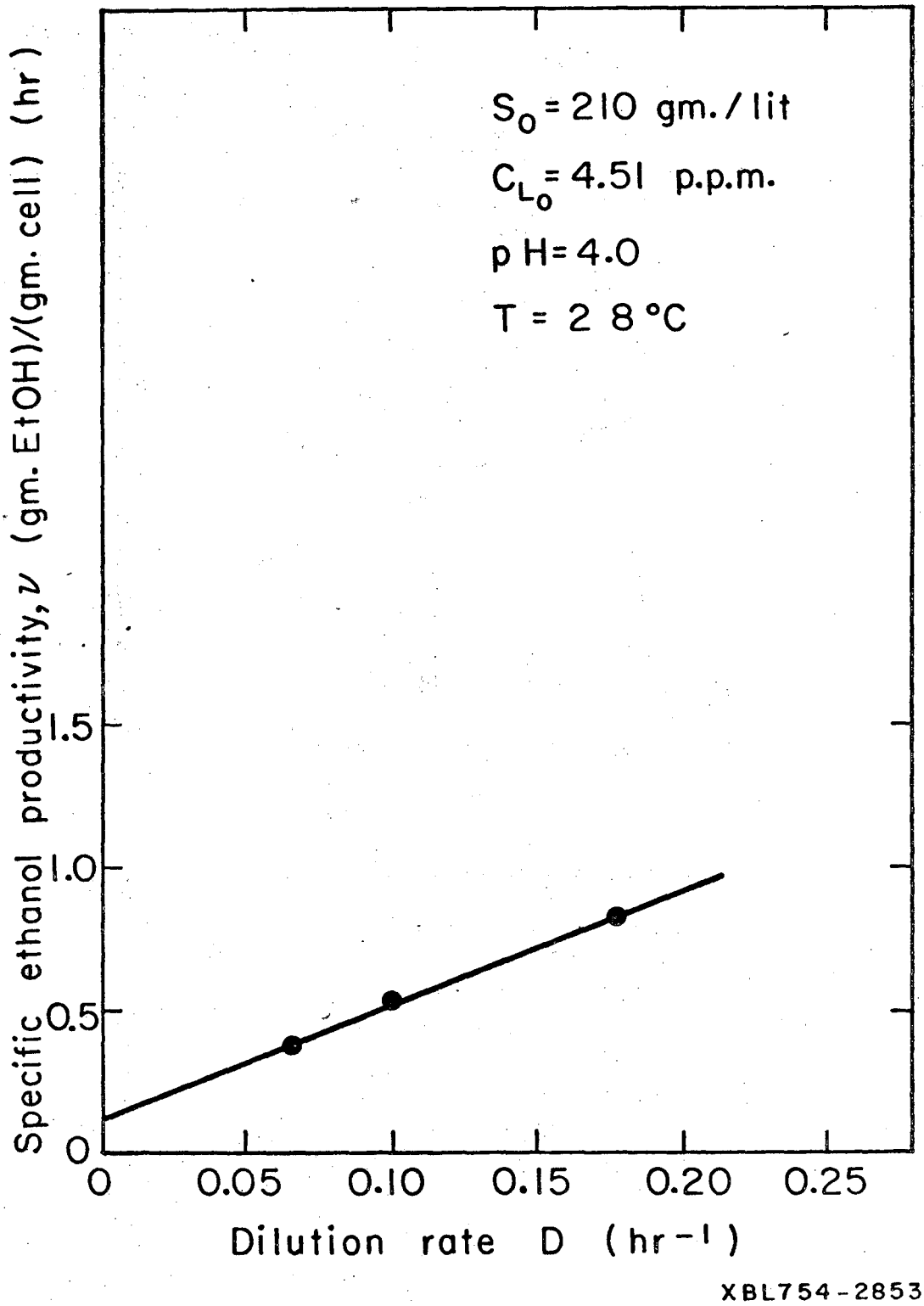

Fig. 6.36. Specific ethanol productivity for Run G.

Table 6.8 Summary of Data for Run G

S_0 = 210 gm. glu/lit C_{L0} = 4.51 p.p.m. pH = 4.0 T = 28°C

Dilution Rate D (hr^{-1})	Cell Mass X (gm/lit)	Glucose S (gm/lit)	Ethanol P (gm/lit)	$Y_{X/S}$	$Y_{P/S}$	Specific Ethanol Productivity ν^* (hr^{-1})	Cell Productivity DX	Ethanol Productivity DP	1/D (hr)	$1/Y_{X/S}$	Rate of Glucose Uptake Rg** (hr^{-1})
0.066	1.75	170.0	10.0	0.044	0.25	0.377	0.116	0.66	15.15	22.7	1.51
0.10	1.60	190.0	8.5	0.080	0.425	0.531	0.16	0.85	10.0	12.5	1.25
0.178	1.30	196.0	6.0	0.093	0.428	0.821	0.23	1.07	5.62	10.8	1.92
0.231	0	210.0	0	-	-	-	-	-	-	-	-

*ν = gm. EtOH/hr. gm. cell

**Rg = gm. glucose consumed/hr. gm. cell

6.6.5 Summary of Results for Runs A, C, E, G.

The effect of glucose concentration on the specific ethanol productivity ν is shown in Figure 6.37. Those data were obtained from the steady-state results of runs A, C, E, and G. Each curve represents a constant dilution rate D which is equal to μ. At a given D the values of ν corresponding to glucose concentration values S were obtained from Figures 6.14, 6.21, 6.28 and 6.34 respectively and plotted as shown in Figure 6.37. At a given constant value of μ the specific ethanol productivity increases with S, reaches a maximum, and then further increases in S results in decreasing values of ν. This decrease in ν at high values of S is in agreement with the glucose repression effect as explained earlier in Section 6.3. Figure 6.37 also shows that at a given glucose concentration ν increases with increasing values of μ. This is in agreement with the fact that ν and μ are linearly related as shown, for example, in Figure 6.24.

Figure 6.38 is a summary of results for ν against D while Figure 6.39 shows values of $Y_{X/S}$ and $Y_{P/S}$ for runs A, C, E, and G. Table 6.9 is a summary of data for the effect of substrate concentration S on specific ethanol productivity ν. Also shown is the corresponding concentration of ethanol at a given value of S and ν. Results of ethanol inhibition on specific ethanol productivity ν showed that up to approximately 35 gm.

ethanol/lit the inhibitory effects of ethanol on ν is very small (28). For example, at an ethanol concentration of 35 gm/lit the specific ethanol productivity ν is approximately 94% of its value at zero ethanol concentration, while at 50 gm EtOH/lit ν is reduced to about 85% of its value at zero ethanol concentration (28). Therefore, the levels of ethanol concentration shown in Table 6.9 do not affect appreciably the values of specific ethanol productivity ν.

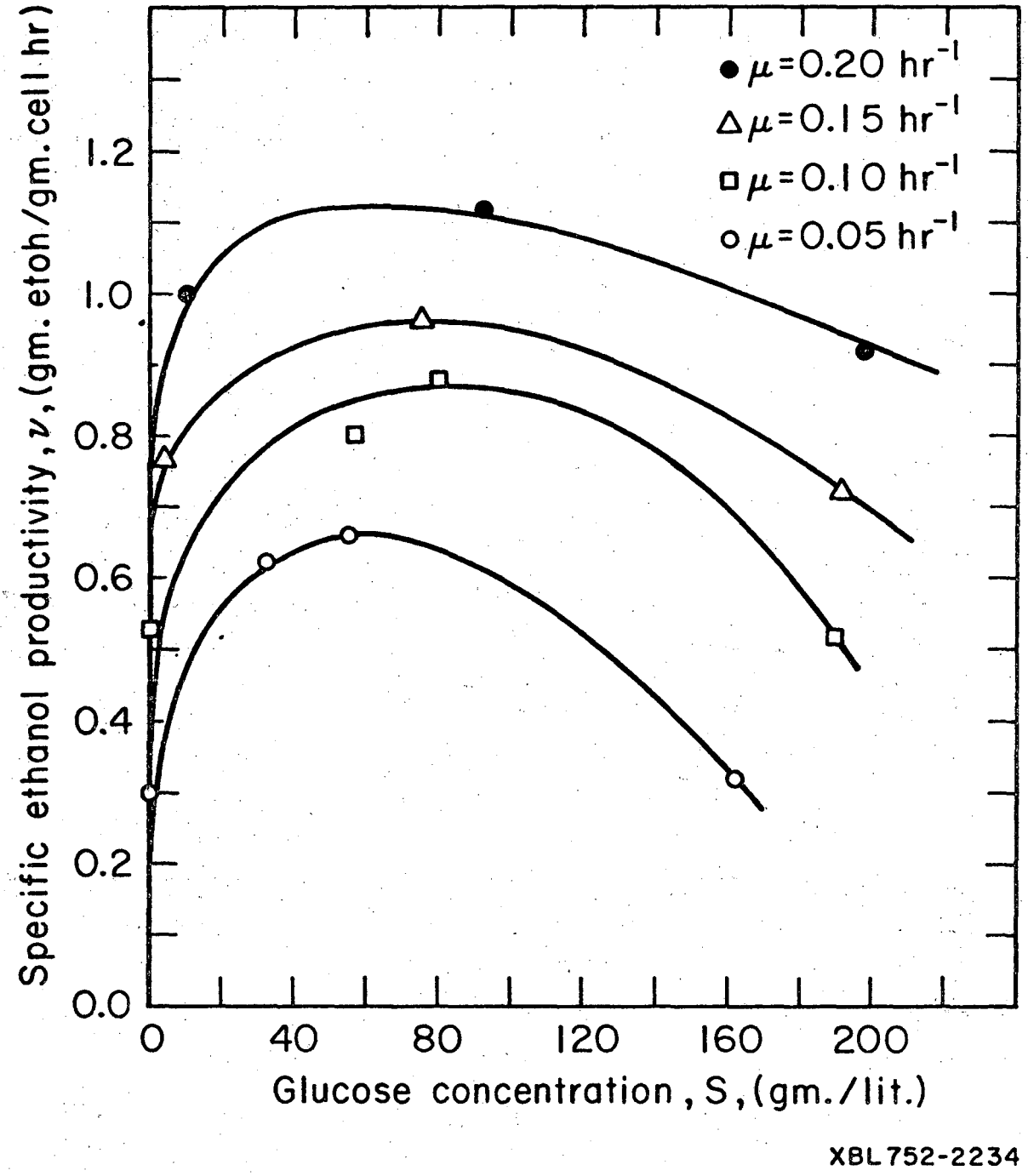

Fig. 6.37. Effect of glucose concentration on specific ethanol productivity for Saccharomyces cerevisiae ATCC 4126.

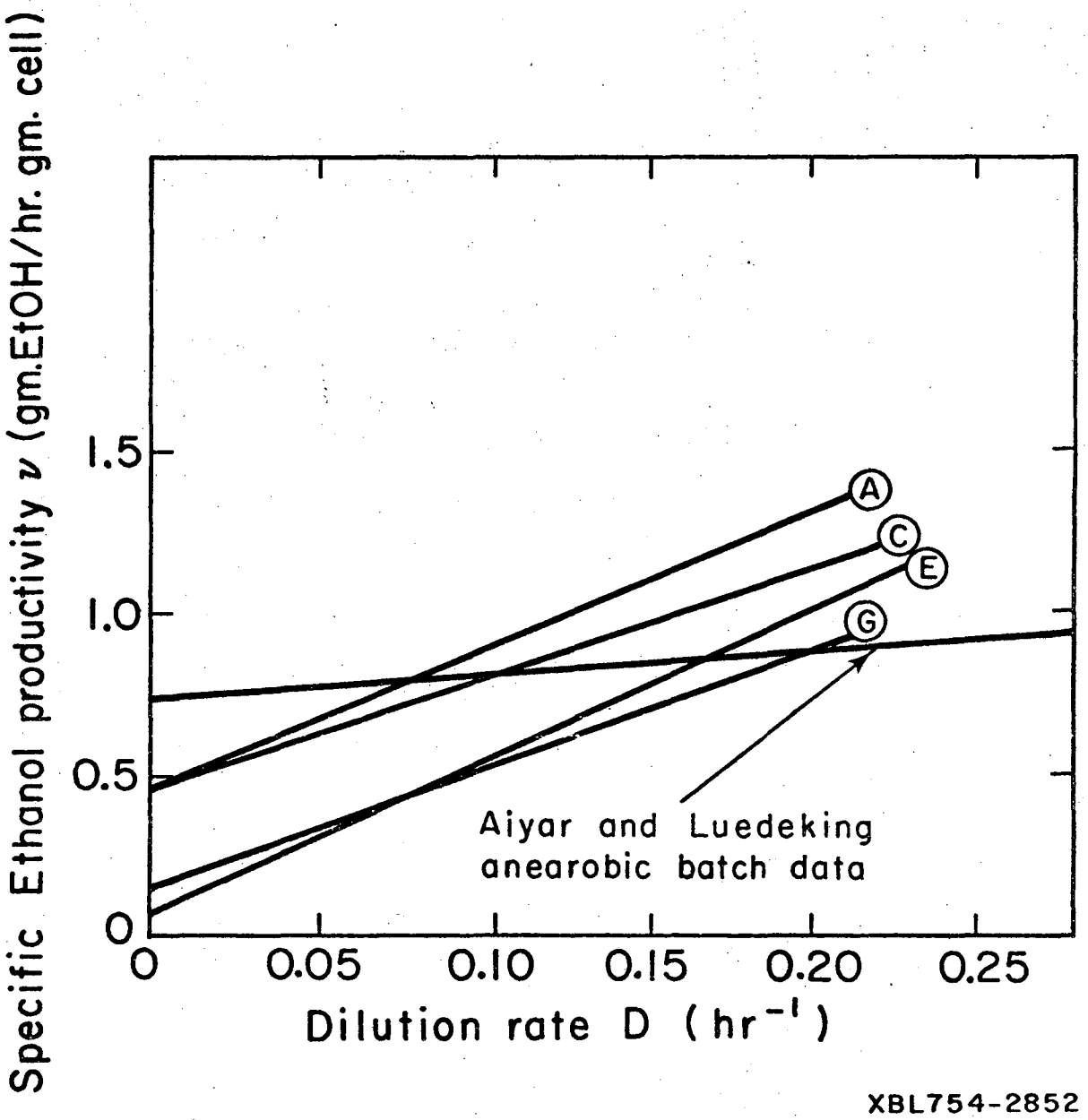

Fig. 6.38. Summary of results for the specific ethanol productivity of Runs A, C, E and G.

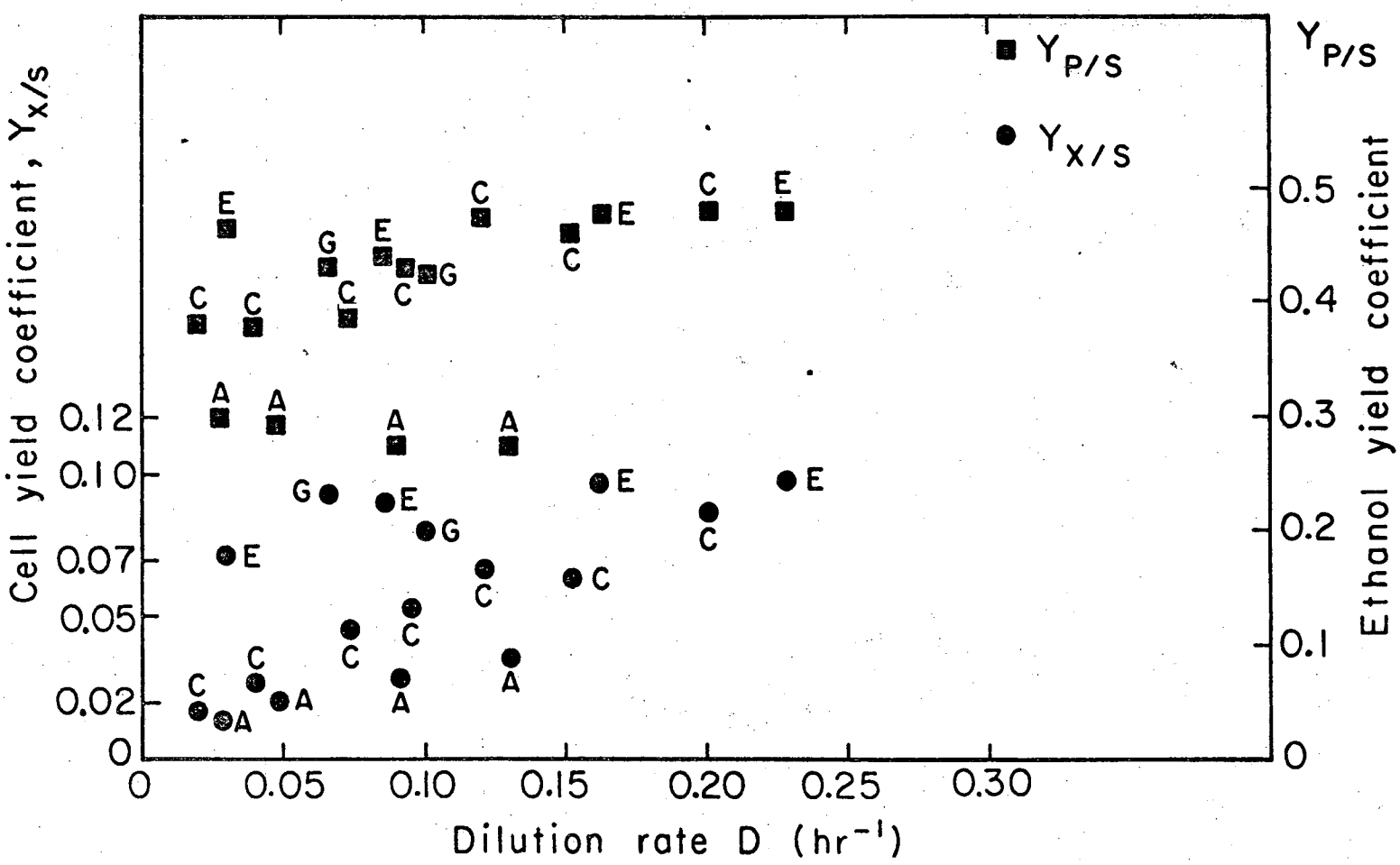

Fig. 6.39. Summary of results for cell and ethanol yield factors of Runs A, C, G and E.

Table 6.9 Summary of Data; Effect of S on ν.

Run	S (gm/lit)	P (gm/lit)	ν*	μ=D (hr^{-1})
A	55	22	0.66	0.05
C	32	30	0.62	0.05
E	0.20	10	0.30	0.05
G	162	10	0.32	0.05
A	80	12	0.88	0.10
C	57	22	0.80	0.10
E	0.80	9.0	0.53	0.10
G	190	9.2	0.52	0.10
C	75	15	0.96	0.15
E	3.6	8.2	0.77	0.15
G	192	7.8	0.72	0.15
C	92	8.0	1.12	0.20
E	9.8	6.0	1.0	0.20
G	198	4.4	0.92	0.20

*ν = gm. EtOH/hr. gm. cell.

6.6.6 Run Y.

This run was designed to measure the respiration rate coefficient of Saccharomyces cerevisiae. The glucose concentration in the feed was 119.3 gm/lit and the oxygen concentration 5.19 p.p.m. or 162.2 M. The oxygen probe was placed inside the fermentor to measure the oxygen concentration at various dilution rates. The only source of oxygen was that coming from the fresh medium in the feed. To prevent the possibility of some oxygen coming in from the top a small nitrogen stream was used periodically to flush the top empty space. It was also found that even in the absence of nitrogen the amount of air coming from outside was almost zero because the top part of the fermentor had a slightly higher than atmospheric pressure due to the accumulation of CO_2.

Equation 6.6.1 is an oxygen mass balance at steady-state conditions for a given dilution rate.

$$FC_{L0} - FC_L - Q_{O_2} X V_L = 0 \qquad 6.6.1$$

or rearranging and since F/V = D we get

$$Q_{O_2} = \frac{D(C_{L0} - C_L)}{X} \qquad 6.6.2$$

where:

Q_{O_2} = respiration rate coefficient, μ moles O_2/hr. gm. cell.

F = volumetric flow rate of fresh medium, lit/hr.

V = fermentor volume, lit.

C_{L0} = oxygen concentration in feed, μ moles/lit.

C_L = oxygen concentration inside the fermentor, μ moles/lit.

X = cell mass concentration, gm/lit.

Equation 6.6.2 gives the respiration rate coefficient at steady-state conditions and when the only oxygen source is that coming from the fresh medium in the feed.

Figure 6.40 is a plot of cell mass, glucose, ethanol and oxygen concentration against dilution rate D. Figure 6.41 is a plot of cell mass and ethanol productivities while Figure 6.42 shows the results on cell and ethanol yield coefficients. Table 6.10 is a summary of data for run Y. The respiration rate coefficient was calculated by using equation 6.62, and plotted against oxygen concentration as shown in Figure 6.43. The relatively low values of Q_{O_2} obtained in this experiment reflect the fact that the respiratory enzymes are repressed at the high glucose concentration ranges from 23.4 gm/lit at D = 0.021 hr^{-1} to a high value of 97.9 gm/lit at D = 0.21 hr^{-1}. These values are much higher than the glucose concentration values reported by Moss et al. (16) as described in Section 6.3. Therefore, when reporting Q_{O_2} values the glucose concentration is an important parameter.

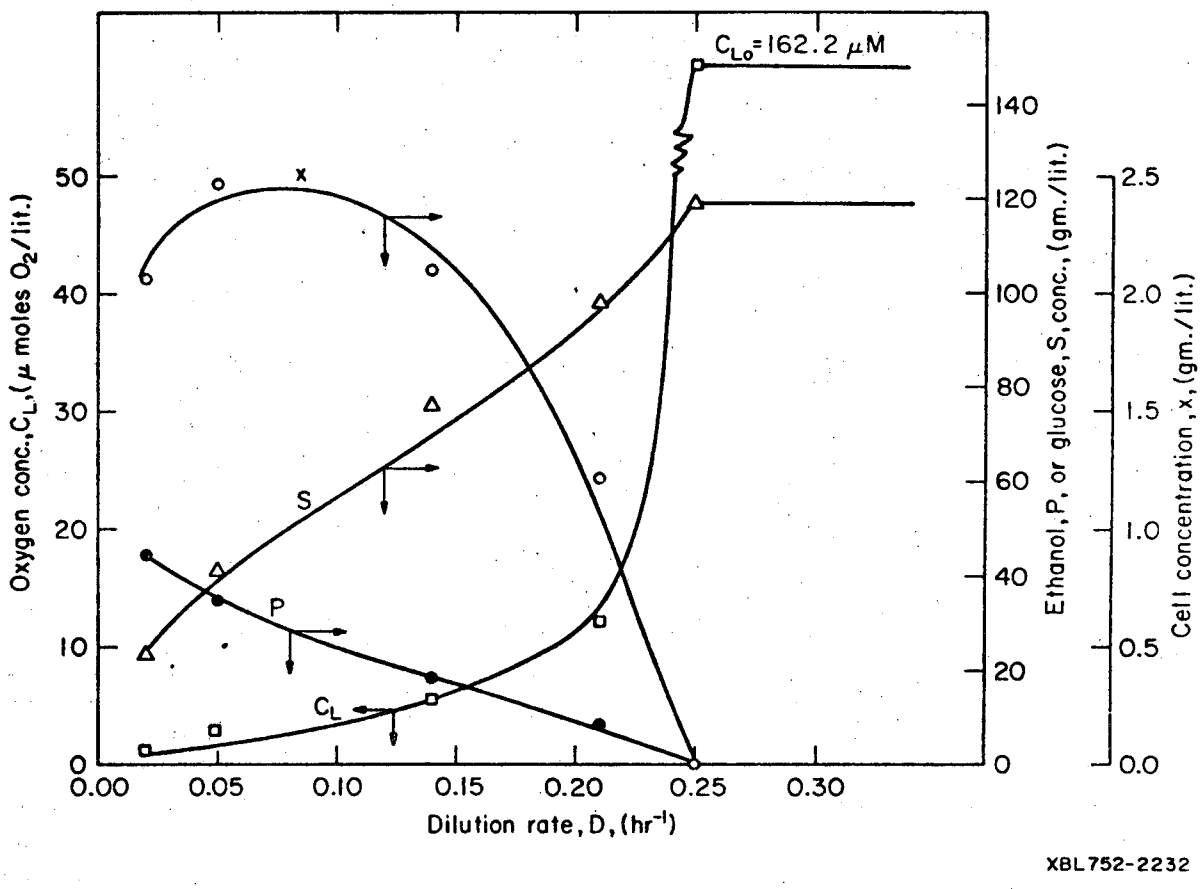

Fig. 6.40. Steady-state growth results for Run Y.

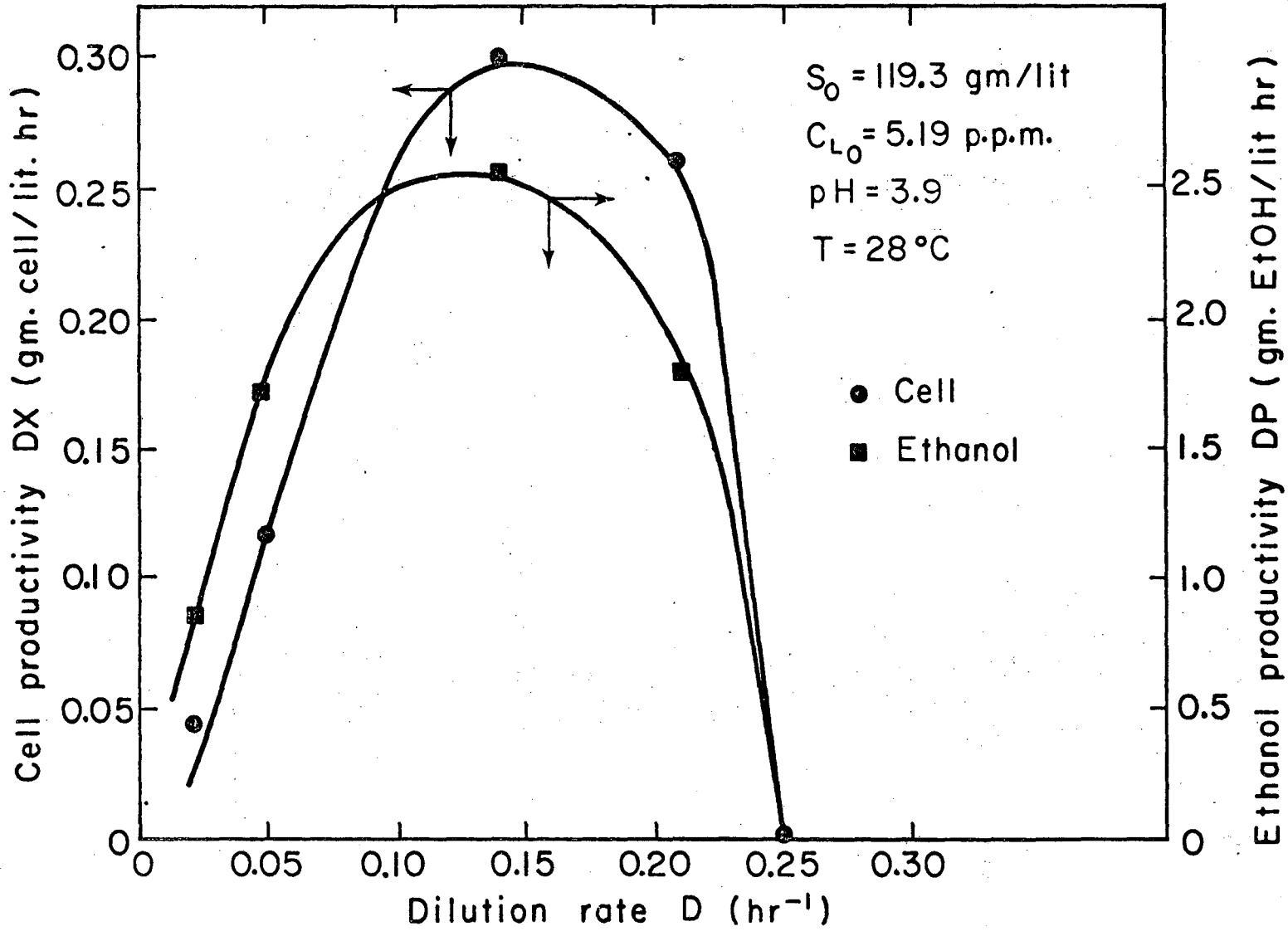

Fig. 6.41. Cell and ethanol productivity results for Run Y.

XBL754-2832

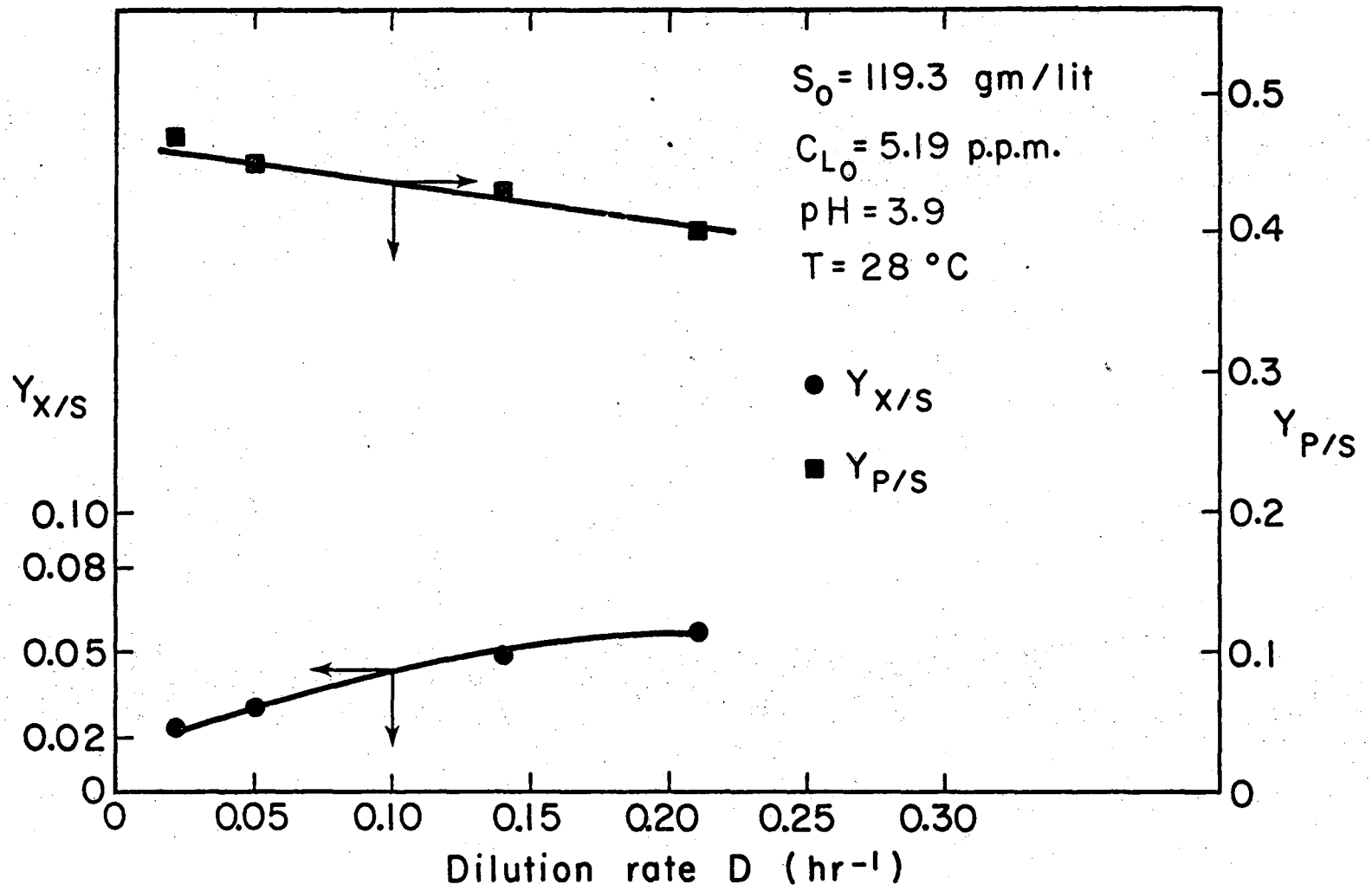

XBL754-2826

Fig. 6.42. Cell and ethanol yield factors for Run Y.

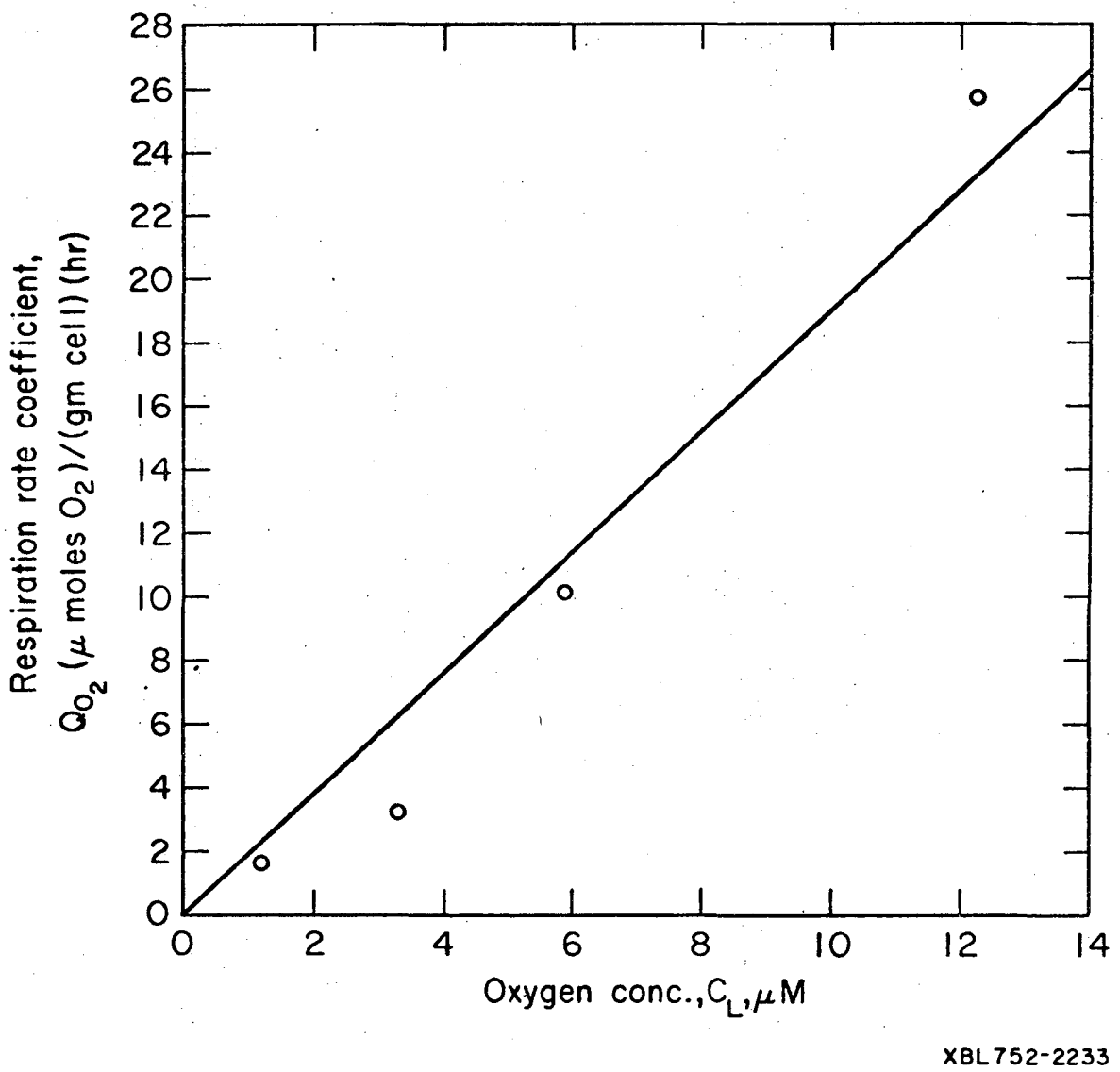

Fig. 6.43. Respiration rate coefficient for Saccharomyces cerevisiae ATCC 4126. Run Y.

Table 6.10 Summary of Data for Run Y

S_0 = 119.34 gm. glu/lit. C_{L0} = 5.19 p.p.m. pH = 3.9 T = 28°C

Dilution Rate D (hr^{-1})	Cell Mass X (gm/lit)	Glucose S (gm/lit)	Ethanol P (gm/lit)	Oxygen Conc. C_L (μM)	$Y_{X/S}$	$Y_{P/S}$	Specific Ethanol Prod. ν^* (hr^{-1})	Cell Prod. DX	EtOH Prod. DP	Rate of Glucose Uptake Rg** (hr^{-1})	Q_{O_2} ***
0.021	2.07	23.4	45.1	1.24	0.022	0.47	0.46	0.043	0.95	0.97	1.63
0.049	2.37	40.8	35.0	3.32	0.030	0.45	0.72	0.116	1.71	1.62	3.28
0.14	2.12	76.5	18.2	5.87	0.049	0.43	1.20	0.30	2.55	2.83	10.32
0.21	1.22	97.9	8.5	12.25	0.057	0.40	1.47	0.26	1.79	3.68	25.72
0.251	0	119.34	0	162.2	-	-	-	0	0	-	-

*ν = gm. EtOH/hr gm. cell.

**Rg = gm. glucose consumed/hr gm. cell

***Q_{O_2} = μMoles O_2/hr. gm. cell

6.6.7 Run OY

This run was designed to find the effect of increasing oxygen concentration at a given constant dilution rate. The glucose concentration in the feed was 93.0 gm/lit. The oxygen concentration inside the fermentor, C_L, was controlled by changing the flow rate of air and/or the speed of the magnetic stirrer. The incoming air was first sterilized and humidified and then sparged through the fermentor as shown in Figure 6.8. Essentially zero oxygen concentration was achieved by sparging the growing liquid culture with high purity nitrogen. The dilution rate for this run was held constant at 0.063 hr^{-1}. Table 6.11 is a summary of experimental results for run OY. The following observations can be made based on results from Table 6.11.

There is an almost seven-fold increase in cell mass concentration X when the oxygen concentration is increased from zero to 21.45 μM. This reflects similar increases in cell yield coefficient $Y_{X/S}$ from 0.048 to 0.151. For the same increase in oxygen concentration, i.e., from zero to 21.45 μM, the amount of unfermentable sugar left over is decreased from a high 51.50 gm/lit to 1.58 gm/lit, while the cell mass productivity increases by a factor of almost seven. If cell mass production is desirable, rather than ethanol, then a moderate amount of aeration improves both cell

production and minimizes the amount of unfermentable sugar.

The specific ethanol productivity ν decreases from 0.66 hr^{-1} at zero oxygen concentration to 0.19 hr^{-1} at 21.45 μM. This decrease in ν is in agreement with theoretical arguments presented in Section 6.3 regarding the "Pasteur effect." Since only 2 ATP are produced per mole of glucose under anaerobic conditions as opposed to 38 ATP under aerobic conditions, the cell will consume less glucose under aerobic than anaerobic conditions to obtain the same amount of ATP needed. This explains the fact that the rate of glucose uptake Rg decreases from 1.300 hr^{-1} to 0.417 hr^{-1} as the oxygen concentration increases from zero to 21.45 μM. Although the specific ethanol productivity decreases, the overall ethanol productivity per unit fermentor volume DP increases from 1.32 gm ethanol/lit hr. at zero oxygen to 2.65 gm ethanol/lit hr. at 21.45 μM. This is due to the fact that the cell concentration is much higher at aerobic than anaerobic conditions thus producing more ethanol per unit fermentor volume. Figure 6.44 shows the results of specific ethanol productivity ν and overall ethanol productivity DP as a function of oxygen concentration C_L. The decrease in ν with increasing oxygen concentration is similar to the results found by Cowland and Maule (29) and is in agreement with the "Pasteur effect" as

explained by Sols (4). Figure 6.45 is a plot of cell and ethanol yield coefficients against oxygen concentration. These results are similar to those obtained by Cowland and Maule (29). Figure 6.46 shows the results on rate of glucose uptake and overall cell productivity. As seen from Figures 6.44 to 6.46, for the growth conditions covered in this experiment, the "critical" oxygen concentration beyond which there is relatively little effect is around 20 μM. Figure 6.47 is a transient run and shows the time it takes for the yeast cell to adapt when it is exposed to a step change in oxygen concentration from 2.84 μM to 45.67 μM. As seen from Figure 6.47 the adaptation is almost complete in a relatively short period of time of 24 hours if one considers the fact that the doubling time corresponding to the dilution rate of 0.063 hr^{-1} is 11 hours. Table 6.12 shows the transient response data due to a step change in oxygen concentration.

Table 6.11 Summary of Data for Run OY

S_0 = 93.0 gm. glu/lit D = 0.063 hr^{-1} pH = 4.0 T = 28.5°C

Aeration	Oxygen Conc. C_L (μM)	Cell Mass X (gm/lit)	Glucose S (gm/lit)	Ethanol P (gm/lit)	$Y_{X/S}$	$Y_{P/S}$	Specific Ethanol Prod. ν^* (hr^{-1})	Cell Prod. DX	EtOH Prod. DP	Rate of Glucose Uptake Rg^{**} (hr^{-1})
Nitrogen	~0	2.01	51.50	21.0	0.048	0.506	0.66	0.127	1.32	1.300
None	2.84	3.35	34.50	31.0	0.051	0.473	0.58	0.211	1.95	1.232
Air	21.45	13.82	1.58	42.0	0.151	0.459	0.19	0.871	2.65	0.417
Air	112.79	14.0	1.62	40.0	0.153	0.438	0.18	0.882	2.52	0.411

*ν = gm. Ethanol/hr. gm. cell.

**Rg = gm. glucose consumed/hr. gm. cell.

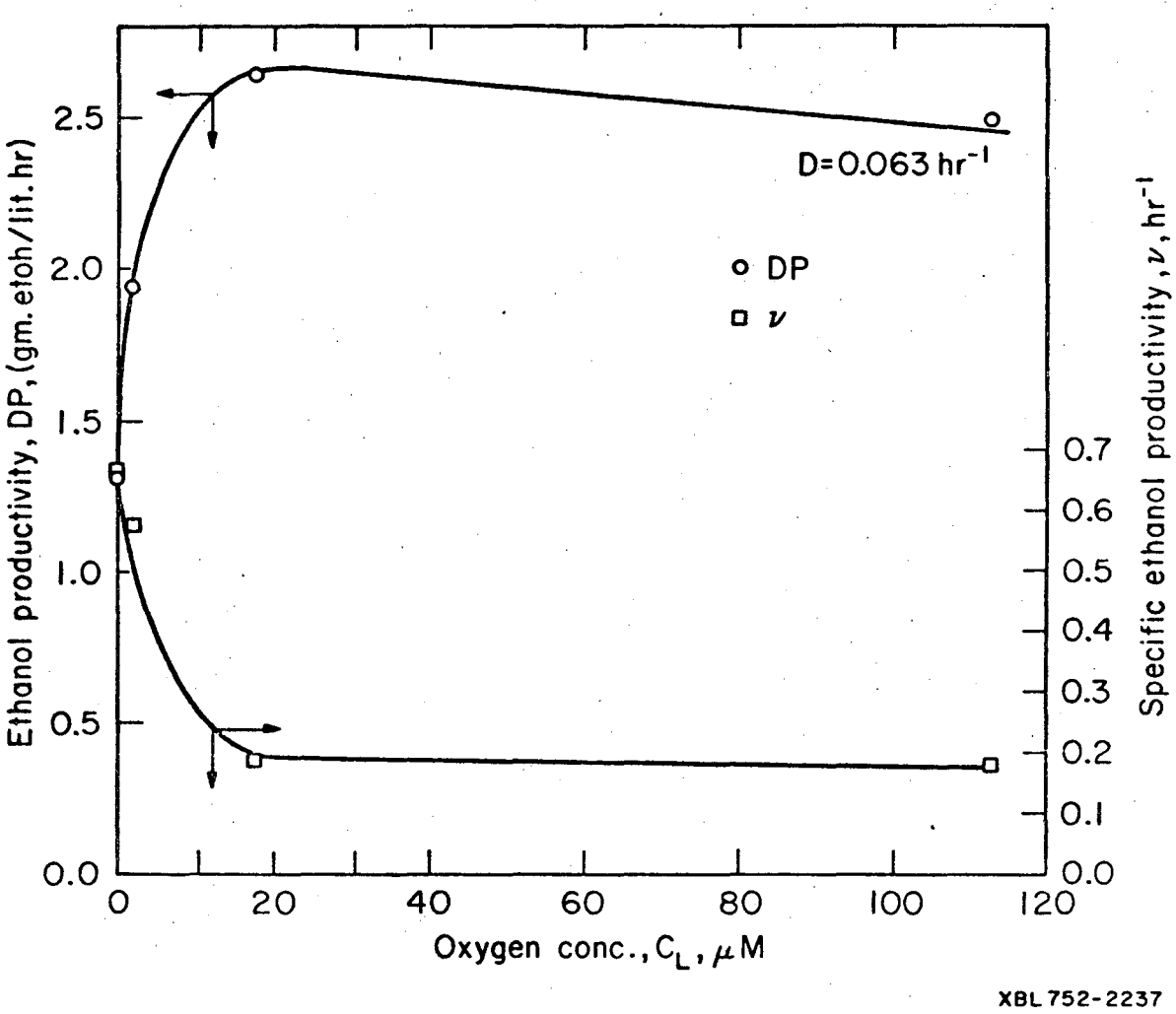

Fig. 6.44. Specific ethanol and ethanol productivity for Run OY.

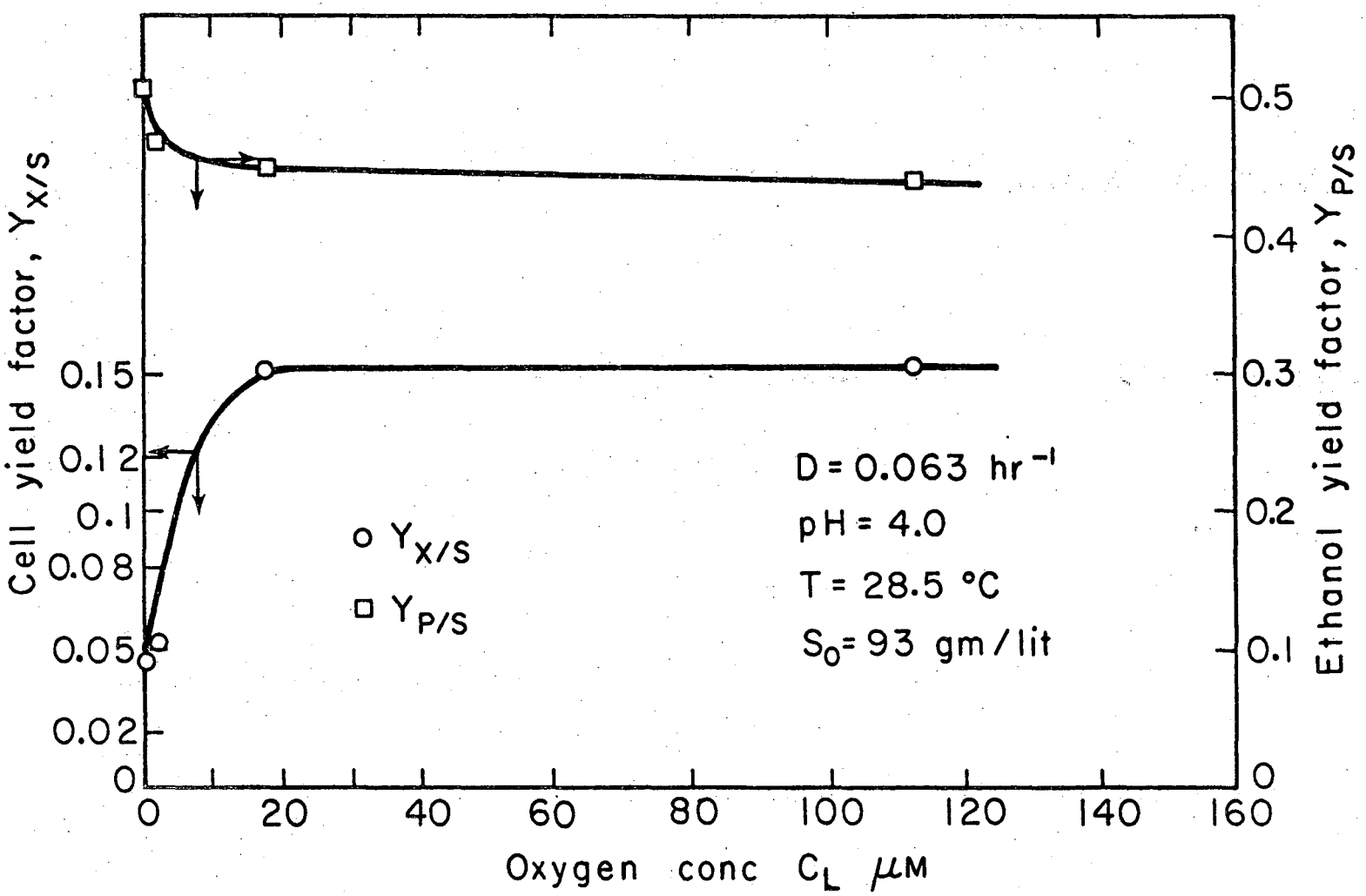

XBL754-2833

Fig. 6.45. Overall cell and ethanol yield factors for Run OY.

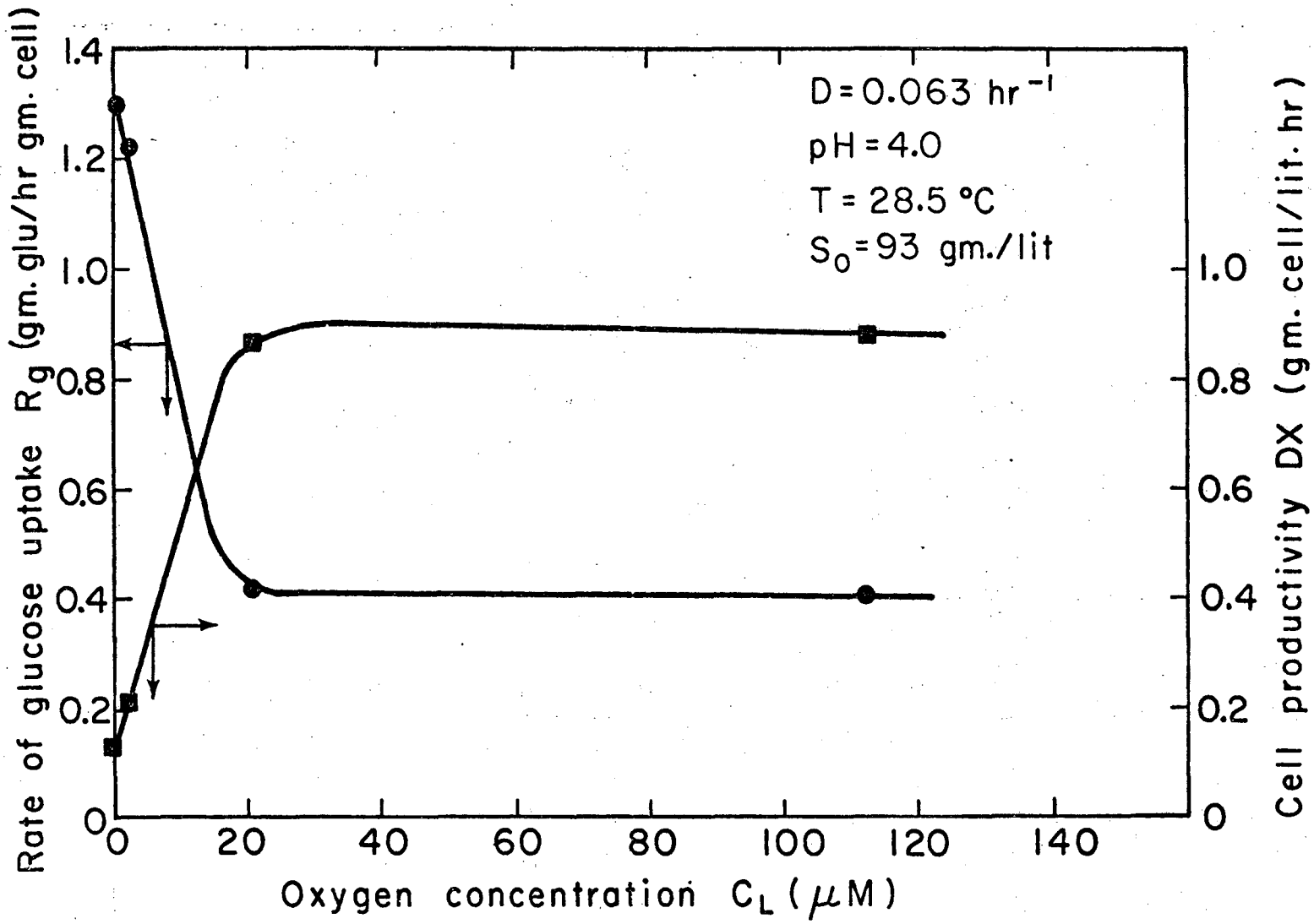

Fig. 6.46. Cell productivity and rate of glucose uptake for Run OY.

XBL754-2829

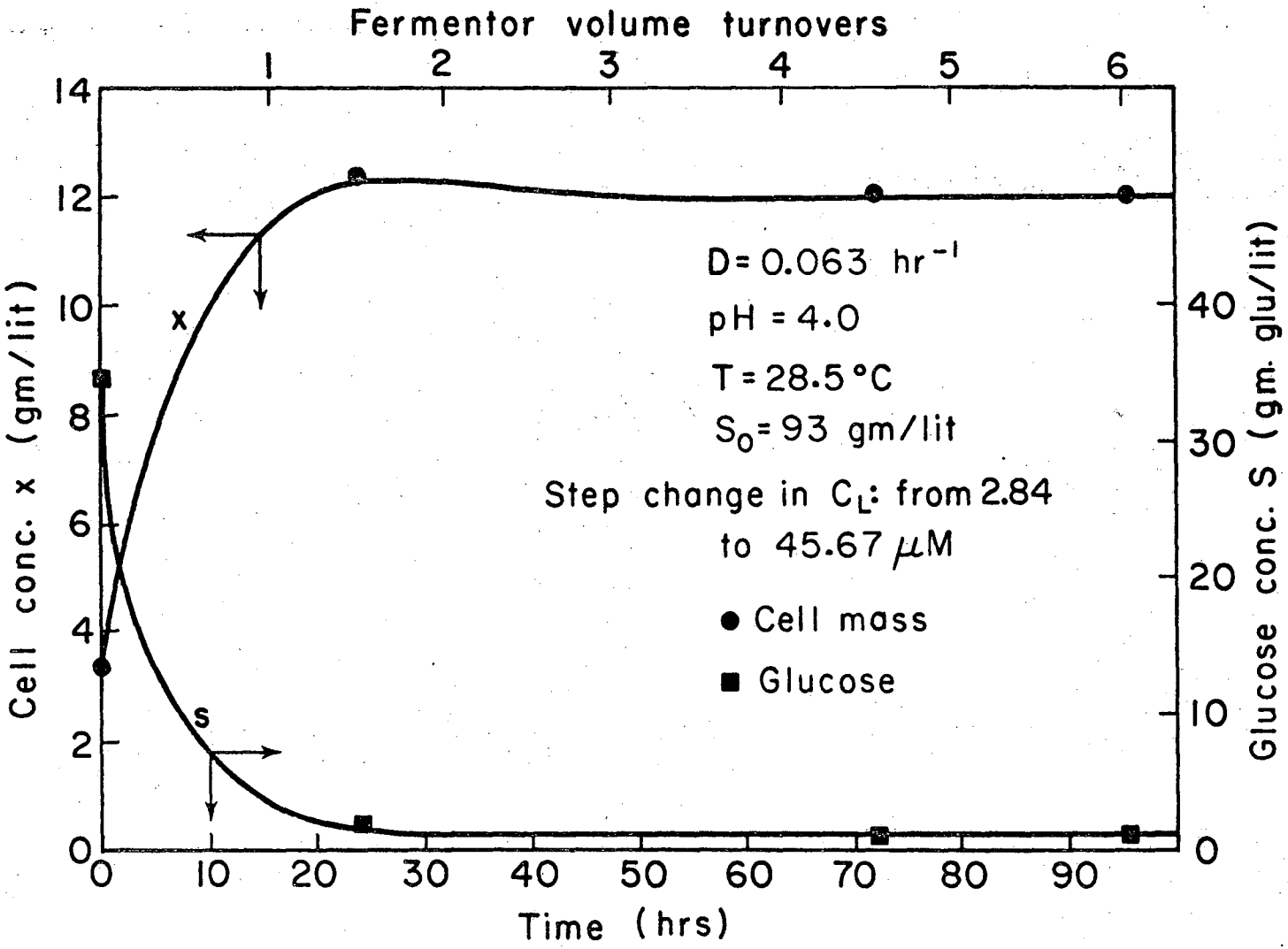

Fig. 6.47. Transient growth results due to step change in oxygen concentration.

XBL754-2828

Table 6.12. Transient Response Data Due to Step Change in Oxygen Concentration from 2.84 μM to 45.67 μM.

S_0 = 93.0 gm/lit D = 0.063 hr^{-1} pH = 4.0 T = 28.5°C

Time from Step Change (hr)	Fermentor Volume Turnovers	Cell Concentration X (gm/lit)	Glucose Concentration S (gm/lit)
0	0	3.37	34.50
24	1.51	12.43	1.80
72	4.52	12.09	1.25
96	6.03	12.09	1.25

6.6.8 Run OX

The dilution rate for this run was held constant at 0.19 hr^{-1} which is almost three times greater than that for run OY. The glucose concentration in the feed was 110 gm/lit and the oxygen concentration inside the fermentor was varied by following the same procedure as that in run OY. The results for run OX are shown in Table 6.13.

Figure 6.48 shows results of specific ethanol productivity ν and rate of glucose uptake Rg as a function of oxygen concentration. The results of run OY are also shown for comparative purposes with those of run OX. As seen from Figure 6.48 the effect of oxygen concentration on specific ethanol productivity is much more pronounced at D = 0.063 hr^{-1} than at D = 0.19 hr^{-1}. For example, at C_L = 20 μM there is a 70% reduction in ν from its value at zero oxygen for D = 0.063 hr^{-1}. This is to be contrasted with a 24% reduction in ν at C_L = 20 μM and D = 0.19 hr^{-1}. This difference in oxygen effect on ν at the same oxygen concentration, but different dilution rates is due to the antagonistic effect of glucose concentration on ν as explained in Section 6.3. The higher dilution rate resulted in much higher glucose concentrations inside the fermentor than those for the lower dilution rate. For example, as seen from the data in Tables 6.11 and 6.13, at C_L = 20 μM the glucose concentration for D = 0.19 hr^{-1} is about 85 gm/lit as opposed to about

1.6 gm/lit at D = 0.063 hr^{-1}. High glucose concentrations tend to minimize the effect of oxygen. The effect of oxygen concentration on rate of glucose uptake Rg follows a similar pattern to that for ν, in agreement with the theory covered in Section 6.3.

Figure 6.49 is a plot of $Y_{P/S}$ and $Y_{X/S}$ against oxygen concentration for both dilution rates 0.063 hr^{-1} and 0.19 hr^{-1}. Again we observe that at the lower glucose concentrations the cell yield factor $Y_{X/S}$ is much higher than the one for 0.19 hr^{-1} at the same oxygen concentration. This finding suggests that if cell mass production rather than ethanol is desired optimal cell yields may be achieved at low glucose concentrations and high oxygen concentrations. In addition, results from Figure 6.49 show that the ethanol yield factor $Y_{P/S}$ is systematically higher at 0.063 hr^{-1} than at the dilution rate of 0.19 hr^{-1}. This again suggests the effect of glucose concentration on $Y_{P/S}$ at a given oxygen concentration. Figure 6.50 shows the overall cell mass and ethanol productivity results for both runs OX and OY at different levels of oxygen concentration. This graph shows that both cell and ethanol productivities are systematically higher at the lower dilution rate of 0.063 hr^{-1} than that at 0.19 hr^{-1} for a given oxygen concentration. These results again show the effects of glucose at a given oxygen

concentration. Figure 6.51 is a plot of percent of glucose in the feed utilized in the fermentor against oxygen concentration. We see that almost all sugar is fermented if the optimal conditions for dilution rate and oxygen concentration are chosen. For a given feed rate low dilution rates imply large fermentor volumes and correspondingly higher capital investment costs which must be offset by increased ethanol and cell productivities per unit fermentor volume. This is clearly a case for optimization of such parameters as dilution rate, glucose concentration, oxygen concentration, depending on what the objective of optimization is.

Table 6.13 Summary of Data for Run OX

S_0 = 110 gm/lit D = 0.19 hr^{-1} pH = 4.1 T = 28°C

Aeration	Oxygen Conc. C_L (μM)	Cell Mass X (gm/lit)	Glucose S (gm/lit)	Ethanol P (gm/lit)	$Y_{X/S}$	$Y_{P/S}$	Specific Ethanol Prod. ν^* (hr^{-1})	Cell Prod. DX	EtOH Prod. DP	Rate of Glucose Uptake Rg^{**} (hr^{-1})
Nitrogen	0.29	1.15	95.00	5.5	0.076	0.37	0.904	0.219	1.04	2.48
None	0.98	1.33	93.75	6.0	0.082	0.36	0.86	0.26	1.14	2.32
Air	6.60	1.50	92.50	6.5	0.086	0.37	0.82	0.29	1.24	2.22
Air	8.93	1.84	89.50	7.4	0.090	0.36	0.77	0.35	1.41	2.12
Air	67.12	3.60	73.25	10.4	0.098	0.28	0.55	0.68	1.98	1.94

*ν = gm. Ethanol/hr. gm. cell.

**Rg = gm. glucose consumed/hr. gm. cell.

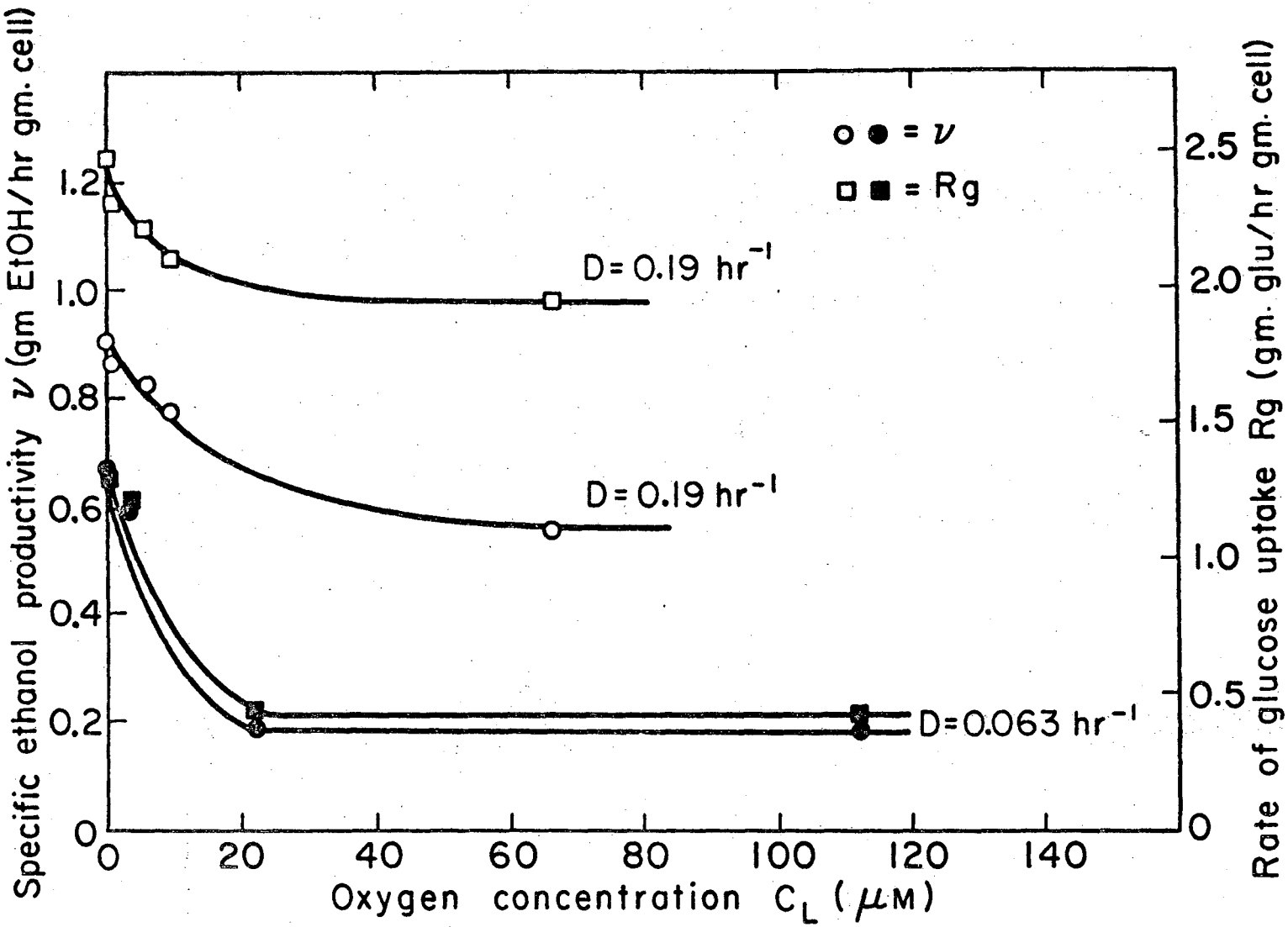

Fig. 6.48. Specific ethanol productivity and rate of glucose uptake for Runs OY and OX.

XBL754-2831

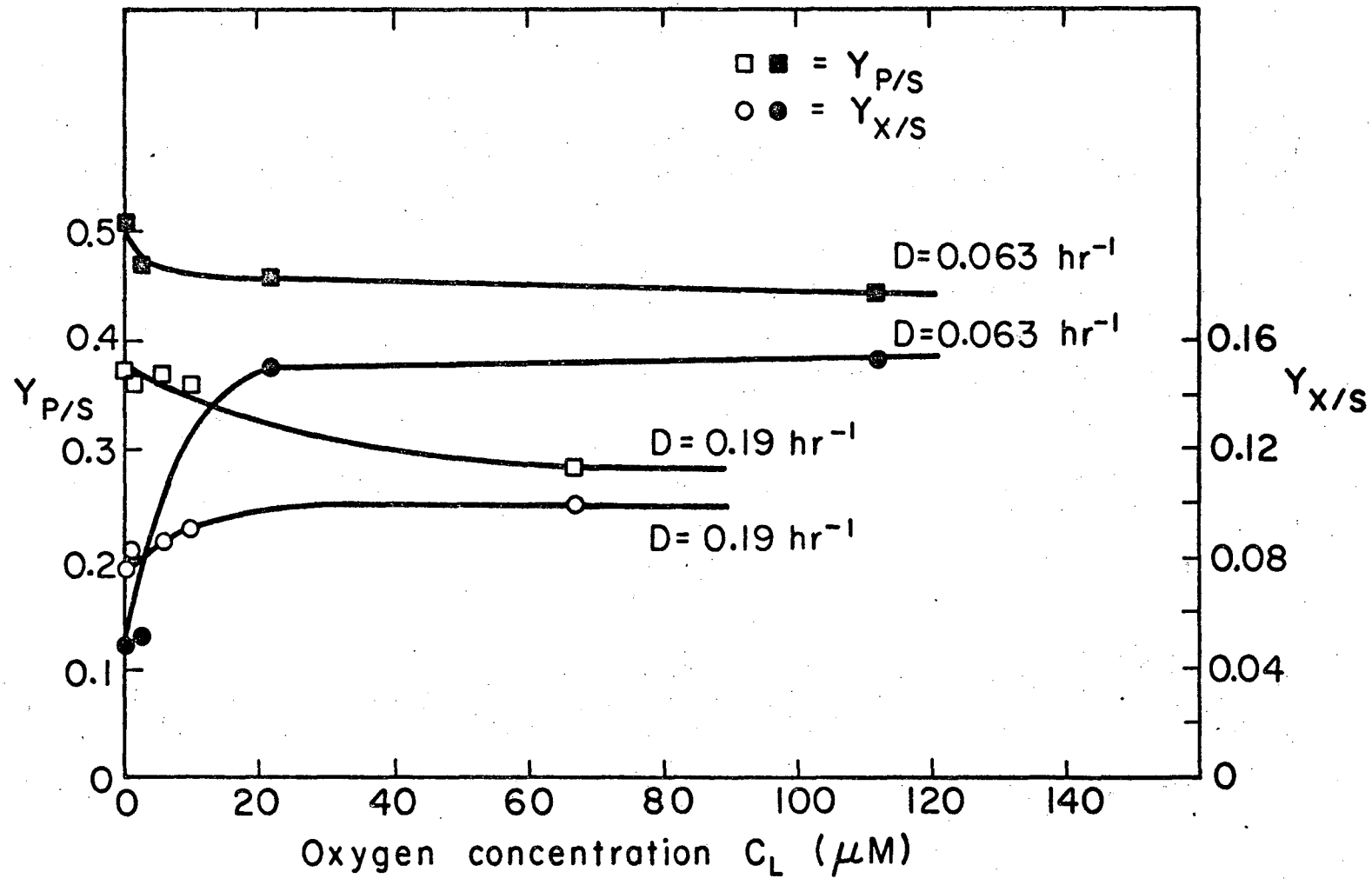

XBL754-2827

Fig. 6.49. Overall cell and ethanol yield factors for Runs OY and OX.

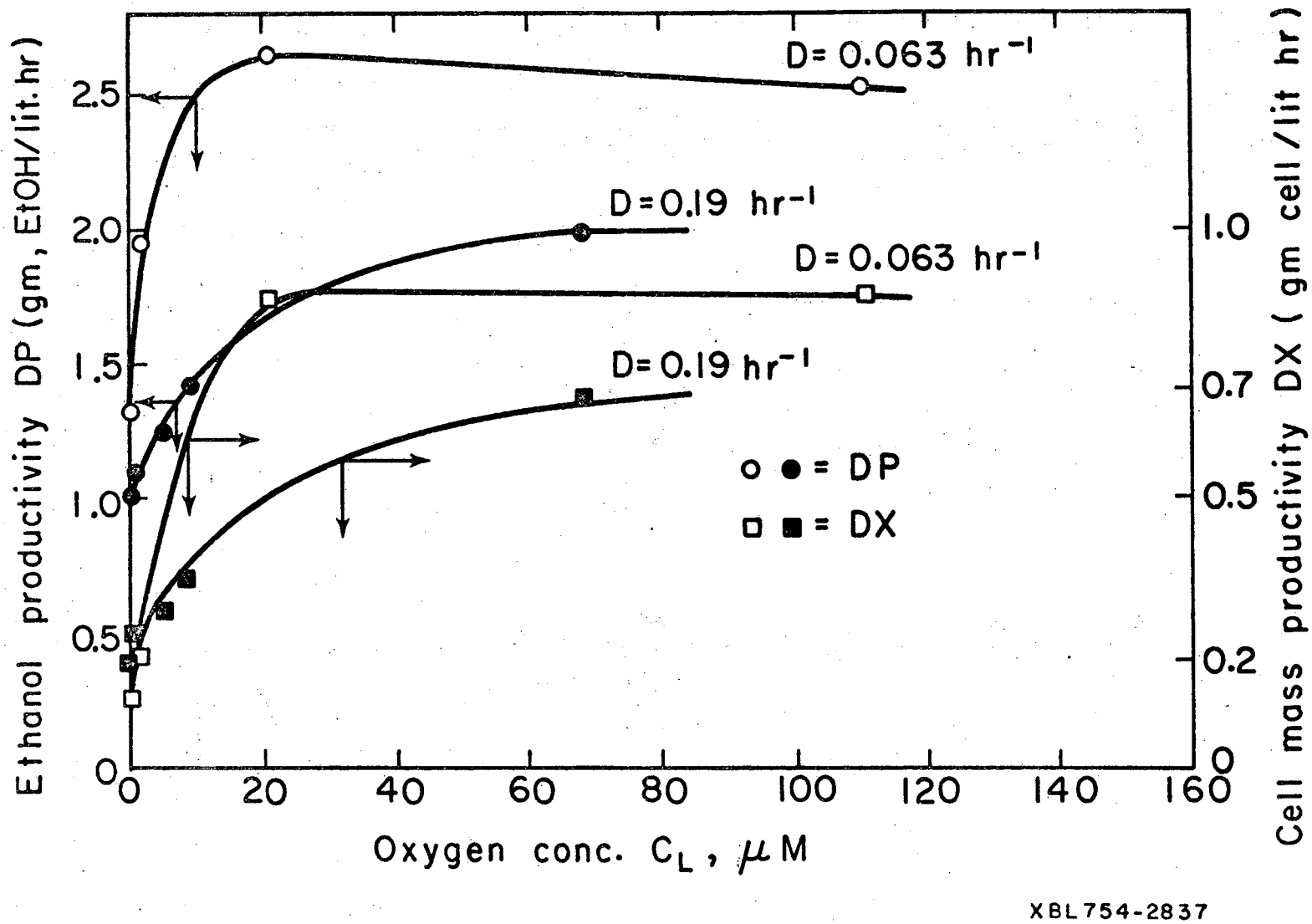

XBL754-2837

Fig. 6.50. Cell and ethanol productivity for Runs OY and OX.

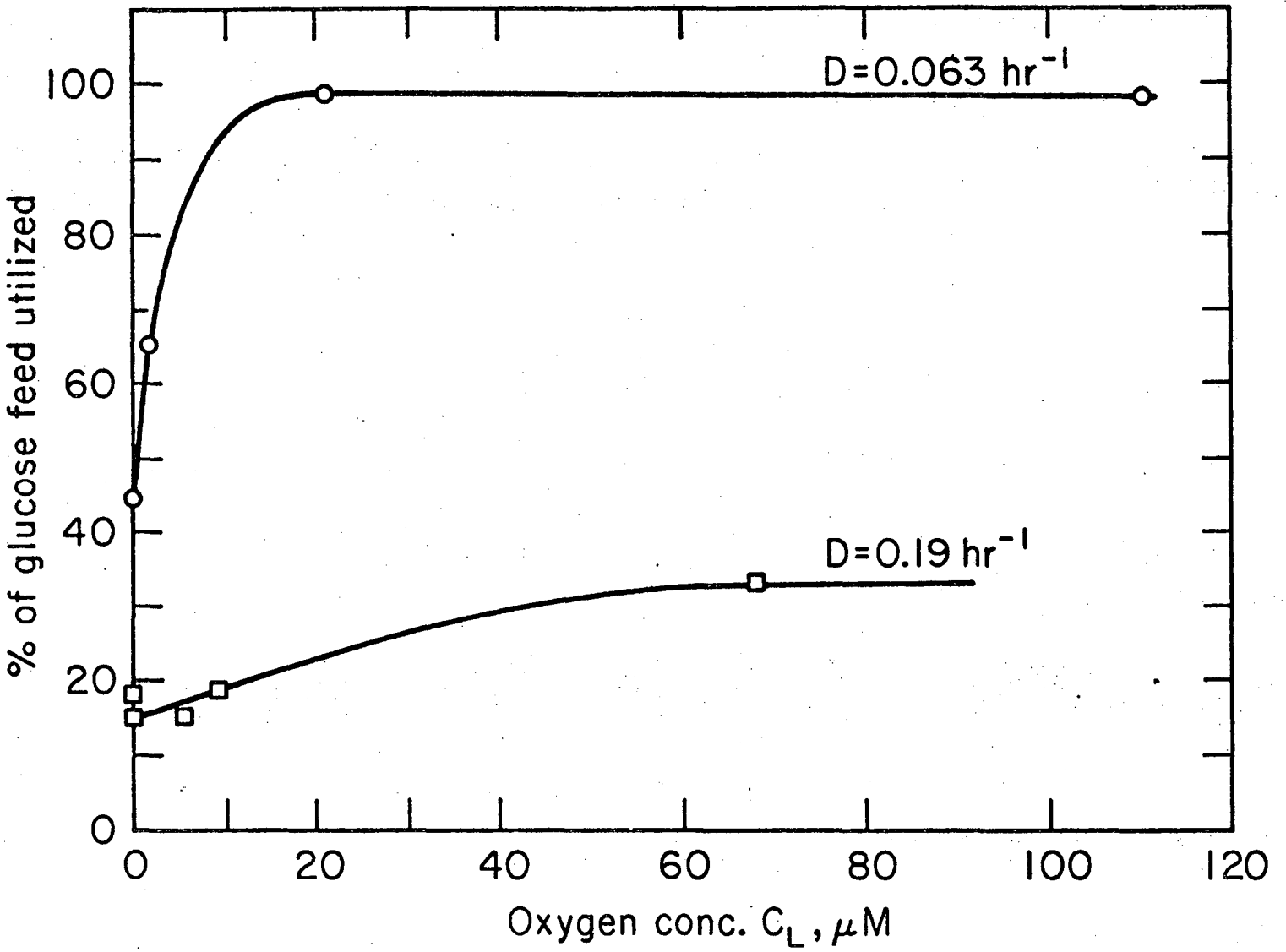

Fig. 6.51. Utilization of glucose in the feed at different oxygen concentrations and constant dilution rate. XBL752-2238

References Cited in Chapter VI

1. Hartwell, H. H., Culotte, J., Pringle, J. R., Reid, B. J., Genetic Control of the Cell Division Cycle in Yeast. Science, 1974, 183, 46-51.

2. de Becze, G., Reproduction of Distillers Yeasts. Biotech. Bioeng., 1964, 6(2), 191-221.

3. Hoffmann, H. P., Avers, C. J., Mitochondrion of Yeast: Ultrastructural Evidence of One Giant, Branched Organelle per Cell. Science, 1973, 181, 749-751.

4. Sols, A., Regulation of Carbohydrate Transport and Metabolism in Yeast. In A. K. Mills (Ed.), Aspects of Yeast Metabolism, Oxford, Blackwell Scientific Publications, 1968. Pp. 47-66.

5. Cirillo, V. P., Ann. Rev. Microbiology, 1961, 15, 197.

6. Oura, E. Effect of Aeration Intensity on the Biochemical Composition of Baker's Yeast. I. Factors Affecting the Type of Metabolism. Biotech. Bioeng., 1974, 16, 1197-1212.

7. Oura, E., II. Activities of the Oxidative Enzymes. Biotech. Bioeng., 1974, 16, 1213-1225.

8. Rogers, P. J. and Stewart, P. R., Respiratory Development in Saccharomyces cerevisiae Grown at Controlled Oxygen Tension. Journ. Bacteriology, 1973, 115(1), 88-97.

9. Richard, P. A. D., Moss, F. J., and Ganez, M. Biotech. Bioeng., 1971, 13, 1-16.

10. Warburg, O., Geissler, A. W., and Lorenz, S., Oxygen, the Creator of Differentiation. In A. K. Mills (Ed.), Aspects of Yeast, Oxford, Blackwell Scientific Publications, 1968. Pp. 327-337.

11. Dickens, F., "The Enzymes," Vol. II, Part 1, J. B. Sumner and K. Myrback (Eds.), New York, Academic Press, 1951.

12. Holzer, H., Biocehmistry of Adaptation in Yeast. In A. K. Mills (Ed.), Aspects of Yeast Metabolism, Oxford, Blackwell Scientific Publications, 1968. Pp. 155-195.

13. Kleinzeller, A., and Kotyk, A, Transport of Monosaccharides in Yeast Cells and its Relationship to Cell Metabolism. In A. K. Mills (Ed.), Aspects of Yeast Metabolism, Oxford, Blackwell Scientific Publications, 1968.

14. Sols, A., and Salas, M. L., in S. P. Colowick and N. O. Kaplan (Eds.), Methods in Enzymology. New York, Academic Press, 1965.

15. Holzer, H. and Witt, J. Biochem. Z., 1958, 330, 545.

16. Moss, F. J., Rickard, P. A. D., Bush, F. E., Ceiger, P., The Response by Microorganisms to Steady-State Growth in Controlled Concentrations of Oxygen and Glucose. II. Saccharomyces carlsbergensis. Biotech. Bioeng., 1971, 13, 63-75.

17. Aiba, S., Shoda, M., and Nagatani, M., Kinetics of Product Inhibition in Alcohol Fermentation. Biotech. Bioeng., 1968, 10, 845-864.

18. Sumner, J. B., and Somero, G. F., "Laboratory Experiments in Biological Chemistry." New York, Academic Press, 1944.

19. Mancy, K. H., Okun, D. A., and Reilley, C. N., J. Electroanal. Chem., 1962, 4, 65.

20. Johnson, M. J., Borkowski, J., and Englblom, C., Biotech. Bioeng., 1964, 6, 457.

21. Robinson, C. W., and Wilke, C. R. Mass Transfer Coefficients and Interfacial Area for Gas Absorption by Agitated Aqueous Electrolyte Solutions UCRL Report #29472, 1971.

22. Vincent, A., Measurement of Dissolved Oxygen. Process Biochemistry, 1974, 19-21.

23. Solomons, G. L., Continuous Culture of Microorganisms, Monograph #12, pp. 233-253, 1961, Society of Chemical Industry.

24. Cook, A. H., The Chemistry and Biology of Yeasts, New York, Academic Press, 1958.

25. Phaff, H. J., Miller, M. W., Mrak, E. M., The Life of Yeasts. Cambridge, Harvard University Press, 1966.

26. Rose, A. H., and Harrison, J. S., The Yeasts, Vol. 3., Yeast Technology, New York, Academic Press, 1970.

27. Aiyar, A. S., and Luedeking, R., A Kinetic Study of the Alcoholic Fermentation of Glucose by S. cerevisiae. Chem. Eng. Progr. Symp. Ser., No. 69, Vol. 62, pp. 55-59.

28. Bazua, C. The Effect of Alcohol Concentration on the Kinetics of Ethanol Production by Saccharomyces cerevisiae. M.S. Thesis, University of California, Berkeley, 1974.

29. Cowland, T. W., Maule, D. R., Some Effects of Aeration on the Growth and Metabolism of S. cerevisiae in Continuous Culture. J. Inst. Brew., 1966, 72, 480-488.

30. Monod, J., La Technique de Culture Continue; Theorie et Applications. Ann. Inst. Pasteur, 1950, 79, 330.

31. Michaelis, L., and Menten, M. L., Biochem. Z. 1913, 49, 333.

32. Luedeking, R., and Piret, E. L., A kinetic study of the lactic acid fermentation. Batch process at controlled pH. J. Biochem. Microbiol. Tech. and Eng., 1959, 1, 393.

APPENDIX B

Table B.1 Calibration of Oxygen Probe

Solution	Temperature °C	Resistance R, (Kilo Ohms)	Voltage V, (mV)	Current I, (μA)	Oxygen Concentration-C_L (μM)
Sulphite	21	7.159	0.050	0.00698	0
"	29.5	"	0.062	0.00866	0
"	35	"	0.082	0.01145	0
"	48	"	0.118	0.01648	0
Saturated Water	30.2	0.200	0.300	1.5000	243.74
Pure Medium	30.0	7.159	2.60	0.36318	57.9

For pure saturated water at 30.2°C net current output $I' = I - I_o = 1.50000 - 0.00900 = 1.491\mu A$. which is proportional to 243.74 H the partial pressure of oxygen, where H = Henry's constant. For pure medium at almost the same temperature, i.e., 30°C the net current output is $I' = I - I_o = 0.36318 - 0.00900 = 0.35418\ \mu A$ which corresponds to

$$C_L = \frac{0.35418\mu A}{H} \times \frac{243.74H}{1.491\mu A} = \frac{86.3278}{1.491} = 57.899\mu M.$$

CHAPTER VII

APPLICATION OF THE ROTORFERMENTOR TO ETHANOL FERMENTATION

In this section the theory on the kinetics of dense cell culture is presented with some batch and transient experimental results on ethanol fermentation. In addition, some attempt is being made to assess the economic feasibility of the Rotorfermentor as a device for potential use in the fermentation industry.

7.1 Transient Operation of the Rotorfermentor

Consider the Rotorfermentor shown in Figure 7.1. A general cell mass balance yields equation 7.1.1.

Rate in - Rate out + Rate of generation = Rate of accumulation

$$0 - BX_r - LX_L + \mu X_r V_r = \frac{dX_r}{dt} \qquad 7.1.1$$

where:

B = cell bleed rate, lit/hr.

L = filtrate flow rate, lit/hr.

V_r = volume of Rotorfermentor, lit.

X_r = cell concentration inside the Rotorfermentor gm/lit.

X_L = cell concentration in the filtrate, gm/lit.

μ = specific growth rate, hr^{-1}.

Similarly, a general mass balance on product P_r such as ethanol, is given by equation 7.1.2.

$$0 - BP_r - LP_r + \mu X_r V_r = \frac{dP_r}{dt} V_r \qquad 7.1.2$$

where:

P_r = concentration of product, gm/lit.

ν = specific productivity, hr^{-1}.

We further define the following dilution rates:

1. Overall dilution rate based on feed rate F_r.

$$D_0 = \frac{F_r}{V_r} = \frac{B}{V_r} + \frac{L}{V_r} \qquad 7.1.3$$

2. Dilution rate based on bleed rate B.

$$D_1 = \frac{B}{V_r} \qquad 7.1.4$$

3. Dilution rate based on filtrate rate L.

$$D_2 = \frac{L}{V_r} \qquad 7.1.5$$

It is obvious then that in general

$$D_0 = D_1 + D_2 \qquad 7.1.6$$

Depending on the way in which the Rotorfermentor is operated equations 7.1.1 and 7.1.2 reduce to the following forms.

Case I: Cell concentration in filtrate is zero, i.e., $X_L = 0$.

Equation 7.1.1 becomes

$$- BX_r + \mu X_r V_r = \frac{dX_r}{dt} V_r \qquad \text{or}$$

$$- D_1 + \mu = \frac{d(\ln X_r)}{dt} \qquad 7.1.7$$

For the product P_r equation 7.1.2 remains the same.

Case II: Bleed rate $B = 0$ and cell concentration in filtrate $X_L = 0$.

For cell mass equation 7.1.1 is reduced to:

$$\mu X_r V_r = \frac{dX_r}{dt} V_r \qquad \text{or}$$

$$\mu = \frac{1}{X_r} \frac{dX_r}{dt} \qquad 7.1.8$$

For product P_r equation 7.1.2 becomes

$$- LP_r + \nu X_r V_r = \frac{dP_r}{dt} V_r \qquad \text{or}$$

$$- D_2 P_r + \nu X_r = \frac{dP_r}{dt} \qquad 7.1.9$$

Case III: Bleed rate $B = 0$ but cell concentration in filtrate $X_L \neq 0$.

Equation 7.1.1 becomes

$$- LX_L + \mu X_r V_r = \frac{dX_r}{dt} V_r \qquad \text{or}$$

$$- D_2 X_L + \mu X_r = \frac{dX_r}{dt} \qquad 7.1.10$$

For product P_r equation 7.1.2 is reduced to

$$- LP_r + \nu X_r V_r = \frac{dP_r}{dt} V_r \qquad \text{or}$$

$$- D_2 P_r + \nu X_r = \frac{dP_r}{dt} \qquad 7.1.11$$

which is the same as in Case II.

The solution to differential equations presented for Cases I, II and III becomes rather cumbersome and depending on existing operating conditions some useful approximations may be made.

7.2. Steady-State Operation of the Rotorfermentor.

Assuming that the cell concentration in the filtrate is zero, i.e., $X_L = 0$, then at steady-state conditions we have the following cell and product mass balance:

Cell mass:

$$- BX_r + \mu X_r V_r = 0$$

or

$$\mu = \frac{B}{V_r} = D_1 \qquad 7.1.12$$

Product P_r:

$$- BP_r - LP_r + \nu X_r V_r = 0 \qquad 7.1.13$$

or

$$\nu X_r V_r = P_r(B + L) = P_r F_r$$

or

$$\nu = \frac{P_r D_0}{X_r} \qquad 7.1.14$$

The cell yield and product yield coefficients $Y_{X/S}$ and $Y_{P/S}$ are given by equations 7.1.15 and 7.1.16 respectively.

$$Y_{X/S} = \frac{\Delta X}{\Delta S} = \frac{BX_r}{F_r S_0^f - LS_r - BS_r}$$

or

$$Y_{X/S} = \frac{BX_r}{F_r(S_0^r - S_r)} \qquad 7.1.15$$

and

$$Y_{P/S} = \frac{\Delta P}{\Delta S} = \frac{LP_r + BP_r}{F_r(S_0^r - S_r)}$$

or

$$Y_{P/S} = \frac{P_r}{(S_0^r - S_r)} \qquad 7.1.16$$

7.3. Comparison of the Rotorfermentor with the C.S.T. Fermentor.

One of the major advantages of the Rotorfermentor is high cell productivities per unit fermentor volume. An expression can be developed which relates the cell productivity of the Rotorfermentor to that of an ordinary C.S.T. fermentor. The two schemes are shown in Figure 7.1.

The cell productivity of the C.S.T. fermentor is given by equation 7.3.1.

$$Q = \frac{FX}{V} \qquad 7.3.1$$

where:

Q = cell productivity, gm. cells/lit hr.

F = volumetric feed flow rate, lit/hr.

V = volume of the C.S.T. fermentor, lit.

X = cell concentration, gm. cells/lit.

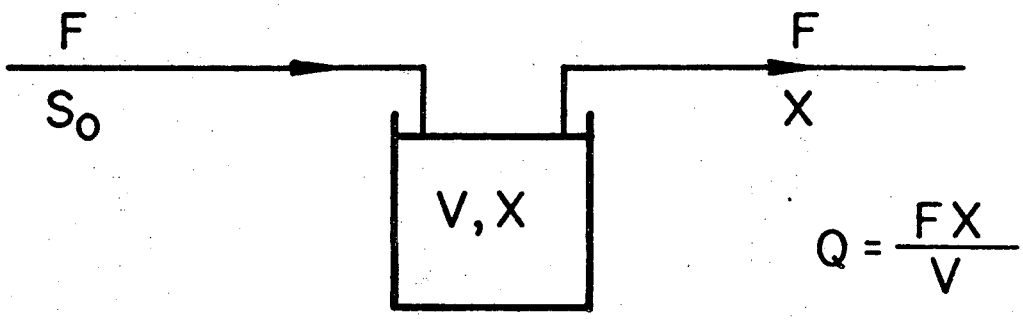

C.S.T. fermentor

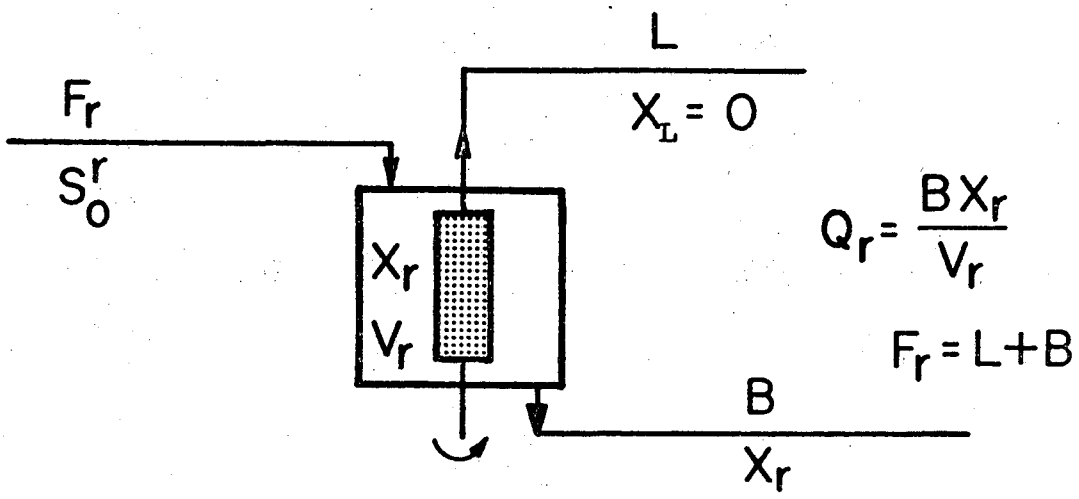

Rotorfermentor

$$R = \frac{Q_r}{Q} = \left(\frac{BV}{FV_r}\right)\left(\frac{X_r}{X}\right)$$

XBL718-4054

Fig. 7.1. Comparison of the Rotorfermentor to C.S.T. fermentor.

The cell productivity for the Rotorfermentor is given by equation 7.3.2:

$$Q_r = \frac{BX_r}{V_r} \qquad 7.3.2$$

where:

Q_r = cell productivity of the Rotorfermentor, gm cells/lit hr.

B = volumetric cell bleed rate, lit/hr.

V_r = net fermentor volume of the Rotorfermentor, lit.

X_r = cell concentration, gm. cells/lit.

The cell productivity ratio of the Rotorfermentor to C.S.T. fermentor, R_X, is given by

$$R_X = \left(\frac{BV}{V_r F}\right)\left(\frac{X_r}{X}\right). \qquad 7.3.3$$

At steady-state the specific growth rate for each system is given by

$$\mu = \frac{F}{V} = \frac{B}{V_r}. \qquad 7.3.4$$

If it is assumed that the Rotorfermentor is operated at the same specific growth rate as the C.S.T. fermentor equation 7.3.3 becomes

$$R_X = \frac{X_r}{X}. \qquad 7.3.5$$

For the C.S.T. fermentor the cell concentration is given by

$$X = Y_{X/S} (S_0 - S) \qquad 7.3.6$$

where

S_0 = concentration of limiting substrate in the feed, gm/lit.

S = concentration of limiting substrate in the fermentor, gm/lit.

$Y_{X/S}$ = cell mass to substrate yield coefficient.

Similarly, for the Rotorfermentor a material balance at steady-state gives

$$X_r = Y_{X/S} (S_0^r - S_r). \qquad 7.3.7$$

Therefore, if the two fermentors are operated at the same level of substrate concentration, i.e., a condition imposed by equation 7.3.4 and assuming the same yield coefficients, equations 7.3.6 and 7.3.7 may be combined to give

$$\frac{X_r}{X} = \frac{F_r}{B} = 1 + \frac{L}{B} \qquad 7.3.8$$

or

$$R_X = 1 + \frac{L}{B} \qquad 7.3.9$$

As shown by equations 7.3.7 and 7.3.8 high cell concentrations and high productivity ratios may be attained

in the Rotorfermentor by employing a high ratio of feed rate to bleed rate. Thus, by suitable choice of flow rates, the Rotorfermentor may fulfill the functions of both an ordinary fermentor and centrifuge cell separator.

Using similar arguments an expression can be developed which gives the productivity ratio for a product such as ethanol. This may be obtained by dividing the ethanol productivity of Rotorfermentor to that of an ordinary C.S.T. fermentor at steady-state conditions. We assume that both the Rotorfermentor and C.S.T. fermentor are operated at the same specific growth rate μ. Under these assumptions the productivity ratio for product P is given by equation 7.3.10.

$$R_P = \frac{(F_r/V_r)\ (P_r)}{(F/V)\ (P)} = \frac{(\frac{B}{V_r} + \frac{L}{V_r})\ (P_r)}{(F/V)\ (P)} \qquad 7.3.10$$

We assume that $\mu = \frac{B}{V_r} = \frac{F}{V}$ 7.3.11

then equation 7.3.10 reduces to

$$R_P = 1 + \left(\frac{D_2}{D_1}\right)\left(\frac{P_r}{P}\right) \qquad 7.3.12$$

where

R_p = Rotorfermentor to C.S.T. fermentor productivity ratio for product P, dimensionless.

$D_2 = \frac{L}{V_r}$, hr_j^{-1} defined by equation 7.1.5.

$D_1 = \frac{B}{V_r}$, hr^{-1} defined by equation 7.1.4.

P_r = product concentration inside the Rotor-fermentor, gm/lit.

P = product concentration inside the C.S.T. fermentor, gm/lit.

As seen from equation 7.3.12 if $P_r \geq P$ then the productivity ratio $R_P > 1$. Thus, by suitable choice of operating conditions for D_2, so that D_2 is maximized while maintaining $P_r \geq P$, it is possible to achieve high productivity ratios for product P.

7.4. Experimental Results

The primary objective of the experiments described in this section is to demonstrate the operational feasibility of the Rotorfermentor as applied to ethanol fermentation. No attempt is being made to optimize the operational variables involved, such as various combinations of flow rates of bleed and filtrate, concentration levels of cells and glucose. Considerable difficulties were experienced in selecting the proper membrane which must be strong and having the proper pore size so that plugging of the pores by yeast cells is not a problem.

7.4.1. Run B

This is a batch run, i.e., no feed of medium. The Rotorfermentor chamber was filled with 12 liters of sterilized medium and inoculated with 500 ml. inoculum that was grown in a Minifermentor. Agitation was provided by the 2-inch diameter rotor at 600 r.p.m. The glucose concentration in the medium was 52 gm/lit. The batch growth results are shown in Figures 7.4.1 and 7.4.2. Table 7.4.1 summarizes the results for Run B.

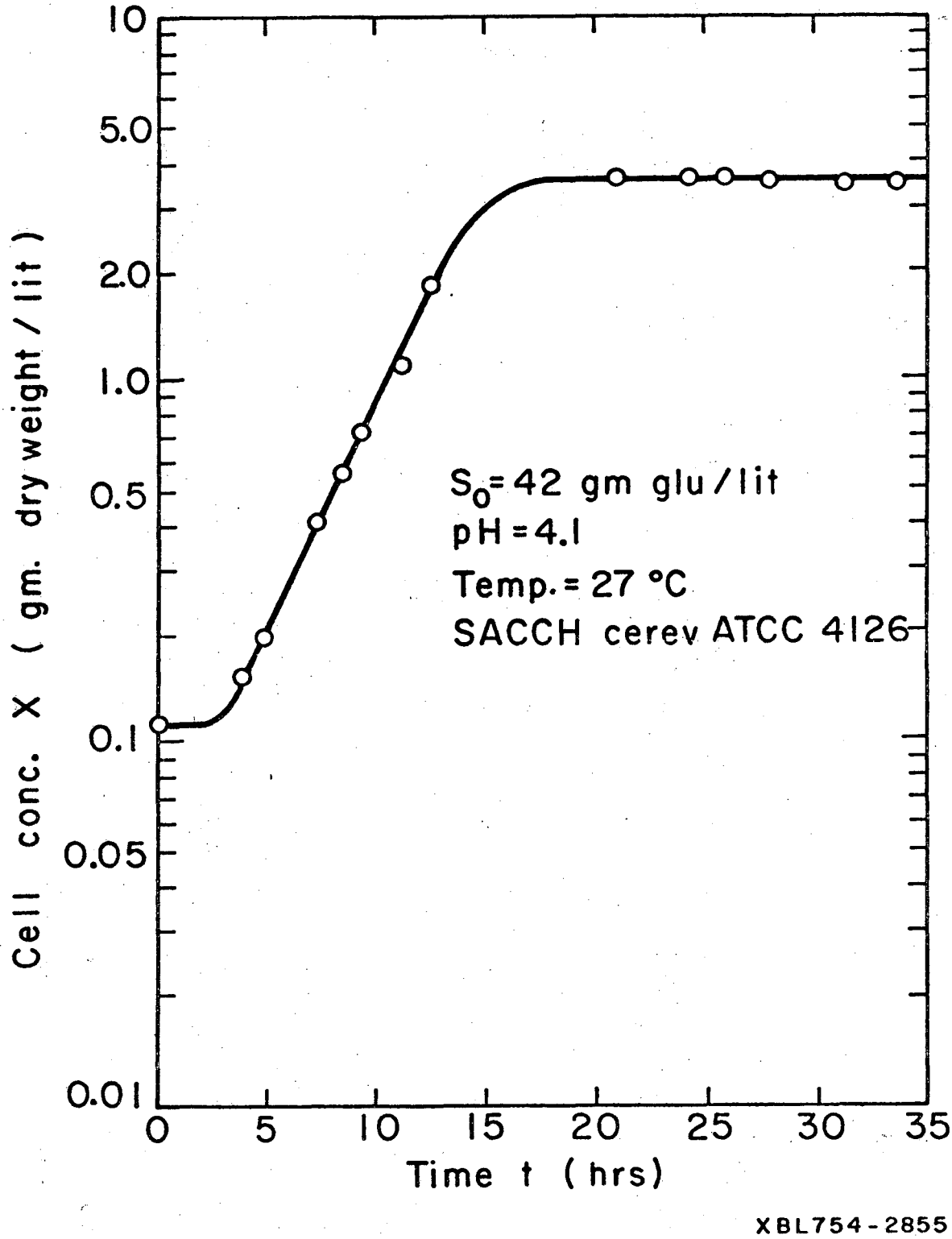

Fig. 7.4.1. Batch growth results for Run B.

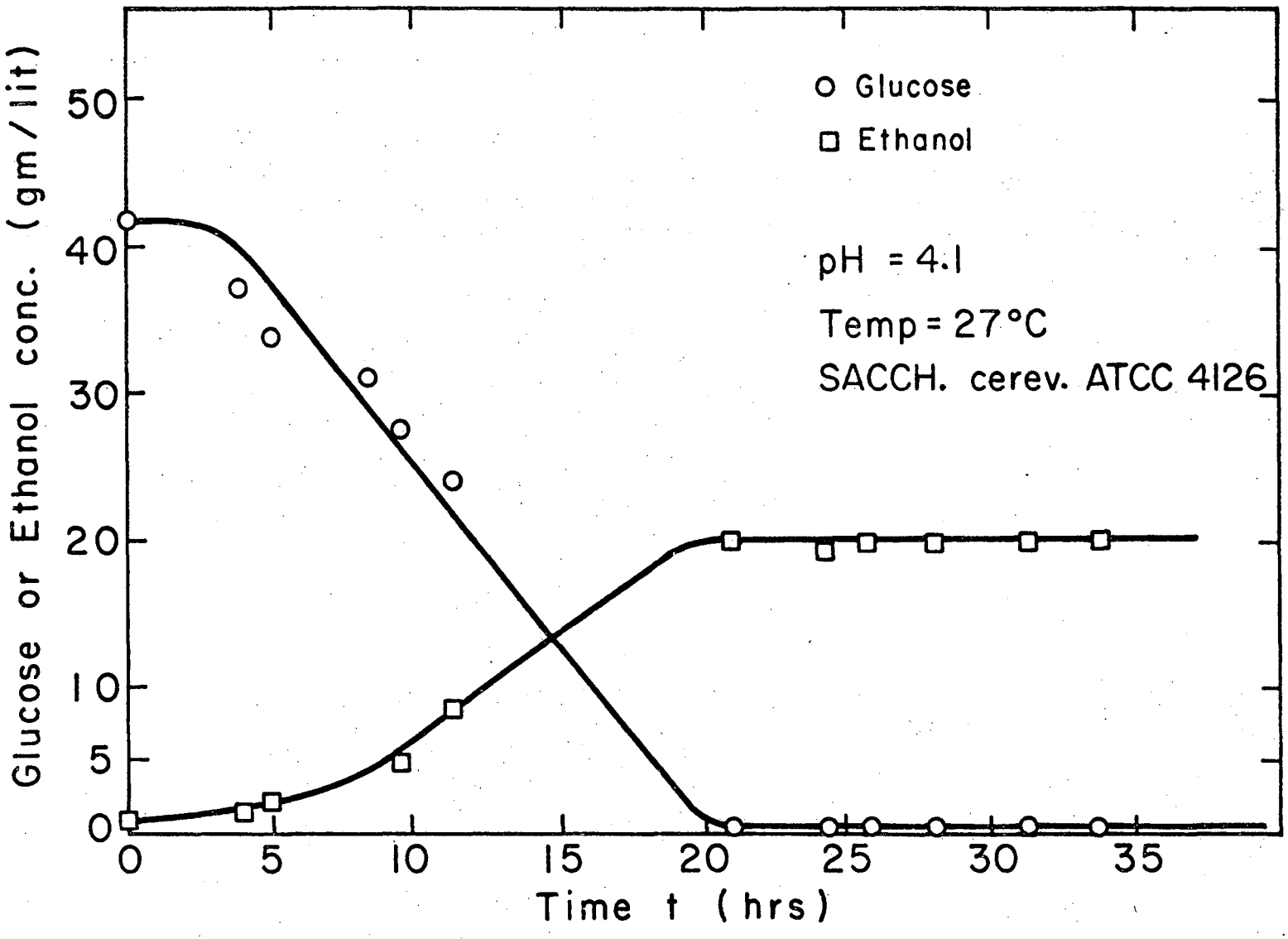

XBL754-2860

Fig. 7.4.2. Batch results for glucose and ethanol. Run B.

Table 7.4.1. Summary of Results for Run B

S_0 = 42 gm/lit. V_L = 12 lit. pH = 4.1 T = 28°C

Time t (hr)	Cell Concentration X (gm/lit)	Glucose Concentration S (gm/lit)	Ethanol Concentration P (gm/lit)	pH
0	0.112	41.8	1.0	4.1
3.92	0.152	37.62	1.5	4.1
4.92	0.195	34.32	2.0	4.1
7.33	0.405	-	-	4.1
8.33	0.55	31.24	-	4.1
9.42	0.72	27.50	5.0	4.1
11.33	1.1	24.20	8.5	4.1
12.67	1.82	-	-	4.1
21.08	3.6	0.25	20.0	4.0
24.33	3.6	0.25	19.0	3.9
25.83	3.6	0.25	20.0	3.9
28.08	3.55	0.25	19.5	3.9
31.33	3.50	0.25	20.0	3.9
33.75	3.50	0.25	20.0	3.9

7.4.2. Run V.

In this run the 2-inch diameter sintered stainless steel membrane shown in Figure 3.1.5 was used. The experimental apparatus shown in Figure 2.1.1 was first sterilized with live steam which was introduced through the Rotorfermentor chamber and medium supply tank. The sterilization was done at 121°C for 45 minutes and then the whole apparatus was left to cool overnight. Approximately 40 liters of medium were prepared separately and sterilized in carbuoy bottles and then transferred aseptically to the supply tank. The glucose concentration in the feed was 170 gm/lit. The temperature was set at 28°C and the pH was equal to 4.1.

The Rotorfermentor was first filled with 8 liters of fresh medium and then inoculated with 800 ml. inoculum prepared in a Minifermentor. The cells were first grown batchwise inside the Rotorfermentor until stationary phase was reached. Then the 2-inch diameter membrane was rotated at 900 r.p.m. while allowing fresh pressurized medium from the supply tank to enter the fermentation chamber. The filtrate came out at the top into the filtrate chamber and then collected in a bottle and weighed. There was no cell bleed and under those conditions the feed rate was equal to filtrate rate while the cell concentration increased with time.

Figure 7.4.3 shows cell concentration as a function of time during batch growth and Rotorfermentor operation with cell filtration. The membrane was rotated for a total of 108 hours without any mechanical difficulties. The pressure inside the fermentation chamber was fluctuating between 11.3 p.s.i. to 13 p.s.i. This fluctuation in pressure was due to the generation of CO_2 which escaped through the rotating membrane. The membrane was the only route of CO_2 escape since the ball valve connecting the G-L separator and fermentation chamber was closed. Thus, during fermentation we have a three-phase system, solid(cells)-liquid-gas. During the course of filtration, it was observed that the filtrate flow rate was slowly decreasing until about 108 hours from the beginning of the growth at which point there was almost no filtrate flow, and the experiment was terminated. Subsequent examination of the filter showed that yeast cells penetrated and plugged most of the membrane pores. Figure 7.4.3 shows that the principle of cell growth and simultaneous filtration works, provided, of course, that adequate measures are taken to minimize pore plugging. This can be done by using much higher membrane r.p.m.'s at the expense of higher power consumption, or using membranes whose pore size is smaller than the size of the yeast cell. Of the two alternatives a membrane

of smaller pore size was chosen since there is a practical limit in increasing the r.p.m. of the membrane beyond which vibrational problems of the rotor unit set in. At the time of experimentation the "5 micron" grade H metallic membrane was the only one available that had the smallest pore size. As new metallic membranes of smaller than 3 micron pores become available plugging of the pores should be minimized.

Figure 7.4.4 shows cell and glucose concentrations inside the Rotorfermentor during filtration. Table 7.4.2 shows the results for run V. Using Figure 7.4.3 one can get μ from the changing slope of the curve during the Rotorfermentor operation. Figure 7.4.5 is a plot of total filtrate collected against time and the filtrate flow rate may be obtained from the slope of this curve.

Table 7.4.2. Summary of Results for Run V

S_0^r = 170 gm/lit. N = 900 r.p.m. pH = 4.1 T = 28°C

2-inch diameter Grade H membrane.

Time t (hr)	Cell Concentration X (gm/lit)	Glucose Concentration S (gm/lit)	Pressure Drop ΔP (p.s.i.)
0	0.25	170	0
1.8	0.20	120	0
8	0.80	-	0
10	1.20	-	0
22.2	3.55	87.5	0
25.8	4.04	80.0	0
49.2	4.80	30.0	0
73.2	4.24	9.0	0
75.2	3.70	30.0	11.3
84.7	3.90	41.0	13.0
98.2	4.60	37.5	11.70
108.2	7.3	32.0	12.2

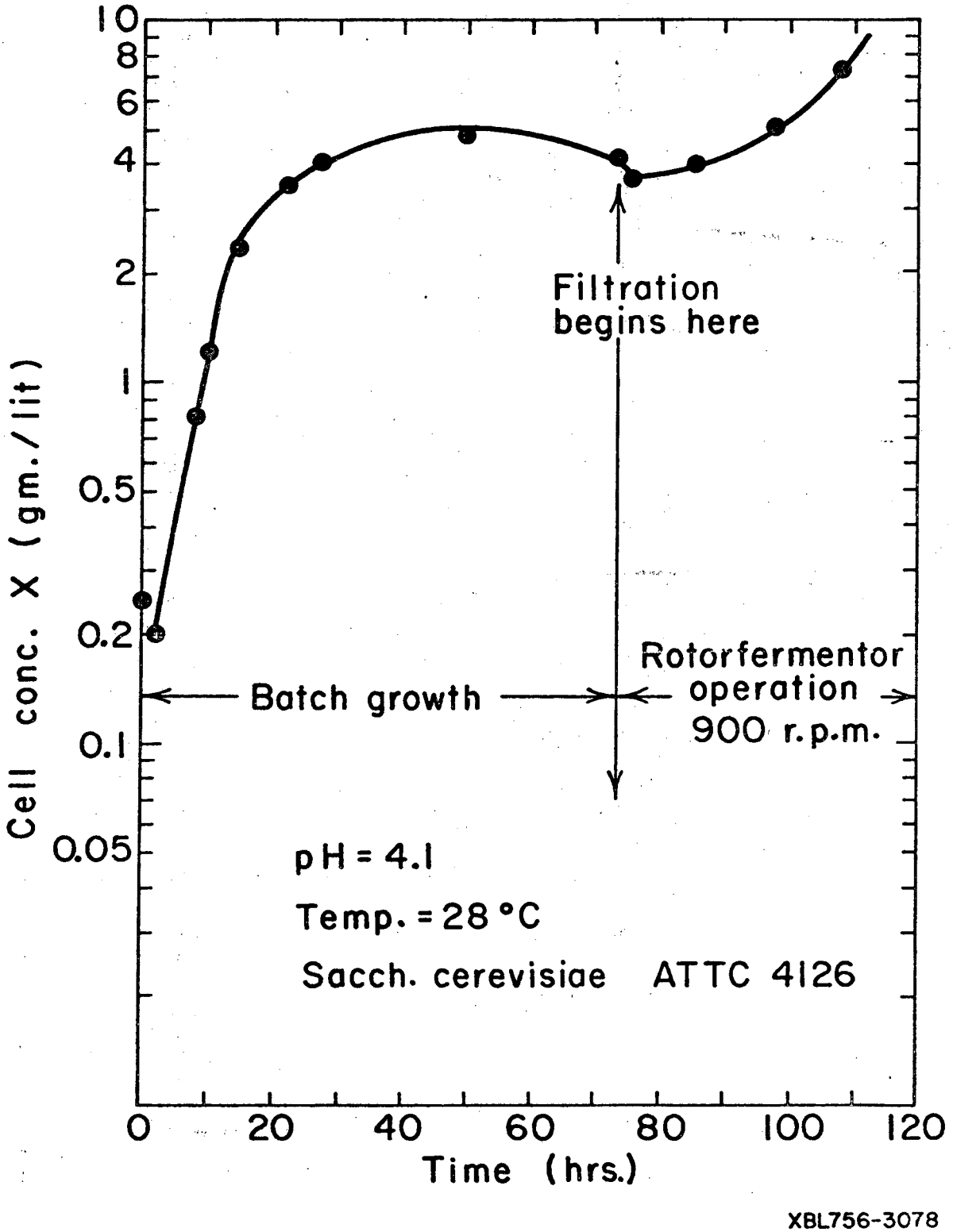

Fig. 7.4.3. Batch and Rotorfermentor Operation. Run V.

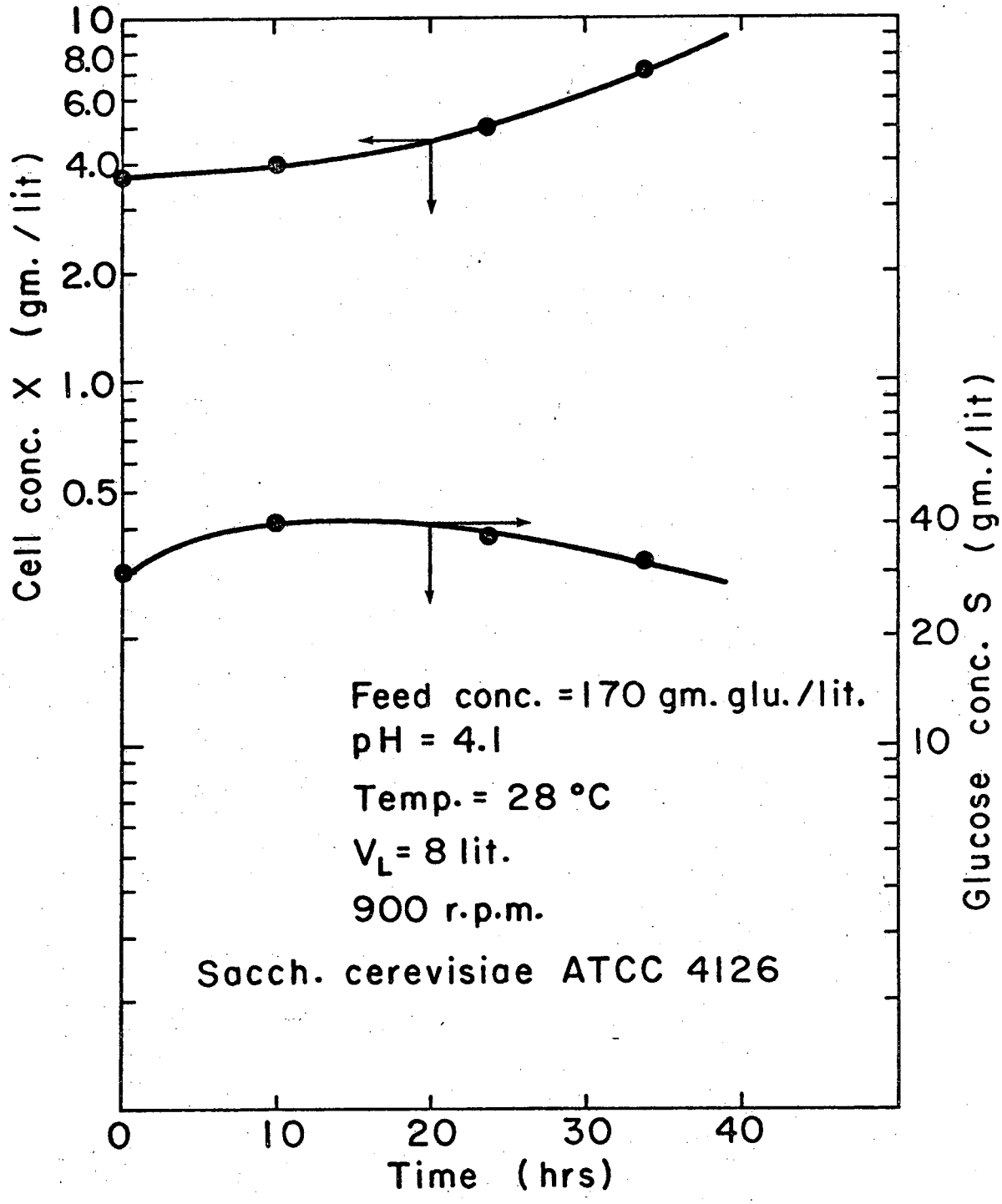

Fig. 7.4.4. Rotorfermentor Operation, Run V.

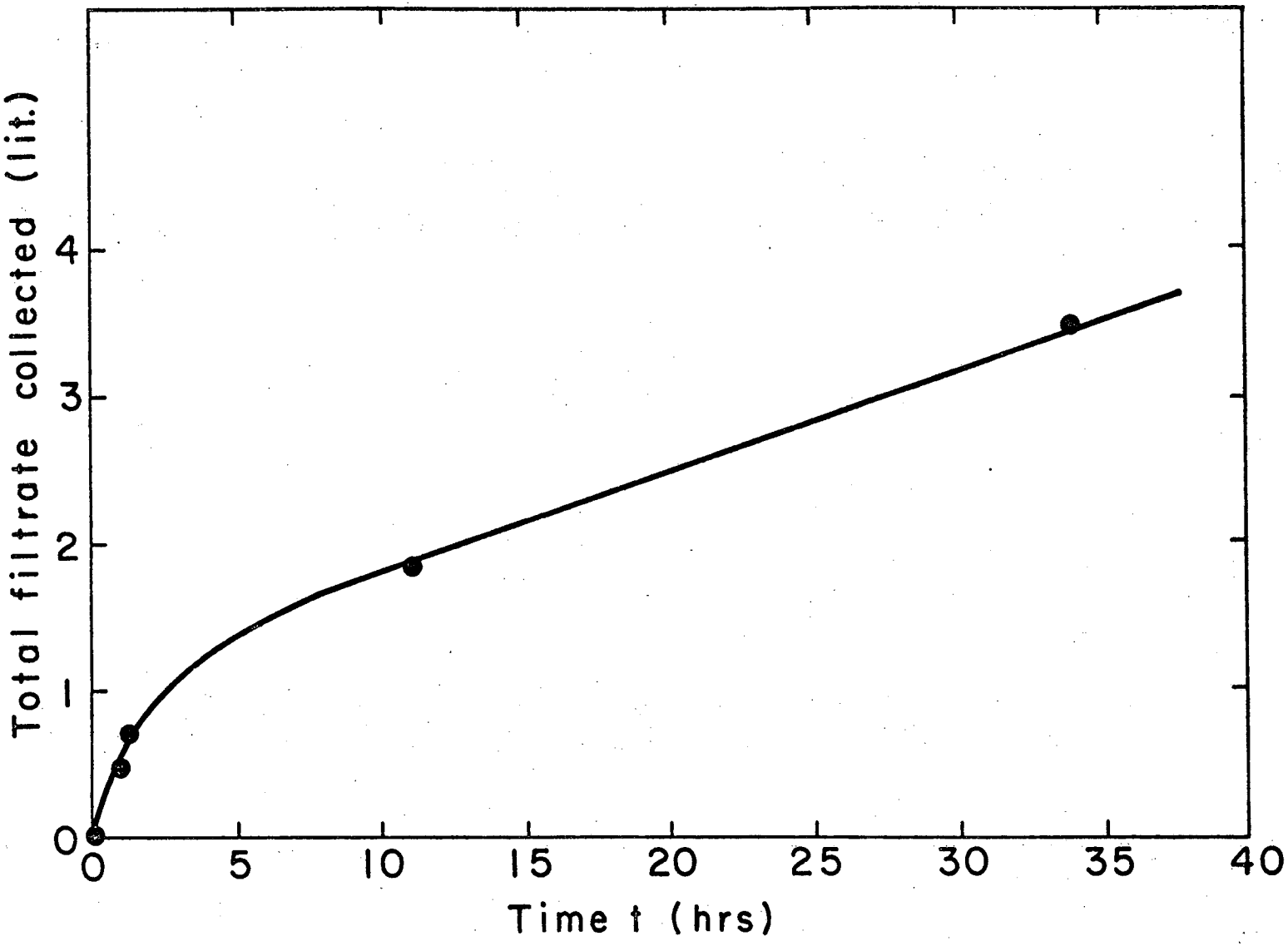

Fig. 7.4.5. Filtrate Collected vs. Time, Run V.

7.4.3. Run HD-1.

For this run a new rotor of 8-inch diameter was installed giving a net filtration area of 1,020 cm^2. This resulted in the decrease of Rotorfermentor volume to 8 liters from the original 14.5 liters when the 2-inch diameter rotor was used. This means that the filtration area to fermentor volume ratio has been increased to 0.128 cm^2/cm^3 from the original value of 0.027 cm^2/cm^3. The advantage of high filtration area to fermentor volume ratio is that it gives high productivities of both cell mass and product.

To minimize pore plugging problems a WS type Millipore membrane of 3 micron pore size was used. This membrane was placed between two sheets of coarse nylon cloth and glued on the supporting metallic screen of the rotor with silicone rubber adhesive RTV 102 made by General Electric. This composite system gave added strength and durability to the membrane which was exposed to high shear forces during rotation.

The membrane and Rotorfermentor chamber were sterilized with 70% v/v ethanol solution since the membrane is not steam sterilizable. The rest of the apparatus was sterilized with live steam as in Run V.

Approximately 60 liters of fresh medium containing 104 gm. glu/lit and 10 mg. ergosterol/lit were prepared and properly sterilized. The Rotorfermentor was first

charged with 7 liters fresh medium and then inoculated with 800 ml. inoculum. The cells were grown batchwise and sparged with air until a cell concentration of 10.4 gm/lit was reached. At that point the air was turned off and the membrane was rotated at 380 r.p.m. and allowing fresh pressurized medium to enter from the supply tank. The fermentor volume was kept at 6.2 lit. in order to allow some portion of the membrane for the escape of CO_2 gas generated. The pressure inside the Rotorfermentor chamber was 2 p.s.i. This pressure is much lower than 13 p.s.i. which was experienced during the plugging of the metallic membrane in Run V. The filtrate rate was high at the beginning and then stabilized around 3.4 lit/hr. as the cake thickness reached its steady-state value. This behavior is similar to the filtration results obtained in Section 5.3.2. The growth experiment was carried out at 28°C and pH = 3.8.

Periodic microscopic examination during growth showed no contamination. Contamination presents a problem when it occurs since the whole run must be aborted and the medium discarded. Table 7.4.3 shows the experimental results during the Rotorfermentor operation at N = 380 r.p.m. Table 7.4.4 shows ethanol productivity results as a function of time. At approximately 13 hours from the start of filtration the ethanol

productivity reaches a value of 26.8 gm. ethanol/lit. hr. Figure 7.4.6 shows the filtration rate and the corresponding ethanol productivity as a function of time. Figure 7.4.7 shows the concentration of cell mass, ethanol and glucose during the course of Rotorfermentor operation.

Table 7.4.3. Summary of Results for Run HD-1

S_0^r = 104.0 gm/lit. N = 380 r.p.m. pH = 3.8 T = 28°C V_r = 6.2 lit.

8-inch diameter WS Millipore membrane

Time t (hr)	Cell Concentration X_r (gm/lit)	Glucose Concentration S_r (gm/lit)	Ethanol Concentration P_r (gm/lit)	Filtrate Rate L (lit/hr)	Pressure Drop ΔP (p.s.i.)
0	10.4	15	37.8	4.74	2
1.44	10.7	12.5	38.5	3.8	2
7.35	15.2	2.6	47.7	3.4	1.6
12.85	24.8	1.6	50.4	3.3	2

Table 7.4.4. Ethanol Productivity Results for Run HD-1.

S_0^r = 104.0 gm/lit. N = 380 r.p.m. ΔP = 2 p.s.i.

V_r = 6.2 lit.

Time t (hr)	Ethanol Concentration P_r (gm/lit)	Filtrate Rate L (lit/hr)	Ethanol Productivity LP/V_r (gm. EtOH/lit.hr)
0	37.8	4.74	28.9
1.44	38.5	3.8	23.6
7.35	47.7	3.4	26.2
12.85	50.4	3.3	26.8

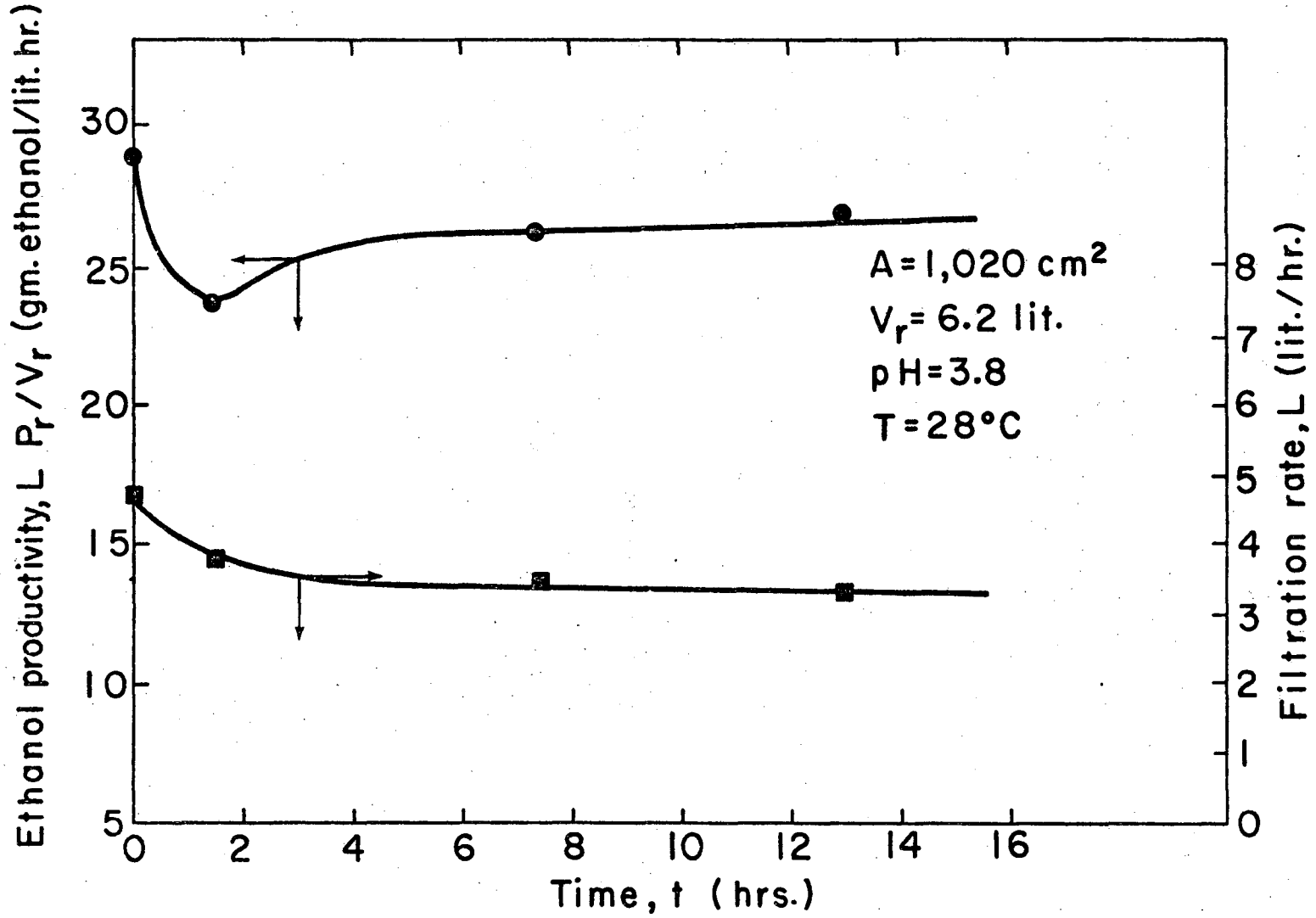

XBL756-3085

Fig. 7.4.6. Filtrate Rate and Ethanol Productivity, Run HD-1.

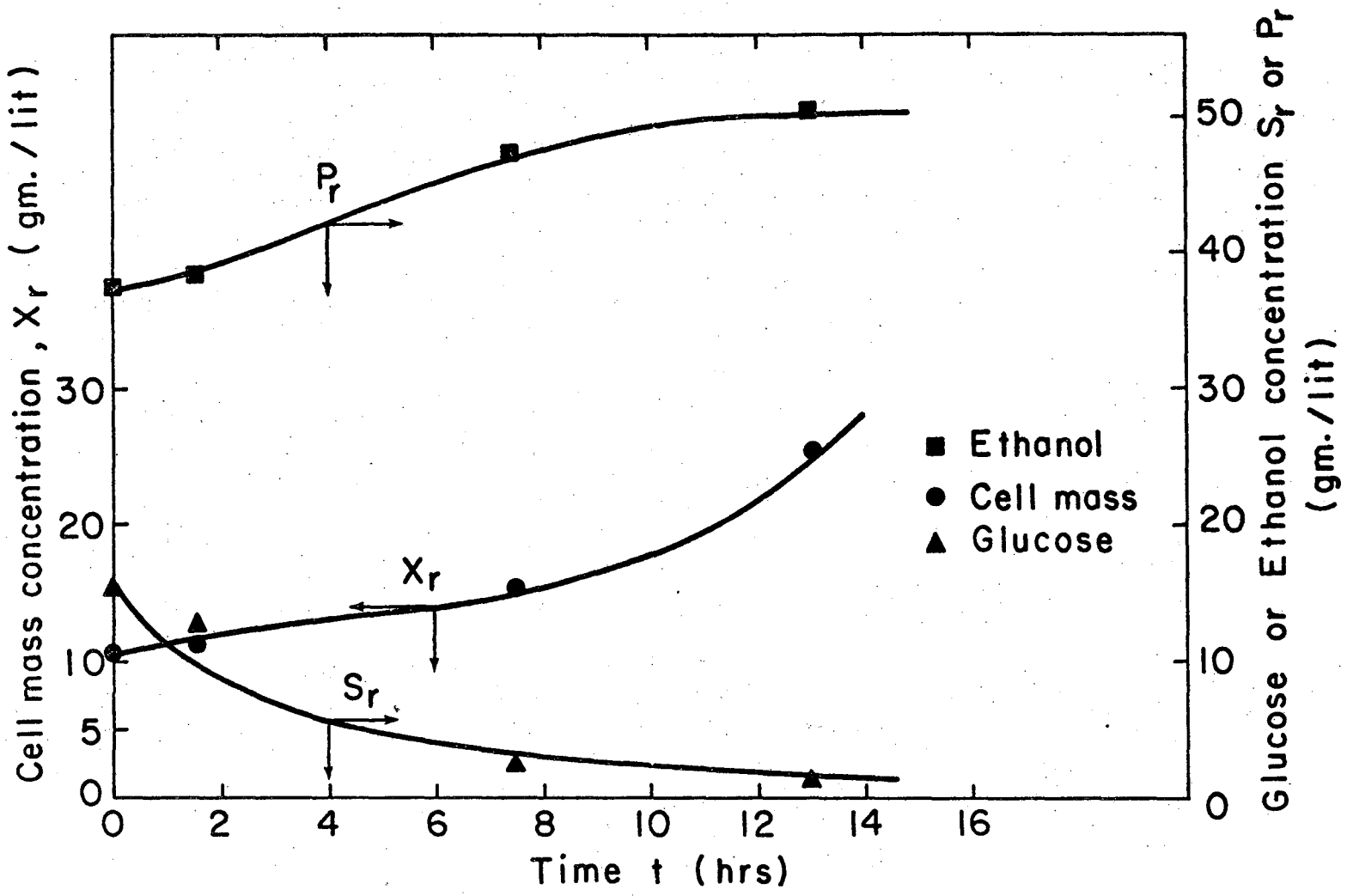

XBL756-3077

Fig. 7.4.7. Ethanol, Cell Mass and Glucose Concentration, Run HD-1.

7.4.4. Run HD-3.

In this run the same 8-inch diameter rotor with the WS type Millipore membrane was used as in run HD-1 described earlier. The main difference between this run and run HD-1 is that air was sparged through the Rotorfermentor throughout the cell growth and filtration operation. This mode of operation was used to check the feasibility of applying the Rotorfermentor to aerobic systems, and, in particular, to find the possible effect of aeration on filtration rates of the rotating membrane.

Approximately 80 liters of fresh medium containing 102 gm. glucose/lit were prepared and sterilized in four carbuoy bottles and then transferred aseptically to the supply tank. The temperature was set at 29°C and the pH was equal to 3.9.

The Rotorfermentor was first sterilized with ethanol and the rest of the apparatus was sterilized with live steam as described in run V. The fermentation chamber was first filled with 6 liters fresh medium and then inoculated with 750 ml. inoculum grown in a Minifermentor. Air was introduced at the rate of 2 standard lit/min, which entered at the bottom of the Rotorfermentor, and then exited through the top of the G-L separator and discharged into the atmosphere through a fine needle valve.

The liquid volume inside the Rotorfermentor was kept at 5.5 liters so that practically no liquid was carried over to the G-L separator. The opening of the needle valve was adjusted so that the pressure of the air was equal to the pressure inside the Rotorfermentor chamber. This pressure varied from 2 to 3 p.s.i. and frequent manual adjustments of the needle valve had to be made to maintain an average pressure of about 2.8 p.s.i. The membrane was rotated at 380 r.p.m. It was found that no air went through the membrane and all the inlet air was discharged through the top of the G-L separator. This also included any amount of free CO_2 gas generated which was discharged along with the incoming air. The filtrate came out at the top in the filtrate chamber and then collected and weighed. There was no cell bleed and the feed rate was equal to filtrate rate while the cell concentration increased with time. Table 7.4.5 is a summary of transient experimental results for run HD-3. As we see the filtrate rate starts at 4.36 lit/hr and then levels off around 3.2 lit/hr. These filtrate rates are in the same range of values as those obtained for run HD-1 with no aeration. Therefore, for the air flow rate used and hydrodynamic conditions of this run there seems to be almost no effect of aeration on filtrate rates of the rotating membrane. It is not known, however, if much higher aeration rates than

the one used in this experiment would adversely affect filtration rates.

As seen from Table 7.4.5 the cell concentration at the end of the run reached a value of 30.9 gm. cell/lit while the ethanol concentration was pretty constant varying between 42 to 47 gm. ethanol/lit. A mass balance shows that this ethanol concentration is about the maximum expected for a glucose concentration in the feed of S_0^r = 102 gm/lit. Because of the relatively high cell concentration inside the Rotorfermentor almost all the glucose is utilized as seen from the glucose concentration levels in Table 7.4.5. Table 7.4.6 shows ethanol productivity results for this run. The ethanol productivity levels off around 27 gm. ethanol/lit hour.

Figure 7.4.8 shows filtrate rate and ethanol productivity results. Figure 7.4.9 is a plot of ethanol, cell, and glucose concentration as a function of time.

Table 7.4.5. Summary of Results for Run HD-3

S_0^r = 102 gm/lit N = 380 r.p.m. pH = 3.9 T = 29°C V_r = 5.5 lit

Air = 2 std lit/min. 8-inch diameter WS Millipore membrane

Time t (hr)	Cell Concentration X_r (gm/lit)	Glucose Concentration S_r (gm/lit)	Ethanol Concentration P_r (gm/lit)	Filtrate Rate L (lit/hr)	Pressure Drop ΔP (p.s.i)
0	9.15	10.14	46.0	4.36	2.0
1.92	12.3	7.8	42.0	3.91	2.8
11	16.2	0.77	46.5	3.28	2.9
14.5	17.85	0.93	45.0	3.15	3.0
18.0	22.1	1.30	47.0	3.10	2.7
22.0	30.9	1.23	47.0	3.20	2.9

Table 7.4.6. Ethanol Productivity Results for Run HD-3

S_0^r = 102 gm/lit N = 380 r.p.m. ΔP = 2.9 p.s.i.

V_r = 5.5 lit.

Time t (hr)	Ethanol Concentration P_r (gm/lit)	Filtrate Rate L (lit/hr)	Ethanol Productivity LP_r/V_r (gm. EtOH/lit hr.)
0	46.0	4.36	36.5
1.92	42.0	3.91	29.9
11	46.5	3.28	27.7
14.5	45.0	3.15	25.8
18.0	47.0	3.10	26.5
22.0	47.0	3.20	27.3

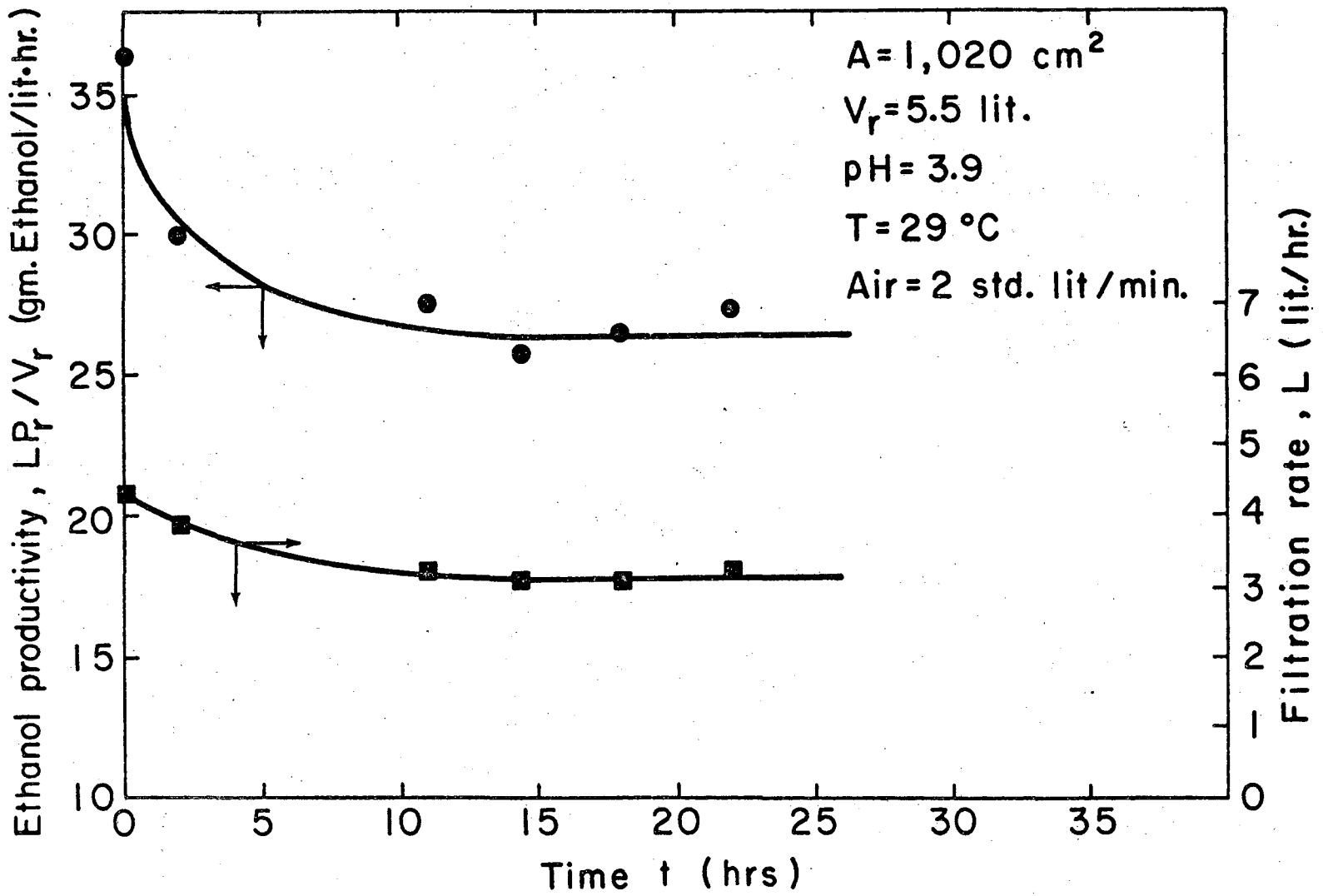

XBL756-3076

Fig. 7.4.8. Filtrate and Ethanol Productivity, Run HD-3.

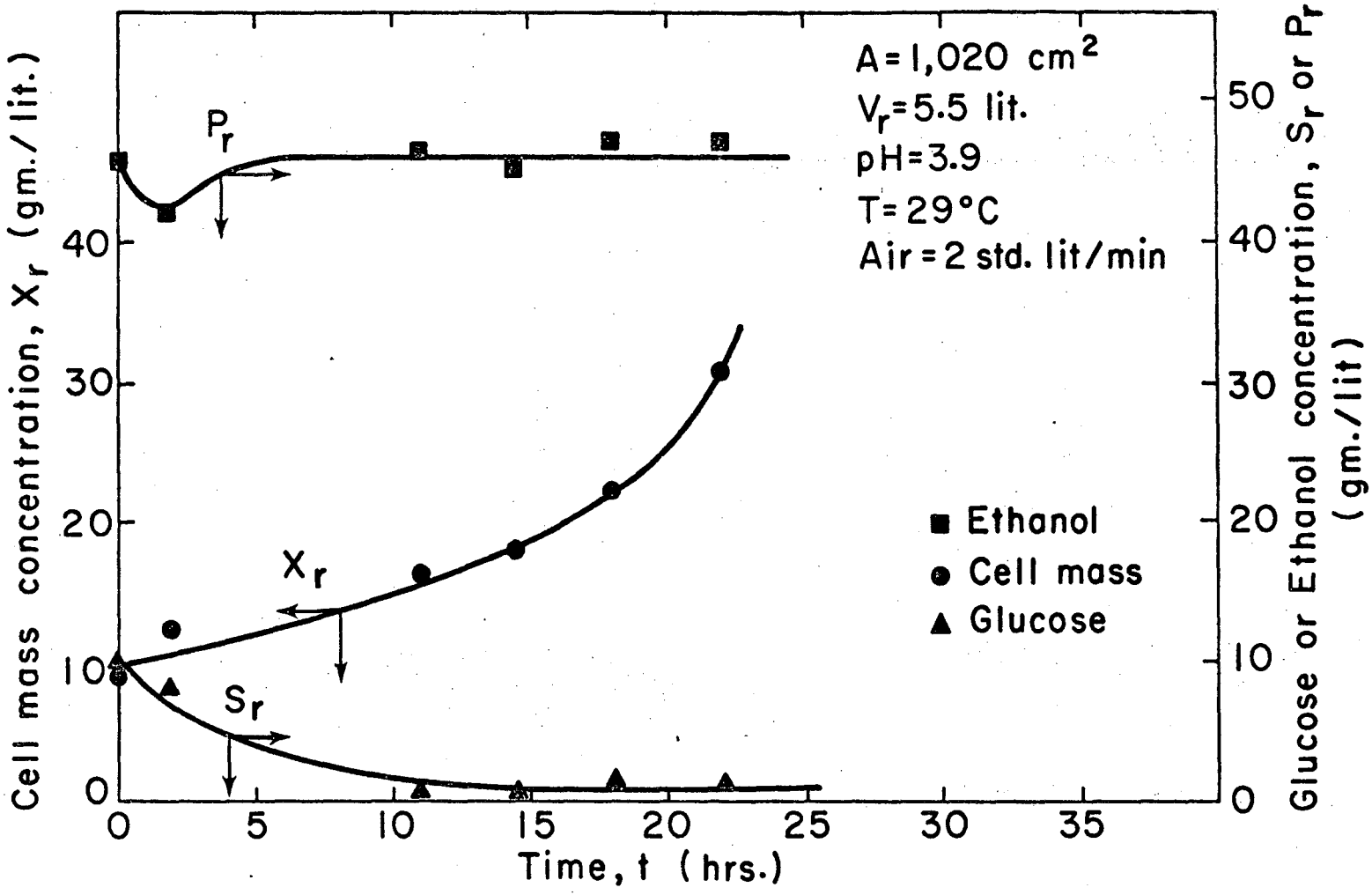

XBL756-3080

Fig. 7.4.9. Ethanol, Cell Mass and Glucose Concentration, Run HD-3.

7.5. Economic Feasibility of the Rotorfermentor

Although no optimization of the operating variables were made a preliminary assessment on the economic feasibility of the Rotorfermentor is possible. Inherent difficulties in projecting cost estimates for a large-scale unit based on information derived from a prototype unit are well understood. In view of this fact an attempt is being made to assess the economic feasibility of the Rotorfermentor when applied to a pilot scale and to an industrial scale process. The latter involves the production of ethanol from glucose and the former is a pilot scale process for the production of cell mass of Pseudomonas aeruginosa which is subsequently used to extract the endoenzyme amidase.

7.5.1. Application of the Rotorfermentor to cell mass production.

In a conventional process where an endocellular product is desired, the first step is cell production in a fermentor followed by cell concentration in a centrifuge, cell disruption and further separation and purification of the final product. Such a process for the continuous pilot scale production of an endoenzyme is described by Lilly and Dunnill (1) employing a wild-type Pseudomonas aeruginosa, a facultative aerobe, to produce the endocellular enzyme amidase. Figure 7.5.1a shows part of the flowsheet based on the given information (1). A C.S.T. 100-liter fermentor was used at a dilution rate D = 0.4 hr^{-1} for maximum enzyme output. The cell concentration leaving the fermentor was 2 to 3 gm. cells/lit. The cells were then fed to a Westphalia centifuge separator model SAOOH-205, which produced a cell slurry of 15 to 25 gm. cells/lit, i.e., a concentration factor of 6 to 8 times. According to information supplied by the manufacturer (private communication) the Westphalia centrifuge separator model SAOOH-205 separates about 80% to 90% of the cells entering. Based on this information, a cell mass balance was made around the centrifuge as shown in Figure 7.5.1a. The concentrated cell output coming out of the centrifuge is estimated to be 96 gm. cells/hr.

Figure 7.5.1b shows the operating conditions of a

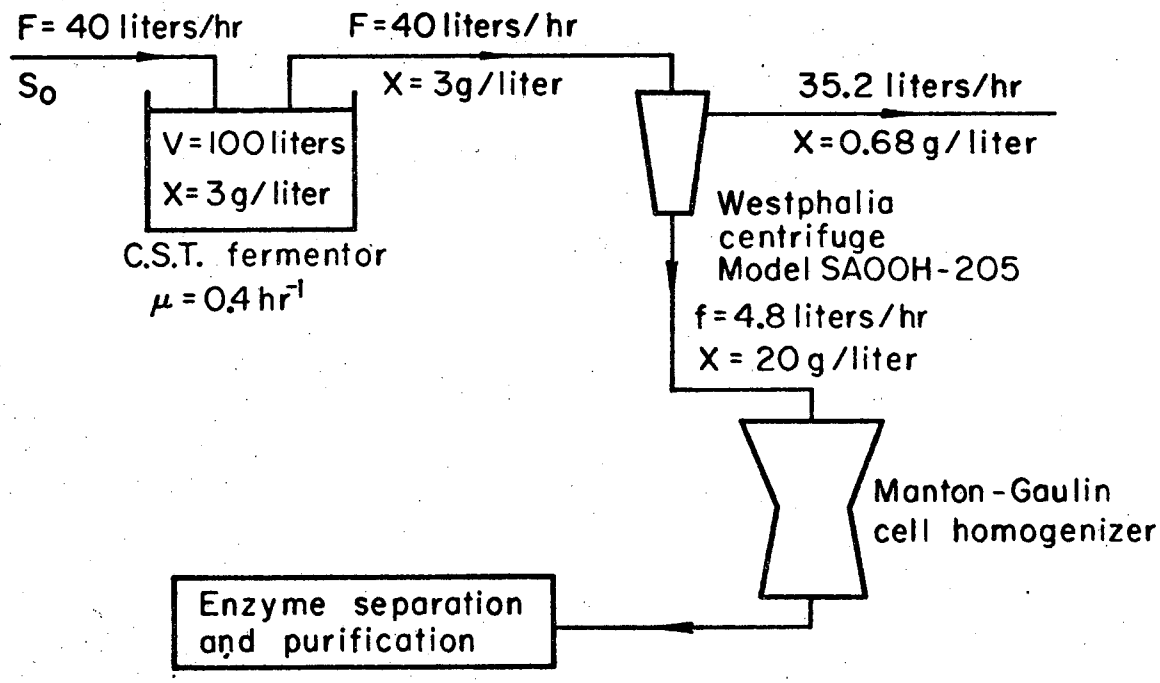

(a) Continuous amidase production

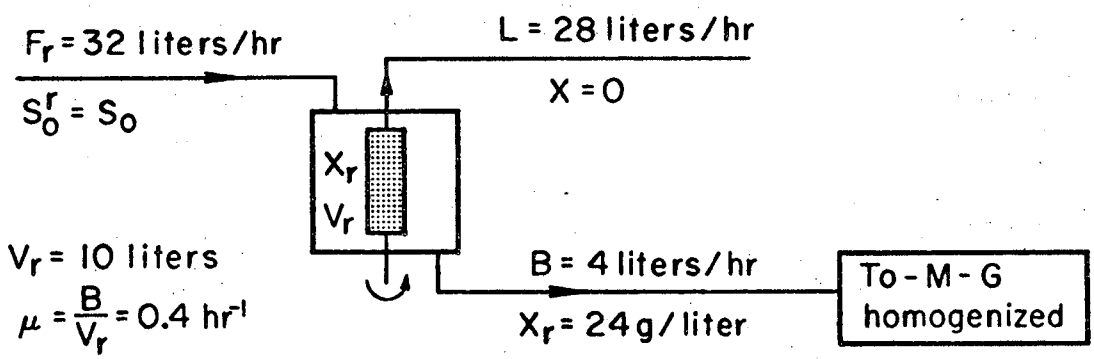

(b) Cell production and concentration by the rotorfermentor

XBL718-4055

Fig. 7.5.1. Application of Rotorfermentor to cell mass production.

12-liter Rotorfermentor (10-liter working volume) designed to give the same cell output as that obtained in Figure 7.5.1a, i.e., 96 gm. cells/hr at the same specific growth rate, 0.4 hr^{-1}, and the same substrate concentration in the feed. Assuming practically all substrate is converted to cell mass, the cell concentration inside the Rotorfermentor, X_r, is 24 gm. cells/lit, and the feed and filtrate rates, F_r and L, are 32 lit/hr and 28 lit/hr, respectively. The specified cell concentration of 24 gm/lit is well below the experimental value obtained by Sortland and Wilke (2) with Streptococcus faecalis.

According to information obtained from the manufacturer (private communication), the Westphalia centrifuge model SAOOH-205 draws 1.5 h.p. power at the start and about 0.9 h.p. once it reaches its final rotational speed. At a typical power input of 3 h.p. per 1,000 gallons liquid for the C.S.T. fermentor and 60% mechanical efficiency, the 100-liter fermentor consumes about 0.13 h.p. Therefore, for the Westphalia and C.S.T. fermentor the total power consumed is 1.03 h.p. to produce 96 gm. cells/hr. Therefore, the energy consumed to produce and concentrate the cells is 3.7 Kwatt-hr/lb-cell mass.

In the case of the Rotorfermentor the rotor has a diameter of 3 inches and 24 inches height giving a

filtration area of 1,460 cm^2. In terms of energy consumption we make a conservative estimate by assuming that the rotor is rotated at high enough speed so that the centrifugal force allows no cake formation at the membrane surface. As seen from Fig. 5.1.2, to maintain a filtrate rate of 28 lit/hr without cake formation for 1 micron particles at μ = 6 c.p., a peripheral velocity of 2,000 cm. per second is required, corresponding to N ≈ 5,000 R.P.M. From Figure 3.1.3 the power consumed by the rotor, P, is 7.95 h.p., which corresponds to 7.43×10^5 ft-lb_f/min ft^3 liquid in the Rotorfermentor. Therefore, the energy consumed to produce and concentrate the cells in the Rotorfermentor is 28.7 Kwatt-hr/lb-cell mass. Thus, for the present example, the Rotorfermentor consumes about 7.7 times more power to do the same job as the C.S.T. fermentor and centrifuge.

The power consumed by the Rotorfermentor is reduced appreciably as the cell size increases. For example, in the above system, if the microorganism size were increased to 5 microns, and for process conditions identical to those given in Figure 7.5.1, the same filtration rate with no cake formation could be obtained, i.e., 28 lit/hr in the Rotorfermentor at 1,130 r.p.m. instead of 5,000. This reduction in rotor speed would reduce the power consumption from 7.95 h.p. to about 0.133 h.p. corresponding to 0.48 Kwatt-hr/lb cell mass, which is less than 3.7 Kwatt-hr/lb-cell mass required for the

C.S.T. fermentor plus centrifuge.

An additional condition pertaining to power input is that sufficient agitation must be provided to disperse oxygen and other substrate constituents throughout the cell suspension at a rate sufficient to sustain the required growth rate. In aerobic systems oxygen supply is usually the limiting factor.

The rate at which oxygen must be supplied to a cell suspension is determined by the respiration rate of the microorganism and the cell concentration. At steady-state this rate must equal the rate of oxygen gransfer from the air bubbles to the gas-liquid interface in the fermentor. This relationship is given by equation 4.1.2.

Hegeman (private communication, University of California, Berkeley) reports that in the case of Pseudomonas aeruginosa approximately 40% of the substrate carbon in the form of succinate is assimilated to form cell mass and the remainder is oxidized. Therefore, for the C.S.T. fermentation conditions reported by Lilly and Dunnill (1), a value of Q_{O_2} may be estimated to be 7.5 m. moles O_2/gm cells hr. From equation 4.1.2 the required value of k_La is 695 hr^{-1} in order to sustain a cell concentration X_r = 24 gm cells/lit in the Rotorfermentor. This value of k_La seems readily attainable at the power input specified above on the basis of

existing mass transfer correlations for agitated fermentor vessels (3). Further analysis of the Rotorfermentor is presented elsewhere (4).

For the pilot scale process comparison given in Figure 7.5.1 the capital equipment cost for the Rotorfermentor system is estimated to be approximately one-third of the capital cost for the C.S.T. fermentor unit plus centrifuge. Further work is needed to determine more accurate power requirements, filtration rates and overall capital costs for large scale processes.

7.5.2 Application of the Rotorfermentor to Ethanol Production.

As mentioned earlier the Rotorfermentor has a dual purpose of cell growth and concentration and in principle may replace the functions of a C.S.T. fermentor and a centrifuge. The experimental results obtained in Chapters VI and VII are used as a basis for a preliminary economic feasibility study.

An industrial scale C.S.T. fermentor is used and a centrifuge with and without cell recycle and then compared with a Rotorfermentor unit for the continuous production of ethanol. Both the C.S.T. fermentor and Rotorfermentor are operated at the same glucose feed concentration and the same specific growth rate assuming the same ethanol production rate. Three fermentor design systems are considered: (1) the C.S.T. fermentor with centrifuge and no cell recycle; (2) the C.S.T. fermentor and centrifuge with cell recycle; and (3) the Rotorfermentor.

All three fermentor systems are rigorously compared to each other by assuming the same design basis, which is derived from results obtained in the C.S.T. fermentor and the Rotorfermentor experiments. As seen from the C.S.T. results of Run OY a rather low dilution rate of 0.063 $hr.^{-1}$ is needed in order to achieve 100% utilization of feed glucose at an oxygen concentration of about 20 μM when the feed glucose concentration

is about 100 gm./lit and the fermentation is carried out at 28°C and pH = 4.0. Furthermore, we assume that the C.S.T. fermentor with cell recycle and the Rotor-fermentor are operated at the same cell concentration of 30 gm./lit. This cell concentration is the same as that obtained experimentally in the Rotorfermentor. In summary then the following common design basis is used to compare the three fermentor design alternatives:

$\mu = 0.063\ hr.^{-1}$

$F = 2{,}500$ lit/hr.

$S_o = 100$ gm. glu./lit

$Y_{x/s} = 0.03$

$Y_{p/s} = 0.45$

Temp. = 28°C

pH = 4.0

100% glucose utilization.

Case I. C.S.T. Fermentor with Centrifuge and No Cell Recycle

Detailed calculations are shown in Appendix C-1. Figure 7.5.2 shows an overall cell and ethanol mass balance for the C.S.T. fermentor and centrifuge when there is no cell recycle. Table 7.5.1 is a summary of equipment costs and power requirements. The total equipment costs for the 13,575 gallon C.S.T. fermentor, the centrifuge and other auxiliary equipment is estimated to be $113,640 while the power required to produce 113 Kg ethanol/hr. is 34 H.P. or 0.22 $\frac{\text{Kwatt-hr.}}{\text{Kg. ethanol}}$.

Case II. C.S.T. Fermentor with Centrifuge and Cell Recycle

This fermentor system is in principle equivalent to the Rotorfermentor system when both are operated at the same cell density. Although no experimental data are available we assume that the viability of the yeast cells is not adversely affected due to centrifugation and pumping during recycling. All calculations are based on the assumption that there is 100% cell viability.

We assume that the C.S.T. fermentor and Rotorfermentor are operated at the same cell density of 30 gm./lit. Figure 7.5.3 shows the results of a cell and ethanol mass balance for the C.S.T. fermentor and centrifuge. Table 7.5.2 is a summary of equipment costs

and power requirements. The total equipment costs for the 1,358 gal. fermentor and centrifuge plus accessories is estimated to be $71,260 while the power required to produce 113 Kg Ethanol/hr. is 11.7 H.P. or 0.077 $\frac{\text{Kwatt-hr.}}{\text{Kg ethanol}}$. Appendix C-2 shows detailed design calculations and basic assumptions made for this case.

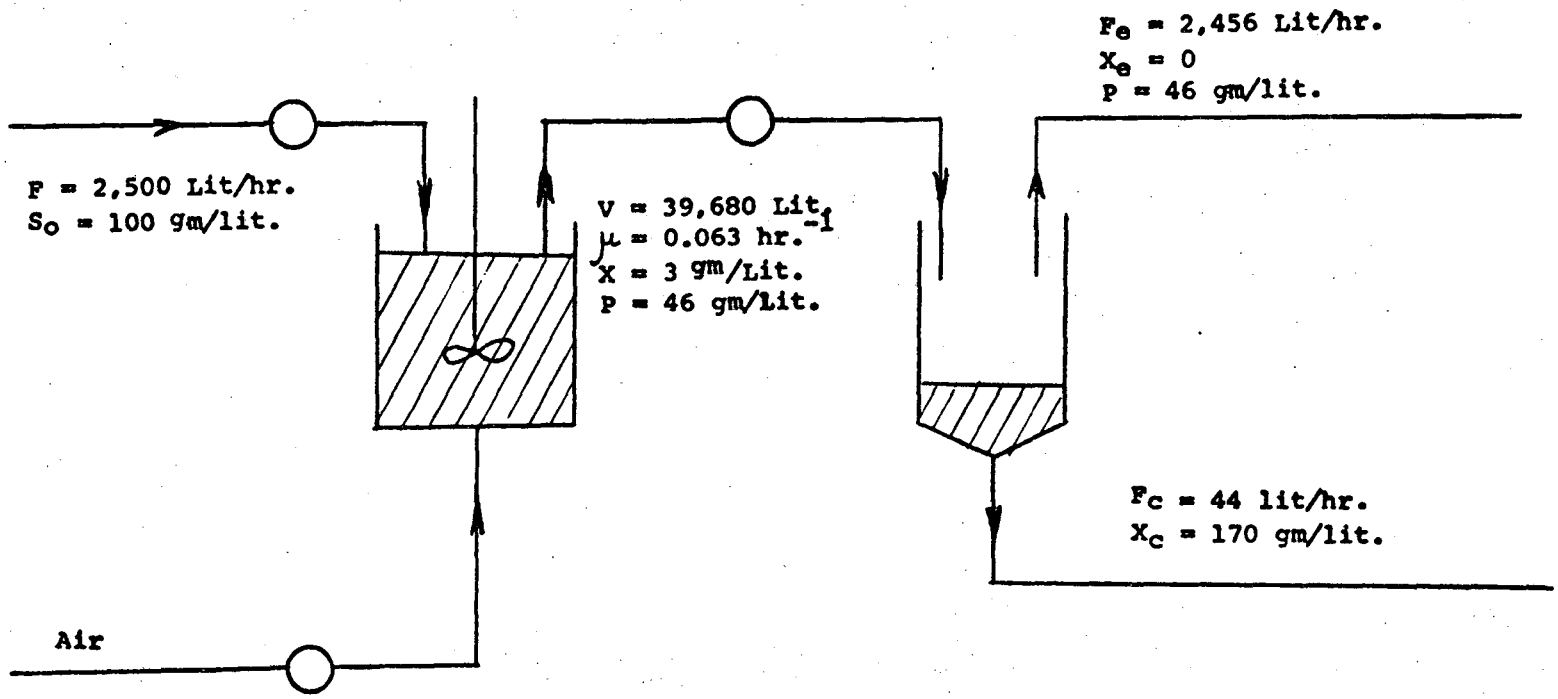

XBL 756-1716

Figure 7.5.2 C.S.T. No Cell Recycle

Table 7.5.1 Summary of Equipment Costs[1] for C.S.T. Fermentor with Centrifuge and No Cell Recycle.

Item	Unit Specification	Unit Cost, $	Total Cost, $
C.S.T. Fermentor	13,575 gallon, agitated stainless steel	62,430	62,430
Continuous Centrifuge	Nozzle type, stainless steel De Laval Type PX-207, 660 gal/hr throughput. 3.5 H.P. motor	36,000	36,000
Air Compressor	Single, reciprocating one-stage (20 to 150 p.s.i.). Capacity 210 S.C.F.M.	10,840	10,840
Pumps (2)	Stainless steel positive displacement, Viking H-724; feed and effluent pumps; 660 G.P.H.; 0.75 H.P.	1,350	2,700
Moyno Pump for Centrifuge Concentrate	Positive displacement stainless steel Moyno pump type 1L2-SSQ; 250 lit/hr	800	800
Motor Drive	To be coupled with 13,575 gal tank. 29.2 H.P.	870	870
		TOTAL	113,640

[1]Cost estimate for the 1st quarter 1975, M.S. Index = 437 (6).

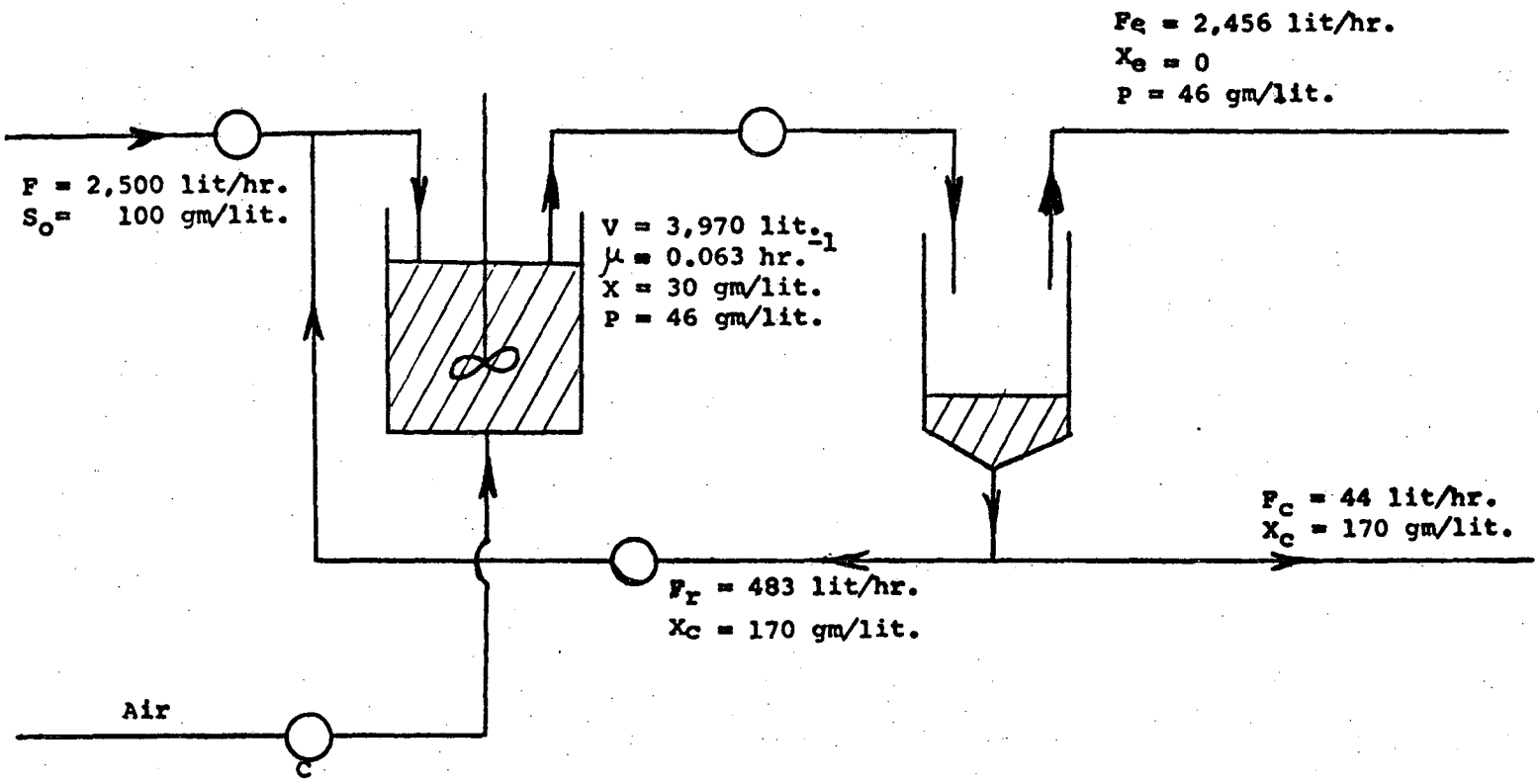

XBL 756-1717

Figure 7.5.3 C.S.T. With Cell Recycle

Table 7.5.2 Summary of Equipment Costs[1] for C.S.T. Fermentor and Centrifuge With Cell Recycle

Item	Unit Specification	Unit Cost, $	Total Cost, $
C.S.T. Fermentor	1,358 gal., agitated stainless steel	19,000	19,000
Continuous Centrifuge	Nozzle type, stainless steel; De Laval type PX-207 660 gal/hr throughput; 3.5 H.P. motor	36,000	36,000
Air Compressor	Single, reciprocating one-stage (20 to 150 p.s.i.). Capacity 210 S.C.F.M.	10,840	10,840
Pumps (2)	Stainless steel positive displacement, Viking H-724; feed and effluent pumps; 660 G.P.H.; 0.75 H.P.	1,350	2,700
Moyno Pump for Centrifuge Concentration	Positive displacement stainless steel Moyno pump type 1L2-SSQ; 250 lit/hr	800	800
Moyno Recycle Pump	Positive displacement stainless steel type 1L3-SSQ; 490 lit/hr; 0.4 H.P.	1,520	1,520
Motor Drive	To be coupled with 1,358 gal tank. 6.3 H.P.	400	400
		TOTAL	71,260

[1]Cost estimate for the 1st quarter 1975, M.S. Index = 437 (6).

Case III. Rotorfermentor

The results of run HD-3 show that the ethanol concentration and ethanol productivity became almost independent of time, i.e., a pseudo-steady-state was reached, while the cell concentration inside the Rotorfermentor increased with time. This may be explained as follows. At a given feed rate, when the cell concentration is low, i.e., a few grams per liter, then the rate of glucose conversion by the cells is less than the rate of glucose supply to the fermentor with resultant amounts of glucose left over in the fermentor. As the cell concentration increases the rate of glucose conversion increases until it becomes equal to the rate of glucose supply at which point the glucose concentration inside the fermentor is zero. Further increases in cell concentration result in a situation where the rate of glucose conversion by the cells is much higher than the rate of glucose supply, and the latter becomes the limiting step. Under those conditions all glucose in the feed is converted resulting in a maximum ethanol concentration which is independent of time. Figure 7.4.9 of run HD-3 shows that the maximum ethanol concentration is about 45 gm/lit which becomes independent of time at about $X_r \geq 16$ gm cell/lit and corresponding to almost 100% utilization of glucose. The ethanol productivity obtained under those conditions is about 26 gm. ethanol/

lit.hr. In this case the Rotorfermentor may be operated either by employing a periodic cell bleed or continuous cell bleed and in order to be on the conservative side we assume that X_r = 30 gm./lit.

Figure 7.5.4 shows a cell and ethanol mass balance for the continuous operation of the Rotorfermentor unit. A small size secondary Westfalia centrifuge is used to further concentrate the cell bleed stream to the same level of 170 gm. cell/lit as that obtained in the C.S.T. fermentor with cell recycle. In this way the two equivalent systems are compared vis-à-vis using the same design basis and the same degree of cell concentration. Table 7.5.3 is a summary of equipment and power requirements for the Rotorfermentor unit. The total equipment cost is estimated to be $41,780 while the power required to produce 113 Kg. ethanol/hr. is 7 H.P. or 0.046 $\frac{\text{Kwatt-hr.}}{\text{Kg. ethanol}}$. Appendix C-3 shows detailed design calculations for the Rotorfermentor case.

Table 7.5.4 is a summary of design calculations results for the three fermentor systems which are compared by assuming the same design basis. Table 7.5.5 summarizes the equipment costs and power requirement results for the three fermentor design alternatives.

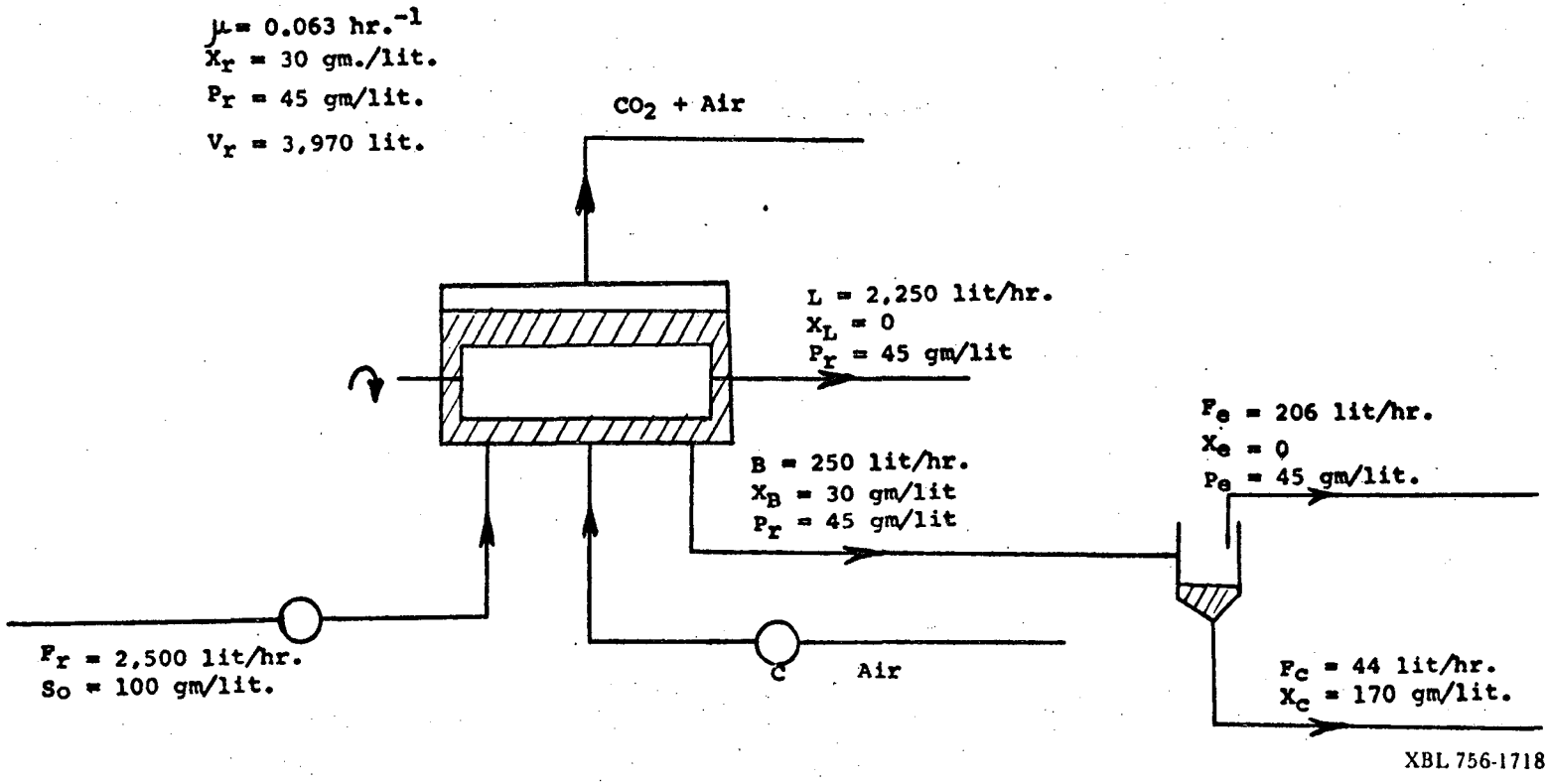

Figure 7.5.4 Rotorfermentor

Table 7.5.3. Summary of Equipment Costs[1] for the Rotorfermentor

Item	Unit Specification	Unit Cost, $	Total Cost, $
Fermentor Vessel	1,358 gal. stainless steel	19,000	19,000
Installed Rotors plus Accessories	20 rotors 6"-diameter x 6' length. Ball bearings, Crane seals, supporting screen, membrane, motor drive units, rotor shaft.	7,630	7,630
Air Compressor	Single, reciprocating one-stage (20 to 150 p.s.i.). Capacity 210 S.C.F.M.	10,800	10,800
Feed Pump	Stainless steel positive displacement, Viking H-724; 660 G.P.H.; 0.75 H.P.	1,350	1,350
Secondary Centrifuge	Westfalia LWA-205; 300 lit/hr. throughput; 0.75 H.P.	3,000	3,000
		TOTAL	41,780

[1]Cost estimate for the 1st quarter 1975, M.S. Index = 437 (6).

Table 7.5.4. Summary of Design Calculations

Basis: 113 Kg ethanol/hr; μ = 0.063 $hr.^{-1}$; So = 100 gm. glu/lit.

Fermentation System	Cell Conc. X (gm/lit)	EtOH Conc. P (gm/lit)	Fermentor Volume V_L (lit)	Cell Prod. (gm.cell/lit.hr)	Ethanol Prod. (gm.EtOH/lit.hr.)
C.S.T. Fermentor and Centrifuge No Cell Recycle	3	46	39,680	0.189	2.89
C.S.T. Fermentor and Centrifuge With Cell Recycle	30	46	3,968	1.89	28.52
Rotorfermentor	30	45	3,968	1.89	28.4

Table 7.5.5. Comparison of Equipment[1] and Power Costs for Ethanol Production

Basis: 113 Kg Ethanol/hr.; $\mu = 0.063\ hr.^{-1}$; $S_0 = 100$ gm glu/lit.

Fermentation System	Purchased Equipment Cost		Power Requirement (Kwatt-hr/Kg ethanol)	
	Total Cost $	Fraction of Rotor-fermentor Cost	Total	Fraction of Rotor-fermentor Power
Rotorfermentor	41,780	1.0	0.046	1.0
C.S.T. Fermentor and Centrifuge No Cell Recycle	113,640	2.7	0.22	4.78
C.S.T. Fermentor and Centrifuge With Cell Recycle	71,260	1.7	0.077	1.67

[1]Cost estimate for the 1st quarter 1975, M.S. Index = 437 (6).

Conclusions

For the process conditions considered in this case a preliminary economic feasibility study indicates that it may be profitable to replace an industrial scale C.S.T. fermentor and centrifuge with a Rotorfermentor unit for the same ethanol production rate.

The equipment cost for the Rotorfermentor is estimated to be $41,780 which is approximately 2.7 times less than the combined equipment costs of a C.S.T. fermentor and centrifuge without cell recycle. Correspondingly, the power consumed by the Rotorfermentor system is estimated to be 0.046 $\frac{\text{Kwatt-hr.}}{\text{Kg ethanol}}$ which is about 4.78 times less than that needed by the C.S.T. fermentor and centrifuge system without cell recycle.

However, when the C.S.T. fermentor and centrifuge system is operated with cell recycle both the equipment costs and power requirements are reduced. Design calculations showed that the Rotorfermentor equipment cost is about 1.7 times less than the combined equipment cost for the C.S.T. fermentor and centrifuge systems with cell recycle. At the same time, the power consumed by the Rotorfermentor system is estimated to be approximately 1.67 times less than that required by the C.S.T. fermentor and centrifuge system operated with cell recycle.

Depending on the type of membrane used and frequency of membrane replacement the maintenance cost of the Rotorfermentor may be different from that of a continuous cell centrifuge. More experimental work is needed to compare maintenance costs based on operational experience of large scale Rotorfermentor and cell centrifuge units.

Appendix C-1

Case I. C.S.T. Fermentor with Centrifuge and No Cell Recycle

This fermentor scheme is shown in Figure 7.5.2.

$F = 2{,}500$ lit/hr.

$S_o = 100$ gm. glu/lit

$\mu = 0.063$ hr.$^{-1}$

$Y_{x/s} = 0.03$

$Y_{p/s} = 0.45$

100% glucose utilization

Overall cell mass balance:

$$2{,}500 \times 100 \times 0.03 = F_c \times 170$$

$$F_c = 44 \text{ lit/hr.}$$

$$F_E = 2{,}500 - 44 = 2{,}456 \text{ lit/hr.}$$

The cell concentration in the centrifuge $X_c = 170$ gm./lit is based on information received from the manufacturer (De Laval, private communication).

Ethanol mass balance:

$$2{,}500 \times 100 \times 0.45 = 2{,}456 \times P$$

$$P = 46 \text{ gm. Ethanol/lit.}$$

Fermentor Volume:

$$\mu = \frac{F}{V}$$

$$V = \frac{2{,}500}{0.063} = 39{,}680 \text{ lit.} = 10{,}443 \text{ gal.}$$

Allow 30% extra volume for foaming, etc., then nominal

volume = 10,443 x 1.3 = 13,575 gal.

Cell concentration in C.S.T. Fermentor:

$$2{,}500 \times 100 \times 0.03 = 2{,}500 \times X$$

$$X = 3 \text{ gm./lit.}$$

Volumetric ethanol productivity:

$$DP = 0.063 \times 46 = 2.89 \text{ gm. EtOH/lit.hr.}$$

Volumetric cell mass productivity:

$$DX = 0.063 \times 3 = 0.189 \text{ gm. cell/lit.hr.}$$

Ethanol production rate:

$$F_E \times P = 2{,}456 \times 46 = 113 \frac{\text{Kg.EtOH}}{\text{hr.}}$$

$K_L a$ required to maintain C_L = 20 μM:

From Figure 6.43, we can extrapolate the value of

Q_{O_2} = 50 μ moles O_2/gm. cell. hr. at C_L = 20 μM.

X = 3.0 gm/lit.

C* = 252 μ moles/lit.

C_L = 20 μ moles/lit.

At steady-state use equation 4.1.2,

$$K_L a = \frac{(40)(3.0)}{232} = 0.52 \text{ hr.}^{-1}$$

This low value of $K_L a$ means that low agitation rates will be more than adequate to satisfy the oxygen requirements of yeast. In this case we assume that low agitation power inputs in the order of 2 H.P. per 1,000 gallons will be enough to provide adequate mixing and

meet oxygen mass transfer requirements.

Assuming 2 H.P. per 1,000 gallons the 10,443 gallon fermentor will consume 20.9 H.P.

Allowing 60% mechanical efficiency, then total power required is 29.0 H.P.

Equipment Cost Estimate:

According to Aries and Newton (5) the purchased equipment cost for an agitated stainless steel tank of 13,575 gal. capacity is estimated to be $23,000 (1949 prices; M.S. Index = 161). The Marshall and Stevens Index for the first quarter 1975 is 437 (6) with M.S. = 100 for 1926.

$$\text{Current cost} = \$23,000 \times \frac{437}{161} = \$62,430.$$

All equipment costs are based on information from Aries and Newton (5) unless otherwise noted.

$$\text{Motor drive unit of 29.0 H.P.} = \$320\ \frac{437}{161} = \$870.$$

We select a stainless steel positive displacement pump for the feed and effluent streams from the C.S.T. fermentor. According to information received from the manufacturer (private communication) a Viking pump type H-724 of 660 G.P.H. capacity draws 0.75 H.P. and has a current cost of $1,350.

$$\text{2 Viking pumps} = 2 \times \$1,350 = \$2,700.$$

Moyno pump for centrifuge concentrate type 1L2-SSQ, 250 lit/hr. has a current cost of $800 (private communication).

Yeast centrifuge:

According to information supplied by the manufacturer (private communication) for a throughput of 2,500 lit/hr. a relatively small size industrial centrifuge De Laval Type PX-207 is recommended. This is a continuous centrifuge nozzle-type which draws 3.5 H.P. and achieves almost 100% yeast separation with a cell concentration in the concentrate of about 17% dry solids. Current purchased cost is $36,000 which does not include instrumentation costs.

Air compressor:

The air compressor required to feed air to the 13,575 gallon tank has a capacity of 210 S.C.F.M. corresponding to 0.16 VVM which is adequate to provide the aeration requirements of yeast. According to Aries and Newton (5) a 210 S.C.F.M. air compressor capacity has a current purchased cost of $\$4{,}000 \times \frac{437}{161} = \$10{,}840$.

Power requirements:

Agitation power for 13,575 tank = 29.0 H.P.

Centrifuge = 3.5 H.P.

Feed and effluent pumps = 1.5 H.P.

This power is used to produce 113 Kg ethanol/hr., i.e.

$$\frac{34 \text{ H.P.}}{113 \text{ Kg ethanol/hr.}} = \frac{34 \times 0.746}{113} = 0.22 \frac{\text{Kwatt-hr.}}{\text{Kg. ethanol}}$$

Appendix C-2

Case II. C.S.T. Fermentor with Centrifuge and Cell Recycle

In order to make a direct comparison with the Rotorfermentor we assume that the C.S.T. fermentor is operated with a cell recycle so that the cell concentration is 30 gm/lit, the same as that for the Rotorfermentor. Furthermore, we assume the same specific growth rate, feed glucose concentration and ethanol production rate as in Case I. Figure 7.5.3 shows the C.S.T. fermentor and centrifuge with cell recycle.

A cell mass balance around the C.S.T. fermentor at steady-state conditions yields equation 7.5.1.

$$\mu = D\left[1 + \omega\left(1 - \frac{X_c}{X}\right)\right] \qquad 7.5.1$$

where:

μ = specific growth rate of cell mass inside the fermentor, $hr.^{-1}$

D = dilution rate = $\frac{F}{V}$, hr^{-1}.

ω = recycle ratio = $\frac{F_R}{F}$,

X_C = cell mass concentration of centrifuge concentrate, gm/lit,

X = cell mass concentration inside the fermentor.

Equation 7.5.2 is the result of a cell mass balance around the centrifuge.

$$\frac{X_C}{X} = \frac{1 + \omega - \frac{F_E}{F} \cdot \frac{X_E}{X}}{1 + \omega - \frac{F_E}{F}} . \qquad 7.5.2$$

Overall cell mass balance:

$$2,500 \times 100 \times 0.03 = F_C \times 170$$

$$F_C = 44 \text{ lit/hr.}$$

$$F_E = 2,500 - 44 = 2,456 \text{ lit/hr.}$$

Overall ethanol balance:

$$2,500 \times 100 \times 0.45 = 2,456 \times P$$

$$P = 46 \text{ gm. ethanol/lit.}$$

In our case

$\mu = 0.063 \text{ hr}^{-1}$,

$X_C = 170$ gm/lit,

$X = 30$ gm/lit,

$X_E = 0$,

$F_E = 2,456$ lit/hr,

$F = 2,500$ lit/hr.

Use equation 7.5.2 to find ω.

$$\frac{170}{30} = \frac{1 + \omega - 0}{1 + \omega - \frac{2,456}{2,500}}$$

$$5.66 = \frac{1 + \omega}{1 + \omega - 0.982}$$

$$\omega = 0.193$$

Recycle rate = $F_R = (0.193)(2,500) = 483$ lit/hr.

Use equation 7.5.1 to find the volume V of the C.S.T. fermentor.

$$0.063 = \frac{2,500}{V} [1 + 0.193 (1 - 5.66)].$$

V = 3,968 lit = 1,044 gal which is the working volume. Allow 30% extra volume for foaming, etc.

Nominal volume = 1,044 x 1.3 = 1,358 gal.

Therefore, cell recycling to maintain a cell concentration of 30 gm/lit and $\mu = 0.063\ hr^{-1}$ reduced the fermentor volume from 10,443 gal. (Case I) to 1,044 gal., i.e., a tenfold reduction. This reduction in the fermentor volume is in agreement with the fact that we have a tenfold increase in cell concentration.

Volumetric cell mass and ethanol productivities:

$$\frac{F_E P}{V} = \frac{2,456 \times 46}{3,968} = 28.5 \frac{\text{gm. EtOH}}{\text{lit.hr.}}$$

$$\frac{F_c X_c}{V} = \frac{44 \times 170}{3,968} = 1.89 \frac{\text{gm. cell}}{\text{lit. hr.}}$$

Both are ten times greater than those obtained in Case I for no cell recycle.

Equipment Cost estimate:

Agitated stainless steel tank (5) of 1,358 gal. capacity = $\$7,000 \times \frac{437}{161} = \$19,000.$

Yeast centrifuge continuous nozzle type De Laval PX-207 = \$36,000, 3.5 H.P.

Air compressor 210 S.C.F.M. = $\$4,000 \times \frac{437}{161} = \$10,840.$

Positive displacement pump Viking H-724 stainless steel 660 G.P.H., 0.75 H.P. = $1,350.

2 pumps = $2,700

Moyno recycle pump positive displacement stainless steel variable speed 1L3-SSQ 490 lit/hr.; 0.4 H.P. = $1,520.

Moyno pump for centrifuge concentrate = $800.

Power requirements:

When the cell concentration increases from X = 3 gm./lit (Case I) to X = 30 gm/lit (Case II) the viscosity of the yeast suspension also increases. Since the power per unit liquid volume in the fermentor also depends on the viscosity it is desirable to estimate the increase in P/V_L due to increase in viscosity assuming that the K_La for both Cases I and II is the same. To estimate the viscosity at X = 30 gm/lit the Kunitz relation is used (7):

$$\frac{\mu_M}{\mu_L} = \frac{1 + 0.5\ \phi_s}{(1 - \phi_s)^4}$$ where

μ_L = viscosity of pure liquid

μ_M = viscosity of suspension

ϕ_s = volume fraction of solids.

From centrifugation results of yeast suspension a packed cell volume of 2.8% was obtained at X = 5.66 gm. cell/lit.

$$\phi_s = 0.028 \times \frac{30}{5.66} = 0.15$$

$$\mu_M = 2.07\ \mu_L = 2.07 \text{ C.P.}$$

if $\mu_L = 1$ C.P.

According to Calderbank and Moo-Young (8)

$$K_L a \propto \left(\frac{P}{V_L}\right)^n \times \left(\frac{1}{\mu}\right)^{1/3}$$

assuming that the density, oxygen diffusivity surface tension do not change appreciably when X increases from 3 to 30 gm./lit. then since we want $(K_L a)_I = (K_L a)_{II}$ then

$$\left(\frac{(P/V_L)_I}{(P/V_L)_{II}}\right)^n = \left(\frac{(\mu_L)_I}{(\mu_L)_{II}}\right)^{1/3}$$

assuming $n = 0.4$ (8), and since $\left(P/V_L\right)_I$ = 2 H.P./1,000 gal and $\left(\mu_L\right)_I$ = 1 C.P. then $\left(\frac{P}{V_L}\right)_{II} = 2 \times 2.07 = 4.3$ H.P./1,000 gal.

the 1,044 gal. fermentor requires $4.3 \times 1.044 = 4.5$ H.P.

Assume 60% mechanical efficiency

motor drive needed = $4.5 \times 1.4 = 6.3$ H.P.

motor drive unit cost = $\$150 \times \frac{437}{161} = \$400$

Agitation power for 1,358 gal. tank = 6.3 H.P.

Centrifuge = 3.5 H.P.

Feed and effluent pumps = 1.5 H.P.

Recycle pump = 0.4 H.P.

Total = 11.7 H.P.

This power is used to produce 113 Kg ethanol/hr. or

$$\frac{11.7 \times 0.746}{113} = 0.077 \frac{\text{Kwatt-hr.}}{\text{Kg. ethanol}}$$

Appendix C-3

Case III. Rotorfermentor

Figure 7.5.4 is a schematic flow diagram of the Rotorfermentor unit.

Overall cell mass balance:

$2,500 \times 100 \times 0.03 = B \times 30$

Cell bleed rate = B = 250 lit/hr.

Filtrate rate = 2,500 - 250 = 2,250 lit/hr.

Ethanol mass balance:

$2,500 \times 100 \times 0.03 = P_r\ (2,250 + 250)$

$P_r = 45$ gm. ethanol/lit.

Fermentor volume:

According to equation 7.1.12

$$\mu = \frac{B}{V_r}$$

$$V_r = \frac{250}{0.063} = 3,968 \text{ lit.}$$

This fermentor volume is the same as for Case II, i.e. C.S.T. fermentor with recycle operated at the same cell concentration of X = 30 gm./lit. Allow 30% extra volume then nominal volume = $3,968 \times 1.3 = 5,158$ lit. =

= 1,358 gal.

Volumetric cell mass and ethanol productivity:

$$\frac{2,500 \times 45}{3,968} = 28.35 \text{ gm. ethanol/lit.hr.}$$

$$\frac{250 \times 30}{3,968} = 1.89 \text{ gm. cell/lit.hr.}$$

Cell mass balance around secondary centrifuge:

This is a small size Westfalia centrifuge which gives 17% solids concentrate and draws 0.75 H.P.

$$\text{centrifuge cell-free effluent} = 250 - \frac{250 \times 30}{170} =$$

$$250 - 44 = 206 \text{ lit./hr.}$$

Rotor calculations:

In order to calculate the filtration area required to accommodate a filtrate rate of L = 2,250 lit/hr., we assume filtration without cake formation, i.e., "centrifugal" filtration. This assumption in terms of energy consumption by the rotating membrane is rather conservative because the energy consumption for "centrifugal" filtration is much higher than that for "cake" filtration. This assumption must be kept in mind when the energy consumed by the Rotorfermentor is compared with that of C.S.T. fermentor with cell recycle.

We assume a rotor of 6-inch diameter operated at 690 r.p.m. which is a mechanically feasible assumption based also on the overall physical dimensions of the Rotorfermentor. Use Equation 5.6 to calculate the filtrate flux u.

$$u = \frac{\Delta\rho D_p^2 V^2}{18\mu R_0} = \frac{(0.06)(25 \times 10^{-8})(30.25 \times 10^4)}{(18 \times 10^{-2})(7.62)} =$$

$= 0.00335\ cm^3/sec\ cm^2 =$

$= 3.1$ gallon/hr ft.^{2}

since

$$u = \frac{L}{A}$$

required filtration area A is given by

$$A = \frac{L}{u} = \frac{2,250/3.8\ gal/hr}{3.1\ gal/hr\ ft^2} = 190\ ft^2.$$

Total length of 6-inch diameter rotor is given by

$$l = \frac{A}{\pi D} = \frac{190\ ft^2}{3.14 \times 0.5} = 121\ ft.$$

Use 20 rotors of 6-inch diameter and 6-feet length which will be mounted horizontally between the two ends of the Rotorfermentor.

Total volume of the rotors $= \frac{\pi(0.5)^2}{4} \times 121 =$

$= 23.7\ ft^3 = 671$ lit.

Equipment Cost estimate:

Agitated stainless steel tank, 1,358 gal. = $19,000

Secondary centrifuge Westfalia LWA-205; 300 lit/hr. throughput; 0.75 H.P. = $3,000

Air compressor = $10,800

Feed pump = $1,350

Rotor Cost Estimate

Membrane cost at $5.9/ft^2 for Millipore membrane type WSWP00010 is 190 ft^2 x $5.9/ft^2 = $1,120. Assume supporting stainless steel perforated screen = 190 ft^2 x $2.30/ft^2 = $437.0. Use 1-inch Crane seals and ball bearings to support rotors.

Total number of seals = 2 x 20 = 40,

Total number of ball bearings = 2 x 20 = 40,

Total cost of Crane seals = 40 x \$90 = \$3,600,

Total cost of ball bearings = 40 x \$20 = \$800.

Use 5 motor units to drive the 20 rotors by grouping 4 rotors together through a common gear drive.

need 1 H.P. per motor

1 H.P. motor = $\$70 \times \frac{437}{161} = \$190.0$

Total cost of motor drive units = 5 x \$190.0 =

= \$950.0

Rotor shaft cost: assume stainless steel 1-inch diameter rod of 120 ft. total length.

Rotor shaft cost = 120 x \$6 = \$720.

The total rotor cost is:

Membrane	\$1,120
Supporting screen	437
Crane seals	3,600
Ball bearings	800
Rotor shaft	720
Motor drives	950
Total	\$7,627

Power requirements:

Use Equation 3.1.3 to estimate the power consumed by the rotating membrane.

$P = (1.272 \times 10^{-8})(f\rho LD^4N^3)$ where

f = friction factor

$\rho = 62.4$ lb./ft^3

L = 120 ft.

D = 0.5 ft.

N = 690 r.p.m.

In our case the membrane used is a Millipore Grade WS made from cellulose ester and has a very smooth surface. The Reynold's number of the rotating membrane is $N_{RE} = 3.19 \times 10^6$ and from the experimental data of Theodorsen and Regier (9) for smooth cylinders we get $f = 0.002$.

$$P = (1.272 \times 10^{-8})[0.002 \times 62.4 \times 120 \times (0.5)^4 (690)^3] =$$

$$= 3.9 \text{ H.P.}$$

assuming 60% mechanical efficiency

rotor power required = 3.9 x 1.4 = 5.5 H.P.

Rotor power = 5.5 H.P.

Feed pump = 0.75 H.P.

Centrifuge LWA-205 = 0.75 H.P.

Total = 7.0 H.P.

This power is used to produce 113 Kg ethanol/hr. or

$$\frac{7.0 \times 0.746}{113} = 0.046 \frac{\text{Kwatt-hr.}}{\text{Kg. ethanol}}$$

References Cited in Chapter VII

1. Lilly, M. D., and Dunnill, P. Isolation of intracellular enzymes from microorganisms--the development of a continuous process. Fermentation Advances, pp. 225-247, D. Perlman, ed., Academic Press, New York (1969).

2. Sortland, L. D., and Wilke, C. R. Kinetics of a dense culture fermentation. Lawrence Radiation Laboratory Report UCRL-18340 (1968).

3. Robinson, C. W., and Wilke, C. R. Mass transfer coefficients and interfacial area for gas absorption by agitated aqueous electrolyte solutions. Lawrence Radiation Laboratory Report UCRL-20472 (1971).

4. Margaritis, A. and C. R. Wilke. Engineering Analysis of the Rotorfermentor. Developments in Industrial Microbiology, Vol. 13, pp. 159-176 (1972).

5. Aries, R. S., and Newton, R. D. Chemical Engineering Cost Estimation, McGraw-Hill Book Company, New York (1955).

6. Chemical Engineering, May 26, 1975. McGraw-Hill Book Company, New York.

7. Perry, J. H., Chilton, C. H., and Kirkpatrick, S. D. Chemical Engineers' Handbook. 4th edition, McGraw-Hill, New York (1963).

8. Calderbank, P. H., and Moo-Young, M. M. Chem. Eng. Sci., 16 39(1961).

CHAPTER VIII

CONCLUSIONS AND RECOMMENDATIONS

In this dissertation the theoretical basis of design and operation of the Rotorfermentor is presented along with experimental results on ethanol fermentation. In addition, basic ethanol fermentation kinetic studies are reported by employing an ordinary continuous stirred tank (C.S.T.) fermentor. A bench scale pilot plant shown in Figure 2.1.1 was designed and built to test the feasibility of the Rotorfermentor, while the experimental apparatus shown in Figure 6.8 was designed to study the kinetics of ethanol fermentation under batch and continuous growth conditions. All the alcohol fermentation experiments were carried out at 28°C and pH = 4.0±0.1 using Saccharomyces cerevisiae ATCC #4126. A literature survey revealed that no previous work has been done on alcohol fermentation kinetics of this yeast strain. This is a high temperature ethanol producing yeast strain which has been chosen for subsequent use in the fermentation of reducing sugars obtained from the enzymatic hydrolysis of waste cellulose. The effects of varying glucose and oxygen concentration were studied on such metabolic parameters as specific ethanol productivity, cell and ethanol yield factor, rate of glucose

uptake, ethanol and cell productivity and endogenous metabolism. In general, it was found that at high glucose concentrations increases in oxygen concentration produced very small results while at low glucose concentrations the oxygen effect was maximized. This was found to be in agreement with theoretical arguments on the glucose repression effect presented in Section 6.3.

As seen from Figure 6.37 at a given constant specific growth rate the specific ethanol productivity increases with increasing glucose concentration, reaches a maximum and then decreases at high glucose concentrations due to the repression of the enzyme alcohol dehydrogenase.

A linear relationship between specific ethanol productivity and specific growth rate was found, thus fitting the Luedeking-Piret model. However, both the slope and intercept of the straight line were found to depend on both glucose and oxygen concentration. No previous work has been done to assess the effects of glucose and oxygen concentration on the parameters α and β of the Luedeking-Piret model given by equation 6.4.16. As seen from Table 6.5 the kinetic parameters α and β obtained by Aiyar and Luedeking for anaerobic batch fermentation differ from the results for continuous fermentation obtained in the present study.

The experimental results of runs A and C showed that oxygen in the feed can be a limiting substrate. For example, increasing the feed oxygen concentration by a

factor of about three, i.e., from 0.93 p.p.m. to 2.95 p.p.m., there was an almost threefold increase in maximum cell mass productivity and about 2.5 times increase in ethanol productivity.

For all continuous runs a plot of $1/Y_{X/S}$ against 1/D revealed the presence of endogenous metabolism according to equation 6.4.13. It was found that both parameters M and Yg depend on the level of glucose and oxygen concentration. Such a dependence of endogenous metabolism on either glucose or oxygen concentration was not studied by previous workers.

Figure 6.43 shows the respiratory requirements for Saccharomyces cerevisiae ATCC #4126. The respiration rate coefficient varies from zero at zero oxygen concentration to 25.72 μMoles O_2/hr. gm. cell at 12.25 μM oxygen concentration. The relatively low values of Q_{O_2} obtained reflect the fact that the respiratory enzymes are repressed at the high glucose concentration ranges from 23.4 gm. glu/lit at D = 0.21 hr^{-1} to 97.9 gm. glu/lit at D = 0.21 hr^{-1}. These values of glucose concentration are much higher than those reported by Moss et al. (Reference 16, Chapter VI) at which repression of the respiratory enzymes was found. Therefore, when reporting Q_{O_2} values the glucose concentration is an important parameter.

Increasing the oxygen concentration while maintaining a constant dilution rate affects the specific

ethanol productivity, the cell and ethanol yield factor and the ethanol and cell mass productivity. As shown from the results in Table 6.11 for a constant value of $D = 0.063\ hr^{-1}$ there is an almost seven-fold increase in cell mass concentration when the oxygen concentration is increased from zero to 21.45 μM. This reflects similar increases in cell yield coefficient $Y_{X/S}$ from 0.048 to 0.151. For the same increase in oxygen concentration, i.e., from zero to 21.45 μM, the amount of unfermentable sugar left over is decreased from a high 51.50 gm/lit to 1.58 gm/lit, while the cell mass productivity increases by a factor of almost seven. The specific ethanol productivity decreases from $0.66\ hr^{-1}$ at zero oxygen concentration to $0.19\ hr^{-1}$ at 21.45 μM. This decrease is in agreement with theoretical arguments regarding the "Pasteur effect" as explained by Sols (Reference 4, Chapter VI). Although the specific ethanol productivity ν decreases, the overall ethanol productivity per unit fermentor volume increases from 1.32 gm. ethanol/lit. hr. at zero oxygen concentration to 2.65 gm. ethanol/lit. hr. at 21.45 μM. Figure 6.51 shows that at a dilution rate $D = 0.063\ hr^{-1}$ almost 100% utilization of the glucose in the feed is achieved when the oxygen concentration is maintained at about 20 μM. At a higher dilution rate of $D = 0.19\ hr^{-1}$ the maximum amount of glucose feed utilized is only about 40%. It is concluded that in order to achieve 100%

utilization of glucose in a single stage fermentor for the growth conditions covered here a low dilution rate is desirable and an oxygen concentration of about 20 μM which seems to be the "critical" oxygen level.

The second part of this dissertation is devoted to the characterization and assessment of the Rotorfermentor as a device for potential use in the fermentation industry. In summary, the following experiments were conducted:

1. Power requirements and filtration characteristics of the rotating membrane.

2. Measurement of oxygen mass transfer coefficient K_La at different agitation and aeration conditions.

3. Some transient ethanol fermentation experiments to assess the operational feasibility of the Rotor-fermentor.

The K_La values obtained ranged from 72.5 to 109 hr^{-1} corresponding to power per unit liquid volume inputs of 0.527 and 2.863 H.P./1,000 gallons. These K_La values are more than adequate to satisfy the respiratory requirements of yeast under conditions of ethanol fermentation studied here.

Transient fermentation runs with the Rotorfermentor were conducted using a 3 micron Millipore membrane attached to an 8-inch diameter rotor.

The results of run HD-3 show that it is possible to extend the use of Rotorfermentor to aerobic systems where

the continuous supply of air is necessary. For this run air was introduced at the rate of 2 standard lit/min and then exited through the top of the G-L separator. No air escaped through the membrane. The pressure inside the Rotorfermentor was maintained at about 2.8 p.s.i giving a steady-state filtrate rate of 3.2 lit/hr which corresponds to a filtrate flux of 0.77 gal/ft^2 hr. or 0.0523 cm^3/cm^2 min. Much higher filtrate rates should be obtained at higher pressures inside the fermentor. Under those conditions the maximum cell concentration obtained inside the Rotrofermentor was 30.9 gm/lit while the ethanol concentration was pretty constant varying between 42 to 47 gm. ethanol/lit. Because of the relatively high cell concentration inside the Rotor-fermentor almost all feed glucose is utilized giving an ethanol productivity of 27 gm. ethanol/lit hr. The maximum ethanol productivity obtained in a C.S.T. fermentor at the same glucose feed concentration temperature and pH was 2.65 gm. ethanol/lit hr.

Further work is needed in order to optimize the operating conditions of the Rotorfermentor by trying various combinations of bleed and filtrate flow rates, rotor speed, as well as different concentration levels of glucose and ethanol. Much higher filtrate rates should be possible by the proper use of newly developed metallic membranes which have small enough pores to avoid possible plugging.

A preliminary process economic feasibility study indicates that the Rotorfermentor might be a potential alternative in replacing the functions of both an ordinary C.S.T. fermentor and centrifuge separator. Depending on the conditions of a particular process application the Rotorfermentor may result in lower capital investment costs than a combination of a C.S.T. fermentor plus a centrifuge separator. Further work is needed to determine more accurate power requirements filtration rates and overall capital costs for large scale processes.

TECHNICAL INFORMATION DIVISION
LAWRENCE BERKELEY LABORATORY
UNIVERSITY OF CALIFORNIA
BERKELEY, CALIFORNIA 94720